Coastal and Hydraulics Laboratory   Technical Report CHL-98-32

US Army Corps
of Engineers®
Engineer Research and
Development Center

Coastal Inlets Research Program

Shinnecock Inlet, New York, Site Investigation

Report 4, Evaluation of Flood and Ebb Shoal Sediment Source Alternatives for the West of Shinnecock Interim Project, New York

Adele Militello and Nicholas C. Kraus

March 2001

20010515 036

Coastal Inlets Research Program

Technical Report CHL-98-32
March 2001

Shinnecock Inlet, New York, Site Investigation

Report 4, Evaluation of Flood and Ebb Shoal Sediment Source Alternatives for the West of Shinnecock Interim Project, New York

by Adele Militello, Nicholas C. Kraus

Coastal and Hydraulics Laboratory
U.S. Army Engineer Research and Development Center
3909 Halls Ferry Road
Vicksburg, MS 39180-6199

Final report

Prepared for U.S. Army Engineer District, New York
26 Federal Building
New York, NY 10278-0090

and U.S. Army Corps of Engineers
Washington, DC 20314-1000

Contents

Preface ix

Conversion Factors, Non-SI to SI Units of Measurement x

1—Introduction 1

Shinnecock Inlet Navigation Project 2
Overview of Coastal Processes at Shinnecock Inlet 4
Objectives of Study 7

2—Alternative Designs 9

3—Hydrodynamic Data 23

Water Level 23
Current 26
Discharge and Tidal Prism 29

4—Circulation and Wave Modeling 32

Circulation Modeling 32
Wave Modeling 77

5—Engineering Analysis of Inlet Morphology Change 81

Inlet Stability 81
Ebb Shoal 84
Flood Shoal 87
Inlet Morphology Reservoir Model 94

6—Discussion and Conclusions 108

Inlet Stability 109
Evolution of the Ebb Shoal and Bypassing 109
Mining of the Flood Shoal 110
Deposition Basin 110
Changes in Erosion and Deposition Patterns 111
Navigation Benefits 111

References 115

Appendix A: Plots of Calculated Velocity A1

Appendix B: Plots of Calculated Change in Current Speed B1

Appendix C: Analysis of Alternative 16 .... C1

SF 298

List of Figures

Figure 1. Location map for Shinnecock Inlet 2

Figure 2. Shinnecock Inlet, entrance channel, and deposition basin 3

Figure 3. View of Shinnecock Inlet and beach to west, 20 November 1997 4

Figure 4. Ebb shoal at Shinnecock Inlet, 22 April 1997 6

Figure 5. Flood shoal at Shinnecock Inlet, 10 April 1997 7

Figure 6. Detail map of Shinnecock Inlet and Bay 10

Figure 7. Alternative 0: No action 15

Figure 8. Alternatives 1, 2, and 3: Dredge area of compatible material 15

Figure 9. Alternative 4: Dredge area of compatible material following contours 16

Figure 10. Alternative 5: Dredge western portion of flood shoal 16

Figure 11. Alternative 6: Dredge a channel northeast from Ponquogue Bridge 17

Figure 12. Alternative 7: Dredge Ponquogue attachment bar 17

Figure 13. Alternative 8: Lengthen west jetty 18

Figure 14. Alternative 9: Shorten east jetty 18

Figure 15. Alternative 10: Dredge a wedge-shaped channel in flood shoal 19

Figure 16. Alternative 11: Dredge a wedge-shaped channel in flood shoal and channel northeast from Ponquogue Bridge 19

Figure 17. Alternative 12: Dredge an extended wedge-shaped channel in flood shoal 20

Figure 18. Alternative 13: Dredge a rotated wedge-shaped channel in flood shoal 20

Figure 19. Alternative 14: Relocate deposition basin over channel thalweg..... 21

Figure 20. Alternative 15: Relocate deposition basin with orientation toward the southeast 21

Figure 21. Area of compatible material showing northern limit of allowable dredging as requested by the Southampton Town Trustees 22

Figure 22. Locations of historic NOS water-level gauges 24

Figure 23. Shinnecock Inlet and Bay monitoring plan 25

Figure 24. Bin-averaged current speed in Shinnecock Inlet, 13 November through 10 December 1998 28

Figure 25. Bin-averaged current speed in Shinnecock Inlet, 3-4 December 1998 28

Figure 26. Measured discharge in Shinnecock Inlet, 4 December 1997 and 22 July 1998 29

Figure 27. Regional ADCIRC mesh covering New York Bight, south shore of Long Island, and Long Island Sound 34

Figure 28. ADCIRC mesh at Shinnecock Bay 34

Figure 29. ADCIRC mesh for Shinnecock Bay flood shoal and inlet 35

Figure 30. ADCIRC mesh at Shinnecock Inlet 35

Figure 31. Water level and current speed at Shinnecock Canal 36

Figure 32. Comparison of measured and calculated water level at P1 39

Figure 33. Comparison of measured and calculated water level at P2 40

Figure 34. Comparison of measured and calculated water level at P3 40

Figure 35. Comparison of measured and calculated water level at P4 41

Figure 36. Comparison of measured and calculated water level at C4 42

Figure 37. Comparison of measured and calculated water level at C2 43

Figure 38. Comparison of measured and calculated water level at C3 43

Figure 39. Calculated discharge through Shinnecock Inlet, 3 November through 2 December 1998 44

Figure 40. Time-averaged discharge through Shinnecock Inlet 45

Figure 41. Alternative 0 velocity vectors and speed at flood shoal, peak flood tide 46

Figure 42. Alternative 0 velocity vectors and speed at flood shoal, peak ebb tide 47

Figure 43. Alternative 0 velocity vectors and speed at inlet and ebb shoal, peak ebb tide 48

Figure 44. Eddy migration and associated jet orientation and shape 49

Figure 45. Vector plots of measured ebb current 50

Figure 46. Regions identified for evaluating change in current speed 52

Figure 47. Change in current speed for Alternative 3, flood tide 53

Figure 48. Change in current speed for Alternative 3, ebb tide 54

Figure 49. Change in current speed for Alternative 5, flood tide 55

Figure 50. Change in current speed for Alternative 5, ebb tide 55

Figure 51. Change in current speed for Alternative 7, flood tide 56

Figure 52. Change in current speed for Alternative 7, ebb tide 57

Figure 53. Change in current speed for Alternative 8a, flood tide 58

Figure 54. Change in current speed for Alternative 8a, ebb tide 59

Figure 55. Change in current speed for Alternative 9a, flood tide 60

Figure 56. Change in current speed for Alternative 9a, ebb tide 60

Figure 57. Change in current speed for Alternative 12, flood tide 61

Figure 58. Change in current speed for Alternative 12, ebb tide 62

Figure 59. Change in current speed for Alternative 15, flood tide 63

Figure 60. Change in current speed for Alternative 15, ebb tide 63

Figure 61. Alternative 8a velocity vectors and speed at inlet and ebb shoal, peak ebb tide 65

Figure 62. Inlet discharge over 2-day interval for Alternatives 0 and 9a 68

Figure 63. Critical depth-averaged speed for initiation of suspension 69

Figure 64. Water depth vs. critical depth-averaged velocity for $d_{50} = 0.54$ mm 70

Figure 65. Excess suspension at peak flood tide for Alternative 0 71

Figure 66. Excess suspension at peak ebb tide for Alternative 0 71

Figure 67. Excess suspension at peak flood tide for Alternative 1 72

Figure 68. Excess suspension at peak ebb tide for Alternative 1 73

Figure 69. Excess suspension at peak flood tide for Alternative 5 74

Figure 70. Excess suspension at peak ebb tide for Alternative 5 74

Figure 71. Shinnecock Inlet discharge for Shinnecock Canal gated (existing condition) and closed 75

Figure 72. Water level between inlet and flood shoal for Shinnecock Canal gated (existing condition) and closed 76

Figure 73. Output locations for wave calculations 78

Figure 74. Definition sketch for the Escoffier (1940) stability diagram 82

Figure 75. Closure curve for Shinnecock Inlet 84

Figure 76. Depth contours in Shinnecock Inlet from 1998 survey 84

Figure 77. Volume of ebb shoal calculated with measured tidal prism 86

Figure 78. Morphologic notation for flood shoals 87

Figure 79. Bathymetry of Shinnecock Bay in the vicinity of the present location of the inlet 90

Figure 80. Growth of flood shoal from September 1933 to May 1998 92

Figure 81. Volume of flood shoal calculated from the measured tidal prism 94

Figure 82. Sensitivity analysis for predicted volume of the ebb shoal, V_{Ee} fixed 97

Figure 83. Sensitivity analysis for predicted volume of the ebb shoal, Q_{in} fixed 99

Figure 84. Predicted bypassing rate from the ebbs shoal to the beach 100

Figure 85. Sediment paths defining the inlet morphology reservoir model 101

Figure 86. Calculated volumes of ebb shoal and bypassing bar, and flood shoal 106

Figure 87. Calculated bypassing or output rate from morphologic feature 106

Figure 88. Evolution of the volume of the flood shoal after mining 107

List of Tables

Table 1. List of Project Alternatives 11

Table 2. Definitions of Projects Alternatives 12

Table 3. Mined Depth and Volume of Sand Removed for Alternatives 14

Table 4. Tidal Datums (ft) for Shinnecock Tide Gauges 24

Table 5. Tidal Datums (ft) for Shinnecock Tide Gauges for April - June 1998 26

Table 6. Difference in Tidal Datums (ft), NOS 1987 and 1991 vs. 1998 26

Table 7. Tidal Prism and Minimum Inlet Cross-Sectional Area 31

Table 8. Sources of Bathymetric Data and Regions of Application 33

Table 9. Comparison of Measured and Calculated Water Level and Current 41

Table 10. Alternative Groups 52

Table 11. Inlet Discharge Quantities for Alternatives 67

Table 12. Wave Properties at Numerical Stations 80

Table 13. Volume of Ebb Shoal and Flood Shoal 86

Table 14. Values of Reservoir Model Input Parameters for Base Run 104

Table 15. Comparison of Navigation Benefits of Alternatives 113

Preface

This study of hydrodynamic and geomorphic processes at Shinnecock Inlet, Long Island, New York, was conducted by the U.S. Army Engineer Research and Development Center (ERDC), Coastal and Hydraulics Laboratory (CHL) for the U.S. Army Engineer District, New York. Ms. Diane S. Rahoy was the New York District Project Manager, and this report was prepared by Dr. Adele Militello, CHL, Coastal Hydrodynamics Branch (HN-C), and by Dr. Nicholas C. Kraus, CHL, Senior Scientists Group. Dr. Militello was the Principal Investigator for the study.

Partial support for this study was provided by the Inlet Modeling System (IMS) Work Unit of the Coastal Inlets Research Program (CIRP) of Headquarters, U.S. Army Corps of Engineers. Dr. Kraus was the CIRP Technical Leader, and Dr. Militello was the Principal Investigator for the IMS Work Unit. This study was authorized in September 1999, and a draft of this report was submitted to the New York District for review in April 2000.

This work benefited from a field monitoring system sponsored by the New York District, the New York State Department of Environmental Conservation, and the CIRP. The U.S. Coast Guard Station, Shinnecock, contributed onsite resources in support of the monitoring system. The monitoring system was maintained by Mr. William G. Grosskopf, Offshore and Coastal Technologies, Inc. (OCTI), and by Mr. Thomas C. Wilson of the Marine Sciences Research Center, State University of New York at Stony Brook, under contract with OCTI. Mr. Mitchell E. Brown, Mevatec, Inc. assisted in performing the numerical simulations of the tidal hydrodynamics. Dr. Andew Morang, CHL, Coastal Sediments and Engineering Branch, provided data and technical assistance. Mr. Grosskopf also provided background information for the sand mining alternatives. The Suffolk County Department of Public Works provided detailed records and other information on the tidal gate at the Shinnecock Canal.

Work was performed under the general administrative supervision of Dr. Zeki Demirbilek, Acting Chief, HN-C, Mr. Thomas Richardson, Acting Director, CHL, and Dr. James R. Houston, former Director, CHL.

At the time of publication of this report, Dr. James R. Houston was Director of ERDC, and COL James S. Weller, EN, was Commander.

Conversion Factors, Non-SI to SI Units of Measurement

Non-SI units of measurement used in this report can be converted to SI units as follows:

Multiply	By	To Obtain
acres	4,046.873	square meters
cubic feet	0.028317	cubic meters
cubic yards	0.7645549	cubic meters
feet	0.3048	meters
miles (U.S. nautical)	1.852	kilometers
miles (U.S. statute)	1.609347	kilometers

1 Introduction

This report documents a study performed to examine the consequences of mining sand from the flood-tidal shoal at Shinnecock Inlet, Long Island, New York. The mined material, if compatible, would be placed on the eroding beach located adjacent to the west jetty at the inlet. The flood shoal represents a potential renewable source of material for further placement operations. In addition to being a low-cost sand resource, as compared to mining open-ocean borrow sites, modification of the shoal might bring navigation improvement and other benefits through a number of ways that are considered in this report.

The study methodology relied in part on numerical simulation modeling of the tidal hydrodynamics at the inlet. The model was established for the site under the Coastal Inlets Research Program (CIRP), a research and development program supported by Headquarters, U.S. Army Corps of Engineers (USACE). Extensive measurements required to understand the hydrodynamics of the inlet and to calibrate the model were obtained through an ongoing cooperative field-data collection effort sponsored by the U.S. Army Engineer District, New York (New York District), the New York State Department of Environmental Conservation (DEC), and the CIRP.

This report describes the methods applied and results obtained to evaluate the feasibility of 15 action alternatives for material removal and improvement of flow properties within Shinnecock Inlet and Bay and along the ocean shore. Quantitative estimates of the growth of the flood and ebb shoals are also made. Chapter 1 gives an introduction to Shinnecock Inlet, relevant literature, and project objectives. Chapter 2 describes the design alternatives and their rationale. Chapter 3 presents and interprets physical processes data collected within the project area. Chapter 4 describes the circulation and wave modeling conducted to evaluate the alternatives and determine the properties of waves propagating over the ebb-tidal shoal. Chapter 5 describes the morphodynamic processes and related engineering activities at Shinnecock Inlet. Chapter 6 contains conclusions and recommendations of the study.

Shinnecock Inlet Navigation Project

Shinnecock Inlet connects Shinnecock Bay to the Atlantic Ocean and is the easternmost of six permanent openings along the sandy barrier island on the south shore of Long Island, New York (Figure 1). It is located in the town of Southampton, Suffolk County, 37 miles[1] west of Montauk Point, the eastern tip of the south shore of Long Island, and 95 miles east of the Battery in New York City. The present inlet formed as a breach during the great hurricane of 21-24 September 1938 and was stabilized by local interests in a series of projects. A revetment was constructed on the west side in 1947 (probably to halt westward migration of the inlet. The revetment was extended to a jetty on the west from 1953 to 1955, and the east jetty was constructed from 1952 to 1953). Much of the material that follows in this introductory section is taken from Morang (1999).

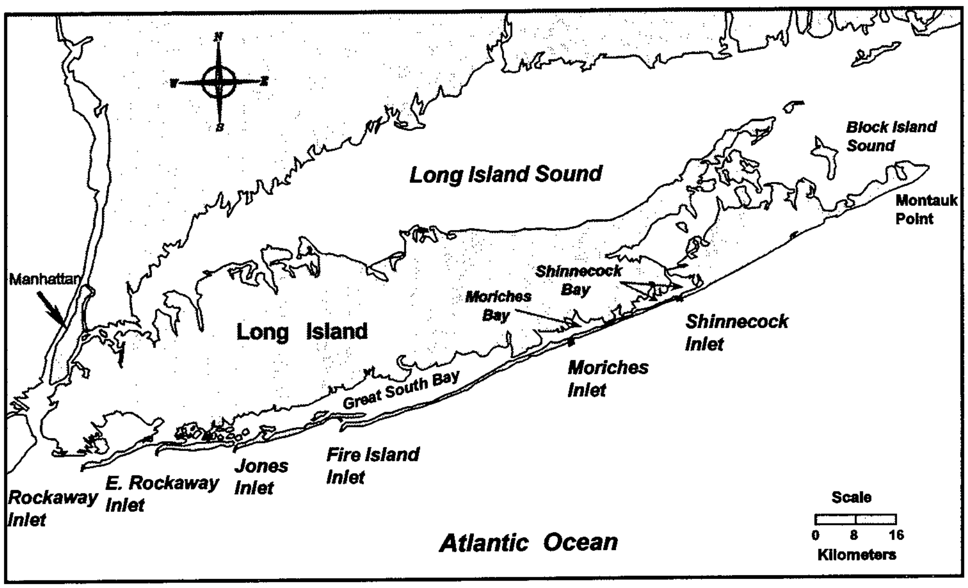

Figure 1. Location map for Shinnecock Inlet

A Federal Navigation Project for Shinnecock Inlet was authorized by the River and Harbor Act of 1960 in accordance with recommendations contained in House Document No. 126, 86th Congress, 1st Session, dated May 1959 (USACE 1988). The primary purpose of the original authorization was to provide safe navigation through the inlet. The Federally authorized entrance channel is 10 ft deep at mean low water (mlw) and 200 ft wide from that depth in the Atlantic Ocean to Shinnecock Bay. The inner bay channel is directed to the west and is 6 ft deep (mlw) and 100 ft wide to the Long Island Intracoastal Waterway

[1] This study involves analysis of historic and recent engineering documents and data with values expressed in American Customary (non-SI) Units. To maintain continuity with the previous body of work, the original units are retained in their context. Measurements and calculations made as part of the present study are expressed in SI units. A table of factors for converting non-SI units of measurement to SI units is presented on page x.

(LIWW). One foot each of advance dredging and allowable overdredging can increase these depths by 2 ft.

Although the Federal navigation project at Shinnecock Inlet was authorized in 1960, a local cooperative agreement (with New York State) was not executed until 1990, at which time substantial navigational improvements were initiated. The two jetties were rehabilitated between 1990 and 1992, and, in 1990, a deposition basin was dredged (involving removal of 668,000 yd^3 of material) seaward of the jetties (Figure 2). The design dimensions of the deposition basin are 20 ft deep (mlw), 2,600 ft long, and 800 ft wide. The basin is intended to capture littoral sediment moving from east to west, the predominant direction of transport. It also serves to improve navigation at the entrance.

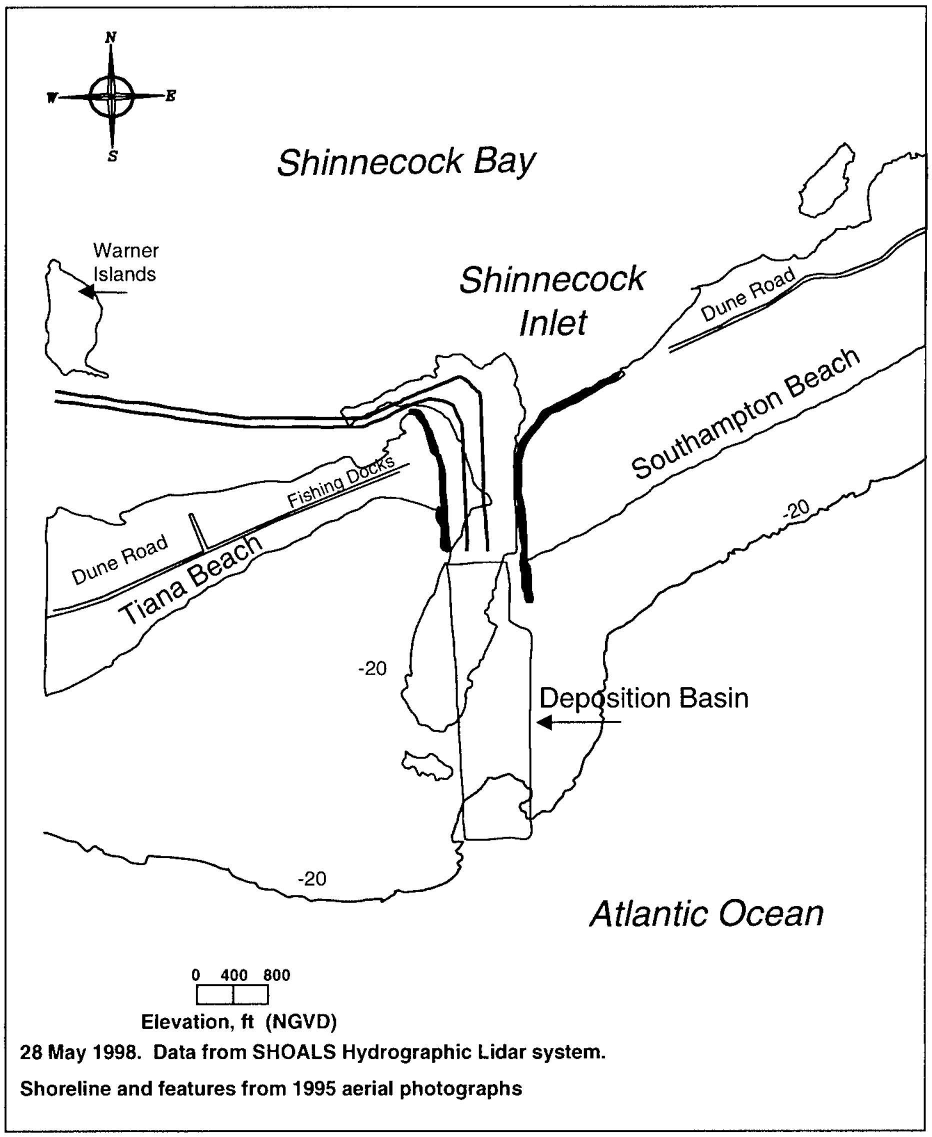

Figure 2. Shinnecock Inlet, entrance channel, and deposition basin

The beach to the west of Shinnecock Inlet experiences persistent erosion (Figure 3) and has almost been breached over recent years during larger storms. Sand dredged from the navigation channel and deposition basin is typically placed on the west beach. The identification of potential economical sources of nourishment material for this beach is the primary motivation for this study. A portion of the flood shoal can be observed in Figure 3. It is believed that the vegetated island on the upper left side of the figure (one of the two islands called Warner Island East and Warner Island West) was created during early dredging (1940s) of the Long Island Intracoastal Waterway.

Figure 3. View of Shinnecock Inlet and beach to west, 20 November 1997

Overview of Coastal Processes at Shinnecock Inlet

Considerable information is available about the geologic and coastal processes along the south shore of Long Island, NY. The present report introduces material sufficient to establish context as needed for the evaluation of alternatives for mining the flood shoal at Shinnecock Inlet. Sediment texture in and around the ebb and flood shoals at Shinnecock Inlet is documented in a comprehensive study conducted by Offshore and Coastal Technologies, Inc., - East Coast (OCTI) (1999).

Gofseyeff (1952), writing as a Senior Engineer of the New York District, summarizes early USACE and other studies together with USACE navigation projects along the south shore of Long Island, including the status of its western inlets. Careful measurement procedures as described by Gofseyeff (1952) give confidence in early measurements such as of the tidal prism, as discussed in Chapter 6. Taney (1961) conducted a pioneering geomorphologic assessment from which much other work follows (e.g., Leatherman and Allen 1985; Kana 1985) applying modern analysis procedures, in particular, accurate shoreline position mapping. Morang (1999) comprehensively documented the geomorphology and coastal processes of Shinnecock Inlet and the south shore of Long Island, New York. Williams, Morang, and Lillycrop (1998) review the coastal processes and discuss possible methods for mechanical bypassing of sand around the inlet. The latter references can be consulted for details and review of the literature.

Estimates of the longshore sand transport rate in the vicinity of Shinnecock Inlet and for the south shore of Long Island have varied in magnitude, as discussed by Rosati, Gravens, and Smith (1999). There is universal agreement that the net transport is directed to the west, with extended periods of reversals typically occurring in the summer. Early estimates of the longshore transport rate, as documented by Kana were based upon impoundment of sand after initial construction of jetties and by the migration of natural inlets, including the celebrated growth of Democrat Point across Fire Island Inlet (Gofseyeff 1952; Panuzio 1968). The early studies give net transport rates at Shinnecock Inlet on the order of 300,000 yd^3/year. This order of magnitude appears consistent with amounts dredged at the inlet entrance channel, accounting for growth of the flood and ebb shoals of the new inlet and bypassing to the downdrift beach.

In a different approach based on wave hindcast data, Kraus, Hanson, and Blomgren (1994) calculated annual net and gross longshore transport rates at Westhampton Beach, located approximately 12 miles to the west of Shinnecock Inlet. For a 20-year hindcast normalized to give a total-record average annual net of 420,000 yd^3, they found maximum and minimum net rates of 117,000 and 685,000 yd^3, and mean, maximum, and minimum gross rates of 610,000, 842,000, and 434,000 yd^3. Although these estimates are considered to be too high, they are representative of the variability in transport rate magnitude and direction.

More recent estimates of the longshore transport rate have been based upon detailed sediment budgets that account for beach nourishment volume, shoreline change, possible onshore transport of sediment, and other considerations. Rosati, Gravens, and Smith (1999) arrived at a net transport value of 150,000 yd^3/year $\pm$ 40,000 yd^3/year and discuss their results in the context of reported values. Longshore transport rates are examined from the perspective of ebb-shoal growth in Chapter 6.

The tidal current flowing through an inlet creates ebb-tidal shoals and flood-tidal shoals comprised predominantly of littoral sediments that are transported along the ocean coast. The entrance channel at an inlet must run through the ebb shoal, and the presence of a flood shoal often requires the inner channel to make

a sharp turn upon exiting into the bay. Such is the case at Shinnecock Inlet. These currents are calculated and discussed in Chapter 4.

The ebb-tidal shoal at Shinnecock Inlet is visible in Figure 4. The ebb shoal is semicircular and skewed to the west, and it attaches to the beach about 4,000 ft west of the west jetty, in the vicinity of the Ponquogue Pavilion. Sand transported to the ebb-tidal shoal is bypassed along the shore to reach the attachment bar and Ponquogue Beach. The large bulge of the attachment bar appears to be isolating the stretch of beach between it and the west jetty. Therefore, one alternative, as discussed in the next chapter, is to mine the attachment bar to allow sediment to return to the west beach during reversals in longshore transport. The semicircular configuration of the ebb shoal tends to focus waves toward the west beach irrespective of the incident wave direction offshore.

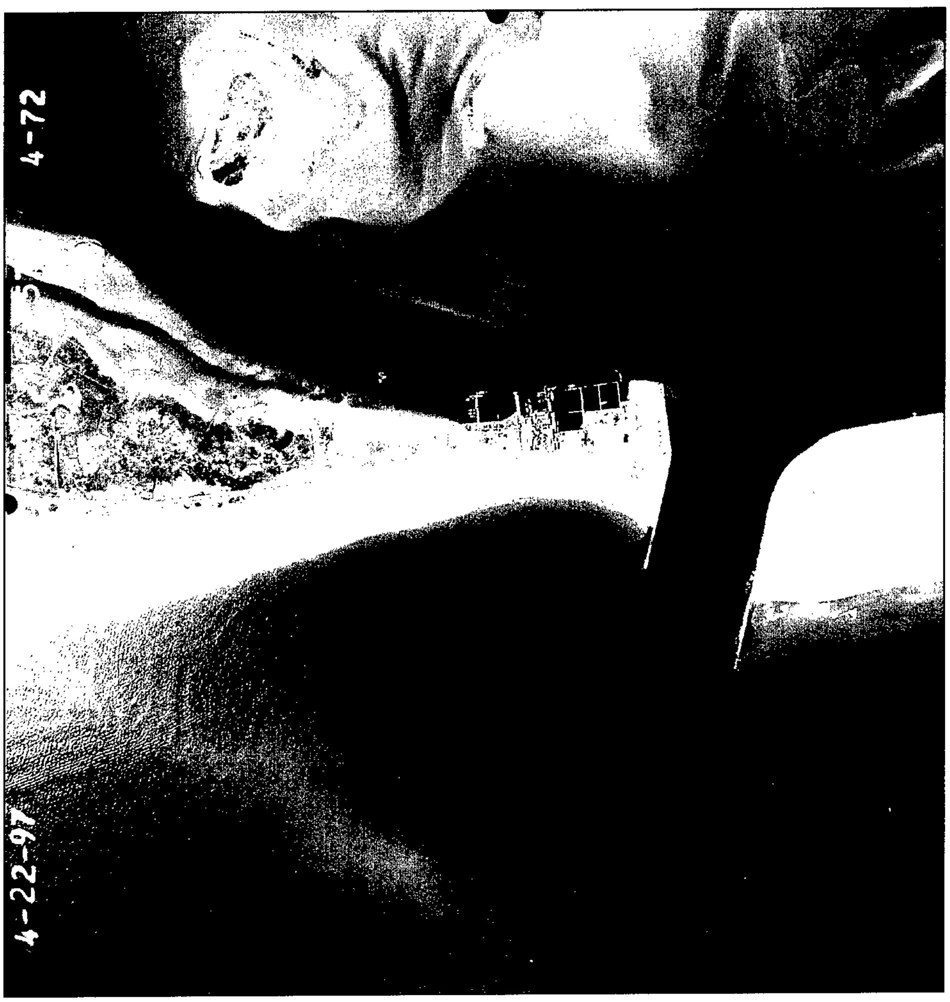

Figure 4. Ebb shoal at Shinnecock Inlet, 22 April 1997

Morang (1999) determined the volume of the ebb-tidal shoal by analysis of survey data. He determined that the ebb shoal accumulated sand at an average

rate of 141,000 yd^3/year over the 60-year period 1938-1998 for a total of 8.453 million yd^3. The deposition basin runs through the large ebb shoal that still appears to be growing (discussed in Chapter 5), and material dredged from the deposition basin reduces the volume of the shoal.

The flood-tidal shoal in 1997 is shown in Figure 5 during a lower tide stage. The tidal range, the difference between mean high water (mhw) and mlw, in Shinnecock Bay near to the flood shoal is about 2.9 ft. Tidal range in Shinnecock Bay is discussed in Chapter 3. During higher tide, most of the flood shoal is submerged.

Figure 5. Flood shoal at Shinnecock Inlet, 10 April 1997

Objectives of Study

The objective of this study is to identify and evaluate new and innovative alternative solutions having the potential of providing sources of sediment for the

beach west of Shinnecock Inlet and to determine the consequences of the borrow site alternatives. The principal innovation is to consider methods of "flood-shoal engineering," by which the flood shoal is mined in an appropriate manner to serve as a beach nourishment source. Dredging of the attachment bar located in the vicinity of the Ponquogue Pavilion, as well as lengthening and shortening of the jetties, are also examined.

Maintained inlets, especially inlets with navigation channels that are assumed by the Federal Government (such as Shinnecock Inlet), often experience problems of engineering concern. Selective dredging of the flood shoal might mitigate some of these problems. A general approach was taken here to understand the integrated hydrodynamics and morphodynamics at Shinnecock Inlet, so that known problems at the inlet could be examined with an aim of alleviating, and certainly not increasing, them. Known and potential problems are:

a. Scour at the bayside ends of the east and west jetties. (The seaward side of the west jetty has experienced scour, but this is believed to be primarily wave related.) The current should not increase greatly in the areas experiencing scour.

b. Difficult navigation of the inlet during ebb tide. The ebb current should not increase greatly at the entrance. A decrease in the ebb current is preferable.

c. Difficult navigation in the West Cut (the bay side part of the navigation channel that connects to the LIWW). The current should not increase greatly in the channel adjacent to the commercial docks.

d. Increased current under the Ponquogue Bridge. The current under the bridge is already strong owing to the constriction by the old and new fishing piers and by the bridge pilings. Increased current strength would induce further scour and be a hazard to boaters and divers (the bridge is a popular scuba diving area).

e. Increased erosion along the beach adjacent to the west jetty.

f. Adverse change in circulation or water exchange in the bay.

g. Greatly increased flow through the inlet that might increase the volume of the ebb shoal or the flood shoal.

h. Adverse change in orientation or shoaling of the navigation channel.

The study was conducted by applying modern tools and analysis procedures, made possible through the availability of high-quality data on the waves, currents, water level, and morphology change at Shinnecock Inlet. In particular, intense numerical simulations of the tidal circulation were made to make objective comparisons of the expected performance or consequences of a large number of alternatives for mining the flood shoal and other areas. A newly developed model of the long-term evolution of the volume of ebb shoals, flood shoals, and adjacent natural and engineered morphologic features was applied as part of the integrated morphology study.

2 Alternative Designs

The West of Shinnecock Interim Project, New York, was developed by the New York District with the aim of establishing cost-effective sand management practice for the beach west of Shinnecock Inlet, as well as enhancing storm damage reduction. The Interim Feasibility Recommended Plan (New York District 1999) includes beach fill with an estimated initial construction volume of 810,400 yd^3 and renourishment volumes of 383,400 yd^3 on a 2-year cycle. During review of the April 1998 draft report, mining of the flood shoal as a potential borrow source was recommended for investigation. This study was conducted to determine the feasibility of mining the flood shoal as a source of material for the beach west of Shinnecock Inlet. Fifteen action alternatives were developed that included dredging and structural modifications. This report discusses the methods applied to assess the feasibility of the alternatives and provides recommendations.

Analysis of flood-shoal material by OCTI (1999) for the New York District defined an approximate area of sand that is compatible with material on the beach west of Shinnecock Inlet. This area, shown in Figure 6, is referred to herein as the "area of compatible material." In addition to dredging the area of compatible material, alternatives were developed that include:

a. Dredging of the Ponquogue attachment bar, East Cut, western flood shoal, and a channel aligned toward the northeast from the Ponquogue Bridge.

b. Relocation and alignment of the deposition basin.

c. Modification of the jetties.

Alternatives were developed through discussion between staff of the Coastal and Hydraulics Laboratory (CHL) and the New York District. The alternatives are listed in Table 1, described in Table 2, and shown in Figures 7 through 20[1]. For alternatives that require sediment mining, areas to be mined are denoted as filled polygons with dimmed contours beneath.

[1] An additional alternative (Alternative 16) was evaluated at the request of the U.S. Army Engineer District, New York, which specifies dredging to –17.7 ft mtl over the seaward half of the area of compatible material. The description and analysis of Alternative 16 are presented in Appendix C.

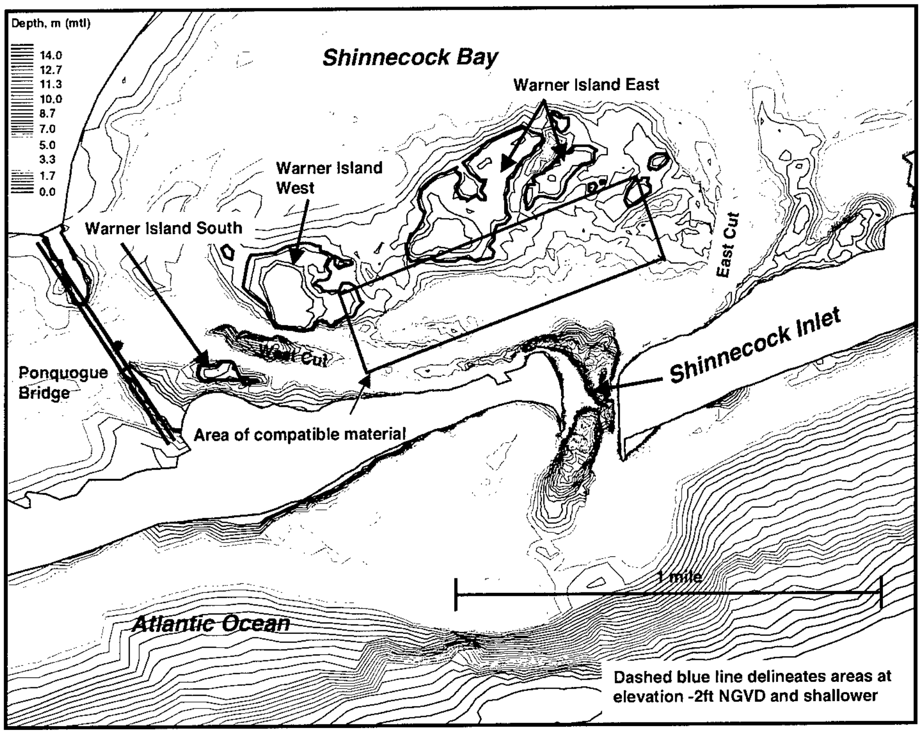

Figure 6. Detail map of Shinnecock Inlet and Bay

Development of alternatives included requirements of the New York District Environmental Branch to avoid dredging any area located at or shallower than -2 ft National Geodetic Vertical Datum (NGVD) 1929 or (-0.78 m) mean tide level[1] (mtl). These shallow areas are feeding and nesting areas for birds. Warner Islands are nesting areas for terns, gulls, and wading birds. These islands support large colonies of common terns and two colonies of the endangered roseate tern. The shallow areas and islands are also feeding habitat for shore birds, including the threatened piping plover. Areas contained within the –2 ft NGVD contour and the Warner Islands are indicated in Figure 6.

The dredging depth and corresponding volume of material removed for each alternative are listed in Table 3. Differences in bottom elevation between the existing condition and each alternative were computed from the circulation model meshes (Chapter 4). Volumes for Alternatives 1 and 2 are comparable to, but less than, those calculated by OCTI (1999) for dredging the area of compatible material. OCTI calculated material volumes of 800,000 m^3 (1,050,000 yd^3) and 1,450,000 m^3 (1,900,000 yd^3) for mined depths of 10.5 and

[1] Relationships between tidal datums and NGVD at Shinnecock Inlet are described in Morang (1999), pp. 12-13. These relationships were established many years ago and should be reviewed based on data recently collected in the recent New York District monitoring program.

13.5 ft referenced to mean sea level[1] (msl), respectively. Volumes of material removed in the present study are 700,000 m^3 (920,000 yd^3) and 1,220,000 m^3 (1,600,000 yd^3) for the 10.5 and 13.5 ft mined depths, respectively. The smaller volumes owe to not removing material at elevation –2 ft NGVD and shallower for preservation of bird habitat.

Table 1
List of Project Alternatives

Alternative	Description
0	No action.
1	Dredge the flood shoal to –10.5 ft mtl over area of compatible material.
2	Dredge the flood shoal to –4.1 ft mtl over area of compatible material.
3	Dredge the flood shoal –12.6 ft mlw (-14.3 ft mtl) over area of compatible material.
4	Dredge the flood shoal –12.6 ft mlw (-14.3 ft mtl) over area of compatible following contours where possible.
5	Dredge on western portion of shoal.
6	Dredge a relief channel extending northeast from the Ponquogue Bridge.
7	Dredge Ponquogue attachment.
8	Lengthen west jetty.
9	Shorten east jetty.
10	Dredge a wedge-shaped channel in the flood shoal extending from north of the inlet across the shoal.
11	Combine Alternatives 6 and 10.
12	Dredge an extended wedge-shaped channel in the flood shoal.
13	Dredge a rotated wedge-shaped channel in the flood shoal.
14	Reposition deposition basin so that its primary axis is parallel to and overlaid on the channel thalweg.
15	Reposition deposition basin so that its primary axis trends southeast from the inlet.

On 28 April 2000, the Southampton Town Trustees, New York District, and CHL made a site visit and discussed potential dredging configurations. The northern portion of the area of compatible material is a shell fishing ground. The town trustees requested that dredging should occur only in the southern portion of the area of compatible material, as shown in Figure 21. Circulation modeling already completed in this study simulated removal of material over the entire area of compatible material.

[1] The term msl refers to the average of all water level readings (customarily, the hourly readings) during a continuous period of record, whereas mtl refers to the tidal datum midway between mhw and mlw for the record. At Shinnecock Inlet, because the tide is dominated by the M_2 component, msl and mtl are expected to lie within a few centimeters of one another.

Table 2
Definitions of Project Alternatives

Alternative	Description
0	1998 bathymetry and no change to bottom or structures. This alternative provides a base condition for comparison of action alternatives.
1	Dredge the flood shoal to –10.5 ft mtl over area of compatible material as defined in the 1999 OCTI report "Evaluation of Flood and Ebb Shoal Sediment Source Alternatives, West of Shinnecock Interim Project, New York" (hereafter "OCTI Report"). Material mined from the shoal placed on the beach west of the inlet. Areas shallower than –2 ft NGVD contained within the defined area of compatible material would not be mined. Mined area was modified to remove a ridge that would remain south of the area of compatible material if dredging took place only in this area.
2	Dredge the flood shoal to –4.1 ft mtl over area of compatible material as defined in the OCTI Report. Material mined from this shoal would be placed on the beach west of the inlet. Areas shallower than –2 ft NGVD contained within the defined area of compatible material would not be mined. Mined area was modified to remove a ridge that would remain south of the area of compatible material if dredging took place only in this area.
3	Dredge the flood shoal –12.6 ft mlw (-14.3 ft mtl) (Referenced to historic NOS tide datums at Shinnecock Inlet of which the difference between mtl and mlw is 1.7 ft) over area of compatible material as defined in the OCTI Report. Material mined from this shoal would be applied to nourish the beach west of the inlet. Areas shallower than –2 ft NGVD contained within the defined area of compatible material would not be mined. Mined area was modified to remove a ridge that would remain south of the area of compatible material if dredging took place only in this area.
4	Dredge the flood shoal –12.6 ft mlw over area of compatible material as defined in the OCTI Report, but modify bounds of dredging to follow contours where possible. Material mined from this shoal would be applied to nourish the beach west of the inlet. Areas shallower than –2 ft NGVD contained within the defined area of compatible material would not be mined.
5	Dredge on western portion of shoal to –12.6 ft mlw in areas deeper than –2 ft NGVD. Removing material from the western shoal may reduce encroachment of the shoal into the navigation channel. Deepening of the western shoal may also provide a path for water movement across the shoal. This change in flow pattern may improve the circulation in the inlet by reducing strong flow on the eastern edge (near scour hole).
6	Dredge a relief channel to –19.3 ft mlw (-21.0 ft mtl) extending northeast from the Ponquogue Bridge. A channel aligned to the northeast may redirect a portion of the ebb flow to the northeast and reduce flow in the navigation channel. This reduction in flow may reduce the current magnitude that impinges on the northeastern side of the inlet near the scour hole.
7	Dredge Ponquogue attachment bar to –11.4 ft mlw (-13.1 ft mtl) and place material on beach west of the inlet. Dredging could be conducted as a land-based operation for cost reduction. This type of operation would limit the distance offshore that could be mined so that the bypassing bar extending from the ebb shoal to the attachment would remain. The attachment bar would eventually re-emerge as sand bypasses the inlet and accumulates on shore.
8	Lengthen west jetty by 558 ft (170 m) to change circulation patterns. Jetty length would be increased from 1,470 ft (448.1 m) to 2,028 ft (618 m). This structural modification is expected to extend the distance offshore in which eddies would form and may reduce the longshore current velocity near the shore west of the inlet. Lengthening of the west jetty may also reduce the tendency of the ebb jet to swing westward. This alternative would have two parts; (a) jetty lengthening, and (b) jetty lengthening plus mining of the flood shoal as described for Alternative 3. The configuration for mining of the shoal is expected to be that of Alternative 4 with placement of material as described for that alternative.

9	Shorten east jetty by 558 ft (170 m) to change circulation patterns. The jetty length would be shortened from 1,363 ft (415.4 m) to 805 ft (245.4 m). This structural modification would bypass sand to the west beach and change flow patterns. Sand impounded by the jetty would be available for transport to the west beach. By aligning the east jetty tip with the west jetty tip, swinging of the ebb jet may be reduced, which could reduce the current speed near the west beach to decrease the erosion there. This alternative would have two parts; (a) jetty shortening, and (b) jetty shortening plus mining of the flood shoal as described for Alternative 3. The configuration for mining of the shoal is expected to be that of Alternative 4 with placement of material as described for that alternative.
10	Dredge a wedge-shaped channel to -16 ft mlw (-14.3 ft mtl) in the flood shoal extending from north of the inlet across the shoal. Although all of the material may not be compatible with beach material west of the inlet, the incompatible portion of material may be placed beneath the compatible material on the beach. Dredging of the channel would provide a straight path for water to flow between the ocean and the bay. This alternative may alleviate problems encountered within the inlet that arise from the severe turns in the channel toward the east and west as it enters the bay.
11	Combine Alternatives 6 and 10 to reduce flow in navigation channel and provide enhanced north-south flow over the flood shoal. This alternative would combine benefits of Alternatives 6 and 10.
12	Dredge a wedge-shaped channel in the flood shoal to -16 ft mlw that covers the area defined by Alternative 10 and extends eastward such that the southeast edge of the wedge is aligned with the eastern edge of the East Cut.
13	Dredge a wedge-shaped channel in the flood shoal to -16 ft mlw that extends from the north inlet over the eastern portion of the flood shoal and East Cut. This dredging orientation requires rotation of the wedge described in Alternative 10 by approximately 25 deg clockwise.
14	Reposition deposition basin so that its primary axis is parallel to and overlaid on the channel thalweg. This change in orientation is a rotation of approximately -19 deg from the present deposition basin orientation.
15	Reposition deposition basin so that its primary axis trends southeast from the inlet. This change in orientation is a rotation of approximately $^{+}$19 deg from the present deposition basin orientation.

Table 3
Mined Depth and Volume of Sand Removed for Alternatives

Alternative	Mined depth (mtl), m (ft)	Volume, m^3 (yd^3)
0	–	–
1[1]	3.2 (10.5)	700,000 (920,000)
2[1]	4.1 (13.5)	1,220,000 (1,600,000)
3[1]	4.36 (14.3)	1,380,000 (1,800,000)
4[1]	4.36 (14.3)	1,330,000 (1,740,000)
5	4.36 (14.3)	1,370.000 (1,790,000)
6	6.4 (21.0)	260,000 (340,000)
7	4.0 (13.1)	700,000 (920,000)
8a	–	–
8b[1]	4.36 (14.3)	1,380,000 (1,800,000)
9a	–	–
9b[1]	4.36 (14.3)	1,380,000 (1,800,000)
10	4.36 (14.3)	1,900,000 (2,490,000)
11	4.36 (14.3) and 6.4 (21.0)	2,160,000 (2,830,000)
12	4.36 (14.3)	2,900,000 (3,790,000)
13	4.36 (14.3)	1,520,000 (1,980,000)
14	6.6 (21.7)	150,000 (200,000)
15	6.6 (21.7)	270,000 (350,000)

[1] Volumes are for mining over entire area of compatible material. Restrictions requested by Town Trustees (see Figure 21) would reduce volume shown.

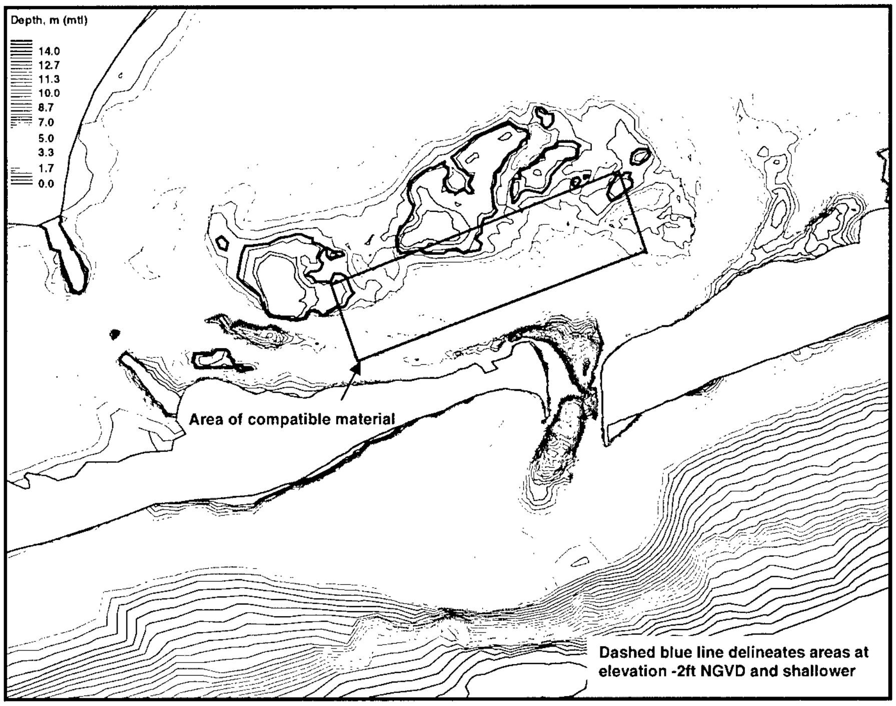

Figure 7. Alternative 0: No action

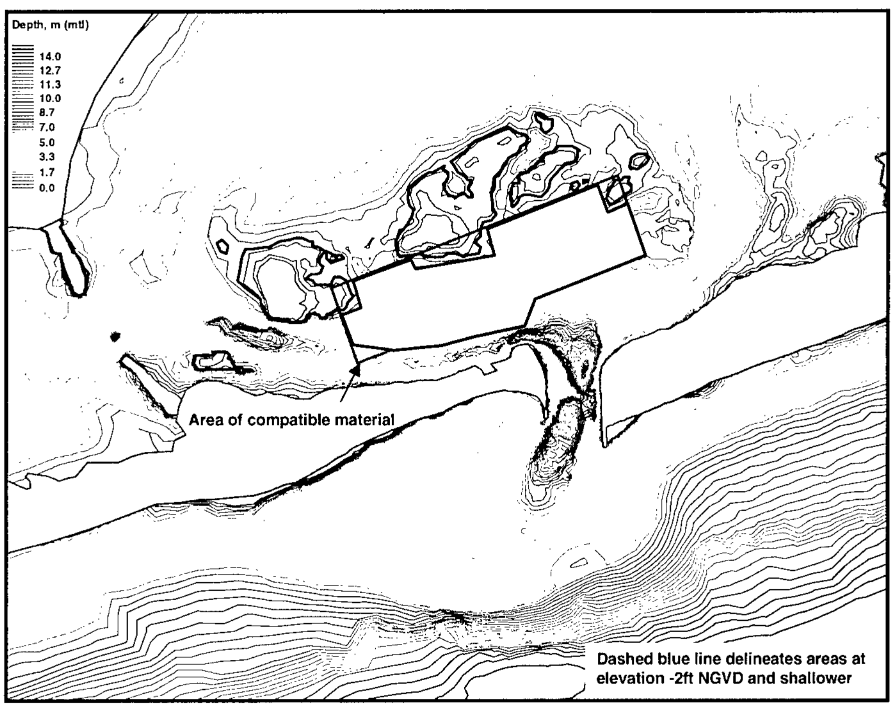

Figure 8. Alternatives 1, 2, and 3: Dredge area of compatible material

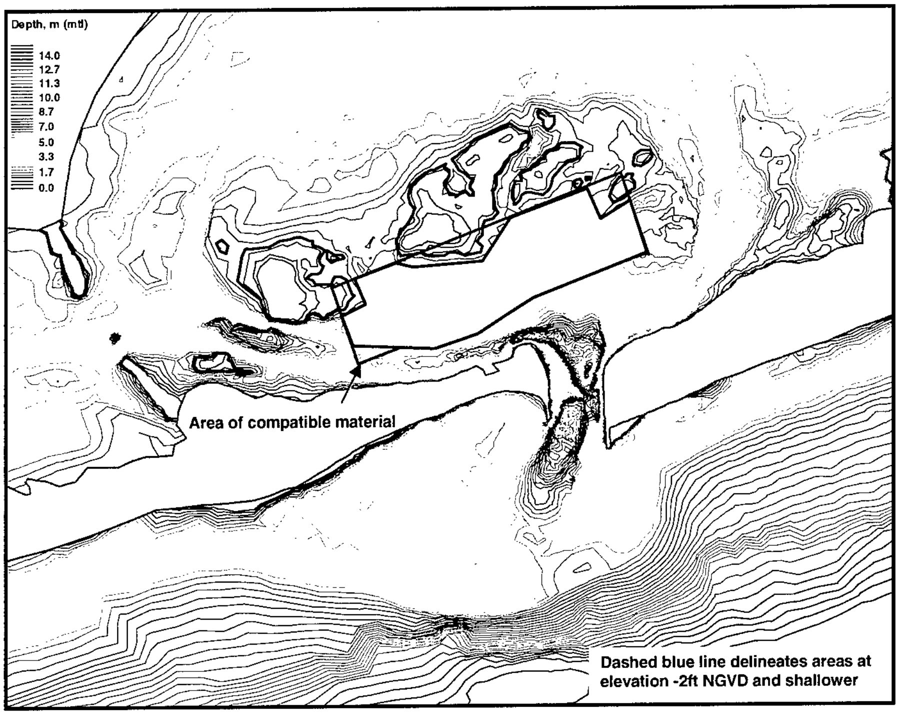

Figure 9. Alternative 4: Dredge area of compatible material following contours

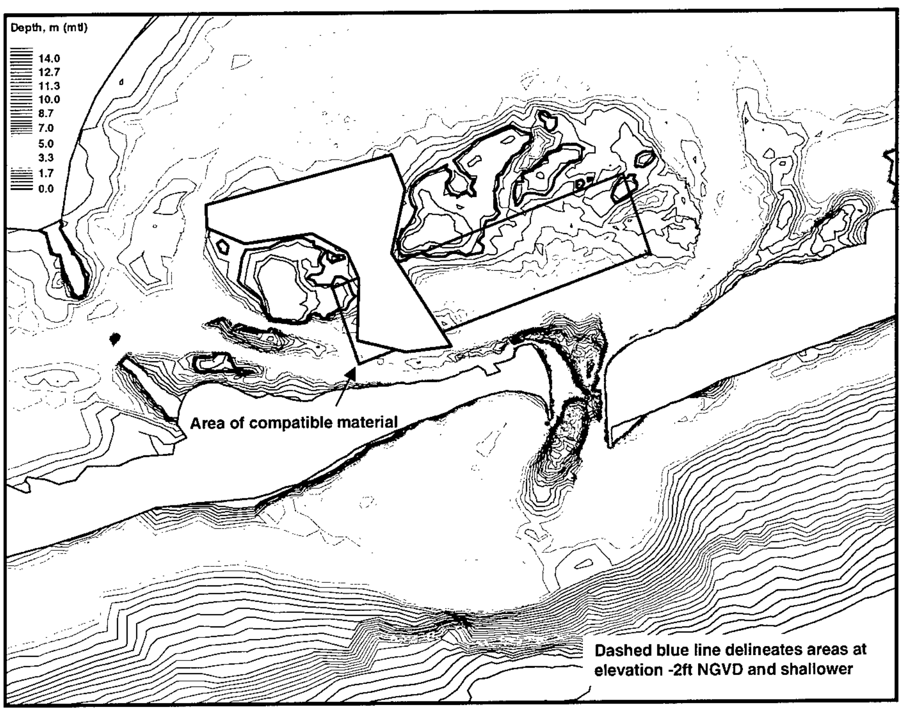

Figure 10. Alternative 5: Dredge western portion of flood shoal

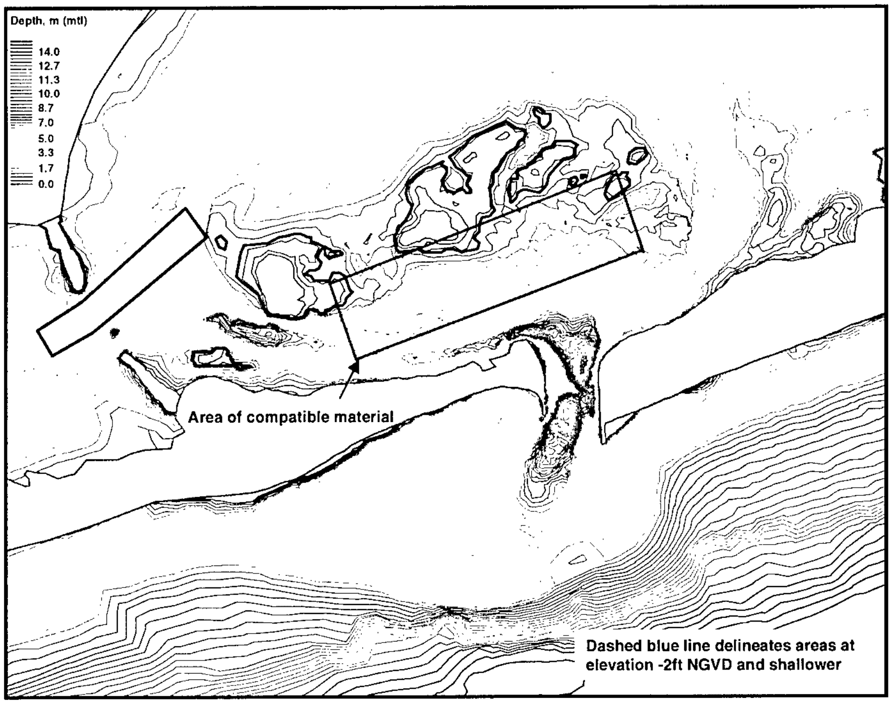

Figure 11. Alternative 6: Dredge a channel northeast from Ponquogue Bridge

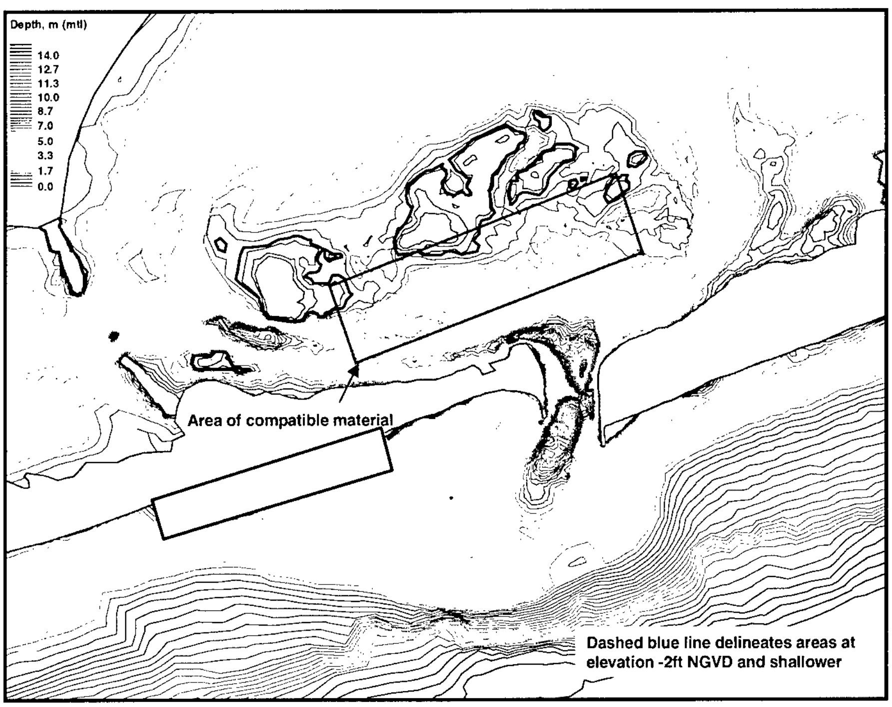

Figure 12. Alternative 7: Dredge Ponquogue attachment bar

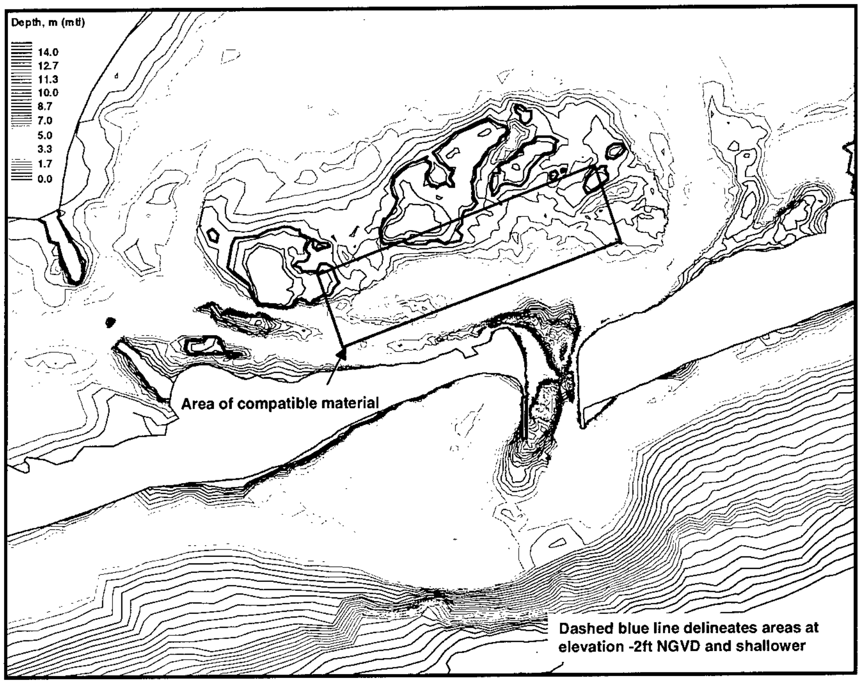

Figure 13. Alternative 8: Lengthen west jetty: (8a) No dredging, (8b) Dredge area of compatible material

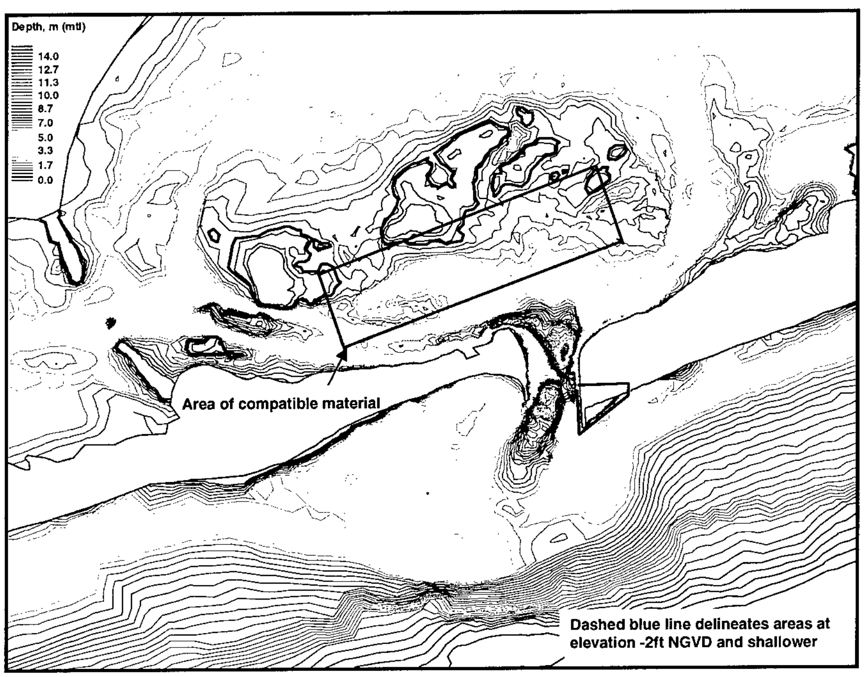

Figure 14. Alternative 9: Shorten east jetty: (9a) No dredging, (9b) Dredge area of compatible material

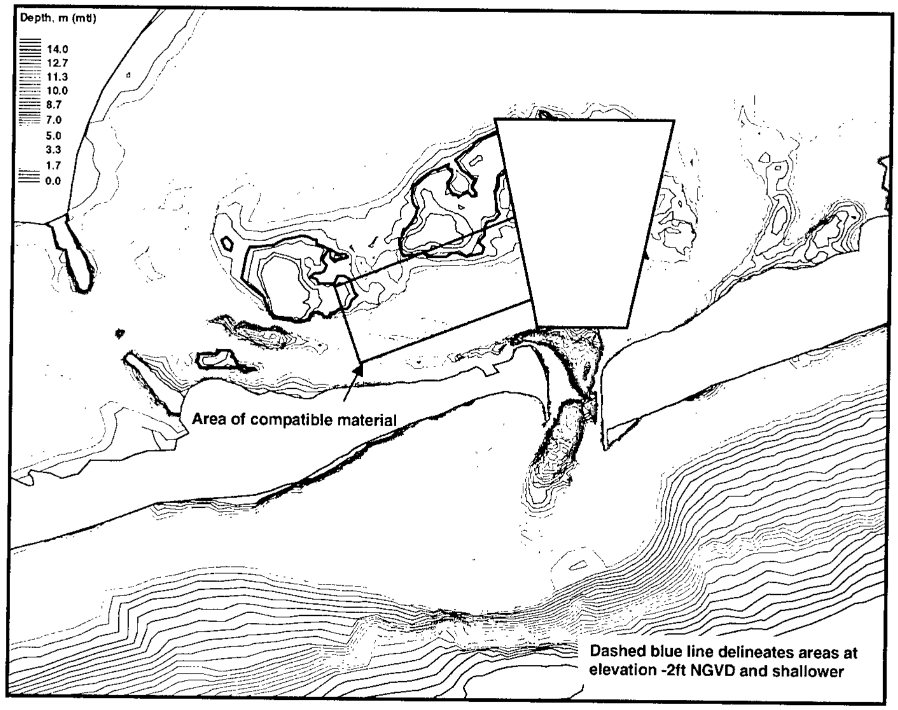

Figure 15. Alternative 10: Dredge wedge-shaped channel in flood shoal

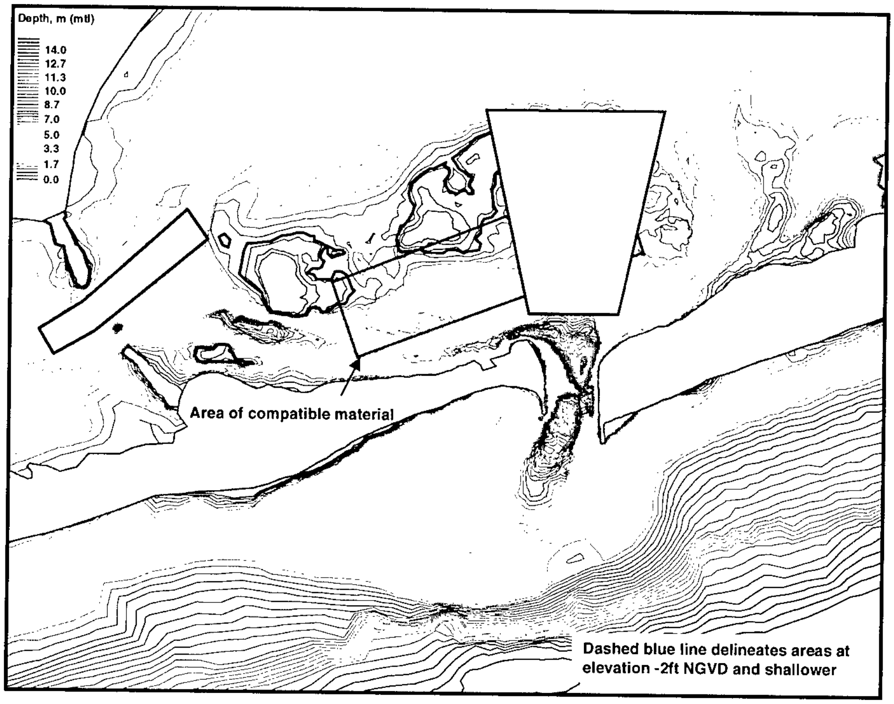

Figure 16. Alternative 11: Dredge wedge-shaped channel in flood shoal and channel northeast from Ponquogue Bridge

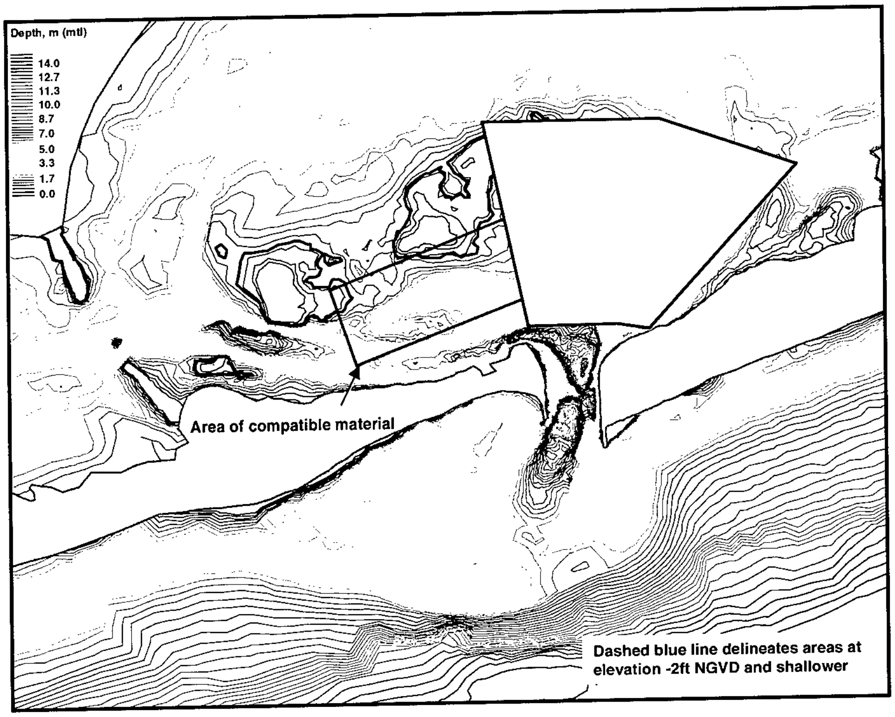

Figure 17. Alternative 12: Dredge extended wedge-shaped channel in flood shoal

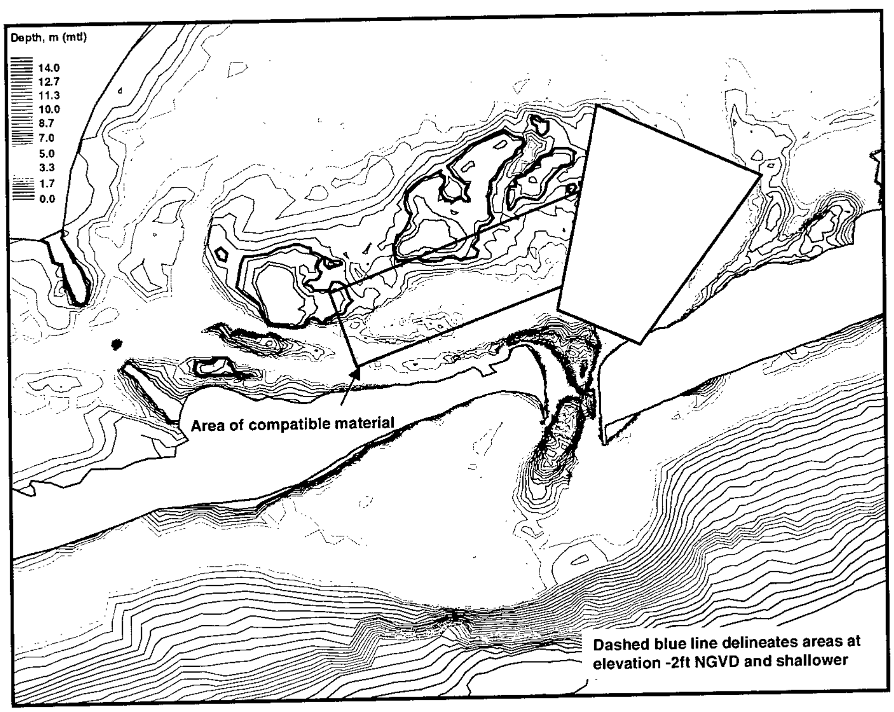

Figure 18. Alternative 13: Dredge a rotated wedge-shaped channel in flood shoal

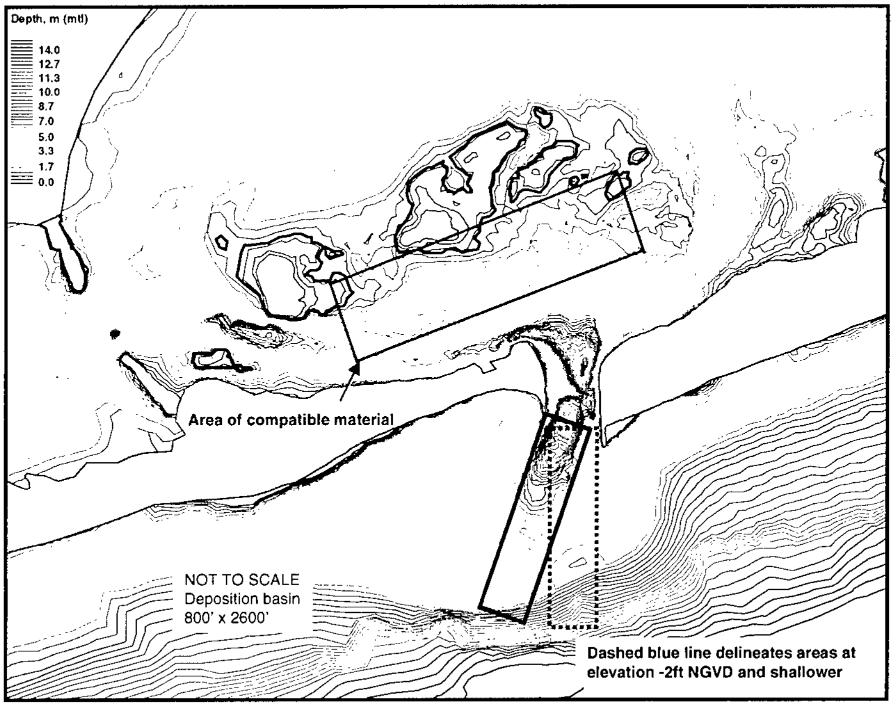

Figure 19. Alternative 14: Relocate deposition basin over channel thalweg

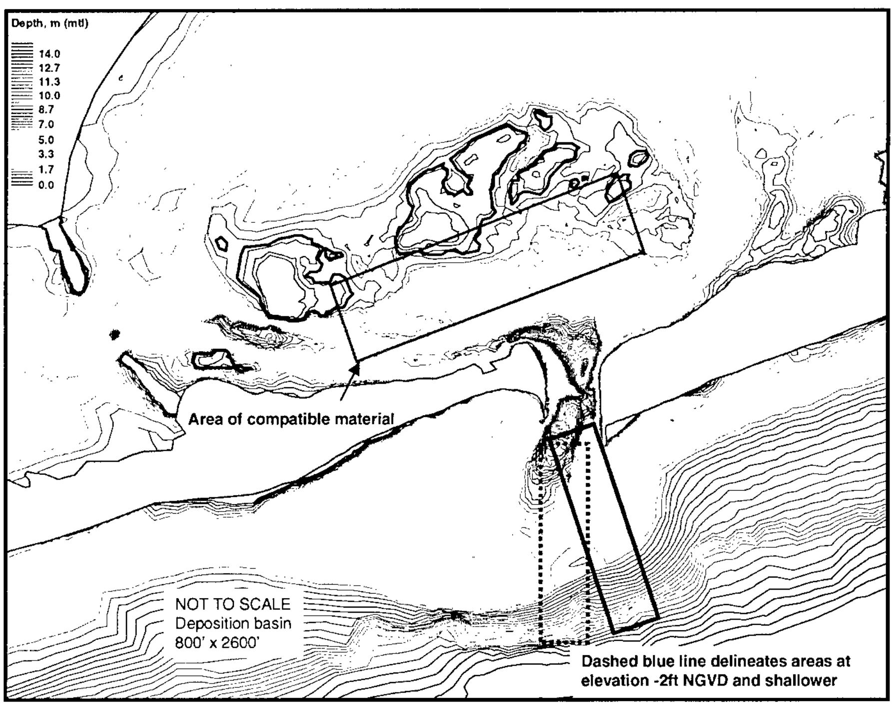

Figure 20. Alternative 15: Relocate deposition basin with orientation toward the southeast

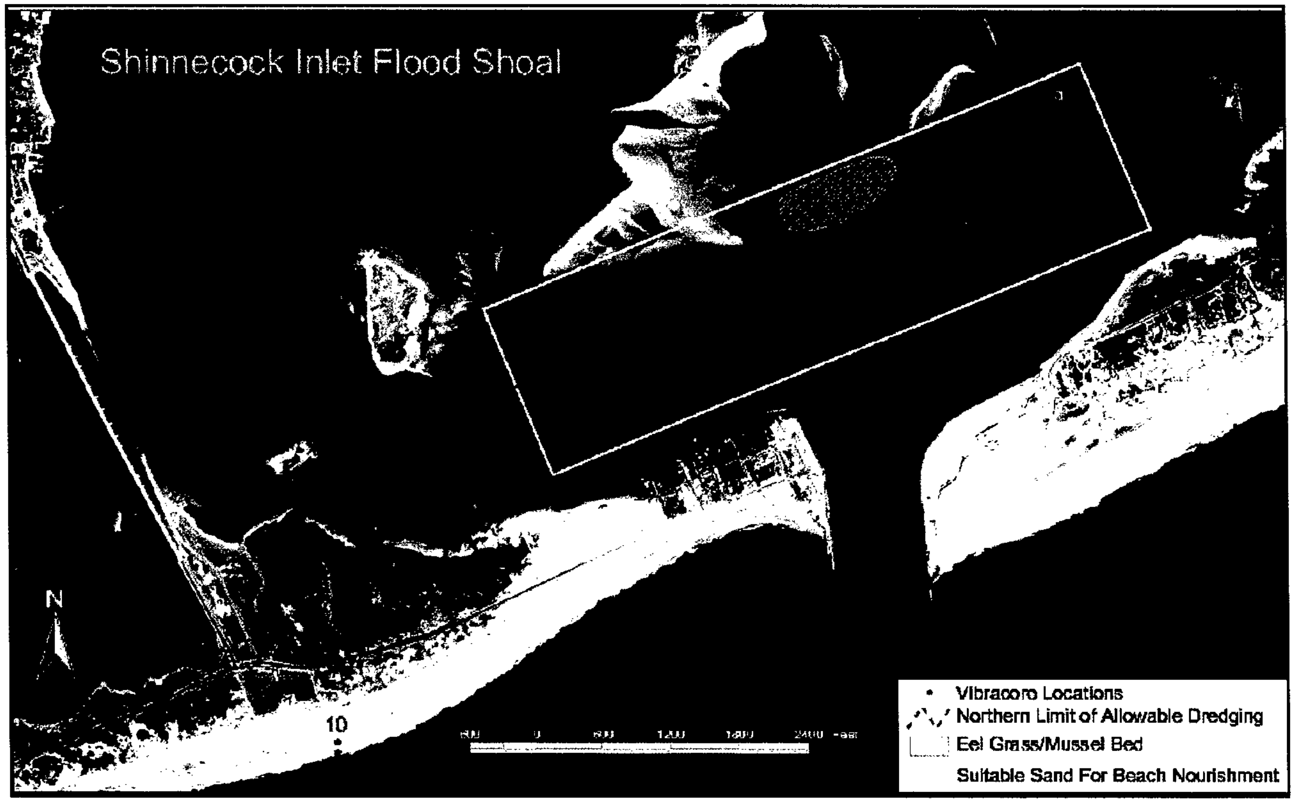

Figure 21. Area of compatible material showing northern limit of allowable dredging as requested by the Southampton Town Trustees

3 Hydrodynamic Data

Williams, Morang, and Lillycrop (1998) and Morang (1999) document the geomorphology and coastal processes at Shinnecock Inlet and thoroughly review the literature. These reports examined inlet formation, beach erosion and accretion, growth of the flood and ebb shoals, channel migration, and sand bypassing. Substantial background material is contained in the references, including historical aerial photographs.

Under the sponsorship of the New York District, DEC, and the CIRP, extensive measurements of water level, current, waves, and wind were made at Shinnecock Inlet, beginning in April 1998. A portion of that data set of relevance to this study is discussed below and in other chapters of this report. The data enabled application and verification of a numerical model of the tidal circulation for Shinnecock Inlet that is part of a regional model of Long Island. The model and results are described in Chapter 4.

This chapter reviews historic and recently-collected hydrodynamic data for Shinnecock Inlet. Changes in the inlet and bay are noted, and these results enter the engineering morphologic analysis for the flood shoal presented in Chapter 5.

Water Level

Czerniak (1977) discusses and provides a plot of bay tide range for the time interval 1940 to 1976 for Moriches Bay and from 1938 to 1956 for Shinnecock Bay. His paper also discusses cross-sectional area of the inlets in relation to tidal range. In the 1970s and up to 1990, at different times the National Ocean Service (NOS) operated three water-level gauges in Shinnecock Bay and in the Atlantic Ocean near Shinnecock Inlet. The locations of these relatively short-term historic NOS gauges are shown in Figure 22. Instruments were deployed for a minimum of 1 year for calculation of tidal datums. It is noted that the gauge termed Shinnecock Bay was located in the western arm of the bay, and the Ponquogue Point gauge was located at the western end of the eastern arm of the bay.

Table 4 lists published tidal datums and deployment dates for the three NOS gauges. The mean range of tide (M_n) is the difference between mhw and mlw. For the Shinnecock Inlet (outside west jetty), Ponquogue Point, and Shinnecock Bay gauges, M_n = 3.31 ft (1.01 m), 2.82 ft (0.86 m), and 2.43 ft (0.74 m),

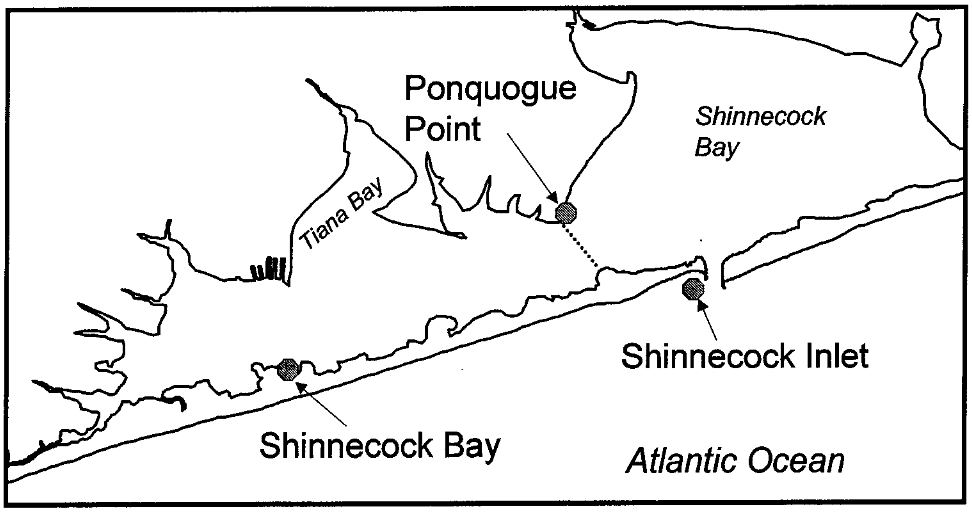

Figure 22. Locations of historic NOS water-level gauges

Table 4
Tidal Datums (ft) for Shinnecock Tide Gauges (NOS 1987, 1991)

Datum[1]	Shinnecock Bay[2]	Ponquogue Point[3]	Shinnecock Inlet[4]
Highest observed water level	5.75 (01/25/79)	4.91 (10/19/89)	7.17 (12/25/78)
mhhw	2.81	3.20	3.78
mhw	2.54	2.94	3.49
mtl	1.32	1.53	1.83
mlw	0.10	0.13	0.16
mllw	0.00	0.00	0.00
Lowest observed water level	-1.66 (04/19/76)	-1.56 (11/12/90)	-1.67 (03/28/1979)

[1] Note: mhhw = mean higher high water, mhw = mean high water, mtl = mean tide level, mlw = mean low water, mllw = mean lower low water
[2] Data collected from 09/77 through 04/79
[3] Data collected from 07/89 through 06/90
[4] Data collected from 06/78 through 05/79

respectively. The decrease in mean range of tide indicates damping of the tidal wave as it propagates through the inlet and into the bay. Between the inlet and bay gauges, the mean range of tide decreases 0.89 ft (0.27 m). The data at these three gauges were not collected simultaneously, but the general relationship among ranges of tide is expected to hold quantitatively because the inlet was not substantially modified over the measurement interval. The inlet was modified after 1990 through rehabilitation of the jetties and dredging of the deposition basin, and these modifications are expected to change the efficiency of exchange of water in the bay, hence the tidal datums.

Monitoring of water level, current, waves, wind, and atmospheric pressure at Shinnecock Inlet and Bay has been ongoing since April 1998. From April 1999 until November 1999, the monitoring system was in place much as shown in Figure 23. In this figure, the symbol "C" with a number attached indicates a current meter; the symbol "P" with a number attached indicates a pressure gauge that records water level; and "M" denotes the meteorology station. Water-level measurements were corrected for atmospheric pressure by applying the barometric pressure from the meteorology station. The gauges denoted by "ADV" with a number denote combined measurements of the dynamic water pressure and the current, yielding the directional wave spectrum.

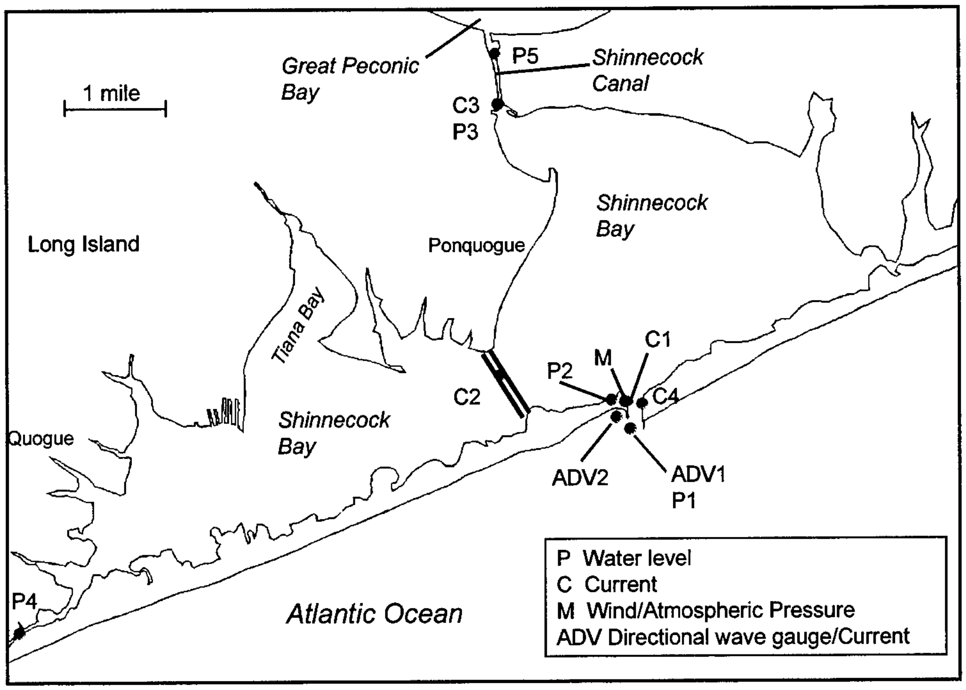

Figure 23. Shinnecock Inlet and Bay monitoring plan

Approximate tidal datums for Stations P1, P2, P3, and P4 were calculated from water-level measurements taken from April to June 1998, and are given in Table 5. Although these datums were computed over a 3-month interval, rather than 1 or more years, they are expected to be approximately correct.[1] The differences in tidal datums between the November 1998 data and the historic (1991 and earlier) data are listed in Table 6. Experience in measurement of water level indicates that an uncertainty of ±0.05 ft should be assigned, meaning that differences within this range should be considered as showing no change.

Inspection of Table 6 shows that the ocean tidal datums showed no change. In contrast, for the same time interval, mhhw and mhw increased 0.016 and

[1] The tidal datums will be computed for a 1-year record in the future to eliminate a seasonal bias.

Table 5 Tidal Datums (ft) for Shinnecock Tide Gauges for April – June 1998				
Datum	**Ocean Gauge P1**	**Town Dock P2**	**Shinnecock Canal P3**	**Quogue Canal P4**
mhhw	3.76	3.36	3.21	2.94
mhw	3.53	3.13	2.97	2.72
mlw	0.12	0.10	0.09	0.08
mllw	0.00	0.00	0.00	0.00

Table 6 Difference in Tidal Datums (ft), NOS 1987 and 1991 vs. 1998[1]			
Datum	**Shinnecock Inlet vs. Ocean**	**Ponquogue Point vs. Town Dock**	**Shinnecock Bay vs. Quogue Canal[2]**
mhhw	-0.02	0.16	0.13
mhw	0.04	0.19	0.18
mlw	-0.04	-0.03	-0.02
mllw (locally defined)	0.00	0.00	0.00

[1] Differences are calculated by 1998 water-level datum minus 1991 and earlier water-level datum
[2] Quogue Canal station is expected to have smaller tidal range than the Shinnecock Bay station because of attenuation of the tide within the Quogue Canal

0.19 ft, respectively, in the eastern arm of the bay, and mhhw and mhw increased 0.13 ft and 0.18 ft, respectively, in the western arm of the bay, while mlw showed no significant change. If the increase in tide range in the bay is correct, then it is an indication that the inlet entrance channel is becoming more efficient, which is consistent with recent (post 1990) dredging. It should be noted that local residents have anecdotally remarked that the tide range seems to be increasing in Shinnecock Bay – for example, residents have noted an apparent rise in reach of the water level at docks.

Current

From December 1999 until the present, only gauges ADV1, ADV2 (removed in May 2000), C4, and P2 have been in place to document changes as might occur owing to future engineering activities. These gauges form part of a regional monitoring network being established for the south shore of Long Island. The current meter C4 is a side-looking current profiler (Acoustic-Doppler Profiler or ADP) set to record the horizontal current in 4-m bins. This gauge is mounted on the east jetty at middepth (approximately 10 ft below mtl); depending on tidal stage, the current meter can reach as far as 160 m across the inlet.

Inlets and bays are often described as either "flood dominated" or "ebb dominated." These terms define properties of the water elevation or velocity curves with respect to the tide. If the water elevation or current has a greater peak value on the flood cycle, the water body is considered to be flood dominated. If the peak is greater on the ebb cycle, then the water body is ebb dominated. For water elevation, peak values are the greatest deviation from the still-water level, taken here as mtl. This deviation corresponds to the greatest water level at high tide and lowest water level at low tide. A typical pattern of flood (ebb) dominance has a greater peak flood (ebb) water level and current speed, and a longer ebb (flood) duration.

To determine the magnitude and dominance of the current through the inlet entrance, the data from Gauge C4 were spatially averaged to obtain net velocity over the bin range extending to 152 m (500 ft) from the east jetty. This range covered 66 percent of the inlet width, including the eastern portion of the inlet where the channel thalweg is located. Figure 24 shows the time-history of the bin-averaged current for the interval YD 317 through 344 (13 November through 10 December 1998). Flood and ebb currents are denoted as positive and negative values, respectively. Peak flood speed exceeds peak ebb speed over the 28-day lunar interval. This bias indicates that Shinnecock Inlet is flood dominated. The pattern of stronger peak flood current is present throughout the time-history of all measurements of the current made in the inlet during the monitoring effort. Although Figure 24 shows values of about 1.5 m/s for the peak flood current and about 1.25 m/s for peak ebb, inspection of the full data record indicates that the flood current can exceed 2 m/s, with maximum ebb currents about 0.2 m/s less.

Figure 25 shows the bin-averaged current in the inlet for the 2-day interval 3 to 4 December 1998 (Year Days 337 to 339) to more clearly observe the flood bias in the velocity through the inlet. The bias in the asymmetric velocity curve gives the appearance that more water flows into Shinnecock Bay than flows out of it. However, the tidal variation in water level is not in phase with the current. While the current is flooding into the inlet, the water level is usually lower than during the ebbing current. This lower water level and greater flooding current balance the higher water level and weaker ebbing current to give a near-zero discharge through the inlet. Therefore, bias in a velocity measurement does not necessarily indicate a bias in the discharge. In fact, the next chapter will demonstrate that there is a small bias toward ebb discharge because of the contribution from the Shinnecock Canal. In addition, possible bias in measurement of the current can be introduced through the location of the sampling volume, because the flood and the ebb tidal current often have different patterns (favored channels).

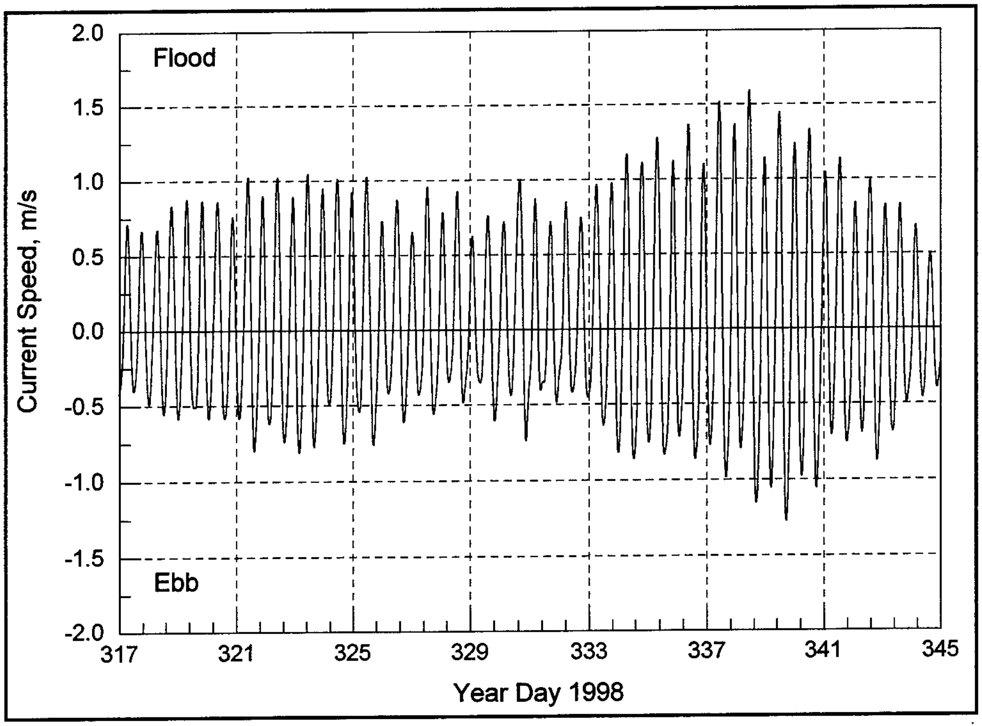

Figure 24. Bin-averaged current speed in Shinnecock Inlet, 13 November through 10 December 1998

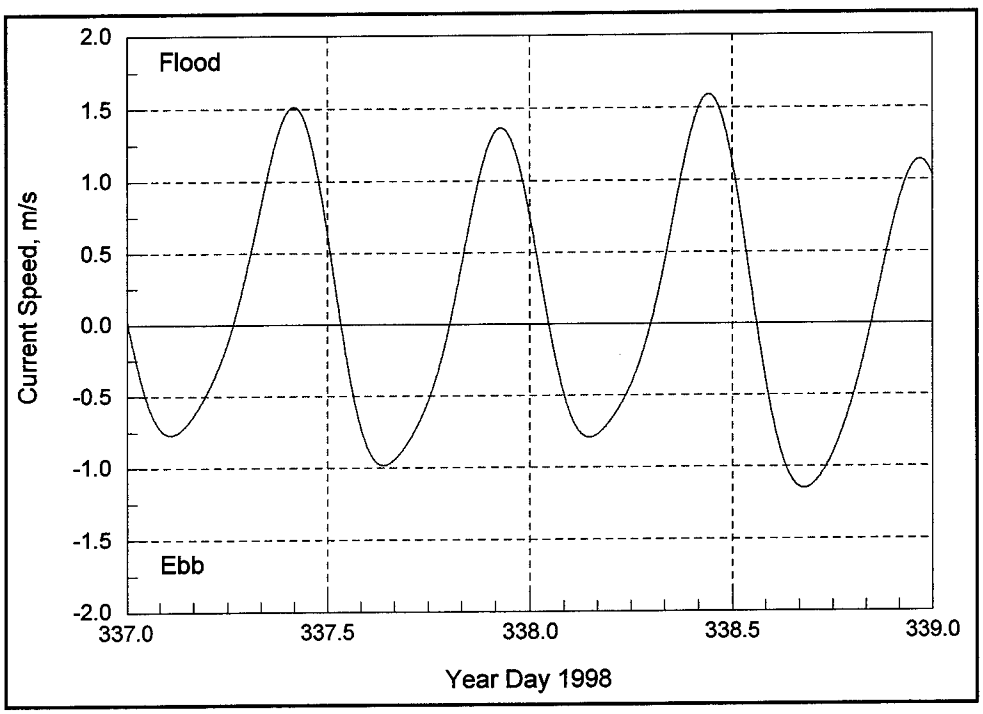

Figure 25. Bin-averaged current speed in Shinnecock Inlet, 3 - 4 December 1998

Discharge and Tidal Prism

The tidal current in Shinnecock Inlet was surveyed in 1997, 1998, and 1999 (Pratt and Stauble 2000). The velocity and discharge were measured along cross-inlet and other transects with an Acoustic Doppler Current Profiler. The discharge is computed by multiplying the average discharge in each bin by the bin area, then summing the bin discharges vertically over the water column then horizontally across the transect. Time series of measured discharge are shown in Figure 26 for 4 December 1997 and 22 July 1998. Flood and ebb discharges are denoted as positive and negative values, respectively. Peak flood discharge is greater than peak ebb discharge for both measurement intervals, consistent with other observations of a flood-dominated system.

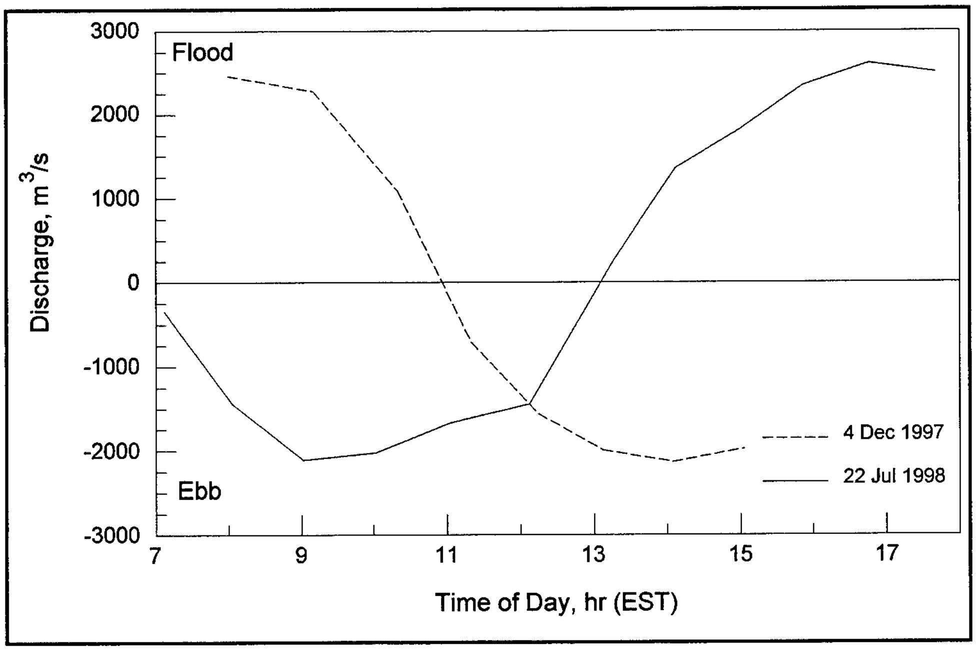

Figure 26. Measured discharge in Shinnecock Inlet, 4 December 1997 and 22 July 1998

The tidal prism is the volume of water exchanged over a tidal cycle (the volume that both enters and exits the bay). Main factors that control the tidal prism are the ocean tide range, inlet cross-sectional area, length of the inlet, and bay area. From a simplified perspective, the tidal prism is the thickness of water between mtl and either mlw or mhw times the bay surface area, assuming the bay empties or fills fully over the flood and ebb half tidal cycles, respectively. Empirical formulas have been developed relating certain properties of inlet morphology to the tidal prism, which can be estimated from the bay surface area and spring or diurnal tidal range. In contrast, modern instrumentation as well as older measurement procedures yield the discharge through the entrance.

If it is assumed that the discharge is solely related to the tidal prism, then the tidal prism can be calculated by knowledge of the discharge and an assumption of the form of the tidal curve for half the tidal cycle. This procedure assumes that no strong river or wind-induced flows occurred during measurement of the discharge. The simplest assumption is to represent the tidal current (discharge) as a single sinusoid, in this case the M_2 component of the tide. Keulegan and Hall (1950) refined this procedure in specifying a sinusoidal discharge so that the tidal prism *P* or volume of water ebbing in half a tidal period *T* is

$$P = \int_{0}^{T/2} D_m \sin\left(\frac{2\pi}{T}t\right)dt \qquad (1)$$

where D_m is the peak or maximum discharge. They introduced a coefficient C_K such that $0.81 \leq C_K \leq 1$ (based upon further analysis and comparison to data) to account for a more realistic non-sinusoidal tide, giving,

$$P = \frac{T}{\pi C_k} D_m \qquad (2)$$

In the present study, we take $C_K = 1$.

Surveys at Shinnecock Inlet conducted since 1940 indicate that both the tidal prism and inlet cross-sectional area have increased over time (Table 7). During the interval from 1940 to 1976, the tidal prism was between 2×10^8 and 4×10^8 ft^3. By 1993, the tidal prism had doubled its 1976 value. As of 1994, the prism was five times greater than it was in 1976. The inlet cross-sectional area began to increase between 1976 and 1984. Since 1990, the cross-sectional area has remained at approximately 1.7×10^4 ft^2. The increase in tidal prism at Shinnecock Bay is related to the increase in inlet cross-sectional area (and, therefore, the current velocity) because the bay surface area and ocean tide range have and are expected to have remained the same.

The apparent increased hydraulic efficiency of the inlet is expected to increase the tide range in the bay. Increase in the cross-sectional area of the inlet owes to scour of the bottom by the current. Further increase in current speed would promote additional scour and potentially increase the tidal prism from its present volume until an equilibrium current velocity was reached corresponding to the new equilibrium cross section of the inlet (see Chapter 5 for further discussion). This situation is to be avoided for stability of the inlet and safe navigation. As part of the evaluation of alternatives for the present study, change in current speed and discharge are investigated through analysis of circulation model calculations. Increased current speed or discharge over that calculated for the existing condition for an alternative, if significant, is evaluated as a negative outcome of that alternative. Decreased current speed or discharge is evaluated as a positive outcome.

Table 7
Tidal Prism and Minimum Inlet Cross-Sectional Area (Augmented Data from Morang 1999)

Survey Date	Prism, m^3	Prism, ft^3	Area, m^2	Area, ft^2
Sep 1940	1.06×10^7	3.75×10^8	–	–
1941	9.30×10^6	3.29×10^8	–	–
Jul-Aug 1949	–	–	5.11×10^2	5.50×10^3
Nov 1955	–	–	3.58×10^2	3.85×10^3
1976[1]	6.20×10^6	2.19×10^8	5.11×10^2	5.50×10^3
11 June 1984	–	–	1.51×10^3	1.63×10^4
Jul 1986	–	–	1.40×10^3	1.51×10^4
Jun 1987	–	–	1.49×10^3	1.60×10^4
Nov 1989	–	–	1.51×10^3	1.63×10^4
9 Aug 1990	–	–	1.61×10^3	1.73×10^4
Dec 1990	–	–	1.51×10^3	1.63×10^4
Aug 1991	–	–	1.64×10^3	1.76×10^4
21 Dec 1992	–	–	1.52×10^3	1.64×10^4
21-23 Jul 1993	2.43×10^7	8.59×10^8	–	–
15 Sep 1993	3.86×10^7	1.36×10^9	–	–
1 Dec 1993	–	–	1.57×10^3	1.69×10^4
3 Aug 1994	–	–	1.54×10^3	1.67×10^4
20-21 Jul 1994	3.32×10^7	1.17×10^9	–	–
8 Sep 1995	–	–	1.53×10^3	1.65×10^4
5 Oct 1995	–	–	1.56×10^3	1.68×10^4
4-6 Mar 1998	–	–	1.54×10^3	1.66×10^4
22 Jul 1998	3.29×10^7	1.16×10^9	–	–

[1] The values in this row are found in Jarrett (1976) and were computed from values of tide range and bay area representative of the 1950s.

4 Circulation and Wave Modeling

The CIRP has designated Shinnecock Inlet as a target site for study and analysis of fundamental inlet processes and their bearing on engineering activities. Through this effort, circulation and wave models were developed and calibrated for the Shinnecock area, and these models were applied in the present study. This chapter describes of the circulation and wave models together with their implementation at Shinnecock Inlet, followed by discussion and interpretation of calculations from the models.

Circulation Modeling

Water-surface elevation and current were calculated by the hydrodynamic model ADvanced CIRCulation (ADCIRC) (Luettich, Westerink, and Scheffner 1992). ADCIRC is a two-dimensional, depth-integrated, finite-element hydrodynamic model developed with the capability of operating over a wide range of element sizes. The finite-element formulation has the advantage of flexibility in resolution over the calculation domain. Coarse resolution can be specified in areas distant from the region of interest, and fine resolution can be specified locally to meet project requirements. In particular, channels and coastal structures can be defined for accurate calculation of flow through and around them.

Specifications for simulations of hydrodynamics at the Shinnecock study area include forcing with tidal constituents, wetting and drying, calculation of nonlinear continuity and advection, and quadratic bottom stress. Open-ocean boundaries were forced by tidal constituents obtained from the Le Provost et al. (1994) database. ADCIRC has robust wetting and drying algorithms to simulate the inundation and exposure of shallow areas such as the flood shoal.

ADCIRC mesh development

Modeling of the Shinnecock study area was conducted within a regional model of the New York Bight and Long Island Sound. The regional model was designed to simulate large-scale processes that contribute to smaller-scale water motion, such as that in the nearshore zone and at inlets. Fine detail was specified in the mesh for the Shinnecock study area for resolution of channels, jetties, and shoals.

Data for mesh development were obtained from several sources. Digitized shoreline coordinates were obtained from the National Oceanic and Atmospheric Administration (NOAA) Medium Resolution Digital Vector Shoreline Database (http://seaserver.nos.noaa.gov/projects/shoreline/shoreline.html). This database contains shoreline locations digitized from NOAA charts. Sources of bathymetric data and the regions where the data were applied are given in Table 8. Dense bathymetry data were collected in 1998 by the Scanning Hydrographic Operational Airborne Lidar System (SHOALS) (Lillycrop, Parson, and Irish 1996) and by traditional boat survey. Together these data covered all of Shinnecock Inlet and Shinnecock Bay, as well as the ebb shoal and nearshore areas east and west of the inlet. All bottom elevations were referenced to mtl in the mesh.

Table 8
Sources of Bathymetric Data and Regions of Application

Data Source	Region of Application
NOAA	Open ocean
GEODAS[1]	Long Island Sound, all bays on South Shore of Long Island with the exception of Shinnecock Bay
Traditional Survey[2]	Shinnecock Bay, except for flood shoal
SHOALS Survey[3]	Shinnecock Inlet, Shinnecock Bay flood shoal, nearshore area of Shinnecock study area, Moriches Inlet
USACE Traditional Survey[4]	Shinnecock Inlet, Jones Inlet

[1] GEOphysical Data System developed by the National Geophysical Data Center. http://www.ngdc.noaa.gov/mgg/geodas/geodas.html
[2] Traditional boat survey conducted in 1998 by State University of New York at Stony Brook
[3] Shinnecock survey conducted in 1998; Moriches survey conducted in 1996
[4] Traditional boat survey data at Shinnecock Inlet supplemented SHOALS data

The regional mesh, shown in Figure 27, has coarse resolution over the open ocean with increasing resolution toward the shore. Highest resolution is within Shinnecock Inlet and minimum node spacing is approximately 40 ft (13 m). Details of the mesh for Shinnecock Bay, the flood shoal, and Shinnecock Inlet are shown in Figures 28 through 30. The number of nodes and elements contained in the regional mesh are 30,296 and 55,553, respectively. Element areas vary greatly over the computational domain with the ratio of the largest to smallest being 8.2×10^6.

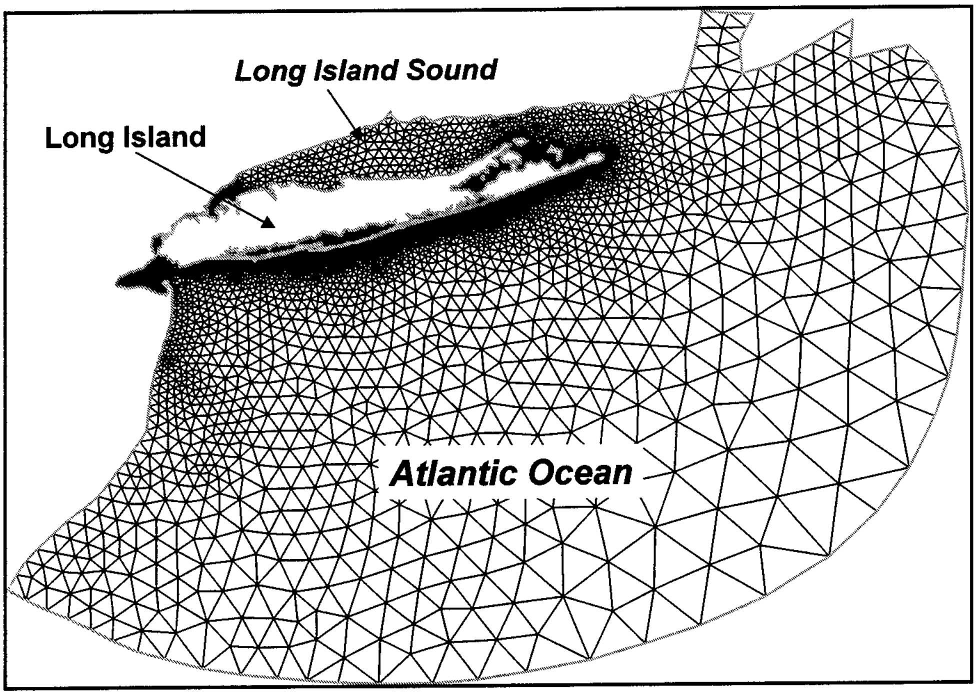

Figure 27. Regional ADCIRC mesh covering New York Bight, south shore of Long Island, and Long Island Sound

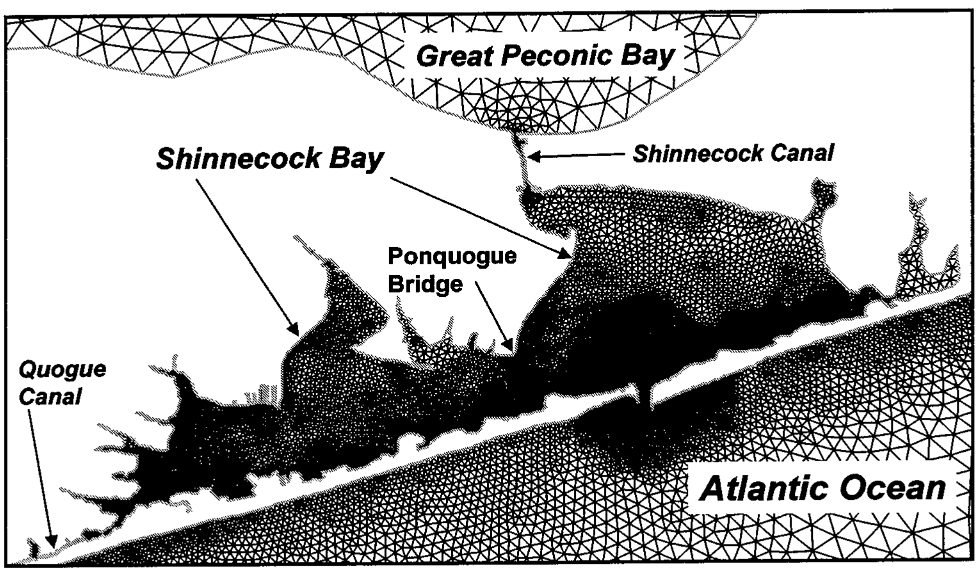

Figure 28. ADCIRC mesh at Shinnecock Bay

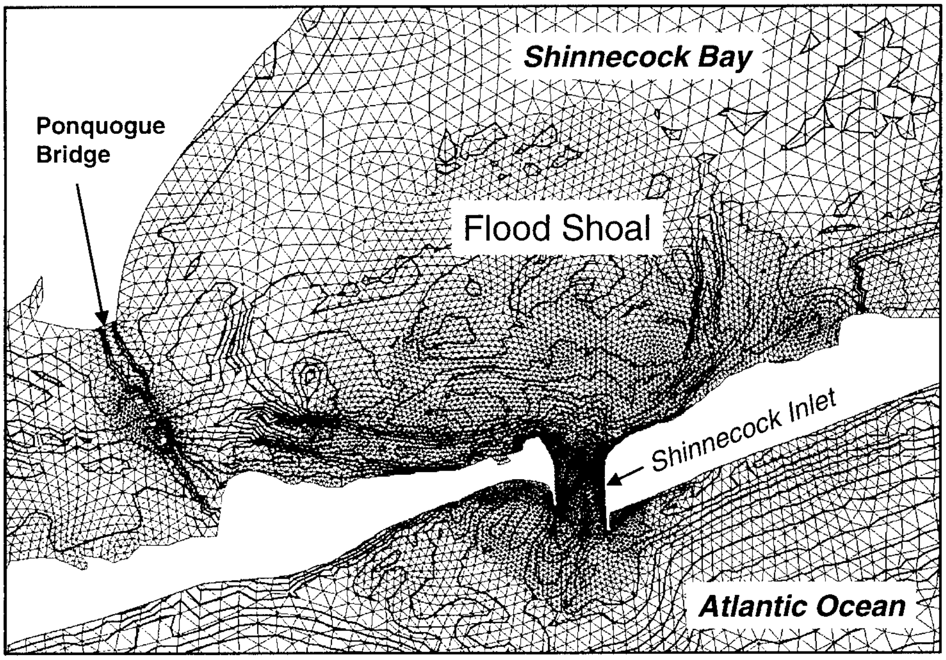

Figure 29. ADCIRC mesh for Shinnecock Bay flood shoal and inlet

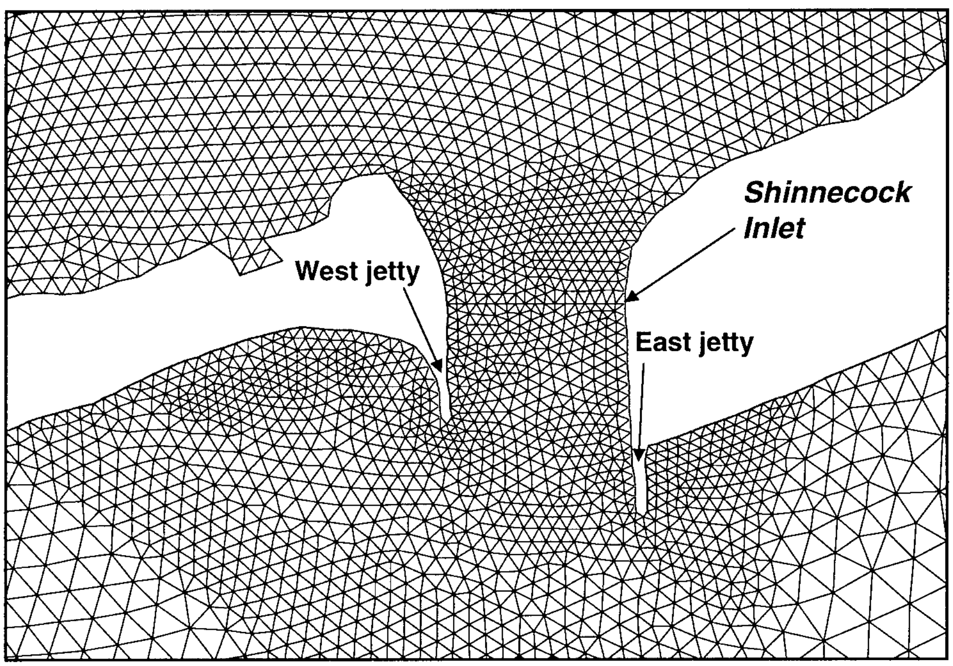

Figure 30. ADCIRC mesh at Shinnecock Inlet

Shinnecock Canal gate

The Shinnecock Canal is an artificially cut and maintained conveyance channel that allows water to flow from Great Peconic Bay to Shinnecock Bay. A gate prohibits water from flowing in the opposite direction. Gate opening and

closing is dictated by the difference in water levels between Great Peconic Bay and Shinnecock Bay. Because the tidal phase is different between the two bays, high tide and low tide occur at different times on each end of the canal. Figure 31 shows water levels measured at each end of the Shinnecock Canal in Great Peconic Bay (Gauge P5) and in Shinnecock Bay (Gauge P3) (refer to Figure 23 for gauge locations). High and low tide stages in Shinnecock Bay occur during the rising and falling tides, respectively, in Great Peconic Bay. Conversely, high and low tide stages in Great Peconic Bay occur during the falling and rising tides, respectively, in Shinnecock Bay.

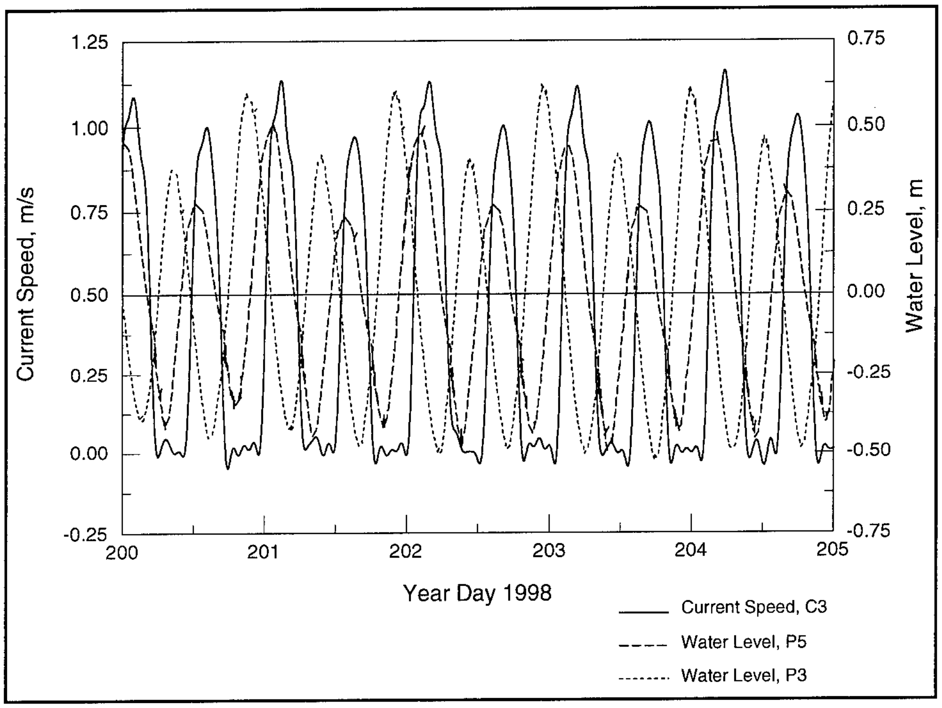

Figure 31. Water level and current speed at Shinnecock Canal

Analysis of the water-level data collected at each end of the Shinnecock Canal (Gauges P3 and P5) revealed that the difference in water level between the two bays is not constant for each opening and closing of the gate, but varies in time depending on the relative tidal elevation. Representative values of water-level difference (water level at P5 minus water level at P3) are 30 cm and -5 cm for gate opening and closing, respectively. These representative values were determined from the 150-day record when Gauges P3, P5, and C3 were deployed. Figure 31 shows representative time series of measured water level and current at the Shinnecock Canal. Data of current speed was low-pass filtered with a cutoff frequency of 10 cycles per day to eliminate high-frequency oscillations (probably resonance within the canal) present in the signal. Intervals when the gate was open and closed can be discerned from the current speed. The gate was open when the current speed rose and fell; the gate was closed when the speed stayed near zero. Figure 31 shows that gate openings occurred when the

water level in Great Peconic Bay (P5) was higher than in Shinnecock Bay (P3). Gate closings occurred when the water levels in the two bays were nearly equal.

To simulate the timing and one-way flow through the Shinnecock Canal, an internal gate boundary condition was implemented within ADCIRC. The numerical gate opens and closes based on the difference in water level between Great Peconic Bay and Shinnecock Bay. Nodes for the water-level difference calculation are located at each end of the canal. When the gate is closed, it will open if the water level in Great Peconic Bay is 30 cm or greater than in Shinnecock Bay. Once the gate is open, water flows through the canal until the water level in Shinnecock Bay is 5 cm higher than in Great Peconic Bay. Once the water level in Shinnecock Bay becomes 5 cm higher than in Great Peconic Bay, the gate is closed. The internal boundary condition simulates opening and closing of the gate by forcing elements in the Shinnecock Canal to wet and dry, respectively. The elements that wet and dry are located in the same position as the gate. When those elements are dry, the flow through the canal is blocked, representing a closed gate. When the elements are wet, they allow full flow through the canal.

Ponquogue Bridge

The Ponquogue Bridge is located directly west of the flood shoal (Figures 6 and 28) and plays a role in determining the current pattern and speed. The bridge spans the bay between the mainland at Ponquogue Point and the barrier island near the Ponquogue Pavilion. Directly east of the bridge, fishing piers have been constructed that extend from landfills built out from the shore. The piers and landfills reduce the width of the opening between the barrier island and the mainland. Bridges can significantly modify the tidal flow in shallow water bodies and must be accounted for in models (Militello and Zarillo 2000). Accurate simulation of the current in the western area of the flood shoal and the West Cut is dependent on representation of the bridge, piers, and landfills.

To describe the flow through and near the bridge, the ADCIRC mesh represented the bridge pilings as physical impediments to flow. Four numerical pilings were placed along the bridge reach. The numerical piling positions and shape were optimized for representation of actual flow conditions. In addition, accuracy of calculations was found to be improved by representation of the fishing piers and landfills associated with them. These structures increase the flow impedance in the vicinity of the Ponquogue Bridge.

Comparison of measured and calculated water level and current

Verification of the circulation model was conducted by comparison of water level and current measurements to calculations at monitoring stations located within the study area. Three error calculations were made to quantify the comparisons; the mean error, root-mean-square (rms) error, and percent error.

The mean error $\bar{E}$ is the arithmetic average of the difference between the calculated and measured value:

$$\bar{E} = \frac{\sum_{i=1}^{N}(\chi_c - \chi_m)}{N} \tag{3}$$

where χ_c is the calculated value of a variable χ, χ_m is the measured value of the variable, and N is the number of points. A positive value of the mean error indicates that on average the calculated values overpredict the measurements and a negative value indicates that the calculated values underpredict the measurements.

The rms error E_{rms} provides an absolute measure of error without regard to over- or underprediction. The rms error is given by

$$E_{rms} = \sqrt{\frac{\sum_{i=1}^{N}(\chi_c - \chi_m)^2}{N}} \tag{4}$$

Percent error E_{pct} is defined in terms of the rms error as

$$E_{pct} = 100\frac{E_{rms}}{R} \tag{5}$$

where R is a representative range of values for the variable χ. For percent error calculations of water level, the difference between mhhw and mllw at a specified NOS station within the study area is taken as R. Percent error values of less than 10 are considered acceptable.

Current speeds do not have datum-type parameters associated with them, making selection of an *R* value arbitrary. For this analysis, *R* was computed from flood and ebb current speed values contained in the measurements. The flood value was computed as the mean of maximum peak flood speed and minimum peak flood speed. The ebb value was computed in the same manner as the flood value but using values for ebb-directed current. A representative range *R* was taken as the sum of the absolute values of the flood and ebb speeds.

Because simulations were conducted with tidal forcing only, a time interval for verification and production runs was selected in which nontidal processes (such as wind) did not contribute significantly to the water level and current motion. To further eliminate nontidal motion, time series of water level and current measurements were high-pass filtered using a cutoff frequency of 0.5 cpd so that motion with 2-day or shorter period was retained. Eliminating longer-period motion from the measurements enhances comparison of calculated and measured tidal processes.

The time interval for verification was 4 November through 4 December 1998 (Year Days (YDs) 308 through 338). Comparisons of measured and calculated water level at P1 (Ocean), P2 (Town Dock), P3 (Shinnecock Canal South), and P4 (Quogue Canal) (see Figure 23 for instrument locations) are shown in Figures 32 through 35. Calculated water level is typically in agreement with measurements, although during some time intervals such as YDs 314 through 317, the tide range was overpredicted.

Table 9 lists error statistics for each of the four water-level gauges. All stations had percent error of 10 or less, with P1 and P3 having the closest agreement (6 percent error). The calculated tidal phase was in close agreement with the measurements, with typical error of 2 deg (4 min) for the M_2 constituent. Spectra of the calculated and measured water level at P4 indicated a phase difference of 20 deg (25 min, 0.42 hr) for the M_2 tidal constituent, where the calculated tide leads the measured tide. For computation of error in water elevation, the calculated water level at P4 was adjusted by 0.42 hr to coincide with measurements. The phase difference is attributed to limitations in accuracy and resolution of the bathymetry in Moriches Bay and parts of the Quogue Canal. Because the Quogue Canal connects Moriches and Shinnecock Bays, tidal motion within the canal is propagated through it from each end. Therefore, there may be a small discrepancy in flow through the Quogue Canal, in which Station P4 is located, between calculations and measurements.

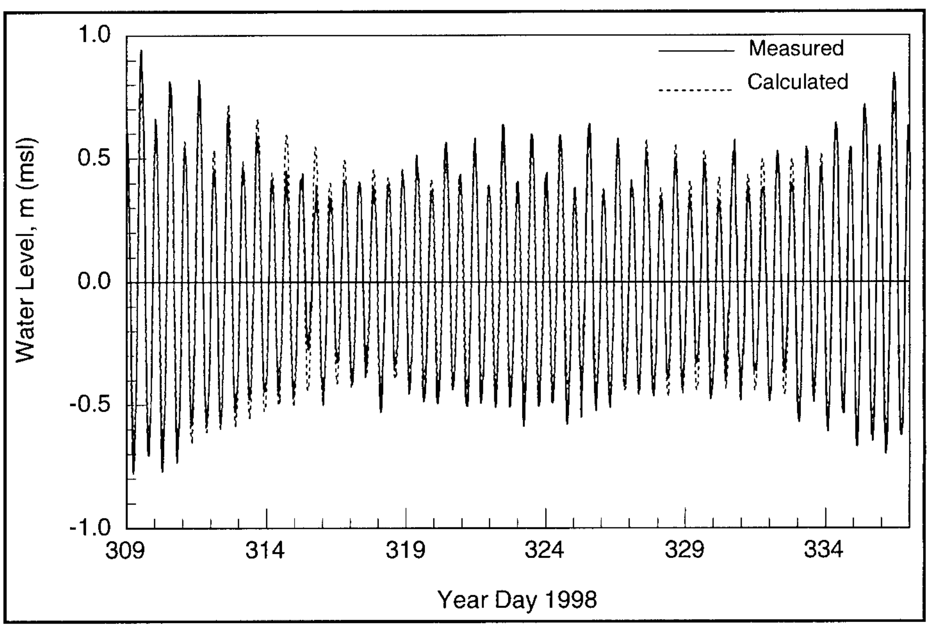

Figure 32. Comparison of measured and calculated water level at P1

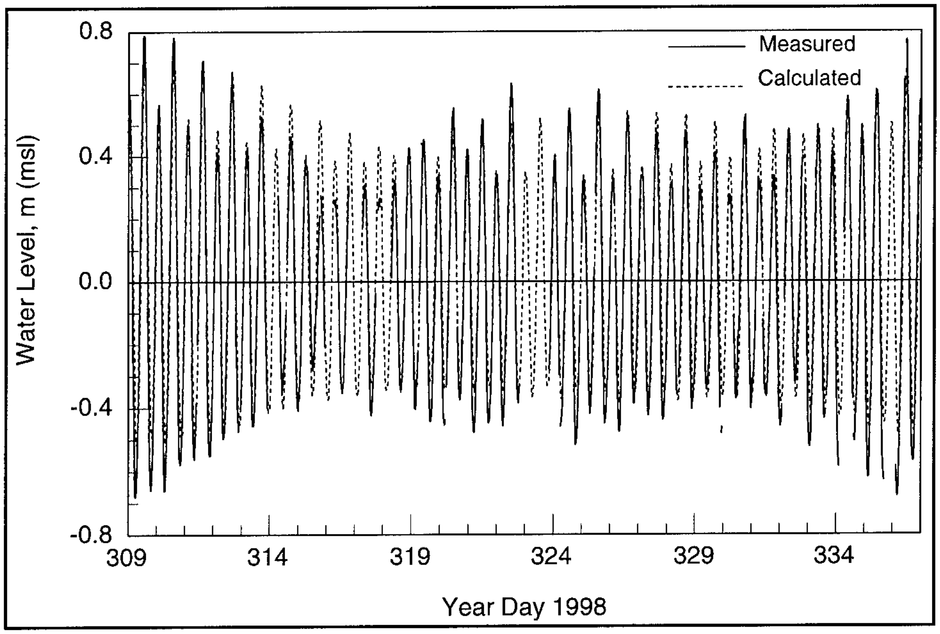

Figure 33. Comparison of measured and calculated water level at P2

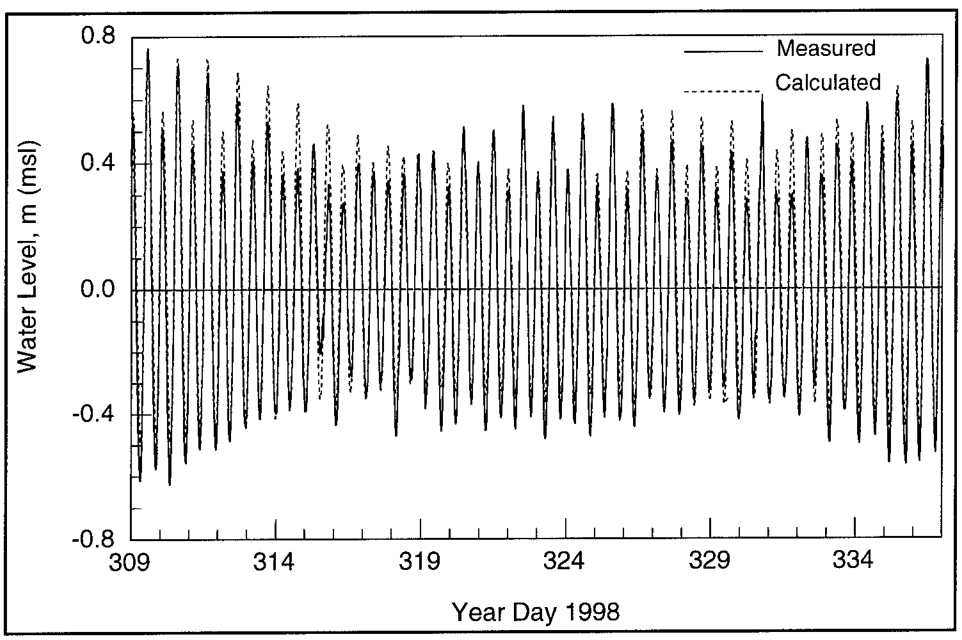

Figure 34. Comparison of measured and calculated water level at P3

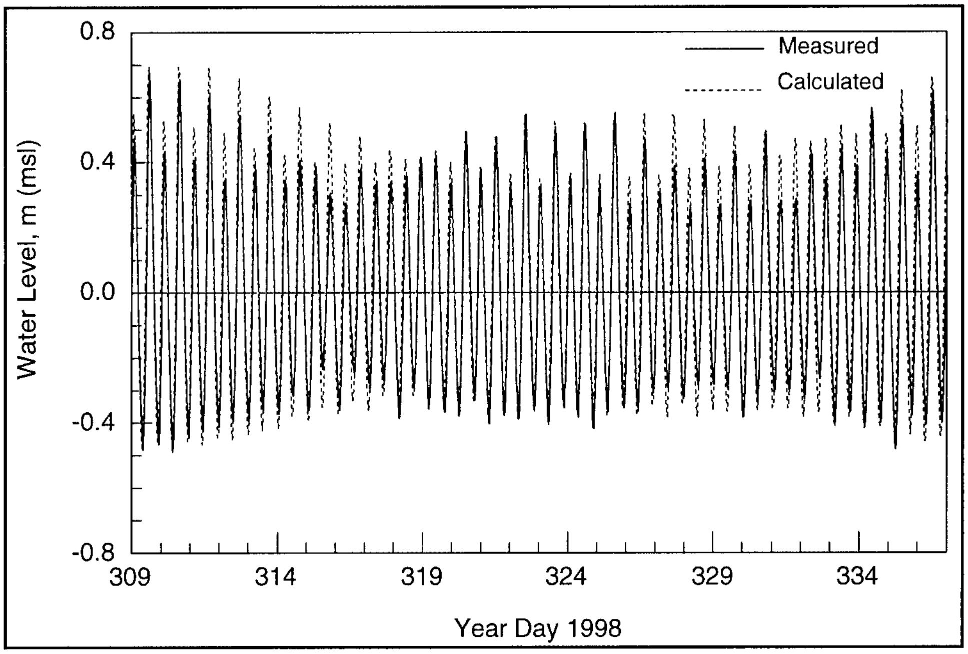

Figure 35. Comparison of measured and calculated water level at P4

Table 9
Comparison of Measured and Calculated Water Level and Current

Water Level Station	Mean Error, m	rms Error, m	Percent Error
P1[1]	0.01	0.07	6
P2[2,3]	0.03	0.10	10
P3[2]	0.05	0.08	8
P4[4,5]	0.03	0.08	9
Current Station	**Mean Error, m/s**	**rms Error, m/s**	**Percent Error**
C2	0.25	0.30	25
C4	0.14	0.37	14

Note: Measured water level was high-pass filtered using a cutoff frequency of 0.5 cpd
[1] Tide range calculated from NOS Shinnecock Inlet gauge datums
[2] Tide range calculated from NOS Ponquogue Point gauge datums
[3] Data gaps of 12.5% may compromise accuracy of error calculations for P2
[4] Tide range calculated from NOS Shinnecock Bay gauge datums
[5] Calculated water level shifted by 0.42 hr to coincide with measured water level for error calculations

Comparison of measured and calculated current speed directed parallel to the east jetty is shown in Figure 36. The current meter bin and calculation point were taken from the area of greatest velocity on the eastern side of the inlet. The time series is shorter than for other comparisons because the data for the current meter were available from YD 313 rather than from YD 308. In general, the model overpredicts both peak ebb and peak flood speed by approximately 0.4 m/s. The greatest difference between measurements and calculations occurs

from YD 327 through 332 during which the measured speed appears to be modified by nontidal forces. The peak measured ebb speed during this time contains more noise than during other parts of the time series and appears to be truncated, indicating that forcing from one or more nontidal sources acted on the current during this interval.

Comparison of measured and calculated current speed at the Ponquogue Bridge is shown in Figure 37. Peak current speed is generally overpredicted, but the phase is accurate. The overprediction owes, in part, to overprediction of the tide range which creates a greater surface slope across the bay than a smaller tide range. A second source of error may be in representation of the bridge piers. Losses for bridge piers were included in the computations, but the calculated turbulent losses may have been too small.

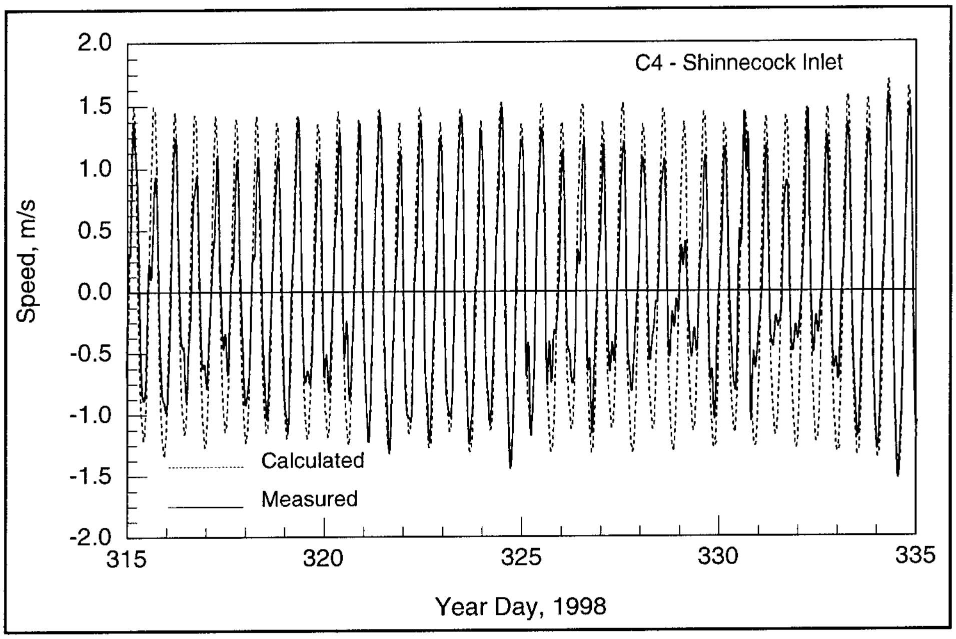

Figure 36. Comparison of measured and calculated current speed at C4

Calculated current speed at the Shinnecock Canal was compared with measurements at Station C3. Measurements were available at Station C3 for three days of the verification interval. Figure 38 compares the calculated and measured current speed in the Shinnecock Canal. The model overpredicts peak measurements by 0.2 to 0.4 m/s, and the difference is attributed primarily to specifying the exact location in the model that corresponds to the gauge location. Figure 38 shows time intervals in which the current speed remains near zero. The beginnings of these intervals correspond to times of gate closing and the ends correspond to gate openings. Timing of the gate closing and opening in the model closely matches the observations.

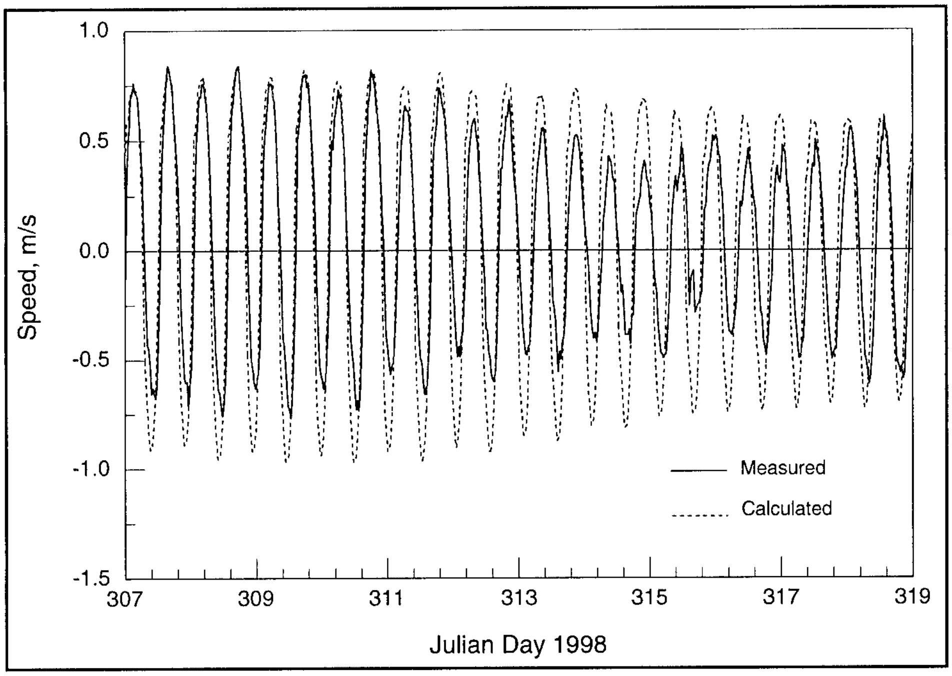

Figure 37. Comparison of measured and calculated current speed at C2

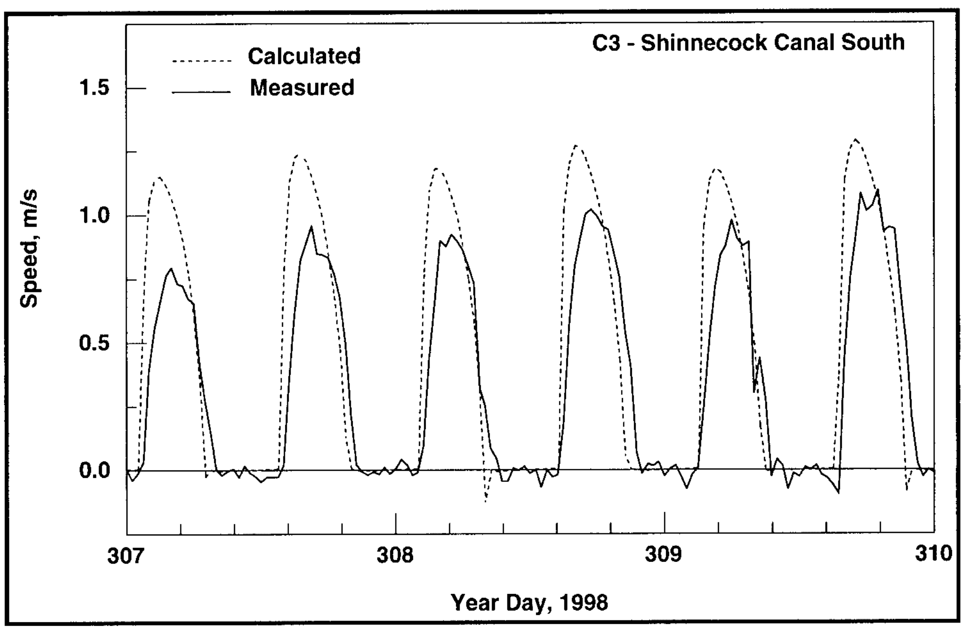

Figure 38. Comparison of measured and calculated current speed at C3

Calculated discharge in Shinnecock Inlet

Discharge was calculated for Shinnecock Inlet for the 3 November through 2 December 1998 simulation interval and is shown in Figure 39 (positive values

denote flood, negative values denote ebb). The calculated discharge is flood dominated, agreeing with measurements (Chapter 3). Although the measurements and calculations do not correspond to the same time, they can be compared as a qualitative check in trends for the calculations. Lines of constant discharge are plotted on Figure 39 that show the peak flood and ebb discharge measured at Shinnecock Inlet on 22 July 1998. Calculated peak discharge is in the range of the measurements.

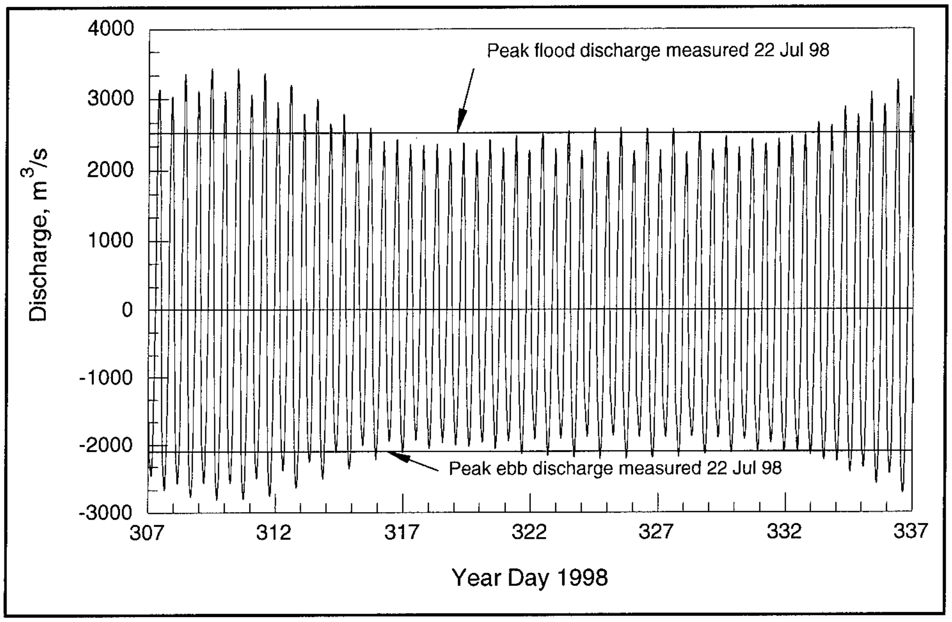

Figure 39. Calculated discharge through Shinnecock Inlet, 3 November through 2 December 1998

The time-averaged discharge D_{TAVG} for Shinnecock Inlet was calculated by

$$D_{TAVG} = \frac{1}{T}\int_0^T D(t)\,dt \qquad (6)$$

where D is discharge, T is the length of time for the integration, and t is time. If Equation 6 is applied for a sufficient length of time, the resulting curve will approach a tidally-averaged discharge into or out of the inlet. Figure 40 shows a time series of D_{TAVG} at Shinnecock Inlet for the interval 3 November through 2 December 1998, which covers spring and neap tide. The curve approaches a mean (tidal average) value of –87 m^3/s, indicating that more water flows from the bay to the ocean than from the ocean to the bay. This apparent loss of water to the ocean is about 4 percent of the typical peak discharge of 2,200 m^3/s. The Shinnecock Canal is the source of additional water into Shinnecock Bay. Thus, the water that flows from Great Peconic Bay to Shinnecock Bay creates an average seaward-directed discharge to the ocean of 87 m^3/s.

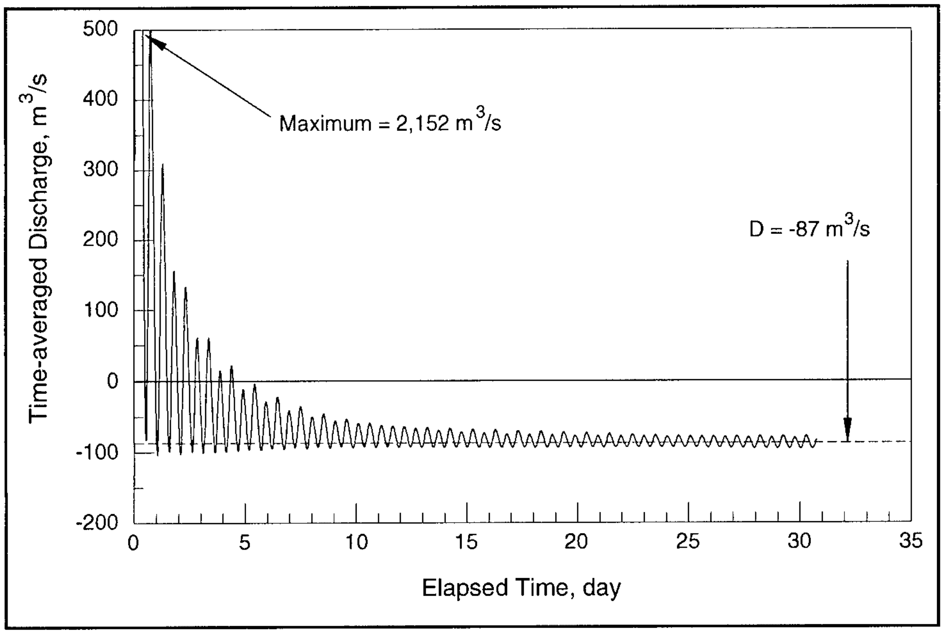

Figure 40. Time-averaged discharge through Shinnecock Inlet

Circulation patterns for existing condition

To establish a reference for evaluating alternatives, the circulation for the existing condition at the inlet and flood shoal is described. Features of the current at peak ebb and flood current are discussed. In addition, the jet and eddies that form and migrate during ebb tide are presented. Plots and current speeds reported are for peak spring tide.

During flood tide, currents are strongest in the center of the inlet and diminish as the inlet opens into the flood shoal, as shown in Figure 41. Peak flood current in the inlet reaches 2.4 m/s during spring tide. The current spreads over the flood shoal, with water moving toward the back bay over the central shoal area, and toward the eastern and western parts of the shoal. A portion of the west-moving current is deflected by the Warner Islands and flows into the West Cut near Warner Island West. Typical speed over the flood shoal is 1 m/s, which diminishes as water passes from the shallow shoal areas into deeper water.

During ebb tide, the current is greatest in the center of the inlet, reaching 2.2 m/s during spring tide, as shown in Figure 42. The East and West Cuts are the primary conduits of water entering the inlet from the bay. Current speed in the East and West Cuts is typically 1 m/s, although it can reach 1.5 m/s. Typical current speed over the flood shoal is 0.3 m/s, although it has a large range over the shoal.

At Shinnecock Inlet, eddies form on the western and eastern sides of the inlet and are termed here as the West Eddy and East Eddy, respectively (Figure 43). Formation of these eddies commences upon the initiation of ebb-directed flow through the inlet. Because the net direction of longshore transport near Shinnecock Inlet is to the west, a large bar has formed and extends from the

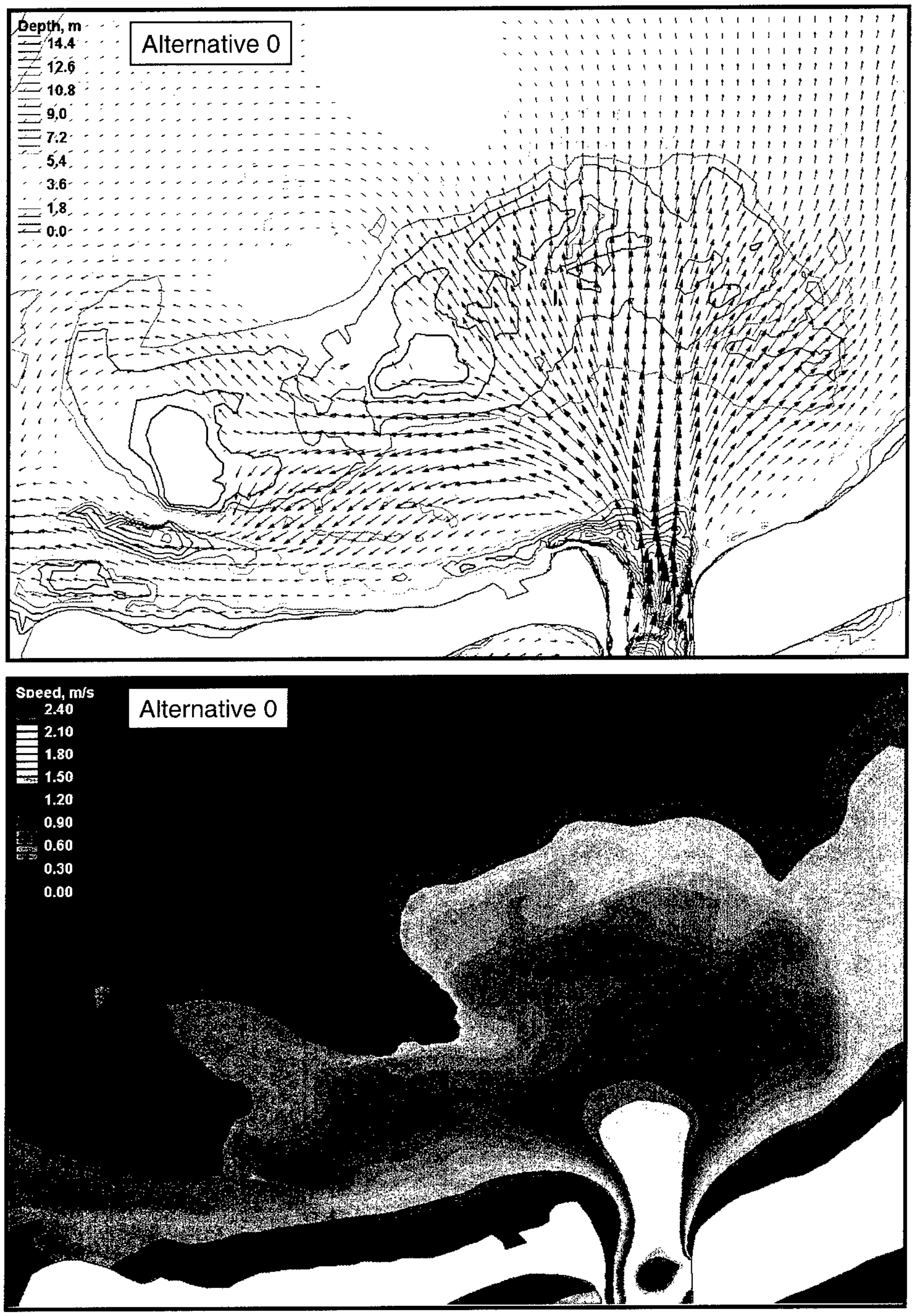

Figure 41. Alternative 0 velocity vectors and speed at flood shoal, peak flood tide

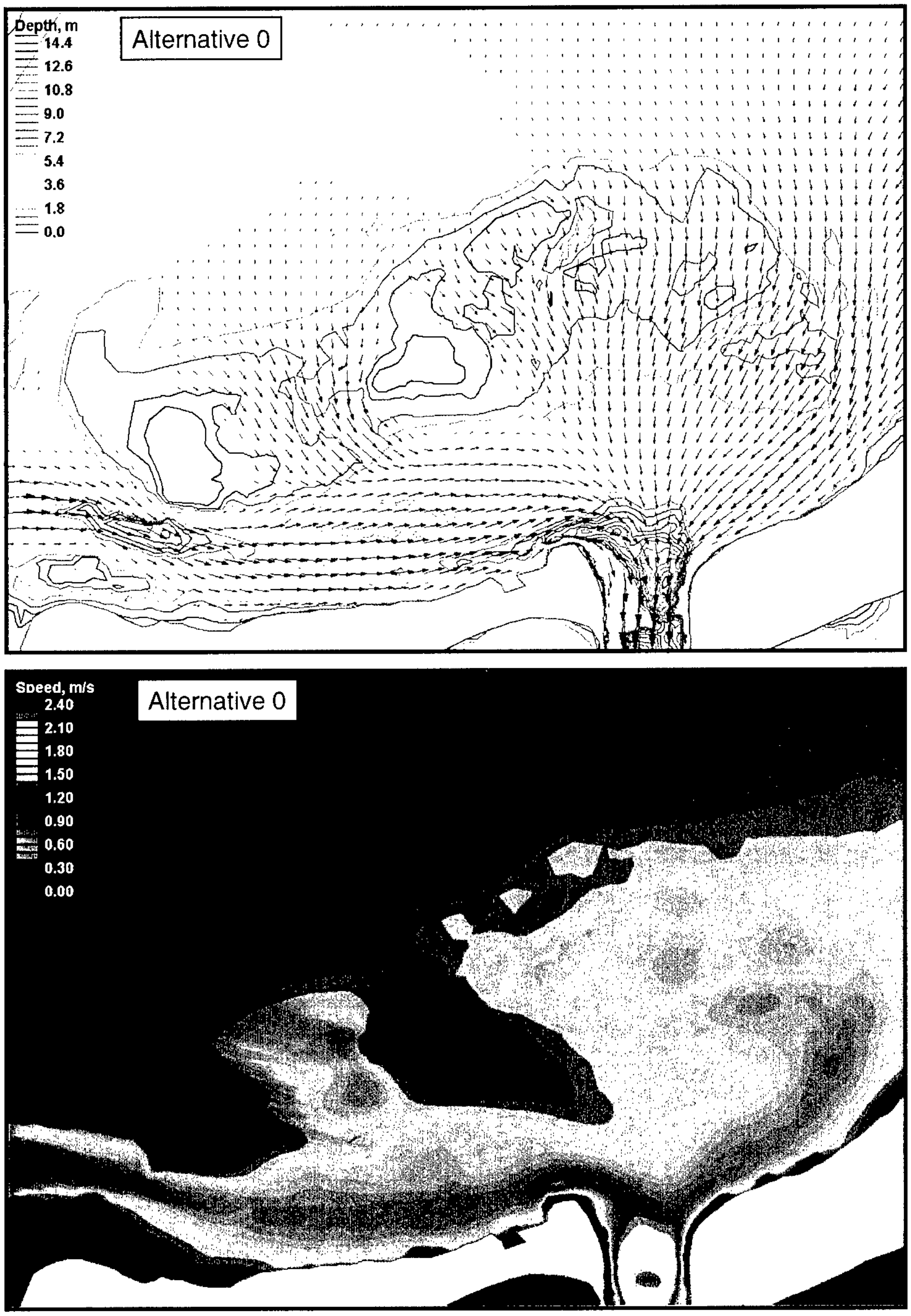

Figure 42. Alternative 0 velocity vectors and speed at flood shoal, peak ebb tide

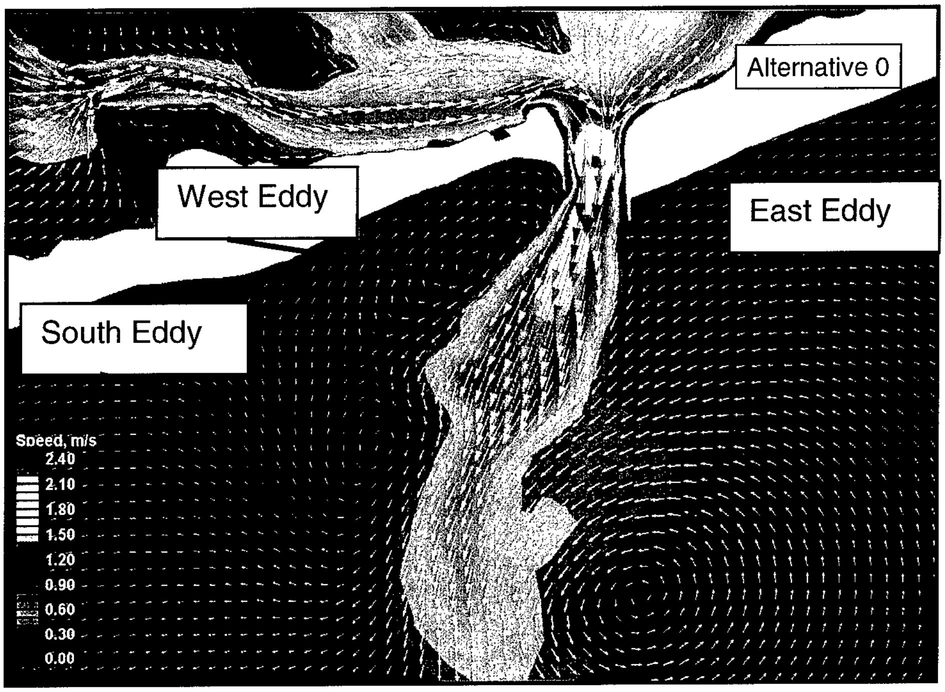

Figure 43. Alternative 0 velocity vectors and speed at inlet and ebb shoal, peak ebb tide

ebb-tidal shoal westward to the beach approximately 1.5 km west of the inlet. Growth and migration of the West Eddy is constrained by the shore and the ebb shoal and bar. During the ebb tidal cycle, the West Eddy's westward extent reaches approximately the bar location, but its migration is limited (Figure 44).

As the ebb jet intensifies over the ebb portion of the tidal cycle, the East Eddy grows and migrates. Figure 44 displays the edges and center line of the jet and centers of eddies at 1-hr intervals for duration of 4 hr. Initial movement of the East Eddy is toward the south-southeast at a nominal rate of 0.1 m/s. This migration corresponds to the lengthening of the ebb jet into the ocean as it strengthens. The ebb jet begins to deform as the eddy expands, as illustrated in Figure 44. During its southward movement, the eye of the eddy circumvents the eastern edge of the ebb shoal. Approximately 3 hr into the ebb cycle, the East Eddy changes heading and propagates toward the southwest at a rate of 0.2 m/s. This change in direction coincides with the turning of the coastal tidal current from east to west. Through a tidal cycle, the East Eddy travels approximately 4.6 km to the southwest at an average speed of 0.13 m/s.

A third eddy, called the South Eddy (Figure 43), forms seaward of the ebb shoal and west of the ebb jet approximately 3 hr into the ebb tide (Figure 44). Formation of the South Eddy occurs simultaneously with the southwest movement of the East Eddy and the seaward extension of the ebb jet past the ebb shoal. The ebb jet becomes squeezed between the East and South Eddies and narrows compared to that portion of the jet located over the ebb shoal. Thus, twice a day over the course of the ebb tidal cycle, the ebb jet is forced to migrate west of its initial position at the entrance and over the ebb shoal. The East and

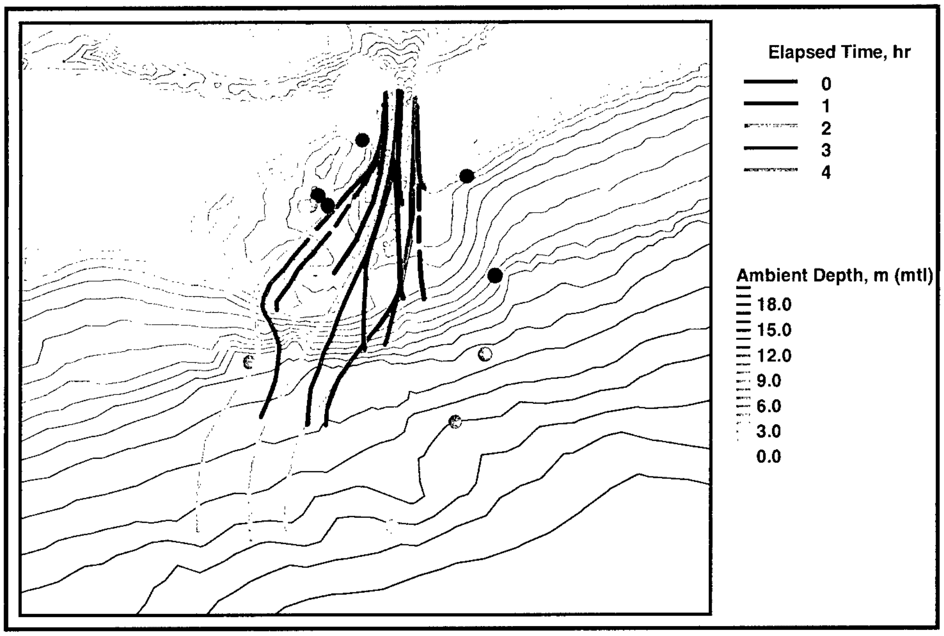

Figure 44. Eddy migration and associated jet orientation and shape. Dots denote center of eddies, solid lines denote jet center line, and dashed lines approximate jet edge. Colors indicate elapsed time of ebb flow since initial formation of eddies.

South Eddies narrow the width of the ebb jet seaward of the ebb shoal, thereby increasing the current speed and tending to scour a channel there.

The eddy and jet patterns occur twice daily, exerting a consistent stress and direction of transport on the bottom sediment. As shown in Figure 44, the center line of the ebb jet at hour 4, a time when the jet is strong and extends relatively far into the ocean, corresponds to the position of the entrance channel between the jetties and outer reach of the ebb shoal.

On 27-28 July 1999, field measurements were made to capture the ebb-jet and eddy motion at Shinnecock Inlet. Seven transects were occupied repeatedly by two boats throughout an ebb tidal cycle, and current through the water column was measured with an acoustic Doppler current profiler. Vectors of measured current are shown in Figure 45 for times (a) 2214 through 2317 EDT on 27 July 1999, and (b) 0008 through 0106 EDT on 28 July 1999. The approximate outlines of the lateral boundaries of the ebb jet are shown in red, and eddies are indicated with red arrows. Because the directions of the jet and eddies are the same where these features merge, delineating boundaries between them is difficult. The measurements exhibit the general pattern of flow predicted by the numerical model in that eddies are present, the ebb jet swings from east to west during ebb flow, and the jet becomes deformed.

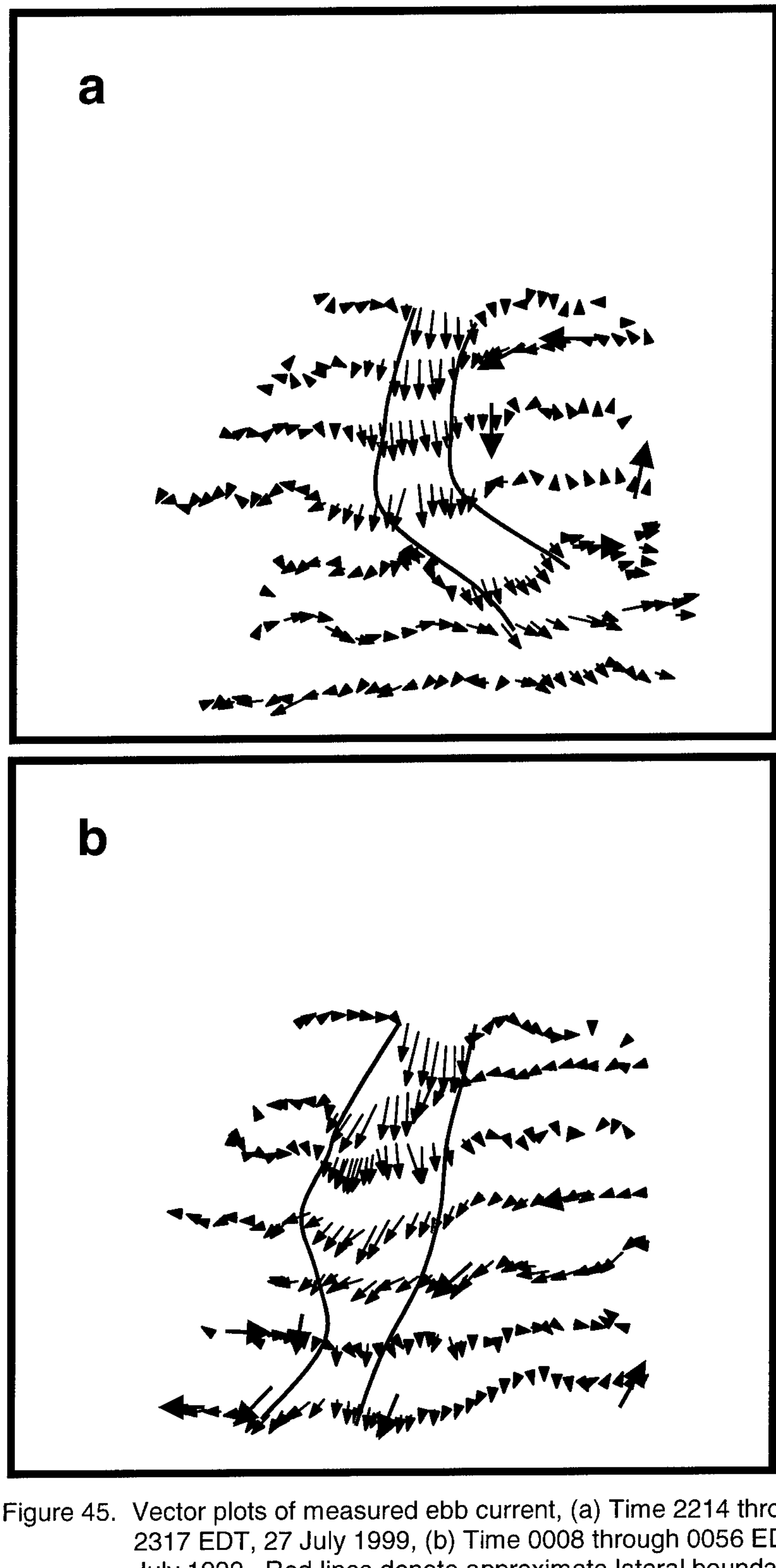

Figure 45. Vector plots of measured ebb current, (a) Time 2214 through 2317 EDT, 27 July 1999, (b) Time 0008 through 0056 EDT, 28 July 1999. Red lines denote approximate lateral boundaries of ebb jet and red arrows denote eddies

Representation of alternatives

Alternatives that consisted of mining in the bay interior or the deposition basin were represented in the ADCIRC mesh by deepening the bottom in the locations of mining. No changes to the mesh (change in number of or relocation of nodes and elements) were required to represent these alternatives. Alternatives 7, 8a, 8b, 9a, and 9b required modification to the model mesh. For Alternative 7, the shoreline was repositioned to make the coast relatively straight, and the bathymetry of the attachment bar and point was modified to simulate dredging.

Jetty lengthening was required for Alternatives 8a and 8b. The west jetty was extended seaward (170 m) to the same distance offshore as the east jetty, requiring modification of the mesh. Bathymetry was altered for Alternative 8b, which included dredging of the flood shoal.

For Alternatives 9a and 9b, the east jetty was shortened by 170 m. This change required modification of the mesh. Bathymetry was modified for Alternative 9b, which included dredging of the flood shoal.

Change in current speed

As part of the evaluation of alternatives, changes in current speed relative to the existing condition were calculated. Changes in current speed in the Shinnecock Inlet region were examined at peak flood and ebb tide.

Change in current speed relative to the existing condition (Alternative 0) for each alternative was calculated for peak flood and ebb tide. Times of flood and ebb tide selected for analysis correspond to those selected for current fields plotted in Appendix A. Eight regions, as indicated in Figure 46, were identified for describing the change in current speed. The most significant changes in current speed for the alternatives occurred in these regions.

Descriptions of change in current speed are presented here by groups of similar alternatives. Appendix B contains further information for each alternative. The groups are defined in Table 10. Change in current speed are shown for flood and ebb tide in plan-view plots. The horizontal extent and speed scale are consistent for all plots. One alternative was selected as representative of that group. Unless indicated otherwise, the selected alternative had the greatest change in speed of the alternatives in its group. Maximum increase and reduction of current speed varies among alternatives, and the reader is referred to Appendix B for additional information.

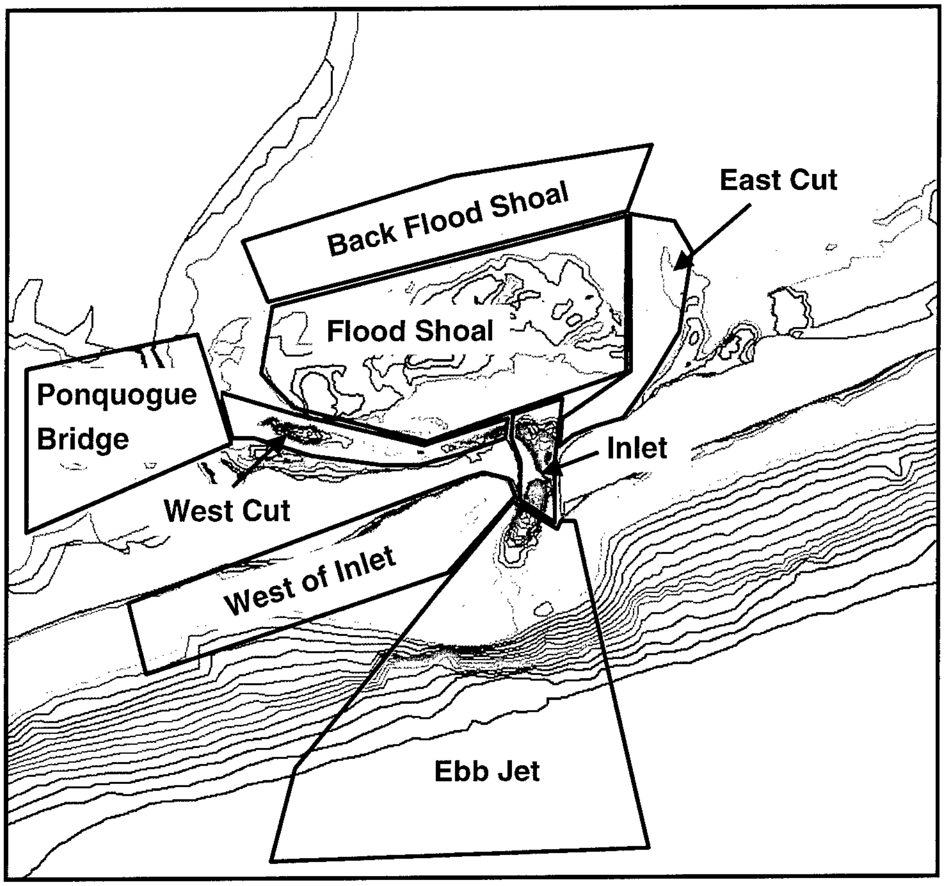

Figure 46. Regions identified for evaluating change in current speed

Table 10
Alternative Groups

Group	Alternatives	Description
A	1, 2, 3, 4	Mine flood shoal area of compatible material
B	5, 6	Mine western flood shoal/channel from Ponquogue Bridge
C	7	Mine Ponquogue Attachment
D	8a, 8b	Lengthen west jetty
E	9a, 9b	Shorten east jetty
F	10, 11, 12, 13	Mine wedge in flood shoal
G	14, 15	Relocate deposition basin

Group A: Mine area of compatible material of flood shoal

a. Flood tide (Figure 47): Current speed is increased where the inlet meets the flood shoal and adjacent to the shoreline along the West and East Cuts over limited reaches. The flood shoal experiences a decrease in current speed, whereas the back flood shoal has increased speed. Speed in the East Cut is reduced, except for a reach adjacent to the shore. Maximum speed increase occurs where the inlet meets the flood shoal and in the eastern back flood shoal. Maximum speed decrease occurs on the eastern flood shoal.

b. Ebb tide (Figure 48): Increased current speed occurs where the inlet meets the flood shoal, and on the western and eastern portions of the flood shoal. Decreased current speed occurs on the flood shoal and in the West and East Cuts.

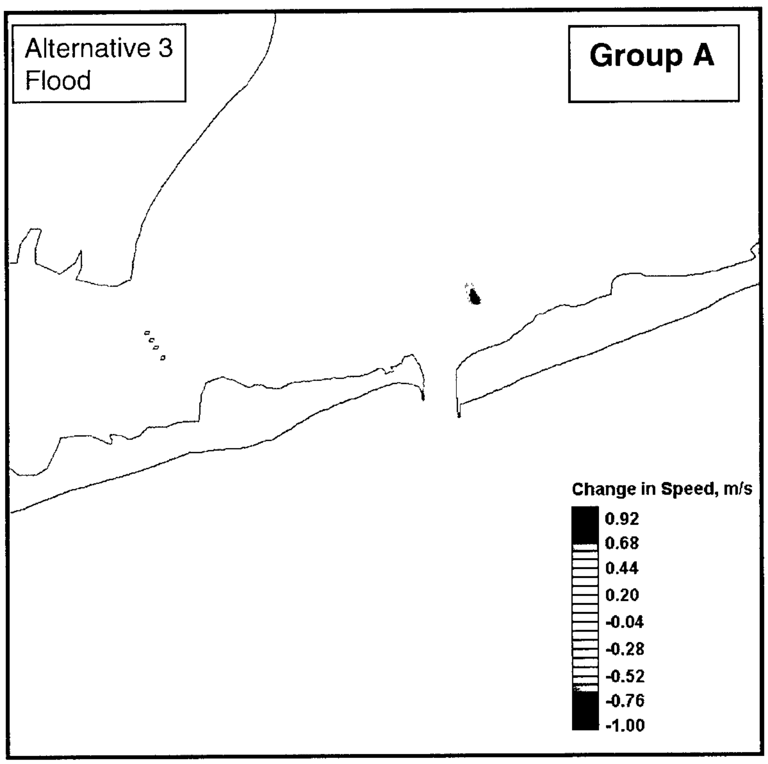

Figure 47. Change in current speed for Alternative 3, flood tide

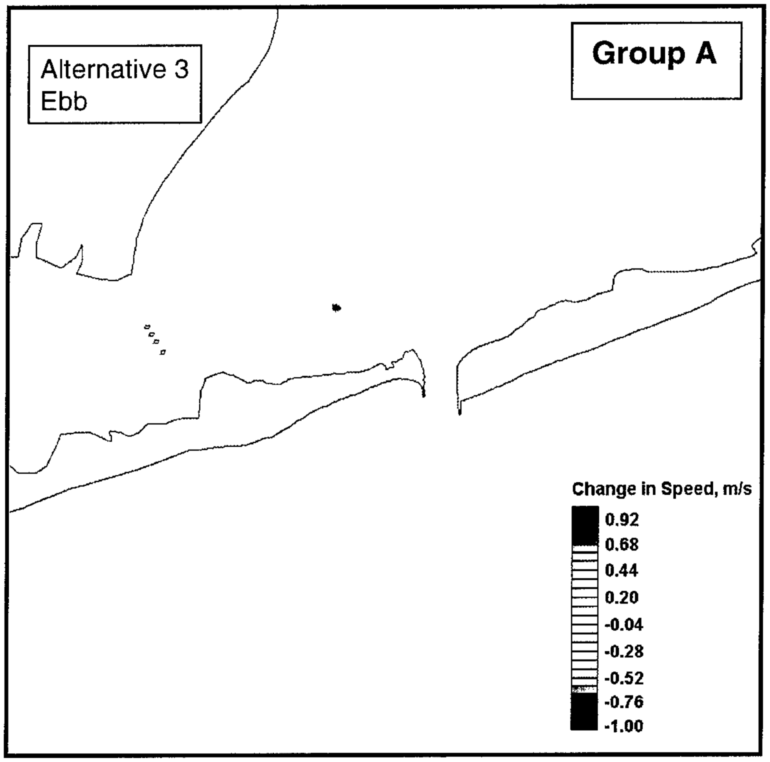

Figure 48. Change in current speed for Alternative 3, ebb tide

Group B: Mine western flood shoal/channel from Ponquogue Bridge

Changes in speed for Alternative 6 were negligible, and only changes for Alternative 5 are described.

a. Flood tide (Figure 49): Increased speed occurs on the flood shoal north of the West Cut (mined area) and on localized regions of the western flood shoal. Current speed is reduced in the East Cut, West Cut, and on localized regions of the western flood shoal.

b. Ebb tide (Figure 50): Current speed is increased on the flood shoal north of the West Cut (mined area), in the western portion of the back flood shoal, on the northwestern flood shoal, and in the center of the inlet. Speed is decreased in the East Cut, West Cut, eastern flood shoal, and localized regions of the western flood shoal.

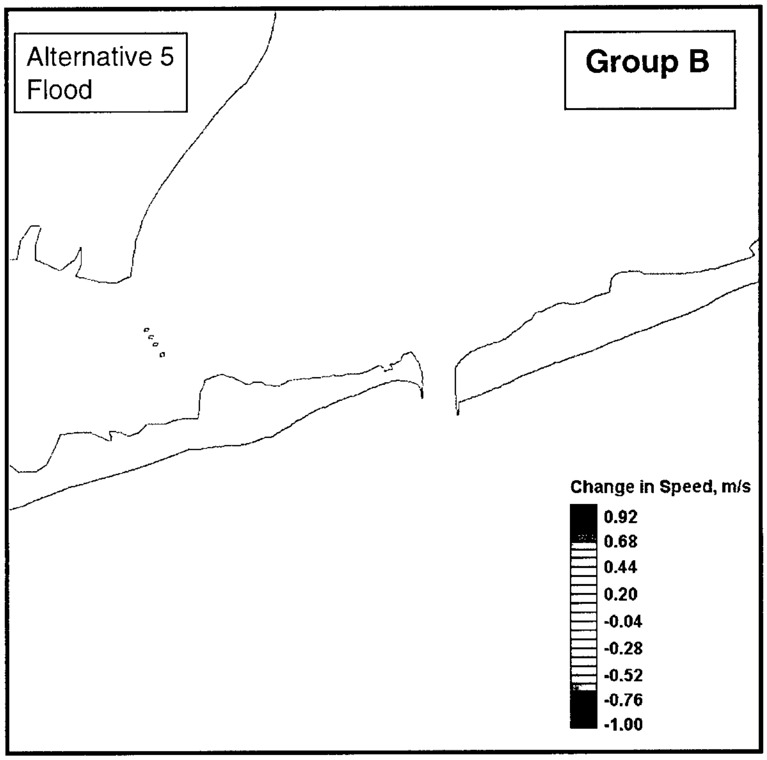

Figure 49. Change in current speed for Alternative 5, flood tide

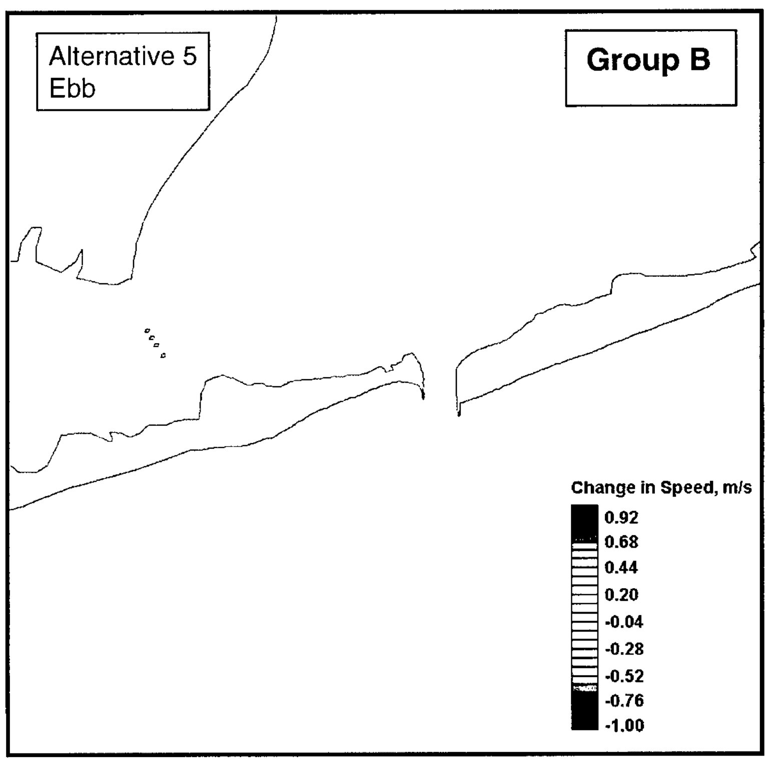

Figure 50. Change in current speed for Alternative 5, ebb tide

Group C: Mine Ponquogue Attachment Bar

a. Flood tide (Figure 51): Increased current speed occurred west of the inlet, within the inlet, on the flood shoal, in the West and East Cuts, and in localized areas near the Ponquogue Bridge. Current speed decreased in localized areas near the Ponquogue Bridge.

b. Ebb tide (Figure 52): Current speed increased on the flood shoal, in the East and West Cuts, in the inlet, and at the ebb jet.

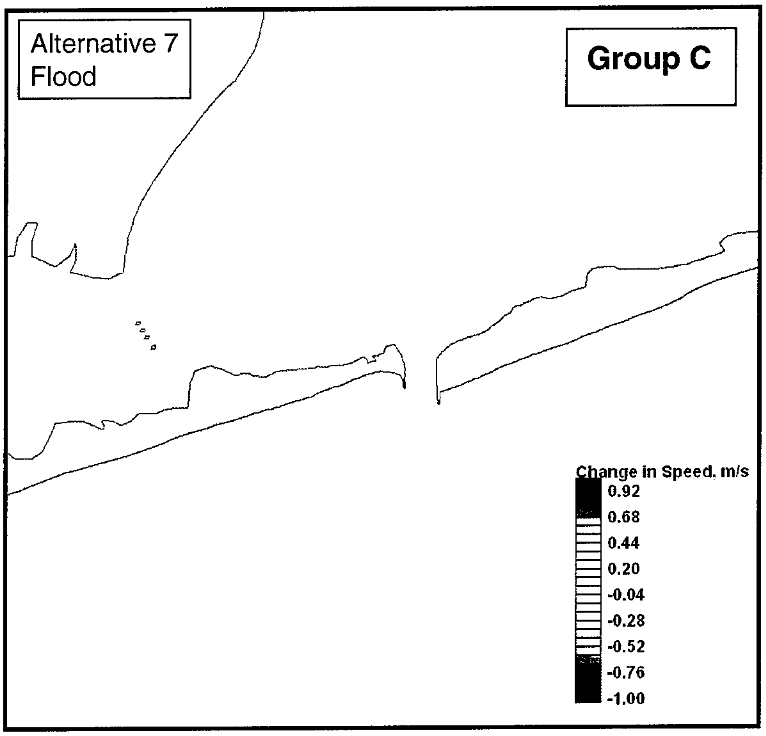

Figure 51. Change in current speed for Alternative 7, flood tide

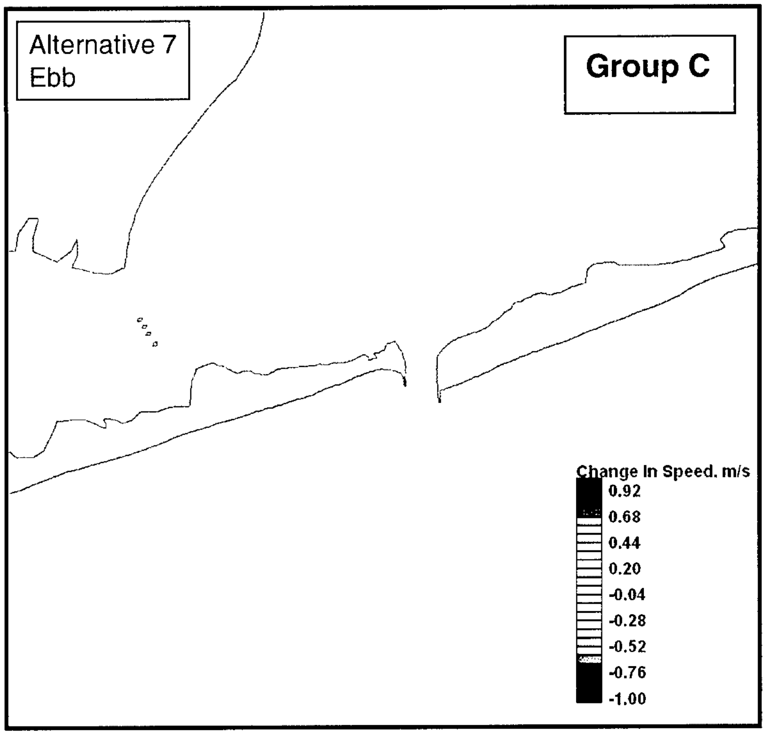

Figure 52. Change in current speed for Alternative 7, ebb tide

Group D: Lengthen West Jetty

Alternatives 8a,b exhibit similar patterns of current speed change everywhere except at the flood shoal and East and West Cuts. At the shoal and cuts, Alternative 8b displays patterns similar to those Alternatives in Group A.

a. Flood tide (Figure 53): For Alternatives 8a,b, the current speed increased at the inlet entrance by approximately 1 m/s. Other regions of increased speed are the inlet, localized areas near the Ponquogue Bridge, and in the ocean southwest of the inlet. Alternative 8a has increased currents in the East and West Cuts and on the western flood shoal. Reduced currents for both alternatives occurred west of the west jetty, on the eastern side of the inlet, and in localized regions near the Ponquogue Bridge and southwest of the inlet. Alternative 8a also had reduced currents northwest of the flood shoal.

b. Ebb tide (Figure 54): Alternatives 8a,b show increased and decreased current speed at the ebb jet. The area of increased speed extends from the inlet entrance generally toward the south and the area of decreased speed lies directly to the west of the area of increased speed. This pattern illustrates that the ebb jet does not migrate as far westward at this time as it does for the existing condition. Instead, the jet is more closely aligned with the inlet. Alternative 8a also has increased speed over limited areas of the flood shoal, and in short reaches bordering the shore in the East and West Cuts. Both alternatives show increased speed in the inlet and decreased speed west of the west jetty.

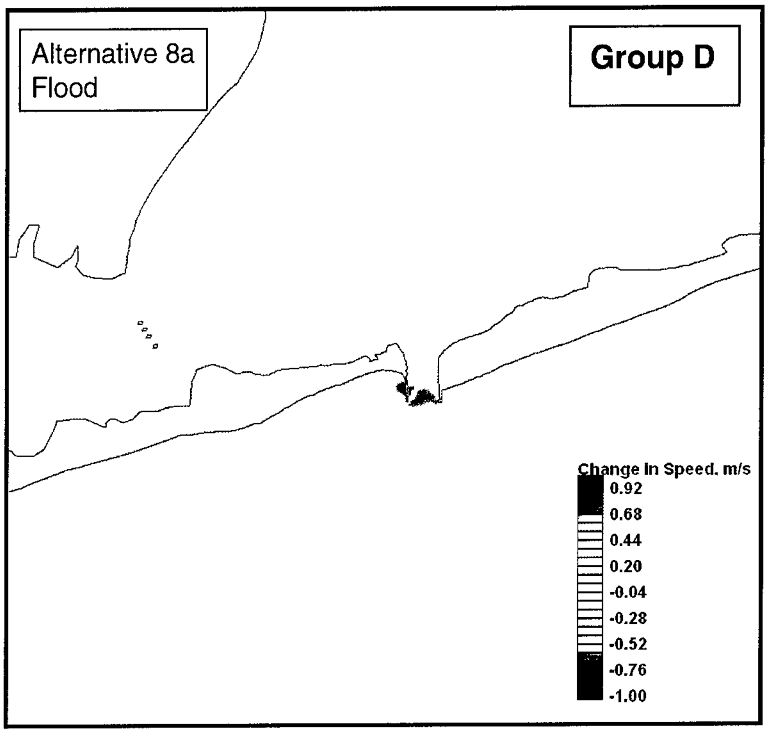

Figure 53. Change in current speed for Alternative 8a, flood tide

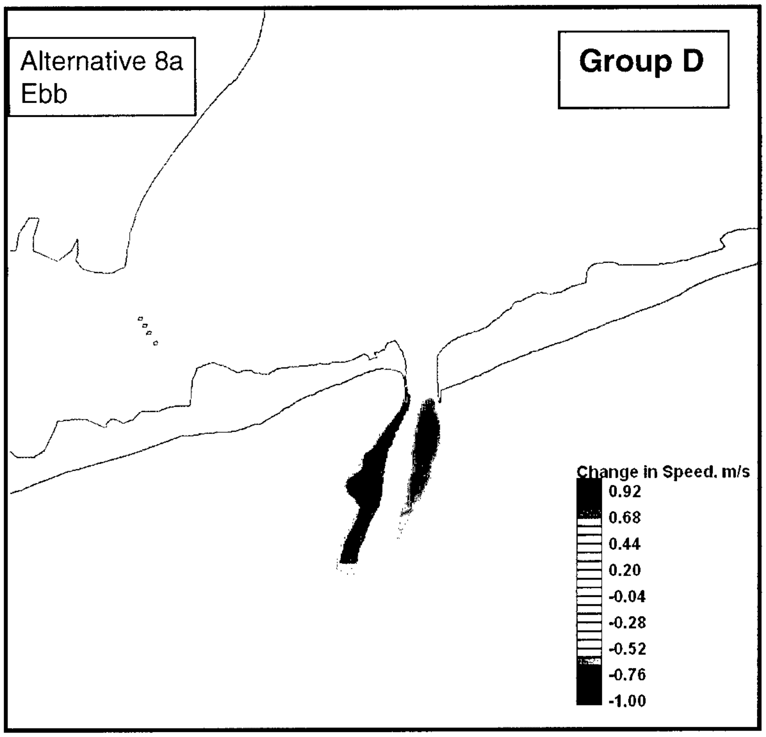

Figure 54. Change in current speed for Alternative 8a, ebb tide

Group E: Shorten East Jetty

Alternatives 9a,b show similar patterns of change in current speed everywhere except at the flood shoal and East and West Cuts. At the shoal and cuts, Alternative 9b displays patterns similar to those alternatives in Group A.

a. Flood tide (Figure 55): Current speed increases within the inlet, east of the east jetty, at the tip of the east jetty, and in a localized area near the Ponquogue Bridge. Within the inlet, the greatest increase is on the western side of the inlet. The large increase at the tip of the east jetty owes to flow being allowed there with the shortened jetty, whereas no flow was there with the present jetty configuration. Alternative 9a shows increased current speed over the flood shoal and in the East and West Cuts. Alternatives 9a,b have decreased speed at the inlet entrance, on the eastern side of the inlet, and in a localized region near the Ponquogue Bridge.

b. Ebb tide (Figure 56): Alternatives 9a,b show increased and decreased current speed at the ebb jet. The area of increased speed extends from the inlet entrance generally toward the south and slightly west, and the area of decreased speed lies directly to the west of the area of increased speed. This pattern illustrates that the ebb jet does not migrate as far westward at this time as it does for the existing condition. Instead, the jet is more closely aligned with the inlet. Alternative 9a also has increased speed over much of the flood shoal and in the East and West Cuts. Both Alternatives show increased speed in the inlet.

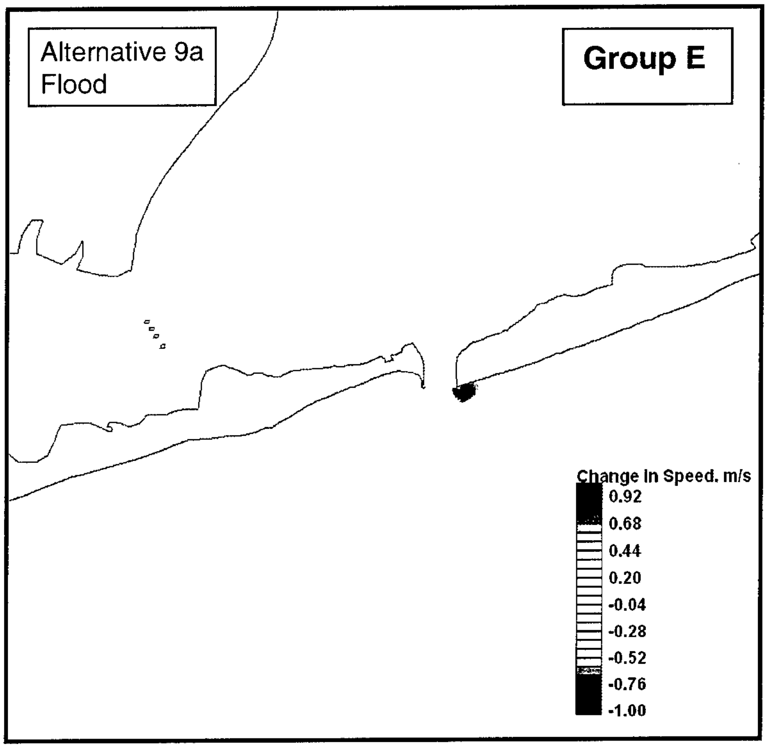

Figure 55. Change in current speed for Alternative 9a, flood tide

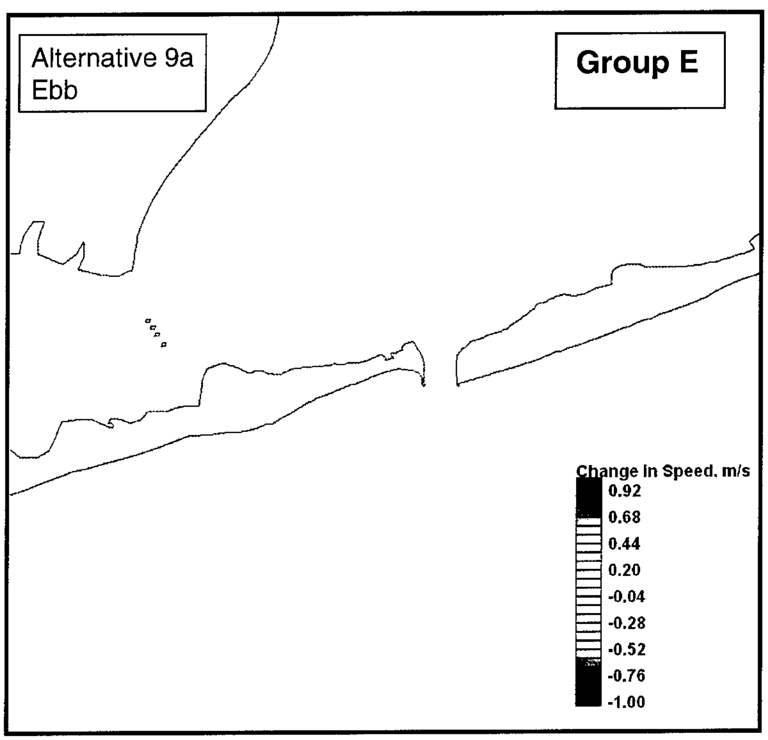

Figure 56. Change in current speed for Alternative 9a, ebb tide

Group F: Mine wedge in flood shoal

Alternative 13 possesses patterns of current change that are different from Alternatives 10, 11, and 12 because the mined wedge is rotated. Refer to Appendix B for details on Alternative 13.

a. Flood tide (Figure 57): Increased current speed occurs in the mined area of the flood shoal, on the back flood shoal, in the area between the flood shoal and the western shore, and in a limited region near the Ponquogue Bridge. The greatest increase occurs on the back flood shoal. Decreased current occurs on the flood shoal (except in the mined area), in the East and West Cuts, on the eastern side of the inlet, and in a limited area near the Ponquogue Bridge. Maximum reduction in current occurs in the area where the flood shoal meets the East Cut.

b. Ebb tide (Figure 58): Increased current occurs in the mined area of the flood shoal, in the back flood shoal, near the Ponquogue Bridge, in the inlet, and at the ebb jet. Decreased current occurs on the flood shoal (except where mined) and in the East and West Cuts.

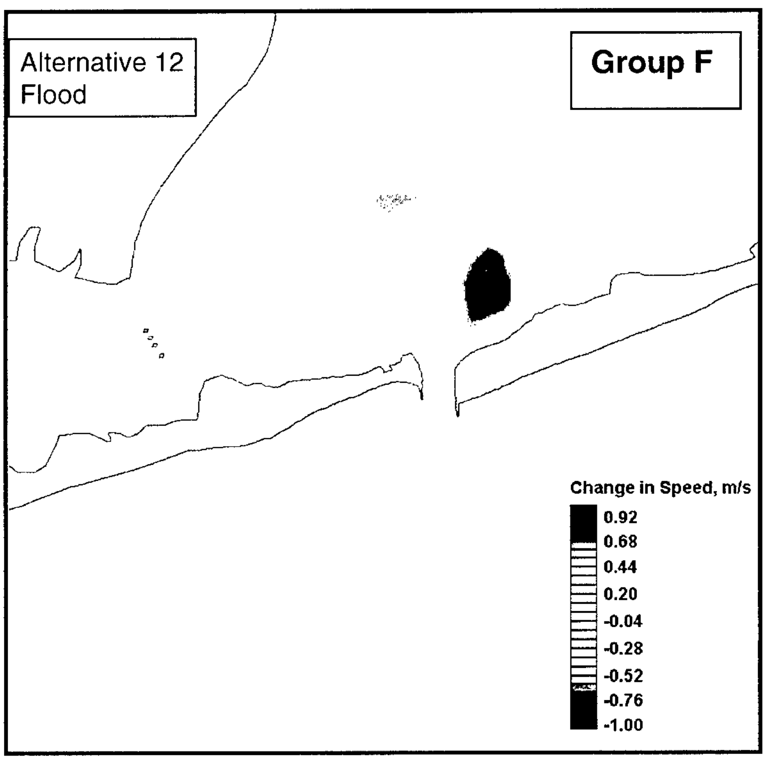

Figure 57. Change in current speed for Alternative 12, flood tide

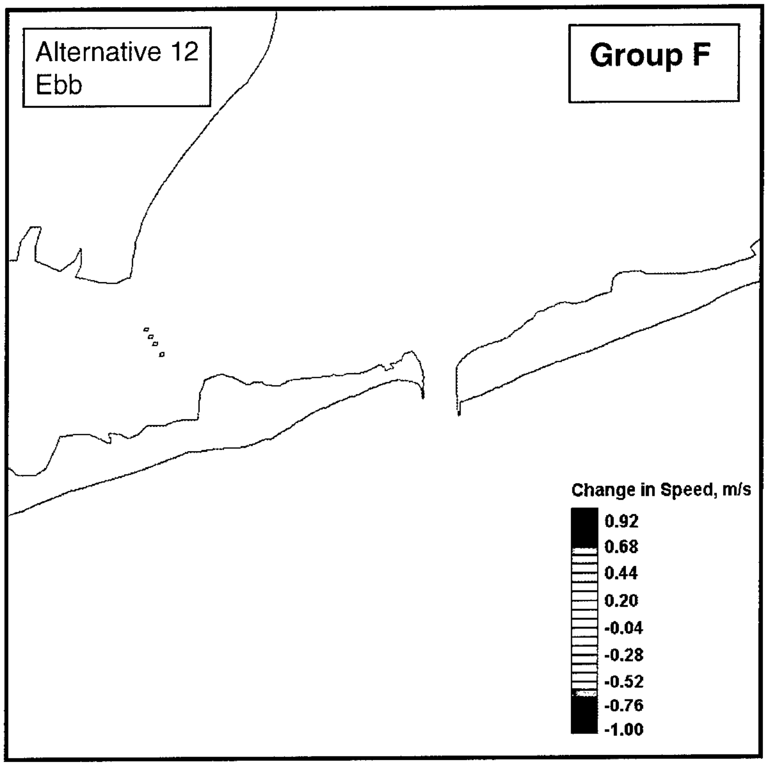

Figure 58. Change in current speed for Alternative 12, ebb tide

Group G: Realign deposition basin

a. Flood tide (Figure 59): Current speed is increased in the inlet on the eastern side adjacent to the east jetty. Alternative 15 also shows increase on the western side of the inlet. Decreased speed occurs at the inlet entrance.

b. Ebb tide (Figure 60): Current speed is increased and decreased at the ebb jet. The area of increased speed extends from the inlet entrance generally toward the south and slightly west, and the area of decreased speed lies directly to the west of the area of increased speed. This pattern illustrates that the ebb jet does not migrates as far westward at this time as it does for the existing condition.

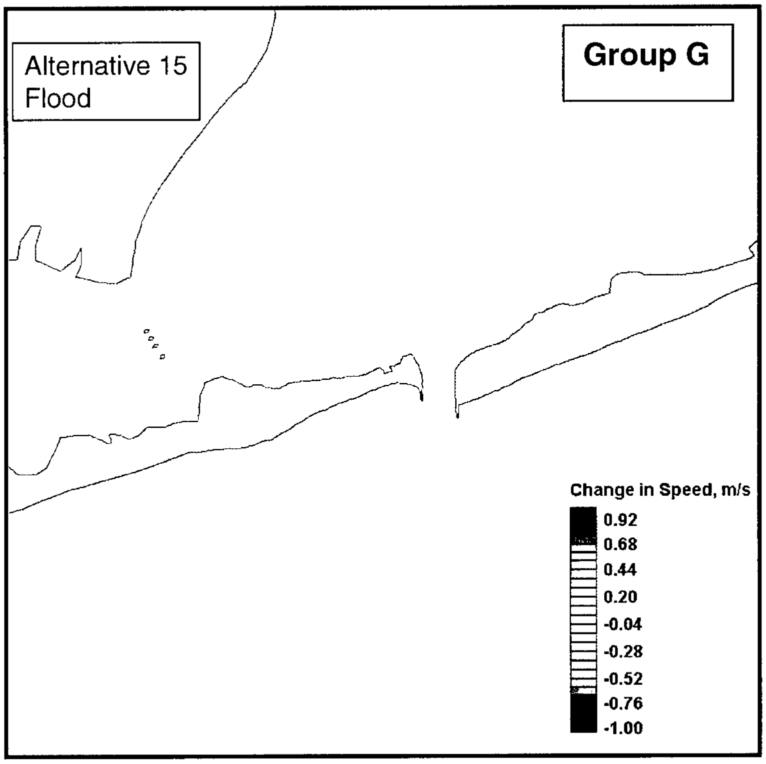

Figure 59. Change in current speed for Alternative 15, flood tide

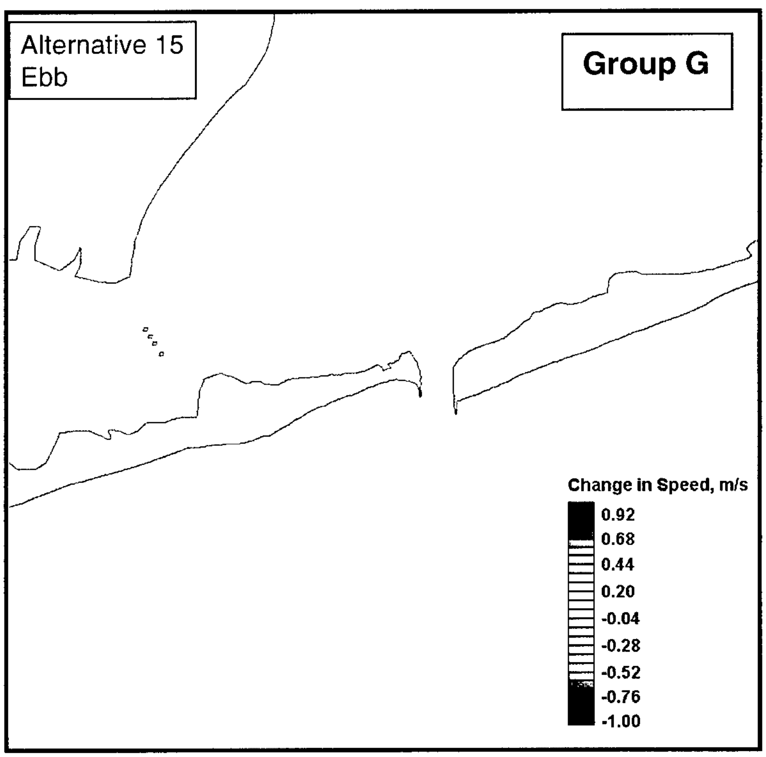

Figure 60. Change in current speed for Alternative 15, ebb tide

Inlet current

Areas of the Shinnecock Inlet and Bay in which change in current speed is of engineering concern are the inlet, flood shoal, beach west of the inlet, the West Cut, and the Ponquogue Bridge. Each of these areas is discussed here with respect to change in speed for the alternatives.

Shinnecock Inlet has experienced scour at two locations, on its southwestern end near the west jetty and on its northeastern end adjacent to the northern section of the east jetty. In addition, strong currents in the inlet pose hazardous conditions for navigation. Improvements within the inlet would include overall reduction in the current speed or reduction in speed in areas of scour. All alternatives that reduce the speed in the inlet do so over limited areas. Reduction in speed along the eastern edge of the inlet occurs on flood tide for Alternatives 8a,b, 9a,b, 10, 11, and 12. The current is not reduced along the eastern edge of the inlet during ebb tide in any alternative. Speed is reduced along the western edge of the inlet during flood tide for Alternatives 8a,b, and 15 and during ebb tide for Alternatives 8a,b. These decreases were located in the seaward half of the inlet. The reductions for Alternatives 8a,b owe to the jetty tip being extended further seaward.

Increased current speed in Shinnecock Inlet would exacerbate scour and navigation problems and could lead to greater change in the tidal prism, thereby potentially altering the inlet stability. Several of the alternatives evaluated here would increase the current speed within the inlet. Alternatives that increased the speed over limited areas of the inlet are Alternatives 5, 10, 11, 12, 14, and 15. Increased current speed over a significant portion of the inlet (50 percent or more of the area) occurs during flood and ebb tide for Alternatives 7, 8a,b, 9a,b, and during ebb tide for Alternatives 10, 11, 12, and 13.

Current near beach adjacent to west jetty

The beach adjacent to the west jetty has experienced chronic erosion. Increased longshore tidal current speed near the beach has the potential to increase erosion there. Decreased current speed could improve the situation by reducing the transport of sand away from the beach.

Alternatives 8a,b reduced the current speed at the west beach during the flood tide. These alternatives also reduced the current speed parallel to shore during ebb tide between the west jetty and the attachment bar, but the reduction did not extend to the shore.

Current speed increased for Alternative 7 between the west jetty and the attachment point (increased west of the attachment point also). The region of speed increase is seaward of the beach shoreline in the area of erosion.

Changes in jetty length for Alternatives 8a,b, and 9a,b modify the eddy and ebb jet structure. Circulation at the beach west of the west jetty can change with modification of the size and center of the West Eddy. The seaward changes for Alternatives 8b and 9b are the same as for 8a and 9a, respectively.

During ebb tide, the jet for Alternatives 8a,b extends from the inlet nearly directly south (Alternative 8a is shown in Figure 61). In comparison, for the existing condition, the jet aligns toward the southwest (Figure 43). The more southerly-directed jet of Alternative 8a modified the size and position of the ebb eddies. The West Eddy is larger than that for the existing condition, and its center is located more toward the southwest. Because the center is at a greater distance from the shore, the velocity on the northern side of the eddy is reduced, as compared to the existing condition (Figure 54). However, the reduction in current speed does not extend to the shore, but is located in the central portion of the eddy.

For Alternative 9a, the strongest part of the ebb jet is positioned east of its corresponding location for the existing condition. However, the western jet edge is in approximately the same location and does not modify the size or position of the West Eddy. Thus, no changes in current west of the west jetty are expected during ebb tide for Alternatives 9a,b.

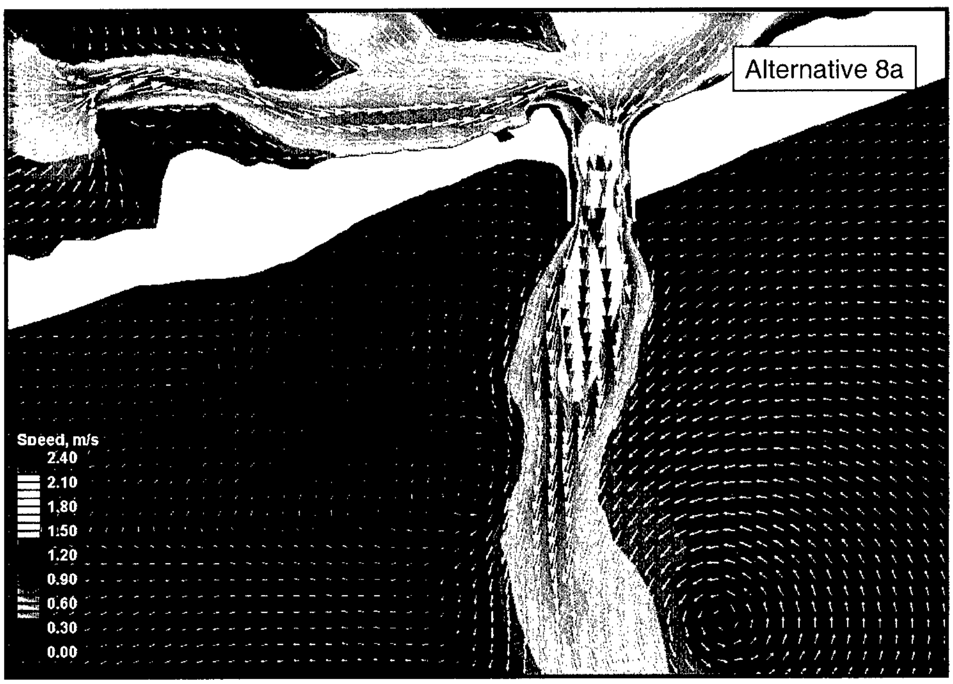

Figure 61. Alternative 8a velocity vectors and speed at inlet and ebb shoal, peak ebb tide

Current speed at the West Cut

Current speed in the West Cut is strong and has resulted in boat groundings on the margin of the flood shoal. Decreased speed in the West Cut would benefit navigability by giving boaters greater control over their vessels. Increased speed would hinder navigation.

Alternatives 1 and 5 reduce current speed in the West Cut west of the docks during both flood and ebb tide. Alternatives 2, 3, 4, 8b, and 9b have areas of both increased and decreased speed west of the docks on flood tide. Near the docks, Alternatives 1, 2, 3, 4, 8b and 9b reduce speed on ebb, and Alternatives 2, 3, 4, 8a,b, 9a,b increase speed on flood. Alternative 1 has both increased and decreased speed during flood tide near the docks. Increased speed occurs on both flood and ebb tide for Alternatives 7 and 9a along the entire West Cut. Speed is decreased along the entire West Cut for Alternatives 10, 12, and 13.

Current speed at the Ponquogue Bridge

The current at the Ponquogue Bridge is strong because the bridge and the nearby fishing piers and landfills constrict the openings through which water can flow to the western portion of Shinnecock Bay. Increased speed at the bridge would be a safety concern for divers and could contribute to scour at bridge pilings.

For the alternatives evaluated, changes in speed at the bridge structure are often accompanied by changes in speed adjacent to the bridge. Speed increase at or near the bridge may occur simultaneously with a decrease at another location at or near the bridge.

Alternatives 1, 2, 3, and 4 produced a decrease in current speed at and to the west of the bridge during flood tide. In all other alternatives in which speed at the bridge changed during flood tide, areas of increased and decreased speed were present west of the bridge. The patterns of speed change appeared as dual lobes extending westward from the bridge in which one lobe had decreased speed and the other had increased speed. Alternatives 5, 10, 11, 12, and 13 produced decreased speed in the northern lobe. Alternatives 7, 8a,b, and 9a,b produced increased speed in the northern lobe.

During ebb tide, changes in speed at the bridge were accompanied by speed changes east of the bridge. The two locations that had changed speed were the channel connecting the bridge to the West Cut, and an area located between the bridge and the flood shoal. Alternatives 7 and 9a,b produced increased current speed east of the bridge, with no decreases. Alternatives 5, 10, 11, 12, and 13 had patterns of decreased speed between the bridge and the West Cut and increased speed between the bridge and the flood shoal. Alternatives 8a,b produced increased speed between the bridge and the West Cut and decreased speed between the bridge and the flood shoal.

Discharge through the inlet

Values of discharge through the inlet for the alternatives, as computed from the 1-month simulation, are listed in Table 11. Maximum flood and ebb discharge values are the greatest instantaneous directional discharges calculated during the simulation. These maxima occurred during spring tide. The time-averaged discharge is the mean of D_{TAVG} (Equation 6) over the last 24.84 hr of the simulation. This time interval was selected because, as shown in Figure 40, the

integral of the discharge has approached an equilibrium value. Positive values of time-averaged discharge denote flood flow, and negative values denote ebb flow.

Table 11
Inlet Discharge Quantities for Alternatives

Alternative	Max Flood Discharge m^3/s (ft^3/s)	Max Ebb Discharge m^3/s (ft^3/s)	Time-averaged Discharge m^3/s (ft^3/s)
0	3,325 (117,406)	2,765 (97,632)	-87 (3,072)
1	3,322 (117,300)	2,789 (98,480)	-88 (3,108)
2	3,312 (116,947)	2,797 (98,762)	-88 (3,108)
3	3,309 (116,841)	2,799 (98,832)	-89 (3,143)
4	3,311 (116,911)	2,799 (98,832)	-89 (3,143)
5	3,310 (116,876)	2,789 (98,480)	-89 (3,143)
6	3,323 (117,335)	2,765 (97,632)	-87 (3,072)
7	3,582 (126,480)	2,951 (104,200)	-96 (3,390)
8a	3,472 (122,596)	2,814 (99,362)	-97 (3,425)
8b	3,460 (122,173)	2,863 (101,093)	-99 (3,496)
9a	3,595 (126,939)	2,975 (105,047)	-61 (2,154)
9b	3,560 (125,704)	3,018 (106,566)	-62 (2,189)
10	3,289 (116,135)	2,853 (100,739)	-91 (3,213)
11	3,288 (116,099)	2,853 (100,739)	-90 (3,178)
12	3,283 (115,923)	2,866 (101,198)	-91 (3,213)
13	3,293 (116,276)	2,842 (100,351)	-90 (3,178)
14	3,353 (118,394)	2,771 (97,844)	-88 (3,108)
15	3,372 (119,065)	2,765 (97,632)	-87 (3,072)

Change in maximum ebb and flood discharge is small, less than 1.5 percent, for Alternatives 1, 2, 3, 4, 5, 6, 14, and 15. Alternatives 10, 11, 12, and 13 have small changes in discharge on flood, and the percent increase ranging from 2.8 to 3.7 on ebb. Greater changes in discharge occur for Alternatives 7, 8a,b, and 9a,b in which both ebb and flood discharges were increased. Alternatives 9a,b have the greatest change with increased flood discharge of 8.1 and 7.1 percent, and the ebb discharge also increased by 7.6 and 9.2 percent, respectively. Alternative 7 has an increase of 7.7 percent on flood and 6.7 percent on ebb. Alternatives 8a,b show typical changes of about 4 percent. Although changes less than about 5 percent can be considered as within range of variability of the system and accuracy of the calculations, all the percentages should be viewed as representing trends in change in the discharge for the given alternative. Increases in discharge would tend to further increase the cross-sectional area of the inlet, although equilibrium inlet theory (Chapter 5) indicates the cross-sectional area will increase in any case.

The larger increases in discharge which occur for Alternatives 7, 9a, and 9b could alter the stability of the inlet. In addition, the flood and ebb shoals may grow because of increased transport capacity of the inlet current.

The time-averaged discharges given in Table 11 reveal that for all alternatives except Alternatives 9a,b, changes in flow through the inlet do not significantly alter the net flow. For Alternatives 9a,b, however, the time-averaged discharges are decreased by 30 percent from the existing condition. This reduction owes primarily to the change in phase relation between the current and water level within the inlet. Figure 62 plots the discharge curves for Alternatives 0 and 9a (jetty modification) for a 2-day interval. The phase is different between the two curves with Alternative 9a discharge lagging that of the existing condition.

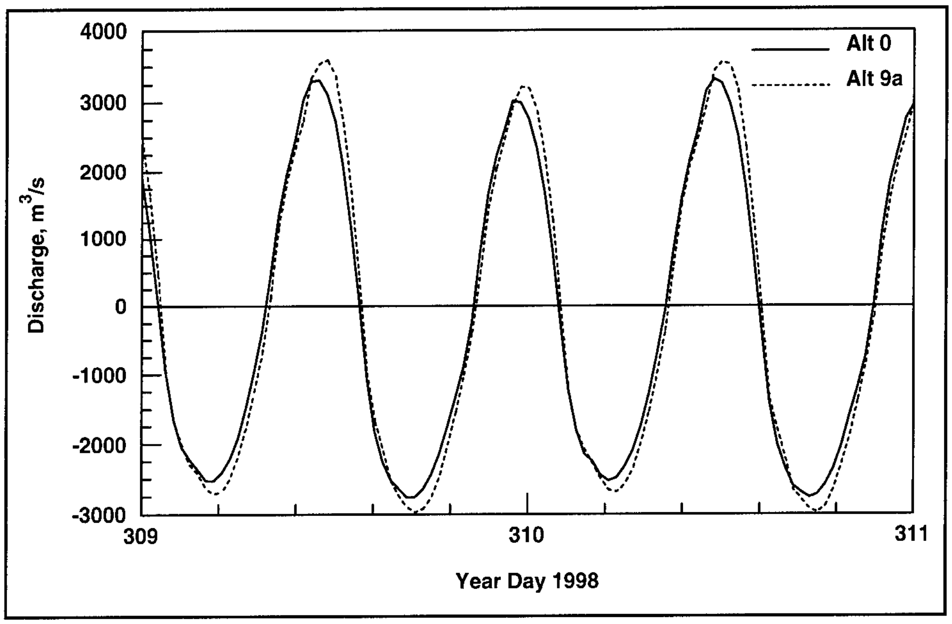

Figure 62. Inlet discharge over 2-day interval for Alternatives 0 and 9a

Changes in patterns of erosion and deposition for selected alternatives

Changes in current strength that occur from removal of sand from the bottom can modify patterns of erosion and deposition. Areas that transition from erosional to depositional or vice versa are calculated here for Alternatives 1, 2, 3, 4, and 5, judged to be the most favorable for possible implementation. The procedure calculates a critical current speed at initiation of suspension to the peak ebb and peak flood speed for the particular alternative. The study area is mapped according to depositional and erosional peak current speed for the alternatives. These maps are compared to an analogous map for the existing condition (Alternative 0) to determine if any areas transition between erosional and depositional.

To establish changes in patterns of erosion and deposition, the critical depth-averaged velocity for initiation of suspension $U_{cr,s}$ was computed and subtracted from the peak flood and ebb velocities. Values of $U_{cr,s}$ are related to the median particle diameter d_{50} and water depth (van Rijn 1993). Although d_{50} varies spatially, the flood shoal was selected as the representative area for specifying grain size because it is the focus of the study. Representative values of d_{50} were obtained from the sieve analysis of Cores 3, 4, 5, and 6 collected on the flood shoal in the area of compatible material (OCTI 1999). These cores were selected as representative because they are located on the area of compatible material or at or near areas of simulated removal of material. Sieve data from the surface portion of the cores entered in the calculation of critical depth-averaged velocity. For the four cores, the d_{50} values ranged from 0.41 to 0.62 mm. The overall representative grain size was approximated by averaging the median diameter values for the four cores, giving a mean d_{50} of 0.54 mm.

Figure 63 (modified from Van Rijn (1993)) relates $U_{cr,s}$ to water depth h and the median grain diameter d_{50}. The depth-averaged speed for initiation of suspension for the subject study area was determined by fitting points from Figure 63 for a mean d_{50} of 0.54 mm to a power curve to establish a relationship between depth and $U_{cr,s}$. The resulting curve is

$$U_{cr,s} = 0.5522\, h^{0.1232} \tag{7}$$

Equation 7 is plotted in Figure 64 for depths ranging from 0 to 20 m.

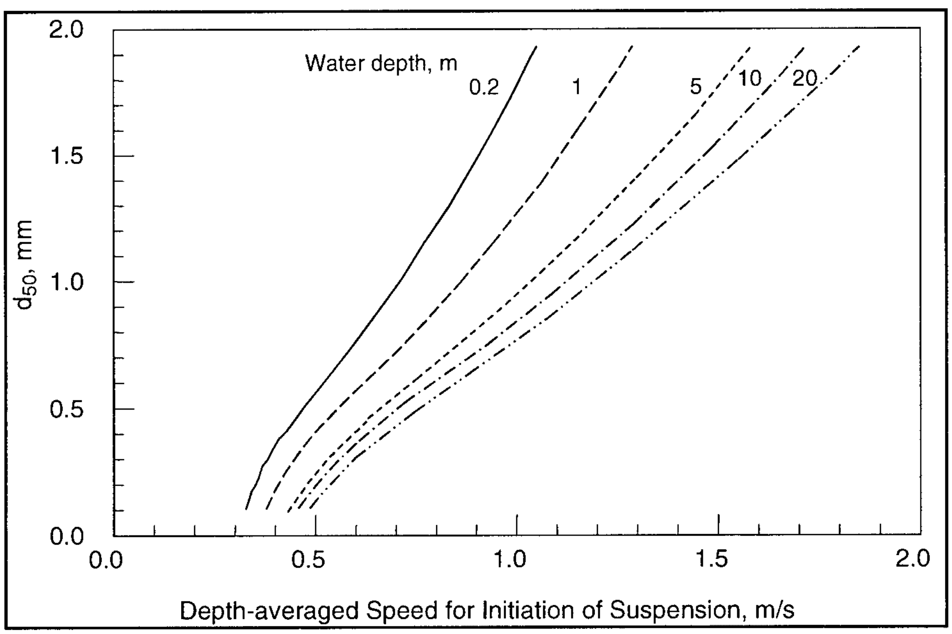

Figure 63. Critical depth-averaged speed for initiation of suspension (modified from van Rijn 1993)

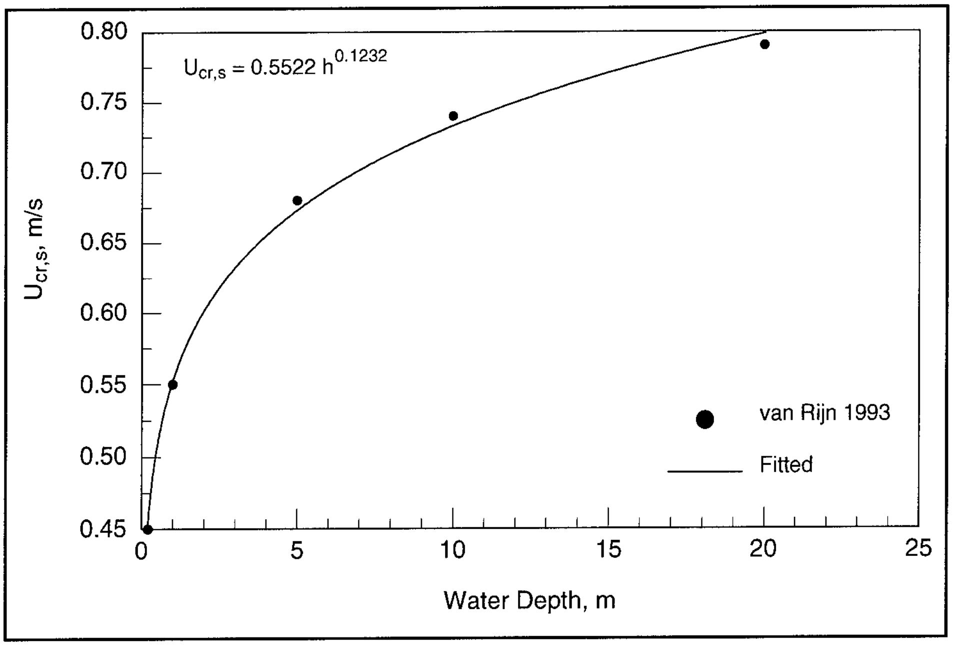

Figure 64. Water depth vs. critical depth-averaged velocity for d_{50} = 0.54 mm

Changes in erosion or deposition patterns for Alternatives 1, 2, 3, 4, and 5 were estimated by subtracting the critical depth-averaged speed of initiation of suspension from the peak ebb and flood current speeds, and comparing those patterns to that for the existing condition (Alternative 0). This speed difference is termed here as the "excess suspension speed" and is calculated as $U - U_{cr,s}$. where U represents the calculated local current speed. The depth-averaged speed for initiation of suspension was calculated for each alternative to account for local changes to this speed owing to deepening by dredging.

Contour plots of excess suspension speed are presented to show areas in which sand with d_{50} = 0.54 mm will be placed in suspension at peak ebb and peak flood current. Colored contours denote excess suspension speed (greater than zero), indicating that the current speed exceeds the depth-averaged speed of initiation of suspension. White areas denote current speed below the critical velocity.

Figure 65 plots the excess suspension speed for Alternative 0, existing condition, at peak flood tide. Areas with excess suspension speed are the inlet, much of the flood shoal, and vicinity of the Ponquogue Bridge. The pattern shown for the flood shoal indicates that material is transported over the front portion of the shoal and onto the middle and back shoal, where it is deposited. There is a strong tendency toward erosion between the jetties (red- and yellow-colored region).

The excess suspension speed at peak ebb tide for Alternative 0 is plotted in Figure 66. Areas in which the current is sufficiently strong to suspend sediment are the East and West Cuts, Ponquogue Bridge, inlet, ebb jet, and limited portions of the flood shoal.

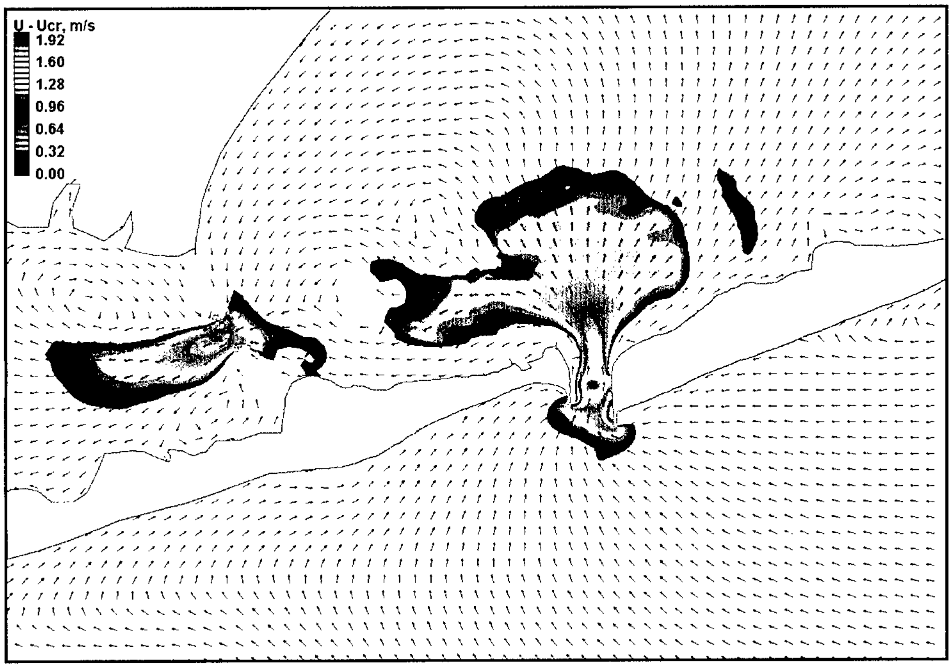

Figure 65. Excess suspension speed at peak flood tide for Alternative 0

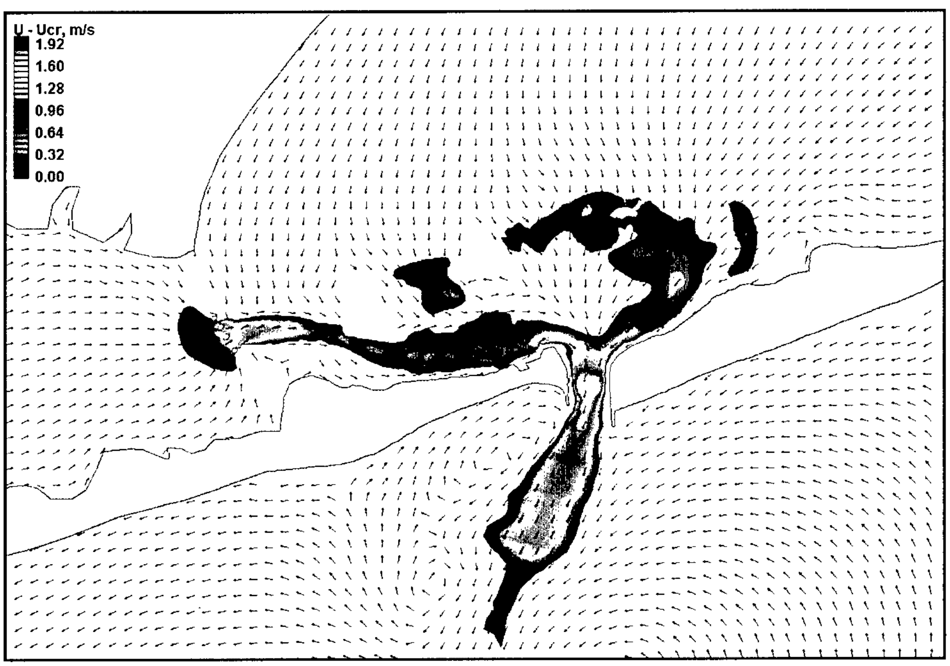

Figure 66. Excess suspension speed at peak ebb tide for Alternative 0

Figure 67 plots the excess suspension speed at peak flood tide for Alternative 1. The patterns are similar to those for Alternative 0 with the exception of an arcuate band of small excess suspension speed located where the fan-shaped flood current weakens. Because this area shows weak initiation of suspension at peak flood flow, it may be depositional over most of the tidal cycle. Thus, the mined area would have a tendency to fill, particularly along its landward edge. Based on this analysis, no areas of Alternative 1 would experience increased erosion as compared to the existing condition during flood tide.

Figure 68 plots the excess suspension speed at peak ebb tide for Alternative 1. The pattern is similar to that for Alternative 0. The eastern portion of the flood shoal shows some small variations from Alternative 0, but significant changes to erosion or deposition are not indicated. The West Cut has a narrower band of excess suspension speed, but the current strength is expected to remain sufficiently strong to carry material out of the channel. Based on this analysis, no areas of Alternative 1 would experience substantial increased erosion over the existing condition during ebb tide.

Alternatives 2, 3, and 4 have excess suspension speeds at peak flood and peak ebb current similar to Alternative 1, and plots are not shown for these alternatives. The only area of notable difference is the arcuate region of weaker current during the flood tide. Alternatives 2, 3, and 4 have weaker excess suspension speed there than Alternative 1, which would tend toward greater deposition in the mined area. Expected erosional and depositional changes are the same as for Alternative 1, with slightly greater deposition on the flood shoal for Alternatives 2, 3, and 4.

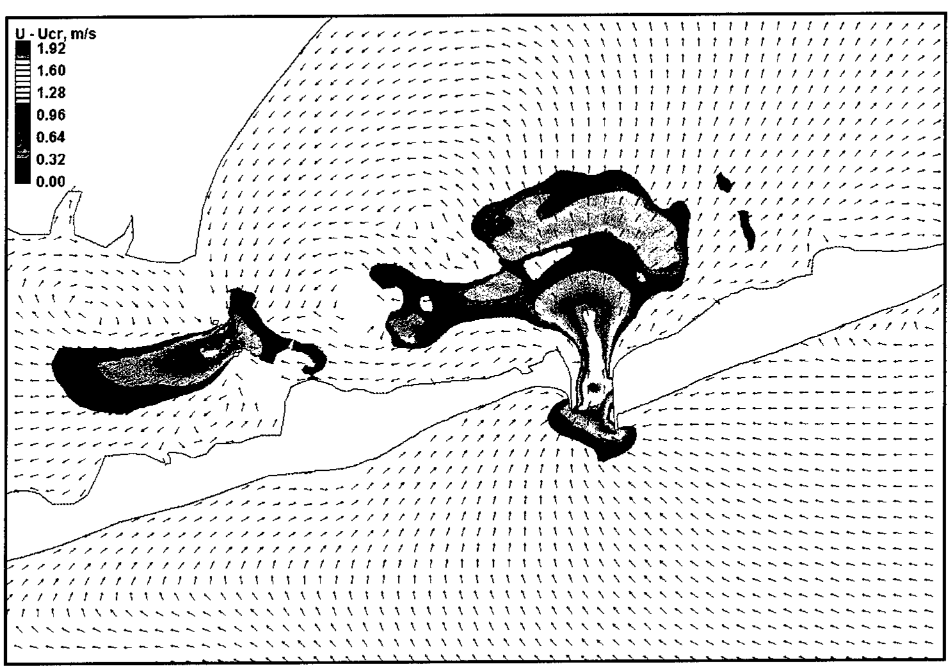

Figure 67. Excess suspension speed at peak flood tide for Alternative 1

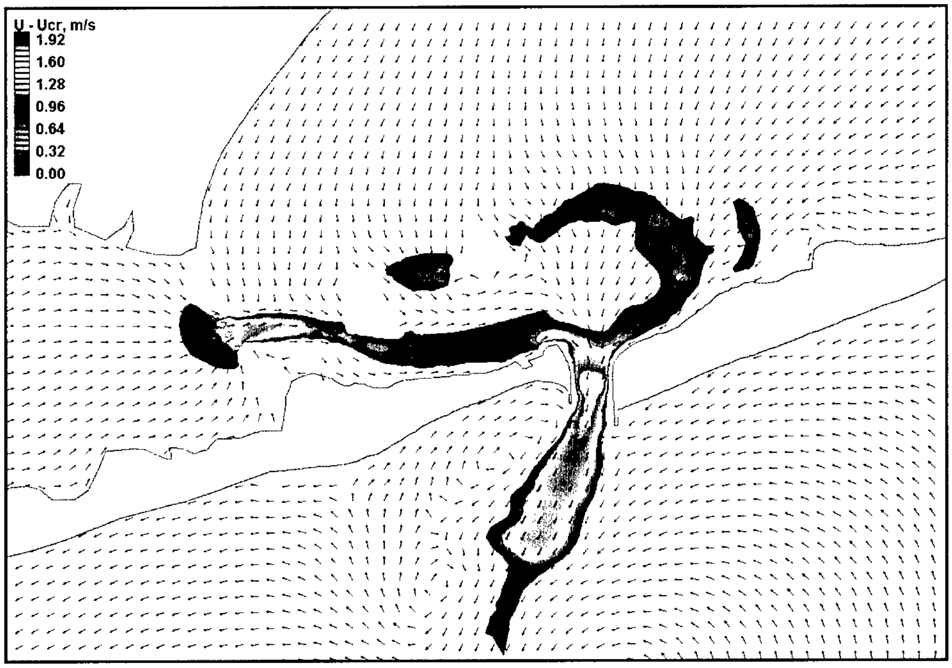

Figure 68. Excess suspension speed at peak ebb tide for Alternative 1

Figure 69 plots the excess suspension speed at peak flood current for Alternative 5. The pattern is similar to that for Alternative 0. The one difference is on the western flood shoal in the area of dredging. There, the excess suspension speed is reduced over that for the existing condition. Deposition of material into the mined area is expected to occur.

The excess suspension speed at peak ebb tide for Alternative 5 is plotted in Figure 70. The pattern shows reduced area of excess suspended speed as compared to that of Alternative 0. Differences are at the east and west flood shoal, East Cut, and West Cut. For these locations, the area of excess suspension speed is decreased for Alternative 5. In particular, the band of excess suspension speed is narrowed and weakened in the West Cut. Alternative 5 would be expected to have increased deposition on portions of the flood shoal, including the mined area, during ebb tide. Because of the weakened current in the West Cut, sand transported south from the flood shoal could be deposited along the northern side of the channel. Erosion is not expected to increase for Alternative 5.

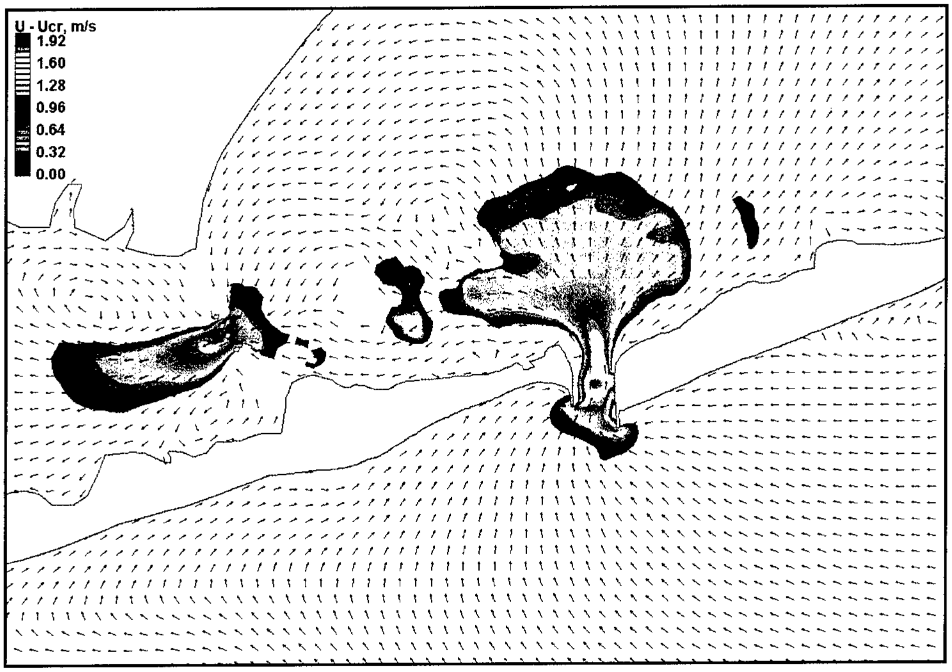

Figure 69. Excess suspension speed at peak flood tide for Alternative 5

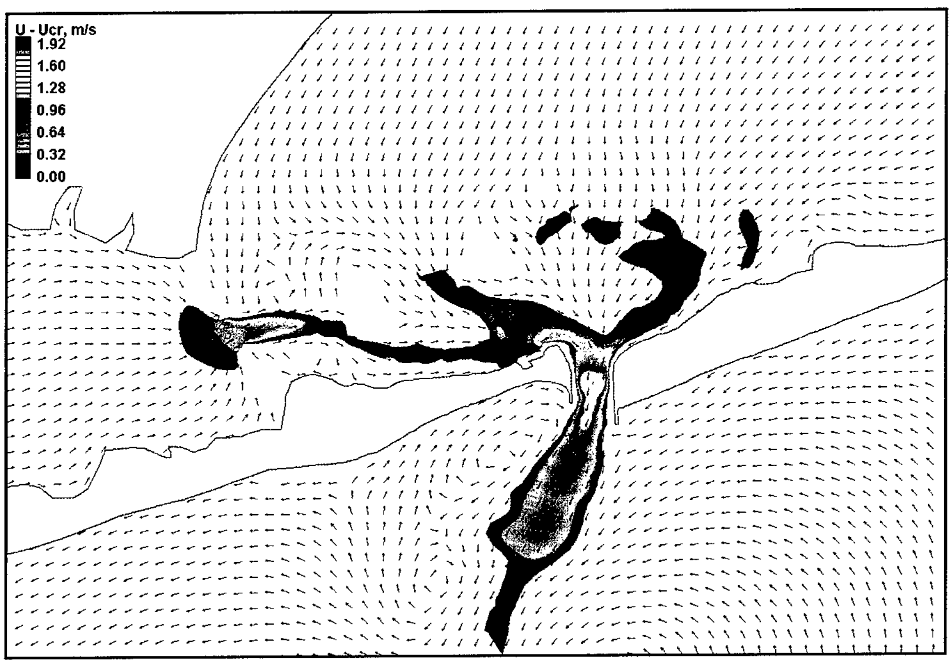

Figure 70. Excess suspension speed at peak ebb tide for Alternative 5

Role of Shinnecock Canal in bay and inlet hydrodynamics

The Shinnecock Canal serves as a one-way conduit (a tidal rectifier) for water to flow from Great Peconic Bay to Shinnecock Bay. To quantify the role of the Shinnecock Canal on the hydrodynamics of Shinnecock Inlet and Bay, a simulation was conducted in which the canal was closed, i.e., water could not enter through the canal. Calculated discharges through Shinnecock Inlet with and without the canal operating are compared in Figure 71. The time series corresponds to a spring tide. Peak flood discharges are almost identical for the two simulations, whereas peak ebb discharges are reduced by 17 percent, on average, for the closed canal. The reduction in discharge during ebb tide with the Shinnecock Canal closed owes to the smaller volume of water in the bay as compared to the present situation of the tidal rectifying gate. In a previous section (see Figure 40), it was shown that the presence of the canal increases the ebb discharge by 4 percent.

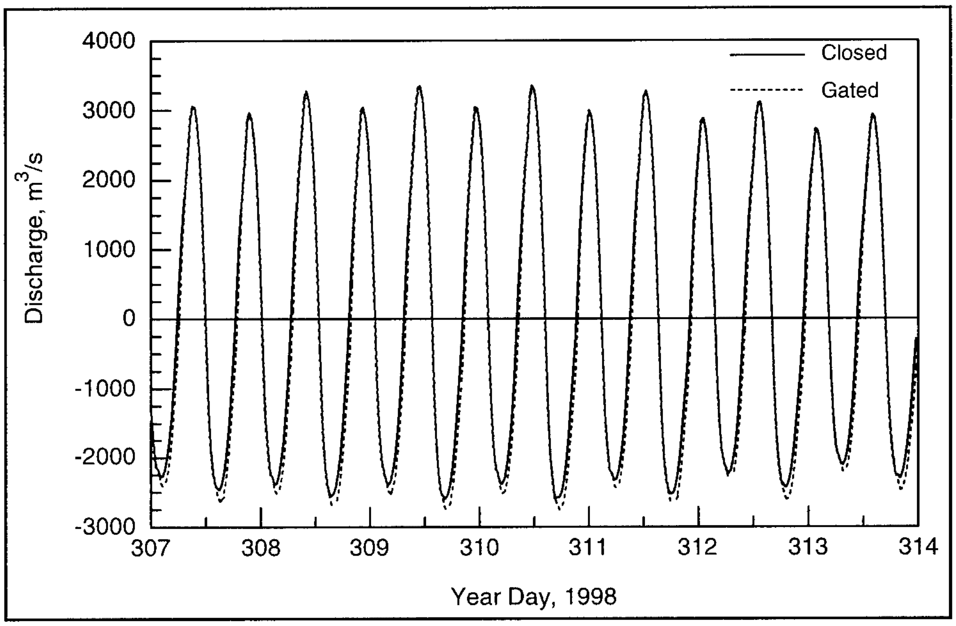

Figure 71. Shinnecock Inlet discharge for Shinnecock Canal gated (existing condition) and closed

Water levels calculated at three points in the bay were compared for the two situations of an operating and a closed canal. The points were located in the western end of the bay near Quogue, the northern bay (north of the flood shoal), and the intersection of the inlet and bay (between the inlet and the flood shoal). For both the open and closed canal, high-tide water level was the same at the respective location. In contrast, the low-tide water levels were lower with the canal closed. Figure 72 compares the water levels for the two situations for the point near the inlet and flood shoal. The low-tide water levels are consistently lower for the closed canal. For the time interval simulated, the minimum water

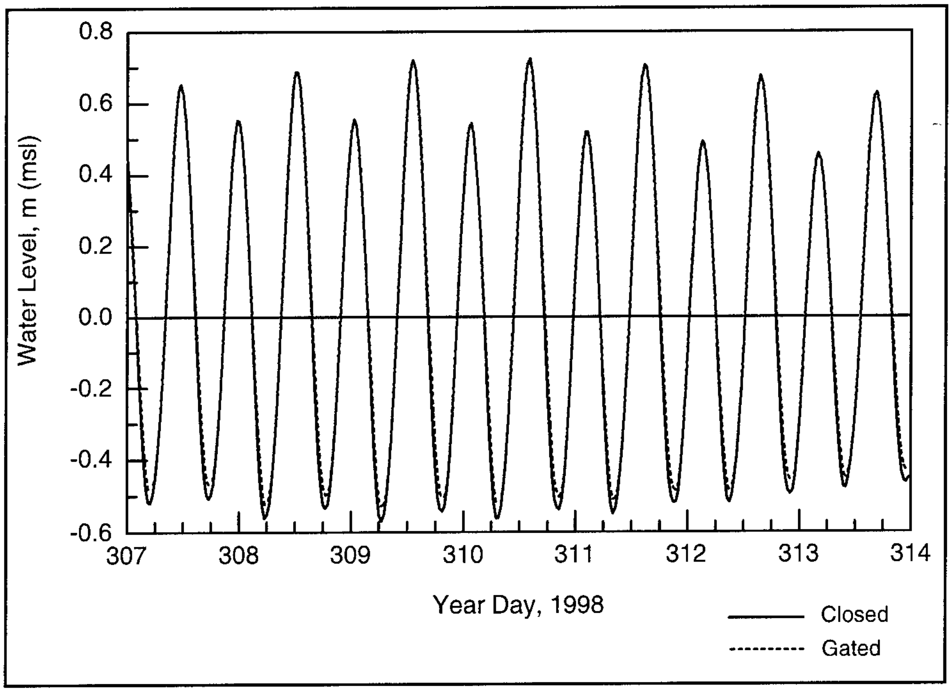

Figure 72. Water level between inlet and flood shoal for Shinnecock Canal gated (existing condition) and closed

levels at ebb tide were reduced by 0.05, 0.07, and 0.04 m for the west bay, north bay, and inlet-flood shoal points, respectively, when the canal was closed.

Summary of circulation modeling for evaluation of alternatives

Preferred alternatives are those that enhance the flow properties of the study site with respect to the study objectives and also do not create or promote adverse conditions. With respect to changes in current speed, Alternatives 1, 2, 3, 4 (Group A), and 5 are preferred. These alternatives do not change the speed within the inlet, with the exception of Alternative 5, which increases the velocity in the center of the inlet during ebb tide. None of these five alternatives change the current seaward of the jetties. In addition, current in the West Cut is generally reduced, with the exception of limited areas near the shore on flood tide. These speed increases are small, ranging approximately between 5 and 15 cm/s (speed values given here are for peak ebb and flood tide and are the maximum values expected to occur).

Alternatives 1, 2, 3, and 4 reduce the current speed west of the Ponquogue Bridge during flood tide and have no change during ebb. Alternative 5 will increase the speed at the bridge slightly (5 to 15 cm/s) during ebb and will create areas of increased and decreased velocity at and west of the bridge on flood tide. These changes in speed will be small (5 to 15 cm/s). However, the current under the bridge under the existing condition is already strong, owing to the constriction created by the bridge pilings, fishing piers, and landfill. If the

current under the bridge is a concern, the most effective remediation would be to reduce the constriction and open the area to more flow.

All of the remaining alternatives, with the exceptions of Alternatives 6 and 7 have both advantageous and disadvantageous flow properties. In particular, alternatives with significantly increased current speed in the inlet, such as Alternatives 8a,b, and 9a,b (Groups D and E) and those with increased discharge, such as 9a,b, must be evaluated to ensure that the enhancements outweigh potential detriments. Alternative 7 increases the velocity on both ebb and flood tide over a wide area ranging from the attachment bar to the Ponquogue Bridge. A significant change in discharge is also expected for Alternative 7 that could alter stability of the inlet. Alternative 6 exhibits small changes in velocity over a limited area east of the Ponquogue Bridge.

An analysis of peak ebb and flood velocity relative to critical velocity for initiation of suspension was conducted for Alternatives 1, 2, 3, 4, and 5. These five alternatives would promote deposition, relative to the existing condition, in the area where material was mined. Thus the mined areas could function as a sediment trap. Erosion is not expected to increase for these five alternatives.

Wave Modeling

Wave properties were calculated for the ebb shoal, inlet, and Ponquogue Attachment areas of the Shinnecock study site by application of the model STeady WAVE (STWAVE) (Resio 1987, 1988; Smith, Resio, and Zundel 1999). The goal of the modeling is to determine the wave transformation and refraction properties for representative wave conditions extending from the attachment to the west jetty. A short description of the model is provided, followed by results of the simulation.

STWAVE numerically solves the equation for steady-state conservation of spectral action along backward-traced wave rays. Source terms include wind input, nonlinear wave-wave interactions, dissipation within the wave field, and surf-zone breaking. STWAVE is a half-plane model, meaning that only waves propagating toward the coast are represented. Wave breaking in the surf zone limits the maximum wave height based on the local water depth and wave steepness. This finite-difference model calculates wave spectra on a rectilinear grid with square cells. Model output is zero-moment wave height, peak wave period, and mean wave direction at all grid points, and two-dimensional spectra at selected grid points.

STWAVE grid development

Two STWAVE grids were developed to calculate wave properties at the site. One grid represents the existing condition and the other represents bathymetry with the Ponquogue Attachment mined (Alternative 7). Bathymetry for the grids was interpolated onto the STWAVE grid from the ADCIRC mesh so that the

depths were the same in both domains. The STWAVE grid is uniformly spaced with cell dimensions of 10 m.

Wave calculations

Three sets of representative waves were developed for the simulations. Each of these sets specified offshore wave height of 1.4 m and peak period of 7.1 s. This combination of height and period was selected because it approximates the annual means of these wave parameters. Offshore wave directions differed for each representative set. The directions were specified as waves propagating from the southwest, south, and southeast. The input was a unidirectional single-peaked narrow spectrum generated by the Surfacewater Modeling System (Environmental Modeling Research Laboratory 1999).

Wave height and direction along the shoreline for the existing condition (Alternative 0) and the mined attachment bar (Alternative 7) were compared. Figure 73 shows the approximate locations of the five numerical stations. Two were specified at the borrow site, and the remaining three were approximately equally-spaced from the eastern end of the borrow site to the west jetty. The positions of Stations 1 and 2 are dependent on the alternative being simulated because the shoreline near the attachment bar changes. The shoreline shown in Figure 73 is for the existing condition. For the mined attachment bar, the shoreline was shifted landward and straightened in the vicinity of the bar (west of Station 3). Numerical stations were located in 2 to 3 m of water.

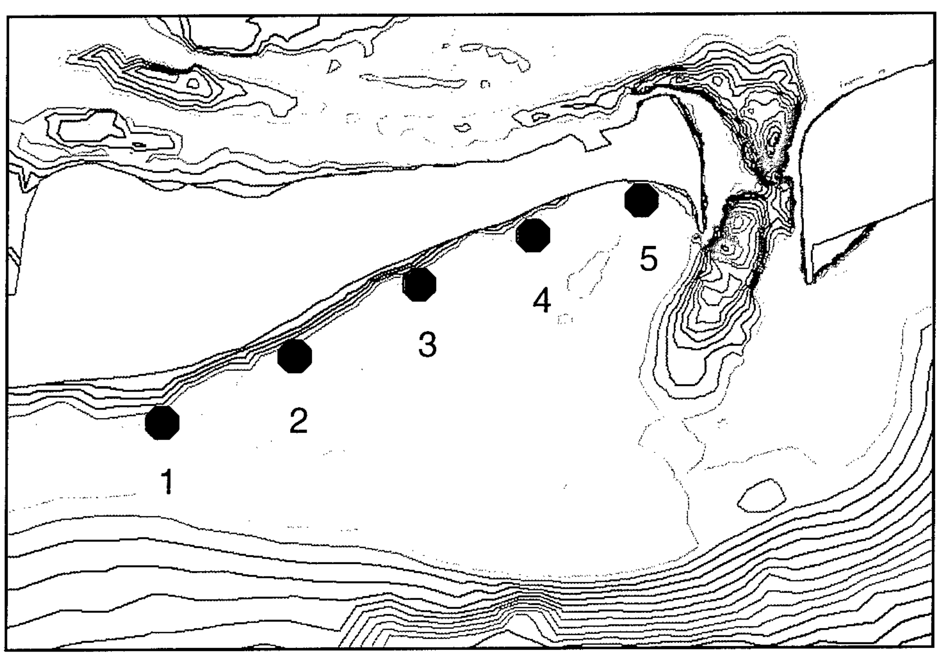

Figure 73. Output locations for wave calculations

Table 12 lists the calculated wave parameters for the numerical stations. Comparison of waves for the existing and mined attachment alternatives gives the following:

SW Waves: West of the ebb shoal attachment bar (Station 1) wave heights increase by 21 percent, and the angle to shoreline becomes more easterly by 4 deg for the mined attachment bar. In the lee of the mined attachment point (Station 3), the wave height increases by 14 percent with no change in direction. To the east, no change in wave properties occurs for the mined attachment.

S Waves: West of the ebb shoal attachment point, waves are not modified by mining of the bar. In the lee of the mined attachment point, the wave height is increased by 14 percent with no change in direction. To the east, no change in wave properties occurs for the mined attachment.

SE Waves: West of the ebb shoal attachment point wave heights increase by 10 percent and direction does not change for the mined attachment. In the lee of the mined attachment point, the wave height is increased by 14 percent with minimal change in direction. To the east, no change in wave properties occurs for the mined attachment.

Comparison of wave properties for the existing condition and the mined attachment bar indicates that change in transport in the erosional area east of the attachment bar will be minimal if the bar is mined. Waves in the lee of the attachment bar (Station 3) experience height increases of approximately 10 percent, increasing wave energy by about 20 percent. This increased energy may impair the safety of swimmers, particularly when storm waves are present. This energy is typical of other locations along this coast. West of the attachment bar, wave heights will increase approximately 20 percent with mining of the bar.

Table 12
Wave Properties at Numerical Stations

Station	Significant Height, m		Peak Period, s		Direction, deg	
	Existing	Mined	Existing	Mined	Existing	Mined
SW Waves						
1	1.07	1.30	7.1	7.1	-38	-34
2	1.00	1.21	7.1	7.1	-29	-35
3	1.04	1.19	7.1	7.1	-15	-13
4	1.28	1.26	7.1	7.1	-15	-14
5	1.11	1.11	7.1	7.1	-32	-32
S Waves						
1	1.35	1.34	7.1	7.1	-23	-21
2	1.44	1.31	7.1	7.1	-13	-14
3	1.04	1.19	7.1	7.1	5	6
4	1.47	1.47	7.1	7.1	1	2
5	1.45	1.44	7.1	7.1	-20	-19
SE Waves						
1	1.22	1.34	7.1	7.1	0	0
2	1.42	1.37	7.1	7.1	16	23
3	1.04	1.19	7.1	7.1	19	21
4	1.30	1.30	7.1	7.1	26	27
5	1.15	1.15	7.1	7.1	-1	0

5 Engineering Analysis of Inlet Morphology Change

This chapter describes an engineering morphologic analysis of the behavior and functioning of the flood shoal and the ebb shoal at Shinnecock Inlet. The flood shoal is part of the inlet morphologic system, and the coastal sediment processes and engineering activity, in particular, dredging, connect these parts. The stability of the inlet is first discussed, and the evolution of the flood and ebb shoals is quantified with a new mathematical model of inlet shoal volume change by which evolution of the volume of the flood shoal after sand mining can be estimated.

Inlet Stability

The phrase "inlet stability" both refers to the location and alignment of an inlet and to its entrance cross section. Jetties have stabilized the location of Shinnecock Inlet and fixed its width at 800 ft. Here, interest is in the stability of the cross section of the inlet, customarily defined as the area of the inlet entrance below mean sea level (msl). Because the width is fixed, the change in cross-sectional area occurs through change in the depth along the channel.

Jarrett (1976) summarized the state of knowledge of cross-sectional area stability for inlets of the United States, including a review of previous empirical correlations and compilation of a large database. He presented predictive relations for the Atlantic, Gulf, and Pacific Ocean coasts classified according to whether the inlets have two, one, or no jetties. For the Atlantic Ocean coast and inlets with two jetties, he found

$$A_C = 5.37 \times 10^{-5} P^{0.95} \tag{8}$$

where A = minimum cross-sectional area of the entrance channel below msl, expressed in ft^2, and P = tidal prism corresponding to the diurnal or spring range of tide, expressed in ft^3. The tidal prism controlling the inlet cross-sectional area is considered to be the mean maximum prism, which is associated with the spring tidal range. Other data, including the tide range in the bay, discharge through the inlet, depth in the inlet, and bay area are available for a stability analysis.

Escoffier (1940) introduced the concept of a closure curve through an inlet stability diagram such as shown schematically in Figure 74. The closure curve is a plot of the velocity through an inlet as a function of the inlet's cross-sectional area. The curve is a balance between the tidal force sweeping sediment out of the channel and the littoral transport bringing sediment to the inlet channel.

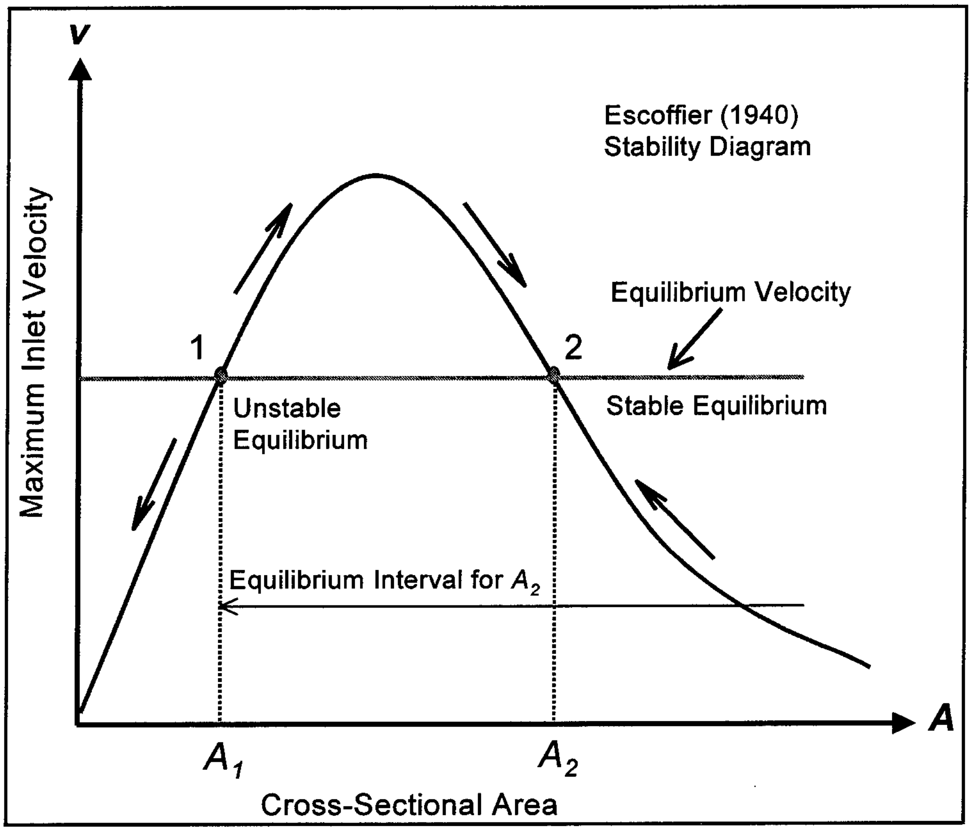

Figure 74. Definition sketch for the Escoffier (1940) stability diagram

The velocity that can maintain an equilibrium or minimum cross-sectional area intersects the closure curve at two locations. The first intersection, denoted by the number 1 at the area A_1, is an unstable equilibrium because if the current velocity through the channel falls below the equilibrium velocity, sediment will accumulate in the inlet, reducing the velocity further by friction, to eventually close the inlet. If the area is slightly greater than A_1, the velocity will increase, and the area of the inlet will increase. The cross-sectional area A_2 is a stable equilibrium because if the channel cross-sectional area increases, the velocity will decrease over the larger cross section, thereby decreasing the area by sweeping less sediment away. Bruun and Gerritsen (1960) and others have shown empirically that the inlet "mean-maximum" velocity necessary to maintain a stable inlet on a sandy shore must be equal to or exceed about 1 m/s (3.3 ft/s). This velocity is the mean of the maximums that would occur for the diurnal tide or spring tide.

The velocity through an inlet changes with the tide and under other forces, as does the amount of sediment brought to the channel by transport along the shore. Therefore, the actual cross-sectional area of a mature inlet will vary with time about the stable equilibrium. An inlet may close if too much sand is deposited in it, as from a storm, because its cross-sectional area falls below A_1 in Figure 74. An inlet can also achieve a larger equilibrium area if dredged to a new depth such as to increase the tidal prism by decreasing the friction through the inlet.

Seabergh and Kraus (1997) developed a software package to compute the Escoffier closure curve and equilibrium velocity based on the tidal prism – inlet area relationships presented by Jarrett (1976). The program can be calibrated by comparing calculations to measurements of the velocity in the inlet and amplitude of the tide in the bay. By referring to Chapter 3, the amplitude of the ocean tide is 1.65 ft; representative measured amplitude of the tide in Shinnecock Bay is 1.4 ft; and a representative mean maximum current velocity in the inlet is in the range of 4 to 5 ft/s. The bay area[1] was taken as 4.09×10^8 ft^2, and the Manning friction coefficient was specified as 0.03. Inlet geometry was width of 800 ft, length of 3,000 ft, and hydraulic radius of 25 ft based on the 1998 SHOALS survey data.

The calibrated model was then run to produce the closure curve for the existing condition, as shown in Figure 75. Several runs were made with reasonable variations of the input parameters, and the closure curve maintained the same general quantitative form.

In 1998, the cross-sectional area of the inlet was 16,000 ft^2 (Morang 1999). This position on the closure curve indicates that Shinnecock Inlet is stable and has velocities near the maximum possible for the given ocean tidal range, bay area, and inlet geometry. With time (after several decades, as discussed in the next section), the cross-sectional area of the inlet will increase, and the current velocity through the inlet will decrease to about 3.2 ft/s from its present mean maximum of about 4.6 ft/s. The reduction in velocity will improve navigation conditions for the inlet through decreased ebb current velocity.

The intersection of the closure and the equilibrium velocity curves indicates a stable cross section of about 29,000 ft^2. With a jetty-to-jetty width of 800 ft, the average depth of the channel is expected to be 36 ft. At present, locations in the channel exceed this depth, as shown in Figure 76. If the ebb flow is not directed down the center of the inlet and the channel takes the same form as present, then the depth will be greater than 36 ft near the northeast corner of the east jetty.

[1] Area calculated by Dr. Andrew Morang, Research Physical Scientist, U.S. Army Engineer Research and Development Center, Coastal and Hydraulics Laboratory, Vicksburg, MS, from the NOAA medium-resolution digital vector shoreline, which represents the high-water shoreline on published nautical charts.

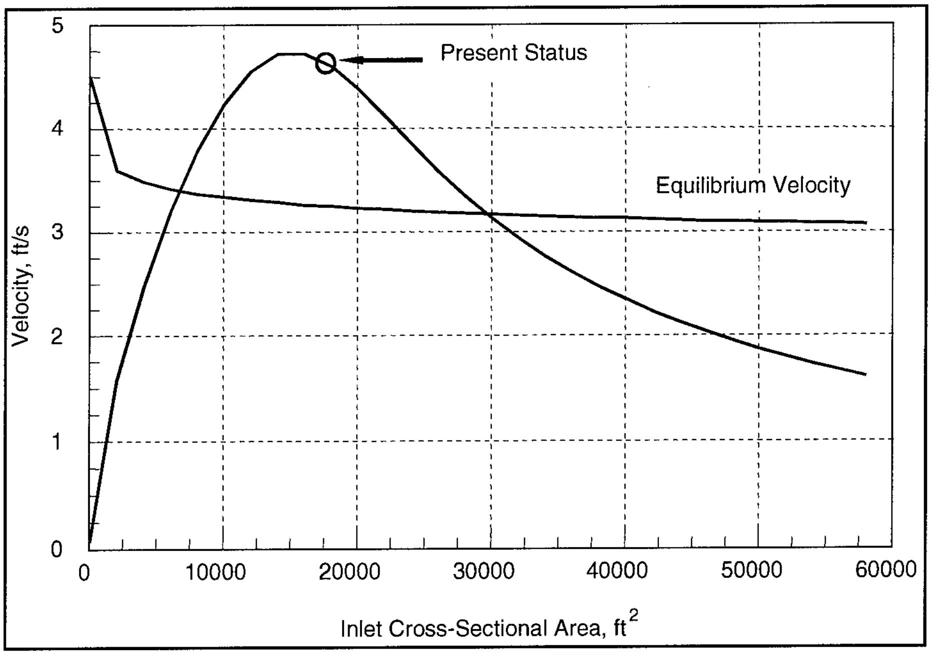

Figure 75. Closure curve for Shinnecock Inlet

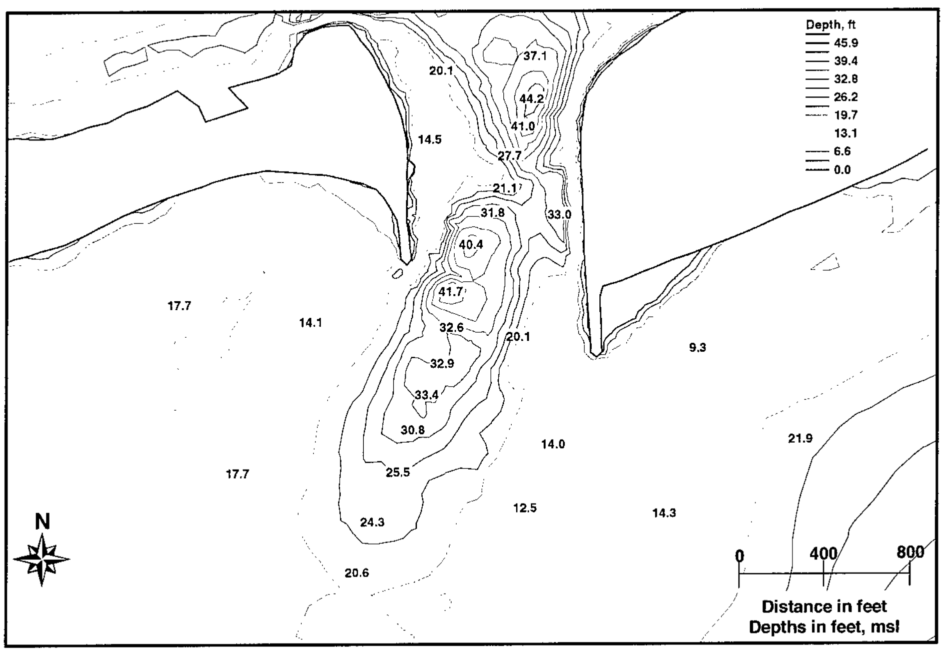

Figure 76. Depth contours in Shinnecock Inlet from 1998 survey

Ebb Shoal

The ebb shoal at Shinnecock Inlet is outlined clearly in Figure 4 (a photograph taken on a calm day). The skewed shape of the ebb shoal indicates that the net longshore sediment transport at the inlet is strongly directed from east

to west. One can infer that sediment moving east reaches the east jetty, and then it either travels along the bar to the seaward portion of the ebb shoal (where it can be bypassed to the attachment bar at the Ponquogue Pavilion) or it is transported into the deposition basin. Other more complex sediment transport paths are possible.

Morang (1999) computed the volume of the ebb shoal from available survey data, as listed in Table 13, and found that its volume has been increasing. Based upon similar but more limited data, Williams, Morang, and Lillycrop (1998) correlated the volume with the predictive relation of Walton and Adams (1976), from which the equilibrium volume of an ebb shoal can be estimated from knowledge of the tidal prism.

Walton and Adams (1976) developed predictive equations for the equilibrium volume of an ebb shoal according to the tidal prism and amount of wave exposure of the coast where, for example, the Pacific Ocean coast is considered highly exposed, and the Gulf of Mexico coast is mildly exposed. The equation for moderately exposed coasts is most applicable to Shinnecock Inlet and is given as

$$V_{Ee} = 10.5 \times 10^{-5} P^{1.23} \tag{9}$$

where V_{Ee} is the volume of the ebb shoal at equilibrium (a mature shoal) expressed in cubic yards, and the prism P is expressed in cubic feet. Walton and Adams (1976) give a value of 10.7×10^{-5} for the empirical coefficient describing all inlets in their database, indicating that Equation 9 will give a reliable estimate for Shinnecock Inlet.

Available measurements of the tidal prism (converted from measurements of the discharge) are listed in Table 7. The values of the prism were entered into Equation 9, and the results are plotted in Figure 77. Although the points plot on an apparent straight line, suggesting a near linear increase in the tidal prism with time, it is probably more accurate to note that the prism changed from that of a nearly natural inlet in the 1940s to that of a dredged inlet with jetties in the 1990s. The inlet was inefficient in the 1940s because it was open to receive sediments moving alongshore. In contrast, in the 1990s, when the jetties were present and the deposition basin was dredged, the inlet became highly efficient. The July 1993 data were evidently taken during neap tide or during a mixed tide and meteorological event that reduced the flow.

On the assumption that the tidal prism will not increase substantially in the future, the volumes shown in Figure 77 that were calculated with Equation 9 indicate that the equilibrium volume of the ebb shoal will reach the range of between 15 to 20 million yd^3. Therefore, according to Table 13, as of 1998 the ebb shoal at Shinnecock Inlet had achieved approximately 50 to 66 percent of its final, equilibrium volume. The growth of the ebb shoal is discussed in the following section on morphology modeling.

Table 13 Volume of Ebb Shoal and Flood Shoal (from Morang 1999)				
Survey Date	Cut, yd^3	Fill, yd^3	Total, yd^3	Total, m^3
Ebb Shoal[1]				
Jul-Aug 1949	17,500	1,043,000	1,025,000	784,000
June 1984	747,000	5,245,000	4,498,000	3,439,000
May 1996	856,000	8,446,000	7,590,000	5,803,000
Aug 1997	712,000	8,544,000	7,832,000	5,988,000
May 1998	933,000	9,385,000	8,453,000	6,463,000
Flood Shoal[2]				
Jul-Aug 1949	445,000	1,123,000	678,000	518,000
Nov 1955	507,000	1,145,000	638,000	488,000
May 1998	4,163,000	3,684,000	-479,000	-366,000

[1] Volumes indicate change from pre-inlet condition, based on 1933 survey data. Does not include sand losses and gains from the barrier island because the 1933 data set did not cover the barrier topography.
[2] Volumes indicate change from pre-inlet condition, based on 1933 survey data. Does not include sand losses and gains from the barrier island. Cut values should be greater because the 1933 survey did not include the area directly north of the present barrier where navigation channels have been dredged.

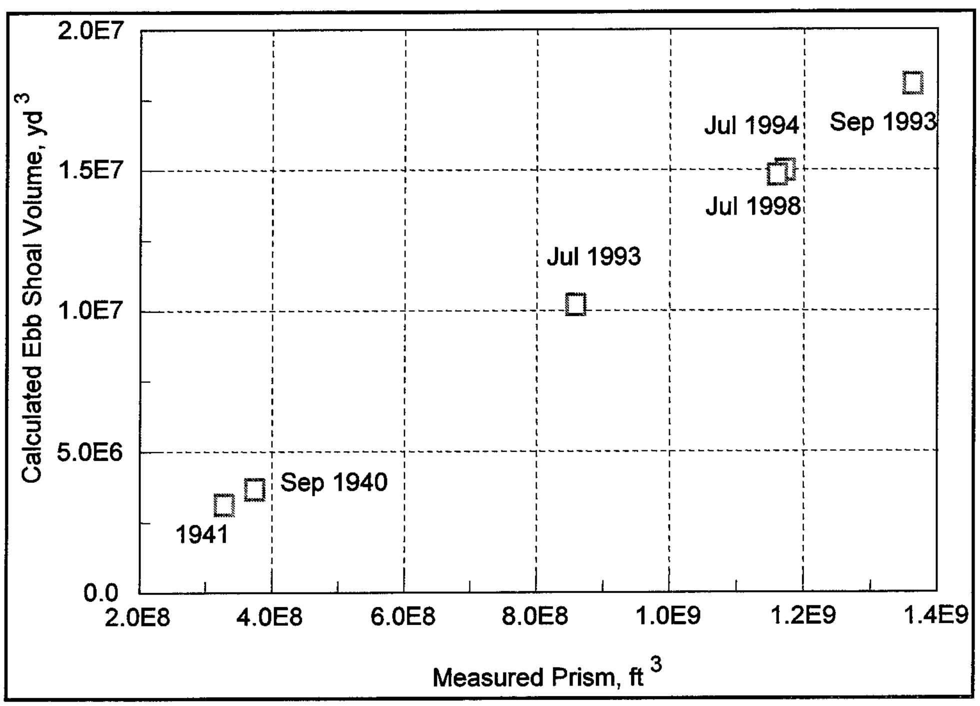

Figure 77. Volume of the ebb shoal calculated with measured tidal prism

Flood Shoal

This section reviews the morphology and evolution of the flood shoal.

Morphology and growth of flood shoal

A flood (tidal) shoal is an accumulation of sediment on the landward side of an inlet. The shoal is formed of sediment that is transported to it by the flood current. Flood shoals are increasingly being identified as persistent causes of sedimentation of navigation channels and waterways (often, intracoastal waterways) that run by them. Figure 78 displays the terminology associated with flood shoals, according to Hayes (1980). In contrast to the relatively regular crescentic shapes of ebb shoals on coasts where there is significant wave action, such as at Shinnecock Inlet, flood shoals are complex morphologic features. Ebb shoals form in a balance of the sediment-transporting forces associated with waves and the ebb jet. In contrast, there is little wave action in the bay or estuary located landward of an inlet, so a flood shoal will tend to spread to fill the bay or to choke the inlet, causing the margin channels around it to migrate.

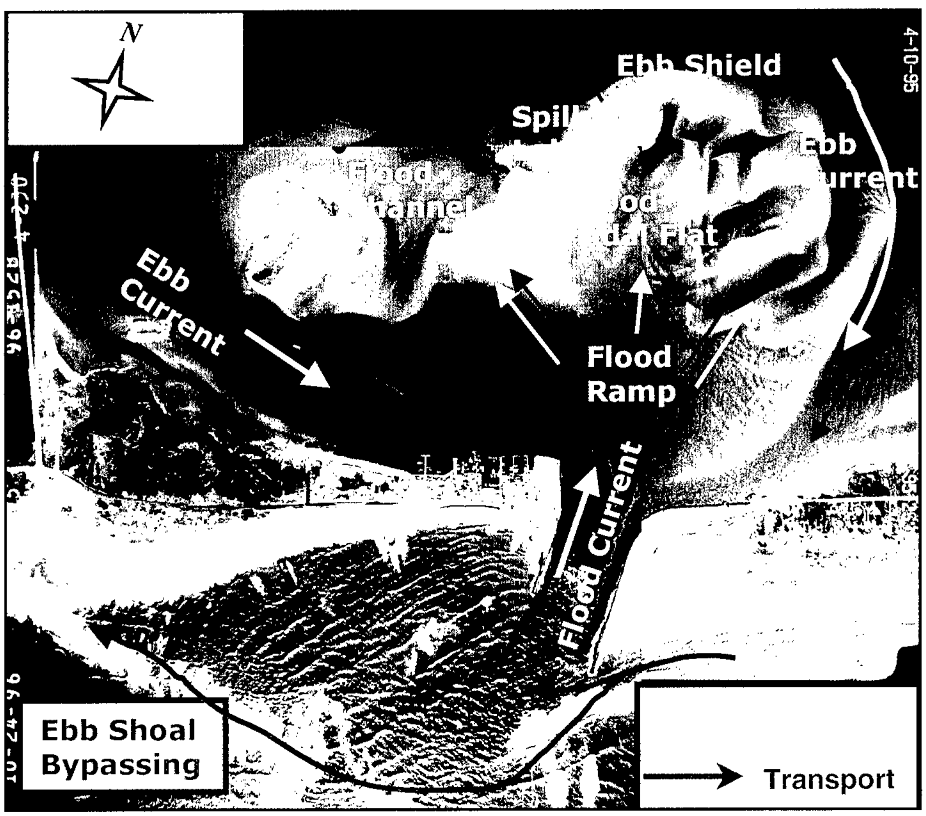

Figure 78. Morphologic notation for flood shoals (composite photographs of 10 April 1995 and 24 October 1996)

The large difference between nearshore and bay bottom configurations is another factor that influences and distinguishes the morphology of flood and ebb shoals (Dean and Walton 1973). The nearshore tends to have a monotonically increasing depth with distance offshore, with the exceptions of local perturbations by longshore bars, whereas the bottom of the landward sides of inlets can vary greatly from inlet to inlet, but is typically flat. Also, the mainland and islands are located at varying distances from inlets, exerting different constraints on the shape of the flood shoals. This discussion is a site-specific simplification of complex morphology formed under different balances of forcing conditions and controlling factors. FitzGerald (1996) can be consulted for more information.

Tidal flow over and around a flood shoal is also complex. On flood flow, water enters the bay in a relatively narrow jet that expands with distance from the inlet, given adequate space. Within the relatively narrow confine of the jet, the flood current carries material over the centrally located ramps, where it disburses and settles in a characteristic fan-shaped form. Flood channels may break through the shoal, creating semidistinct sub units, and spillover lobes are formed from sediment pushed bayward off the shoal. When the water level in the ocean begins to fall, the ebbing current in the bay arrives to the inlet from all directions, with the strongest currents flowing in the deeper water on the sides of the flood shoal, creating ebb spits directed toward the inlet. The hydraulically efficient deeper channels located along the margins of the shoal (at Shinnecock these run along the east and west margins) carry more of the flow because the shallow water over the flood shoal creates stronger resistance. The pattern of current qualitatively described here and indicated in Figure 78 was demonstrated quantitatively in the numerical simulations shown in Chapter 3.

At Shinnecock Inlet, the aerial photographic record (Appendix A in Morang 1999) indicates that local interests favor dredging of the east margin channel (and have tried on occasion to dredge through the center of the shoal). The Federal navigation channel runs to the west and meets the LIWW.

Sediment pathways at inlets are partially understood but have not been quantified. The daily periodic bidirectional tidal current over the flood shoal transports sediment from the inlet channel during flood and furnishes a smaller amount of sediment to the channel during ebb. At one inlet, Smith and FitzGerald (1994) identified sediment pathways and made quantitative estimates of transport rates on an ebb shoal based upon measurements of the current and bathymetry. They found that the sediment transport-paths over and around the shoal depended upon the stage of tidal flow. Smith and FitzGerald concluded that the total quantity of sediment exchanged between morphologic features in gyres or circular paths was large compared to the net longshore transport along the particular coast that would bypass the inlet (cf. review of Komar (1996) for related information).

Flood shoals have received little study compared to ebb shoals, probably because they are complex features, are often modified by dredging of navigation channels, and until recently have held little engineering interest because of potential environmental restrictions that might preclude their modification. Carr (1999) reviewed the state of knowledge on flood-shoal morphology and made several advances of relevance to the present study. Her research concerned inlets

on the east and west coasts of Florida, but the concepts and quantitative results appear to be applicable to Shinnecock Inlet.

Carr (1999) distinguished a flood shoal as consisting of two parts, a "near-field shoal" and a "far-field shoal." (She employed the word "delta" instead of "shoal," but in the present context the meanings are the same.) The near field is that portion of the flood shoal located closer to the inlet and readily discernable in photographs at low tide, whereas the far field is a deeper area of sediment accumulation located landward or bayward of the near field portion. Ebb shoals eventually achieve a dynamic equilibrium volume (Walton and Adams 1976), after which sediment is bypassed to the adjacent beach by longshore currents generated by waves breaking on the shoal. In contrast, Carr (1999) concluded that the near-field portion of a flood shoal approaches an equilibrium value, while serving as a sediment supply for flood currents to sweep sediment bayward to the far-field portion. In the absence of constraints exerted by the bay topography, the far field flood shoal appears capable of potentially unrestricted growth. Carr (1999) also determined predictive expressions for the volume of a flood shoal in terms of the tidal prism, and these are introduced in the following section.

The aerial photographic record and bathymetric surveys indicate that the flood shoal formed rapidly after the inlet opened during the 21-24 September 1938 storm. Some material may have been swept bayward to start the shoal when the barrier island breached. Figure 79 shows contours of the bathymetry from the available surveys from the years 1933, 1949, 1955, and 1998. Elevations are in units of feet referenced to NGVD, and the coordinates are state plane easting and northing expressed in feet. Deeper water is darker blue, zero-depth is white, and elevations above NGVD move toward darker brown with increasing elevation. The blank areas in Figures 79(b-d) indicate sparse data or absence of data. The surveys did not include the barrier island, so the northing limit at the bottom of the figures is located at some distance northward of the island.

Prior to formation of the present inlet in 1938, the depth of the bay bottom closest to the barrier island ranged between approximately 3 to 6 ft, and a 10-ft deep basin occupied the central portion of the bay (Figure 79a). The survey of 1949 (Figure 79b) shows modern incipient flood shoal, which already had elevations at 0 ft in broad areas. In addition, it appears that some sediment in the far field of the shoal had reached the basin. The beginnings of both the east and west margin channels are apparent in 1949.

By 1955 (Figure 79c), the east channel had deepened or had been dredged to about 12-ft depth, and in 1998 (Figure 79d) the shoal had clearly gained substantial elevation in both the near field and far field. The margin channels in 1998 had reached 20-ft depth in some locations. Because the authorized depth of the inner navigation channel is 10 ft plus 1 ft each of overdredging and advance dredging, the deeper water in the channels can be attributed to scour by the tidal current.

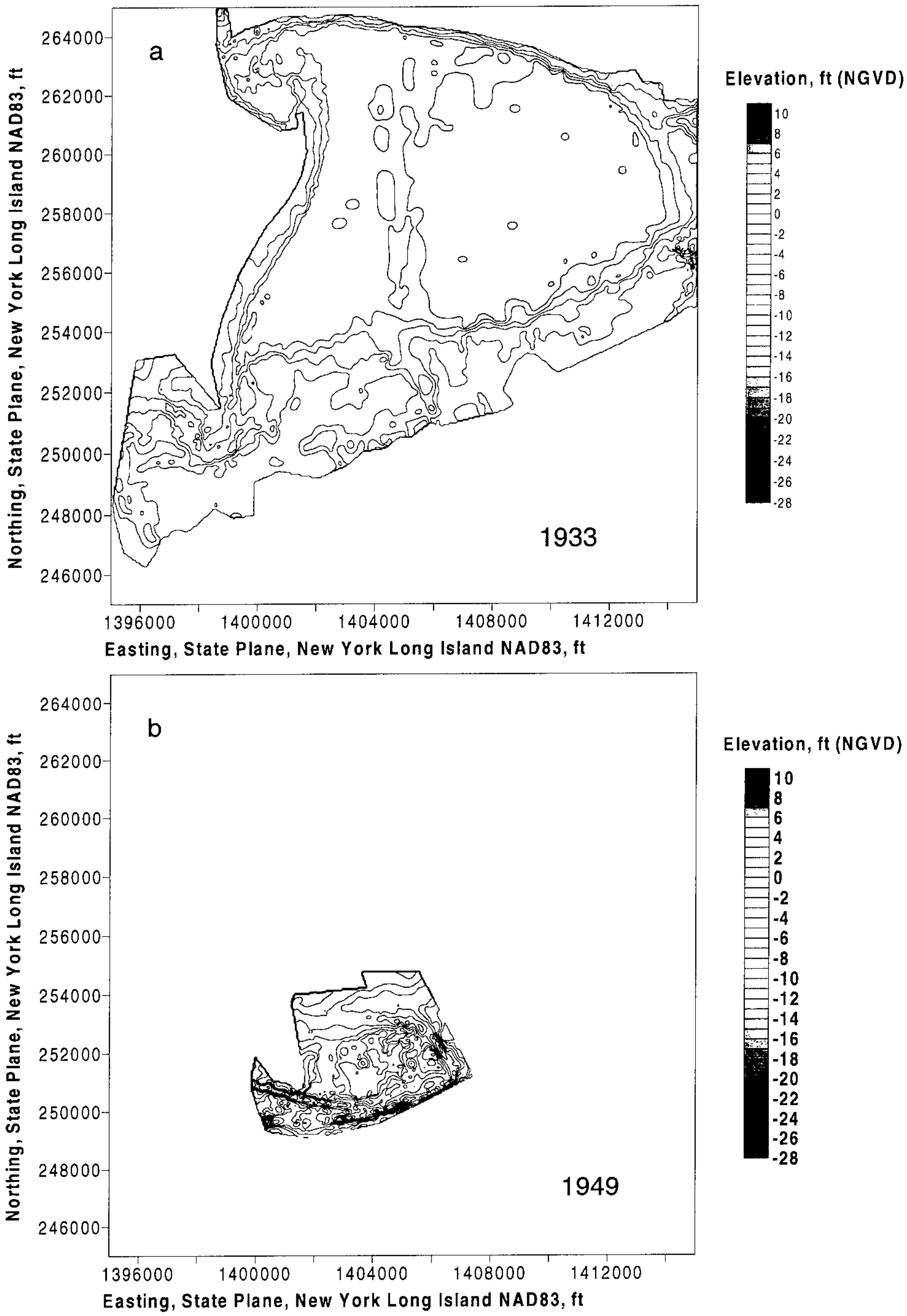

Figure 79. Bathymetry of Shinnecock Bay in the vicinity of the present location of the inlet, indicated by the dark bar and notation "inlet." Data compatible with Morang (1999) (continued)

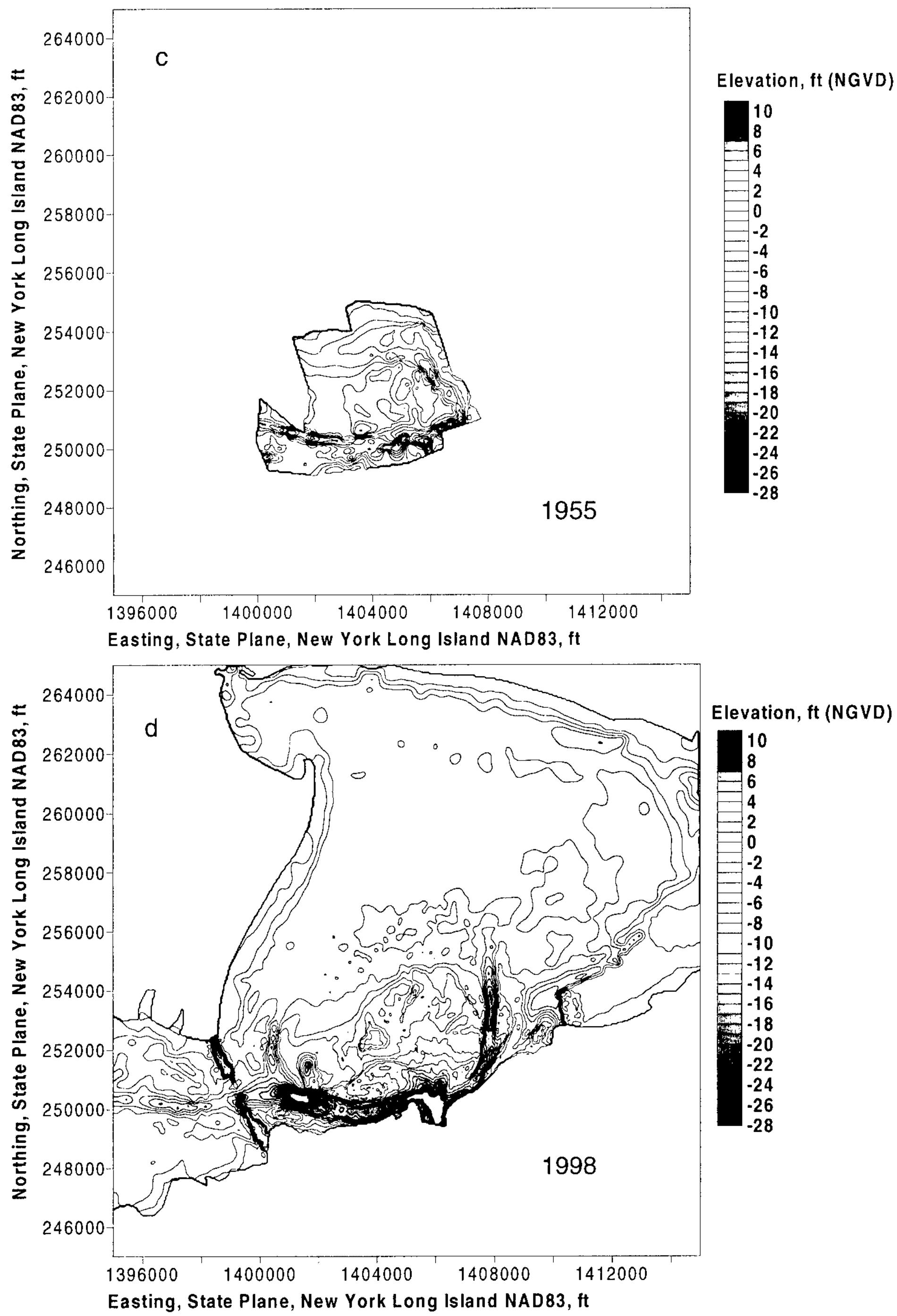

Figure 79. (concluded)

Volume of flood shoal

Morang (1999) calculated the change in volume of the flood shoal by computing the differences in elevations of available bathymetric surveys taken in different years, and his results are listed in Table 13. He found that the region of the bay occupied by the flood shoal and including the margin channels had lost volume since 1933 (Figure 80). The volumes labeled "Cut" in the figure indicate material removed through dredging, and the volumes labeled "Fill" indicate the gain in material evident in aerial photographs. The volume remained constant for the surveys made in July-August 1949 and in November 1955, indicating that either equilibrium volume had been reached for the areas covered by the surveys or that the inlet was closing and becoming inefficient in transporting sand to the flood shoal. Both jetties were in place by 1956, and in 1990 the deposition basin was dredged to –20 ft mllw. It is concluded that the more efficient hydraulic system of jetties and dredging caused the volume of the flood shoal to increase notably.

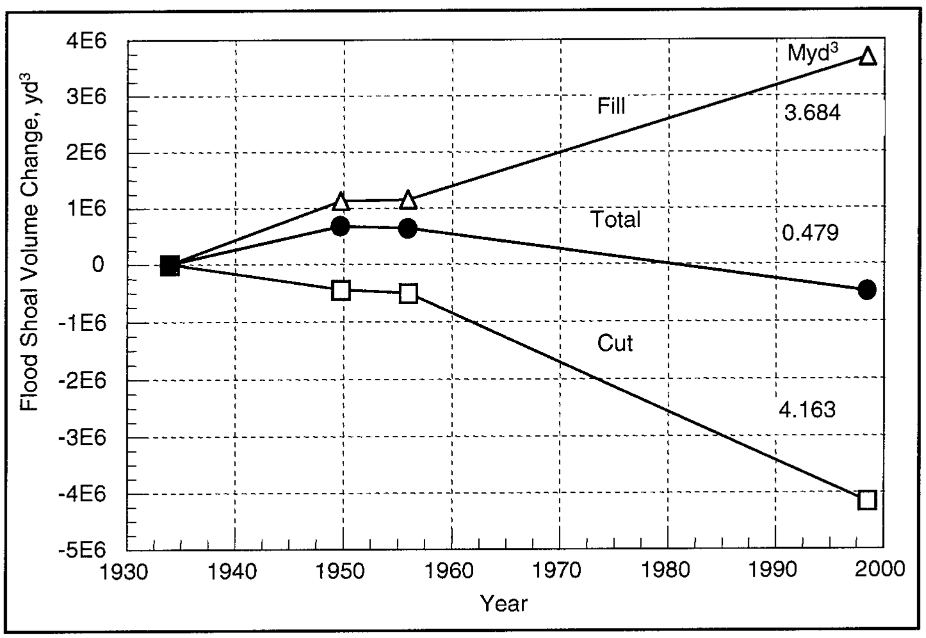

Figure 80. Growth of flood shoal from September 1933 to May 1998 (values from Morang 1999)

The line labeled "Total" in Figure 80 indicates that the shoal area lost volume, but this does not mean the flood shoal itself lost volume from 1955 to 1998. Rather, dredging in the area of the shoal removed more material than was transported to it, in particular in taking material below the ambient bay bottom. Because the flood shoal is growing and encroaching into the east and west channels, these channels have been dredged numerous times. The amount of material expected to comprise the flood shoal, had dredging not occurred, can be estimated by drawing a perimeter of the expected size of the shoal (including

segments of the east and west navigation channels) and multiplying that area by an average thickness of the existing shoal. The April 1995 photograph of the shoal was analyzed to estimate the area of the near-field flood shoal at 20 million ft^2. An average thickness of the existing shoal was specified as 7 ft above the ambient bottom of the bay. These values give a volume of 5 million yd^3 for the potential volume of the near-field portion of the flood shoal in April 1995.

Carr (1999) presents empirical equations to estimate the volume of a flood shoal, based on the tidal prism. The relations were developed by best fit to data for a large number of inlets located on the east and west coasts of Florida. Scatter in the data sets was great, making correlation coefficients low, but visual examination of the fits show that the predictive equations reproduce trends. The equations of Carr (1999) were developed for the tidal prism expressed in cubic meters per second, yielding areas of the shoal in square meters and volumes in cubic meters. Conversion to non-SI units was performed on the calculated results (area and volume). The volume of the near-field portion of a flood shoal *VN* is given as

$$VN = 4.06 \times 10^3 P^{0.314} \tag{10}$$

where the tidal prism is expressed in m^3/s. The total volume VT of the flood shoal (volumes of the near field and the far field), was found to be

$$VT = 2.04 \times 10^4 P^{0.296} \tag{11}$$

Calculation results of Equation 10 and Equation 11 are plotted in Figure 81. The total volume corresponding to recent measurements of the tidal prism approximately agrees with the measurements of fill as shown in Figure 80 and with an estimate of 5 million yd^3 arrived at independently from inspection of a recent aerial photograph. The conclusion is that the predictive relationship of Carr (1999) can give guidance on the volume of the flood shoal at Shinnecock Inlet as a function of the tidal prism and that, if the tidal prism increases, the volume of the flood shoal will increase.

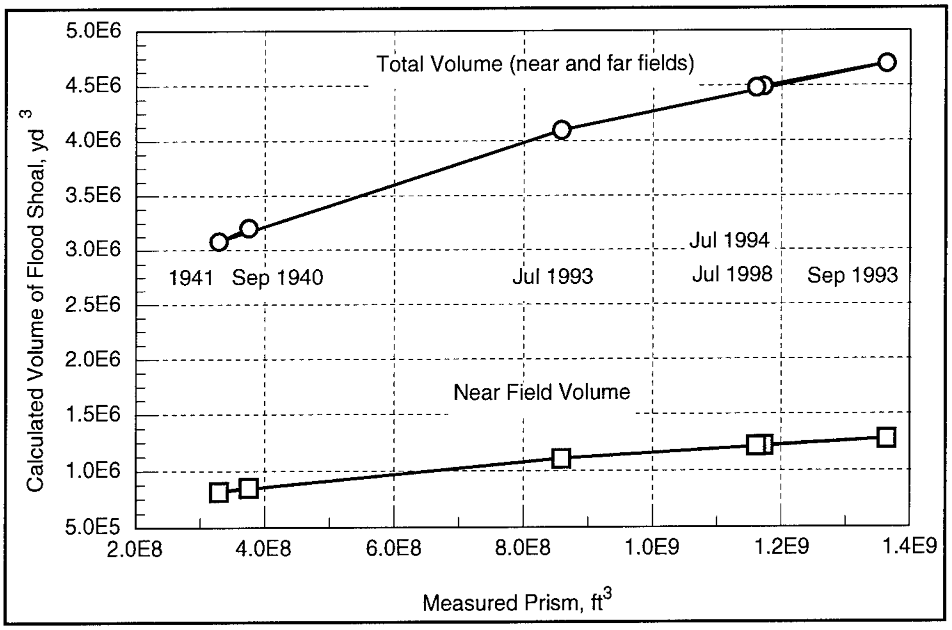

Figure 81. Volume of flood shoal calculated from the measured tidal prism

Inlet Morphology Reservoir Model

As previously discussed, sediment transport paths and mechanisms at inlets are only partially and qualitatively understood, and calculation of morphology change by fundamental principles is beyond present capability. To make progress in describing the evolution of large-scale morphological features, Kraus (2000a,b) introduced an inlet morphology reservoir model that represents sediment pathways and volume change, by analogy to a series of connected reservoirs. In the reservoir model, each morphologic feature is represented by its volume, and the volumetric exchanges among features are connected by equations describing the sediment pathways. Central assumptions of the reservoir model are:

a. Mass (volume) of sediment is conserved.

b. Morphological forms and the sediment pathways among them can be identified, and the morphologic forms evolve while preserving identity.

c. Stable equilibrium of the individual morphologic forms exists.

d. Changes in meso- and macro-morphological forms are reasonably smooth.

e. The amount of material leaving a morphologic feature at a particular time is proportional to its volume and the transport rate to it at that time.

The reservoir model was shown to reproduce the growth of the ebb-tidal shoal at Jupiter Inlet, FL and at Ocean City, MD. The present application is the first project-support use of the model. Results must be reviewed critically until capabilities and limitations of the reservoir model are understood.

The reservoir model will be presented in two applications of increasing complexity. The first application gives an overview of the model by restricting it to calculate the growth of the ebb shoal at Shinnecock Inlet. This application is intended to demonstrate suitability of the model for the study site. Also, the model provides a new perspective and additional information about the inlet and coastal processes. The second application is a generalization of the model to describe the growth of the flood shoal within an active sediment-exchange system that includes the channel, deposition basin, ebb shoal, and other morphologic and engineering features.

Simulation of ebb shoal growth

In this section, a simplified but realistic longshore transport condition is specified to obtain a closed-form mathematical solution by which the main dynamical parameters controlling the growth of an ebb shoal can be identified. The amount of material leaving the shoal, which is the volume that is bypassed to the beach or transported into the deposition basin, is assumed to vary in direct proportion to the volume of the shoal at the particular time. Therefore, the rate of sand leaving or bypassing the ebb shoal, $(Q_E)_{out}$, is specified as

$$(Q_E)_{out} = \frac{V_E}{V_{Ee}} Q_{in} \tag{12}$$

in which V_E is volume of the ebb shoal, and Q_{in} is taken to be a constant average annual rate of sediment transported to the ebb shoal. (The transport rate need not be constant in either direction or time, but is specified as so here to obtain a solution that reveals functional dependencies.) The input rate Q_{in} is expected to be approximately equal to the longshore transport from the east. A portion of this material moves on the arm of the ebb shoal extending seaward from the east jetty, and a portion falls into the deposition basin and is transported to the ebb shoal by the ebb current. It is assumed that impoundment fillet adjacent to the east jetty is filled to capacity, or otherwise a portion of the westward-moving transport would go there.

The continuity equation governing change in the volume V_E of the ebb shoal is expressed as

$$\frac{dV_E}{dt} = Q_{in} - (Q_E)_{out} \tag{13}$$

where t = time. By substituting Equation 13, for $(Q_E)_{out}$,

$$\frac{dV_E}{dt} = Q_{in}\left(1 - \frac{V_E}{V_{Ee}}\right) \tag{14}$$

With the initial condition $V_E(0) = 0$, the solution of Equation 14 is

$$V_E = V_{Ee}\left(1-e^{-\alpha t}\right) \tag{15}$$

in which

$$\alpha = \frac{Q_{in}}{V_{Ee}} \tag{16}$$

The parameter α defines a characteristic time scale for the ebb shoal. From Equation 14, the time t_p at which the volume V_E reaches p percent of V_{Ee} is given by

$$t_p = -\frac{1}{\alpha}\ln\left(1-\frac{p}{100}\right) \tag{17}$$

For representative values for Shinnecock Inlet of $Q_{in} = 2 \times 10^5$ yd^3/year and $V_{Ee} = 1.5 \times 10^7$ yd^3, then $1/\alpha = 75$ years. For these values, the ebb shoal is predicted to reach 66 and 90 percent of its equilibrium volume 81 and 107 years after its creation in 1938, respectively, under the imposed constant and average-annual effective input longshore transport rate. The input transport rate is referred to as "effective" because the model does not account for interactions with the channel and flood shoal. This effective input transport rate pertains to the ebb shoal solely and indicates that the input transport rate for the entire inlet morphologic system should be greater than 2×10^5 yd^3/year.

The predicted increase in volume of the ebb shoal can be compared to measurements and to the expected equilibrium volume. It was estimated above in analysis of the bathymetric survey data that as of 1998 the ebb shoal at Shinnecock Inlet, 60 years after its creation, had achieved approximately 50 to 66 percent of its predicted equilibrium volume. Predictions from the simple model are considered to be compatible with the observations. This topic is explored graphically next.

Growth of the ebb shoal was examined with the reservoir model through a series of simulations in a sensitivity analysis. Based on estimates of the net transport rate given in the literature, as discussed in Chapter 1, Q_{in} was assigned the three values of 1×10^5, 1.5×10^5 and 2×10^5 yd^3/year. Similarly, the ebb shoal equilibrium volume V_{Ee} was assigned the values of 1×10^7, 1.5×10^7, and 2×10^7 yd^3, based on estimates from Equation 9. Predictions made for a 300-year interval 1938-2238 are shown in Figures 82a-c, where each figure contains plots for three Q_{in}-values for a fixed V_{Ee}. Also shown in the plots are values of the volume of the ebb shoal (Table 13) obtained from analysis of bathymetry surveys. If it is assumed that the reservoir model approximates the trend in growth of the ebb shoal, Figure 82a indicates that the recent measurements of its volume cannot be reproduced by the expected range of values of Q_{in} for an equilibrium ebb shoal volume of 1×10^7 yd^3. In contrast, curves in both Figure 82b and Figure 82c fit the trend of the data, with Figure 82c bracketing the recent measurements of ebb shoal volume by Q_{in}-values of 1.5×10^5 and 2×10^5 yd^3/year.

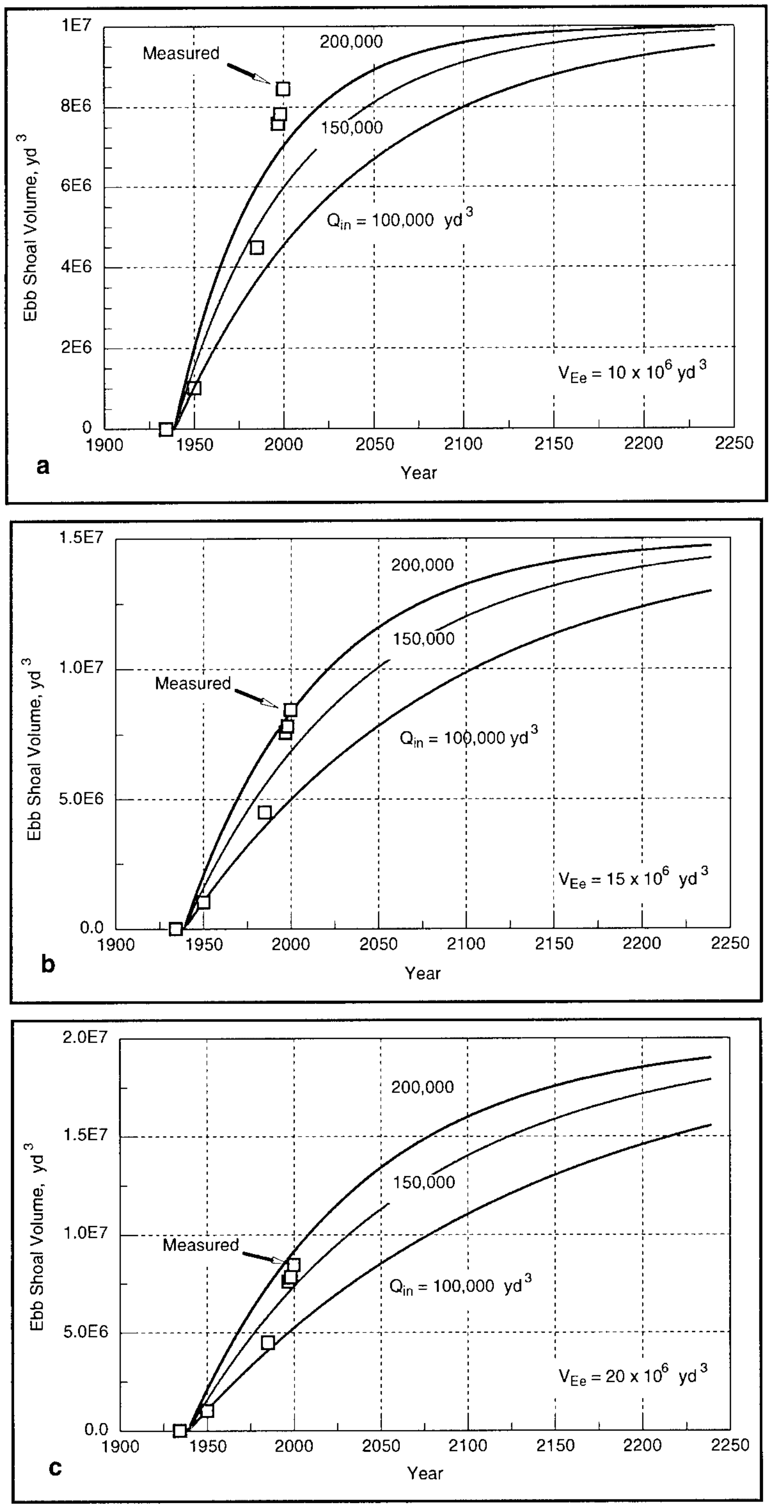

Figure 82. Sensitivity analysis for predicted volume of the ebb shoal, V_{Ee} fixed

The same material is presented in a different way in Figure 83, in which the predicted growth of the ebb shoal is shown in three plots displaying three values of V_{Ee} for fixed values of Q_{in}. Figure 83c indicates that the values of V_{Ee} in the range of 1.5 to 2.0×10^7 yd^3 and $Q_{in} = 2 \times 10^5$ yd^3/year are the most compatible with the recent measurements of those quantities examined.

The bypassing rate to the beach can be estimated by Equation 12. The preceding two paragraphs indicated that Q_{in}=2×10^5 yd^3/year was a reasonable estimate of the input longshore sand transport rate. If we assume that this value approximates the net rate (from east to west), then $(Q_E)_{out}$ gives an estimated bypassing rate to the attachment bar located in front of the Ponquogue Pavilion. Therefore, bypass rates corresponding to the curves in Figure 83c were plotted as shown in Figure 84. The curve corresponding to an equilibrium ebb-shoal volume of 1×10^7 yd^3, which is not a probable value, indicates a bypassing rate of almost 1.5×10^5 yd^3/year (improbably high given the continued increase in volumes of the ebb and flood shoals, and dredging required in the channel) for year 2000.

The curves for V_{Ee} of 1.5 to 2.0×10^7 yd^3 indicate bypassing rates to the attachment bar in the range of about 8 to 11×10^5 yd^3/year in year 2000. As discussed by Kraus (2000a,b), there is a time lag for sand to be bypassed to the beach because first the ebb shoal, bypass bar, and attachment bar must each gain a significant amount of sand to become efficient at bypassing. Bypassing is sacrificed while the shoal features mature. Bypassing values given in Figure 84 are expected to be representative but are probably upper limits to an annual average bypassing rate for the given conditions.

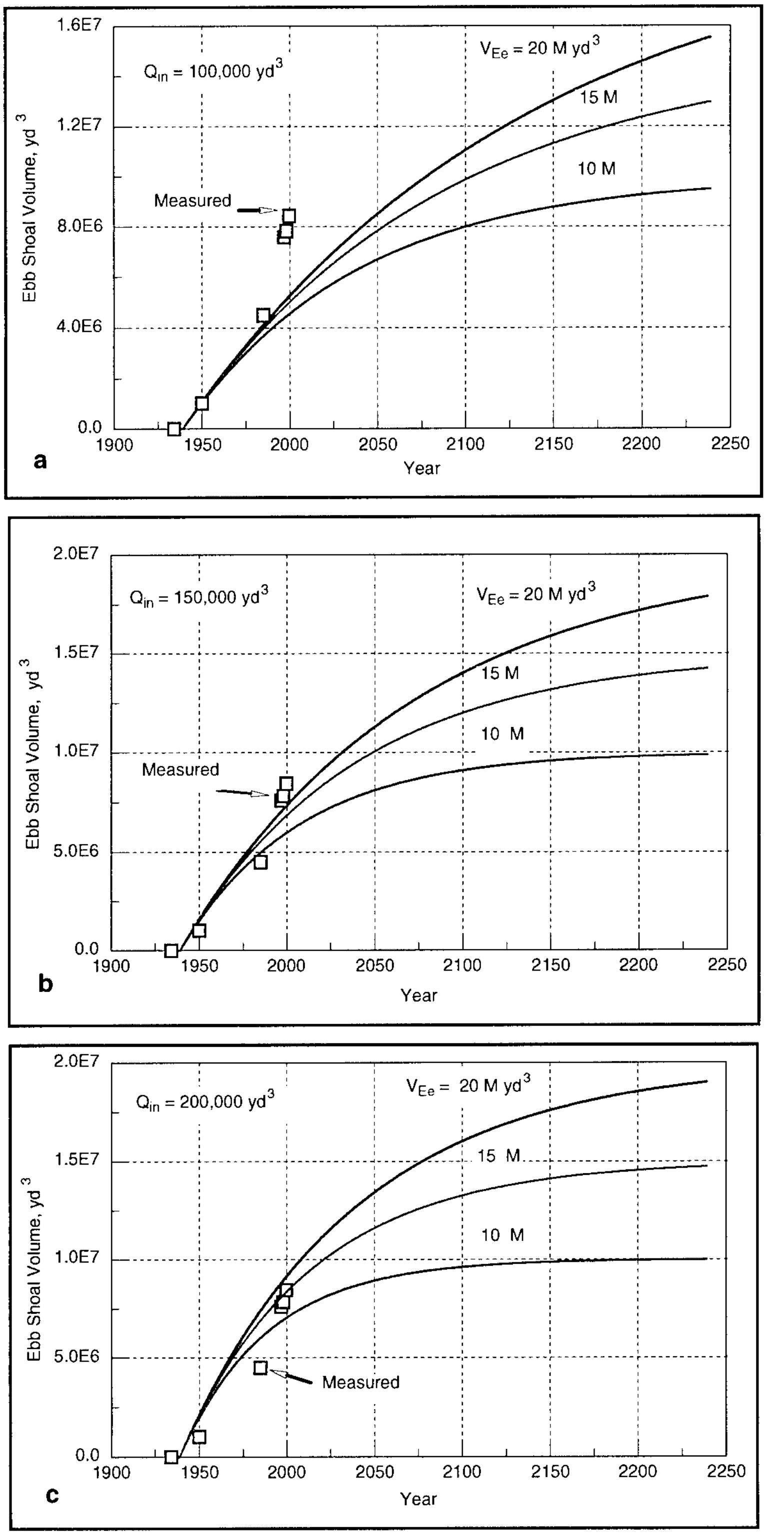

Figure 83. Sensitivity analysis for predicted volume of the ebb shoal, Q_{in} fixed

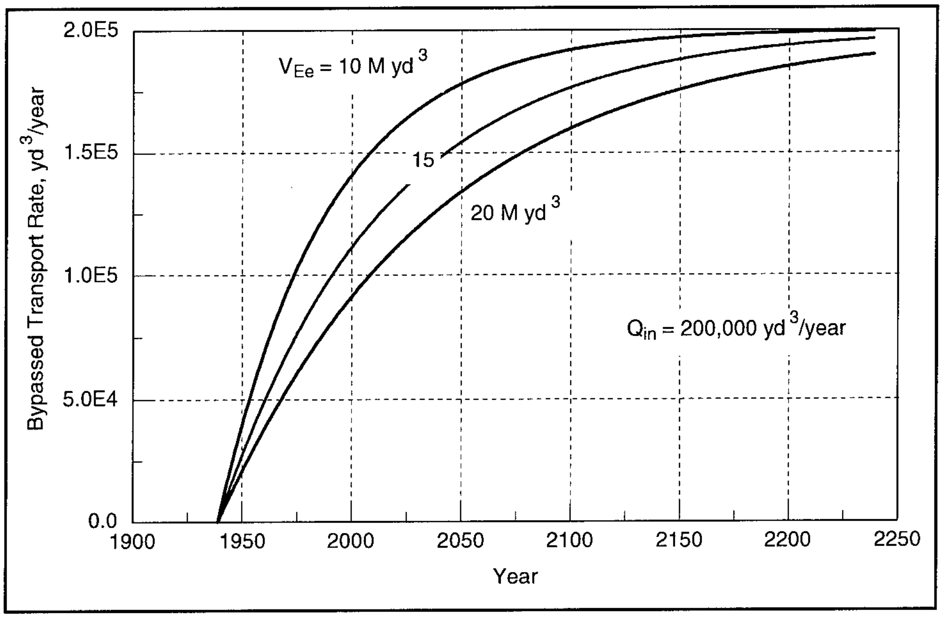

Figure 84. Predicted bypassing rate from the ebb shoal to the beach

Simulation of growth and sediment exchange at major inlet features

Specification of the sediment-transport paths at an inlet quickly becomes complex and ambiguous, and quantification of the transport rate is even more difficult. In the following, the inlet is represented by a more general version of the reservoir model. This version itself is a simplification of a yet-more detailed model, but it is one that allows quantitative examination of transport processes of central interest in this study.

For representation of the inlet in the model, the sediment paths shown in Figure 85 were specified. In doing so, it is assumed that the longshore sand transport was directed primarily from east to west (right to left) so that, for example, sand would bypass the inlet to the west but would not bypass it to the east. This is a purposeful limitation to restrict the number of equations and could be eliminated in a more detailed study. It is also assumed that the average-annual longshore sand transport rate is constant and directed to the right for an observer standing on the beach. Then, as shown in the figure, the arrows define the following sediment path equations expressed through a short-hand notation in which the arrow can be read as "from (right) to (left):"

$$
\begin{aligned}
&Q_R = Q_{RC} + Q_{RD} + Q_{RE} \\
&D \rightarrow C, E \\
&E \rightarrow C, D, B, O \quad \text{(to C prior to October 1990)} \\
&F \rightarrow C, Y \\
&B \rightarrow A, E \\
&A \rightarrow N, S, B \\
&N \rightarrow A, C
\end{aligned}
\tag{18}
$$

For example, the third equation is read as "from the ebb shoal (E) to the channel (C), to the deposition basin (D), to the bypassing bar (B), and to the offshore (O)." The sediment-path equations are written in approximate order of how sediment might enter or bypass the inlet from east to west.

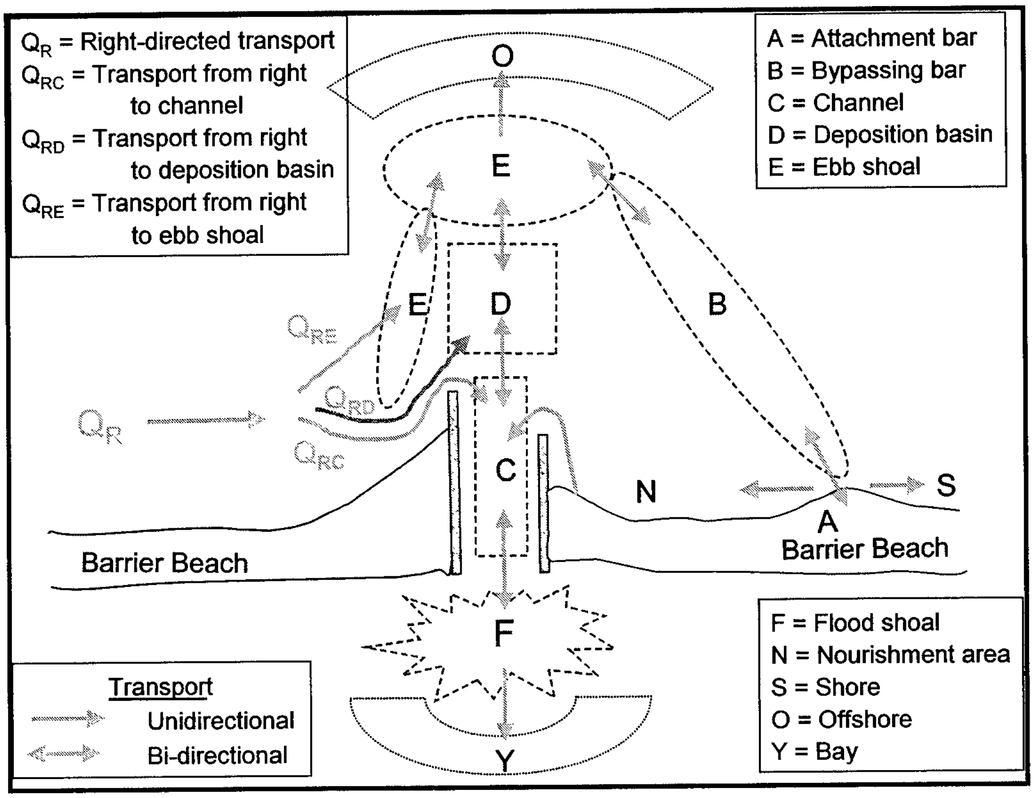

Figure 85. Sediment paths defining the inlet morphology reservoir model

The symbol F denotes the flood shoal. The symbol N denotes the beach segment adjacent to the west jetty in which nourishment is periodically placed through routine dredging of the deposition basin and channels. The symbols O and Y denote the offshore and bay (flood shoal far field), respectively, to which material may go and not return to the system. The symbol A denotes the attachment bar located near the Ponquogue Pavilion, and S denotes the shore west of the attachment bar.

The first of the sediment-path equations introduces a similar notation for the transport rate directed to the right, Q_R, as viewed by an observer on the shore looking seaward, which for this situation also equals Q_{in}. The subscripts on the transport rates in Equation 18 are read as "transport directed to the right equals or splits into transport from the right to the channel, from the right to the deposition basin, and from the right to the ebb shoal."

The subscript notation is carried through to define a central quantity in the reservoir model called the "coupling coefficient." Coupling coefficients allow the modeler to quantify the sediment-path equations. If the sediment path is believed to be correct, then the principal unknown or task of the modeler is to specify values of the coupling coefficients. To see this, two sediment path equations are expressed through coupling coefficients as examples.

The equation describing sediment paths for the right-directed transport can be re-expressed as

$$Q_R = \left(a_{RC} + a_{RD} + a_{RE}\right)Q_R \tag{19}$$

in which the coupling coefficients, a_{RC}, a_{RC}, and a_{RD} are defined through the relations

$$Q_{RC} \triangleq a_{RC}Q_R, \quad Q_{RD} \triangleq a_{RD}Q_R, \text{ and } \; Q_{RE} \triangleq a_{RE}Q_R \tag{20}$$

where the symbol $\triangleq$ denotes "is defined as." Equation 19 indicates that

$$a_{RC} + a_{RD} + a_{RE} = 1 \tag{21}$$

Equation 21 is one equation with three unknowns; two coupling coefficients must be given as input, and then the third is determined. In general, the coupling coefficients are time dependent and will be functions of the sediment-transport processes. At present, however, they are specified as constants by trial and error in reproducing general trends in growth and bypassing rates of measured features.

As a second example defining the coupling coefficients, consider from Equations 18 the sediment path equation $D \rightarrow C, E$. This equation means that the output transport rate, as defined by an equation similar to Equation 12 with the subscript E replaced by D, is distributed in some way between the channel and the ebb shoal. This gives

$$a_{DC} + a_{DE} = 1 \tag{22}$$

which is one equation in two unknowns, indicating that one of the two coupling coefficients must be specified, thereby determining the other. In similar manner, all sediment pathway equations can be prepared.

The full reservoir model is solved numerically, as opposed to the application above for which the analytical solution was developed. Time-dependent longshore transport rates, sand mining, and other time-dependent processes and engineering activities can be represented in the numerical solution. For the present application, a constant average-annual input rate $Q_{in} = Q_R$ was specified, and the coupling coefficients were taken to be time-independent constants with the exceptions of those pertaining to the deposition basin. Because the deposition basin was dredged in October1990, its related coupling coefficients were set to zero prior to 1990, removing this feature from the sediment-path equations.

Numerous runs were made to explore the sensitivity of the reservoir model to variations in coupling coefficients, input transport rate, and equilibrium volumes for each feature. Parameter values considered to represent the overall properties of the system, both in growth in volume and bypassing rates, are listed in Table 14. Considerable more work could be done in applying the model for increasing understanding of the inlet sediment pathways. Here, only the input transport rate and consequences of mining of the shoal are considered.

To reduce degrees of freedom in this initial application of the model, assumptions were made to simplify the evaluation process. The assumptions, documented in Table 14, were examined and found not to be significant for the final balance of sediment pathways. Among them, the equilibrium volume of the flood shoal was assumed to encompass both the near- and far fields, implying that $a_{FY} = 0$. Also, loss to the offshore by the ebb shoal (or from any other morphologic entity) was taken to be zero.

The major simplifying assumption is that Q_R (= Q_{in}) represents the total longshore sand transport rate arriving at the Shinnecock Inlet morphologic and channel system. This approximation may hold only moderately for the first few decades after the inlet formed. However, with growth of the attachment bar at Ponquogue, it is expected that the large bar will impede sediment moving to the east from the beaches located to the west of it.

Table 14
Values of Reservoir Model Input Parameters for Base Run

Parameter Name	Value Before (After) Dredging Deposition Basin	Comment
Q_R	3×10^5 yd^3/year	Upper end of estimates of net rate
a_{RC}	0.4 (0.3)	Key parameter for flood shoal
a_{RD}	0 (0.4)	Same comment as for a_{RC}
a_{RE}	$1 - a_{RC} - a_{RD}$	–
a_{CD}	0 (0.4)	–
a_{CE}	0.1 (0)	–
a_{CF}	$1 - a_{CD} - a_{CE}$	–
a_{ED}	0 (0.2)	–
a_{EC}	0.2 (0)	–
a_{EO}	0 (0)	
a_{EB}	$1 - a_{ED} - a_{ED} - a_{EO}$	
a_{FY}	0	Assume flood shoal volume is total
a_{FC}	$-(1 - a_{FY})$	–
a_{DC}	0 (0.4)	–
a_{DE}	0 $(1 - a_{DC})$	–
a_{BE}	0	Assume no reversal in transport
a_{BA}	$1 - a_{BE}$	–
a_{AN}	0	–
a_{AB}	0	–
a_{AS}	$1 - a_{AN} - a_{AB}$	–
a_{NC}	0.9	–
a_{NA}	$1 - a_{NC}$	–
V_{Ee}	10×10^6 yd^3	Split ebb shoal complex into two-thirds and one-third of predicted equilibrium volume
V_{Be}	5×10^6 yd^3	
V_{Ce}	5×10^5 yd^3	Nominal small value
V_{FE}	5×10^6 yd^3	Nominal small value
V_{Ye}	infinite	–
V_{Ae}	1×10^6 yd^3	Approx. volume of present feature
V_{De}	5×10^5 yd^3	
V_{OSe}	infinite	

It was anticipated that a relatively large value of Q_R would be necessary through considerations associated with the previous example. As an initial estimate, it is known (Morang 1999) that during approximately 60 years the ebb shoal has accumulated about 9×10^6 yd^3 and the flood shoal about 5×10^6 yd^3. In addition, some sand has bypassed the inlet, with a reasonable lower limit

probably being 4×10^6 yd^3 in the 60 years. If one assumes all of this material is associated with right-directed transport, then the total amount 18×10^6 yd^3 divided by 60 years gives an average annual rate of 3×10^5 yd^3/year. This amount, if approximately correct, would be an overestimate of the actual right-directed transport rate, because the estimate inherently includes right- and left-directed transport (but not sand bypassing, which cannot be measured through volume change on inlet features).

As an initial condition, the volume of the flood shoal was set to 5×10^5 yd^3, as an assumed amount of material swept bayward when the inlet opened in September 1938.

The parameter values listed in Table 14 produce the results shown in Figure 86 and Figure 87. The combined volumes of the ebb shoal and the bypassing bar are plotted in Figure 86 because this total entity corresponds to the measurements. The model reproduces the trend of the measurements well, despite no attempt made to determine a best fit. The bypass rates of the individual features show a downward spike for the year 1990, produced by dredging of the deposition basin. The basin introduced a new morphologic features and new pathways, for which time was required for the system to adjust.

The model predicts that in the year 2000, approximately 40,000 yd^3 of material are being contributed from the bypassing bar to the Ponquogue attachment bar. Figure 87 also shows that there is a considerable time lag before material reached the beach from the bypassing bar, because the ebb shoal and bypassing bar had to be established first to some reasonable volume before notable bypassing to the attachment bar and beach could take place. Perceptible bypassing to the attachment bar began from about 1950. If it is assumed that the average rate transported to the attachment bar was about 25,000 yd^3/year beginning in 1950, then in the 40 years following approximately 1×10^6 yd^3 would have accumulated, which is close to the volume of the feature as estimated from bathymetry measurements in Chapter 4.

If the attachment bar at Ponquogue were mined as a nourishment source for updrift and, possibly, downdrift beaches, bypassing of the inlet would re-establish the attachment bar.

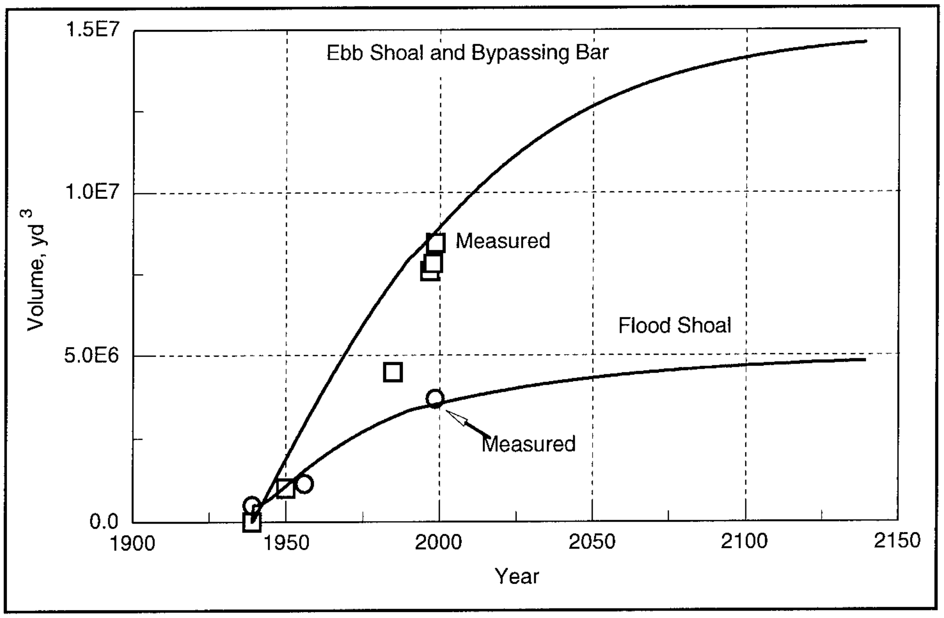

Figure 86. Calculated volumes of ebb shoal and bypassing bar, and flood shoal

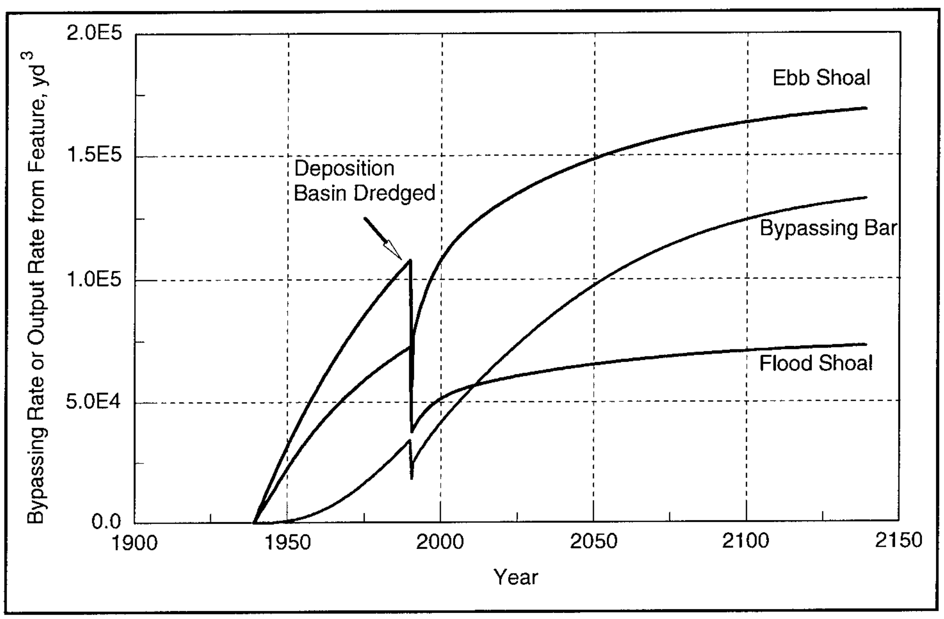

Figure 87. Calculated bypassing or output rate from morphologic feature

Simulation of flood shoal mining

Simulations were performed in which 400,000 and 1×10^6 yd^3, respectively, were mined from the flood shoal in the year 2003. The larger volume of material was removed from the inlet system as an extreme case, although the material would be placed on the west beach and a portion would enter the entrance channel and subsequently be transported to the flood shoal and ebb shoal.

As seen in Figure 88, mining of 400,000 yd^3 translates state of evolution of the flood shoal back in time about 15 years, which is interpreted as the estimated time for recovery to the pre-mining volume. After 15 years, the same area would become available for mining again. The flood shoal can serve as a renewable resource, but the "recharge" rate is on the order of 15 years. The 15-year interval is an upper limit, because some material placed on the west beach is expected to enter the channel and be transported to the flood shoal in a sediment-path cycle. This cycle introduces a source in addition to the littoral drift already accounted for in the reservoir model.

Removal of almost all available designated beach-compatible material, 1×10^6 yd^3, translates growth of shoal volume back about 35 years. In the two mining simulations, no notable change in bypassing rate to the beach was found as a result of the mining, because the already large volumes of the ebb shoal and bypassing bar are in the direct sediment transport path to the beach.

Finally, it is noted that mining of the flood shoal in the locations proposed reduced encroachment of the shoal into the West Cut and thereby reduced dredging frequency in that navigation channel.

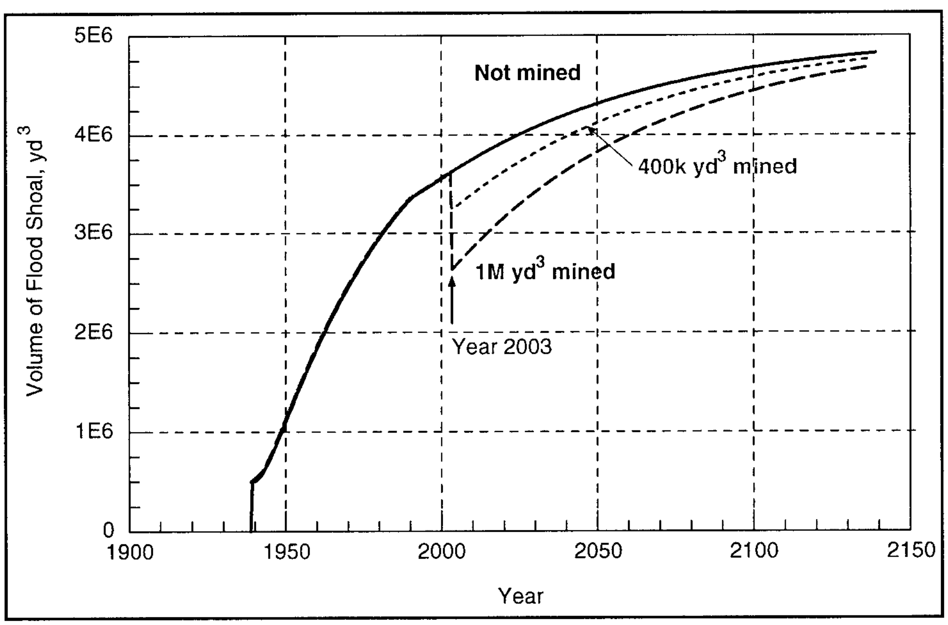

Figure 88. Evolution of the volume of the flood shoal after mining

6 Discussion and Conclusions

The objective of this study was to identify and evaluate potential consequences of mining the flood shoal at Shinnecock Inlet for material to be placed on the ocean-fronting beach adjacent to the west jetty. This study benefited from availability of products from an ongoing comprehensive monitoring project conducted by the New York District and the CIRP at Shinnecock Inlet and Shinnecock Bay. The monitoring provided simultaneous records of waves, currents, water level, and bathymetry. With this information, a model of the tidal circulation could be calibrated and applied to investigate innovative alternatives for mining the flood shoal. Also, stability of the inlet, evolution of the ebb and flood shoals, and natural sand bypassing of the inlet were investigated.

Fifteen action alternatives, with variations within two of the alternatives, were defined and evaluated primarily by comparison to the no-action alternative (existing condition). Six of the alternatives involved mining of the area of designated compatible material located on the southern side of the flood shoal. These mining alternatives consisted of mining only or mining performed together with modification of jetty length. Two alternatives involved repositioning of the deposition basin. The remaining seven alternatives were exploratory and are not discussed in detail in this chapter.

In this discussion, emphasis is given to the alternatives found to be favorable for sediment mining and potential implementation, which are Alternatives 1-5. All alternatives and their properties are listed in Tables 1-3. Alternatives 1, 2, 3 (Figure 8), 4 (Figure 9), and 5 (Figure 10) had favorable consequences based on calculated circulation patterns and magnitudes of the current. For the alternatives involving mining of the area of compatible material, 920,000 to 1,790,000 yd^3 were removed. These amounts are larger than the 200,000 to 400,000 yd^3 that might be removed for placement on the west beach. The smaller amount of material to be mined will produce smaller changes, but trends (such as increases and decreases) should be the same. Trends found, therefore, indicate the most extreme responses to be expected by mining.

Alternatives 1-4 are superior to Alternative 5 because sand compatible with the beach west of the inlet is contained in the designated cut areas. Alternative 5, mining of a large segment on the west side of the flood shoal including an area of finer material, was investigated to determine if it would yield a significantly improved circulation pattern; it did not. Therefore, Alternative 5, although producing similar responses, is not discussed in the same detail as Alternatives 1-4.

The following sections give conclusions of this study, together with supplemental discussion and general observations.

Inlet Stability

Rehabilitation of the jetties and dredging of the deposition basin in 1991 greatly improved the efficiency of Shinnecock Inlet to convey water. Although the authorized depth is 10 ft mllw (plus 1 ft each for advance dredging and overdredging), much of the inlet channel bottom now exceeds 20-ft depth, with some locations reaching 40-ft depth. Deepening of the inlet is concluded to be a response to dredging of the deposition basin.

Analysis indicated that, over the next few decades, the channel cross-sectional area will increase from the present 16,000 ft^2 to approximately 29,000 ft^2 to achieve an average channel depth between the jetties of 36 ft. An increase in tidal range in Shinnecock Bay is expected to accompany an improvement in hydraulic efficiency of the inlet. As the channel cross-sectional area increases, the typical peak ebb (and flood) current speed will decrease from the present approximately 5 to 6 ft/s to the range of 3 to 4 ft/s. The decrease in ebb current velocity will improve navigability, but the increased average depth through the inlet may require monitoring of the toes of the jetties as an alert to possible endangerment of the structures. As much as possible, consideration should be given to actions that may straighten the current and direct it down the center line between the jetties to promote a stable channel alignment.

Evolution of the Ebb Shoal and Bypassing

The equilibrium volume of the ebb shoal was estimated to be between 15 and 20 million yd^3. The present (1998) volume of the ebb shoal is approximately 9 million yd^3. It is anticipated that the volume of the ebb shoal will gradually grow over the next century and reach 90 percent of its equilibrium volume about 40 years from now for the existing jetty configuration. As the ebb shoal grows under the existing tidal prism, greater amounts of material will be bypassed by the action of waves and currents to the downdrift (west) beach. At present, it is estimated that about 40,000 yd^3/year arrive naturally to the Ponquogue attachment bar, and this rate is calculated to increase to about 100,000 yd^3/year by the year 2050, if no significant changes to the jetties or navigation channel are made.

The ebb shoal and flood shoal receive material from the channel (or the deposition basin) and exchange material through the inlet channel. Significant dredging of the deposition basin or channel temporarily reduces the amount of material transported to the flood and ebb shoals. However, mining of the flood shoal for volumes as described in this report will not perceptibly alter the course of sand bypassing along the ebb shoal and bypassing bar because the flood shoal is not in the direct pathway of ebb-shoal bypassing.

Mining of the Flood Shoal

The flood shoal is approaching equilibrium volume, and further growth will be primarily bayward, to the far field. This sand would be lost for mining, because of the limited thickness of the layer. As the far field of the flood shoal grows, the bay bottom will become shallower, which is detrimental from both environmental and navigation considerations.

Mining of the flood shoal, as evaluated in Alternatives 1-4, will reduce encroachment of the shoal into the bay as is occurring now, and the material removed can serve as an economical source for placement on the beach. Such mining is cost effective in that open-ocean operations are eliminated. Uncertainties brought by anticipated unfavorable weather are reduced in making cost estimates. Also, smaller and less-costly equipment can be used, and mining of the flood shoal may bring shorter pipe runs under milder wave and currents as compared to the open ocean. The mined area in the flood shoal would gradually be regenerated, again reaching a thick sand lens for possible future mining. It is estimated that at least one decade will need to pass before the mined area will contain a similar volume of material. Mining of the southern half of the designated beach-compatible area of the flood shoal, as requested by the Southampton Town Board of Trustees, would have the desired benefit of reducing maintenance dredging along the West Cut, and it would also decrease filling of the bay bottom.

Mining of the flood shoal was found to primarily alter only the local circulation, i.e., at the location of mining and sometimes in the inlet. The mining would not change the circulation pattern or water level in the bay. Calculations were done to examine mining of volumes three to four times greater than would actually be removed. Local changes to the circulation by mining would, therefore, be considerably less than estimated in this study. Although not investigated in this study, mining of the flood shoal is not expected to alter hydrodynamics conditions (water level, current) in the bay during a storm, because the storm surge (water elevation above predicted tide and the duration of that elevation) accompanying a storm is the leading factor in controlling water exchange through the inlet and flow within the bay during a storm.

Deposition Basin

The depth along most of the entrance navigation channel is considerably greater than the authorized depth, and the ebb current will continue to increase the depth of the channel. As an alternative to dredging the deposition basin, a potentially more economical and conservative strategy is to perform periodic channel-condition surveys. Such surveys would be made along cross-sectional transects on the order of 2,000 ft to each side of the channel limits. In this way, the channel can be monitored for imminent arrival of a large tip shoal at the east jetty or by a similar large sedimentary body approaching the channel elsewhere. If sand is required for beach nourishment, the morphology model applied in this study could be configured to investigate the consequences of the removal to the overall morphologic system and to natural sand bypassing.

A recommended trial action would be to maintain the entrance bar channel where it naturally tends to be located, that is, in a northeast to southwest alignment. This alignment appears on photos since the jetties have been in place and conforms to the preferred location of the ebb jet.

Evaluation of the functioning of the deposition basin was not an objective of this study, and its functioning was examined primarily for its bearing on evolution of the flood shoal. Because the deposition basin enters significantly in controlling inlet hydrodynamics and cross section, it is recommended that a focused study be done on the performance of the basin and its possible redesign or elimination.

Changes in Erosion and Deposition Patterns

Calculation of excess suspension speed (speed of the tidal current above that required to suspend sand) was conducted for Alternatives 1-5 to infer erosion and deposition patterns. Changes in the speed of the current, as compared to the existing condition, are beneficial for the West Cut and are neutral (minimal change in current speed) for the inlet, area of the Ponquogue Bridge, and for the beach located west of the inlet. These alternatives were estimated to change the discharge though the inlet by about 1 percent or less, and thus would not disturb the stability of the inlet.

The mined regions of these alternatives would experience greater sediment deposition as compared to the existing condition because the deeper water would reduce the speed of the current there. The deposition and erosion patterns of other areas would not change significantly.

Alternatives 1-4 did not modify the current along the beach adjacent to the west jetty. Erosion of the west beach will not be increased by implementation of any of these alternatives.

Navigation Benefits

Dredging and Navigation Safety

As a summary and synthesis of report findings, three criteria are introduced in this section for evaluating potential benefits or detriments of the alternatives to navigation. One criterion is that the strength of the ebb current should not increase notably at the inlet entrance. The second is that the region where vessels enter the West Cut from the inlet should not experience an increase in speed of the current without mitigating factors. For example, a slight increase in speed of the current at the West Cut may be acceptable if the turn into the inlet were made wider by dredging. Reduced maintenance of the West Cut also enters as a benefit. The third criterion is whether any change in the current and sediment-transport patterns would reduce maintenance dredging in the West Cut.

Table 15 compares navigation benefits of the alternatives. Alternatives 1-5 would be expected to have overall positive benefits to navigation. These benefits would come from reduced speed of the current at the inlet entrance to the West

Cut and from reduced maintenance dredging of the West Cut. The speed of the current relative to the existing condition is generally reduced in the West Cut for these five alternatives. The mined region of the flood shoal would trap sediment, making less material available for transport either bayward or to the West Cut. Thus, encroachment of the flood shoal into the West Cut will be slower for these alternatives, as compared to the existing condition, a cost-savings benefit.

Alternatives 6-15 have less favorable benefits for navigation. No significant change is expected for Alternative 6 and, possibly, for Alternatives 14 and 15. Alternatives 8, 9, and 10 have both positive and negative consequences for navigation. These three alternatives increase the speed of the flood current in the region where vessels turn out the inlet to the West Cut. Maintenance of the West Cut would improve because much of the material entering Shinnecock Bay on flood tide is expected to be transported through the opening created in the flood shoal and into the back bay. However, increased transport to the back bay (far field of the flood shoal) is a disadvantage in that the material is lost for possible mining, and depth in the bay will be reduced. Alternatives 7, 11, 12, and 13 have negative consequences for navigation because of increased current speed at the inlet entrance, increased speed of the current at the intersection of the West Cut and inlet, and increased maintenance dredging of the West Cut.

Scour in the Inlet

Changes in speed of the current through the inlet have the potential for promoting or reducing scour. Alternatives 1-6 are not expected to change the scour potential in the inlet. Alternatives 7, and 10-12 would increase the scour potential over the entire inlet because of increased current speed. Alternative 13 has the same scour potential as Alternatives 7 and 10-12 except that no change is predicted adjacent to the east jetty. Alternatives 8a,b would increase the scour potential over the entire inlet except at the west jetty tip where it would be reduced. Alternatives 9a,b have the same scour potential pattern as Alternatives 8a,b except for greater scour potential just inside the inlet near the west jetty. Alternative 14 would increase scour potential adjacent to the east jetty. Alternative 15 would increase scour potential adjacent to the east jetty and on the western side of the inlet.

Shoaling and Navigation Channel Alignment

Alternatives 1-4 are not expected to cause shoaling in the inlet or modify the navigation channel. Alternatives 8, 9, 14, and 15 displace the ebb jet toward the east. Of these, Alternatives 8a,b create the strongest displacement, meaning that the change in peak speed of the ebb current at the location of the displaced jet is greatest. Lengthening of the west jetty for Alternatives 8a,b results in an ebb jet alignment that is approximately parallel to the jetties. This alignment reduces the

Table 15
Comparison of Navigation Benefits of Alternatives
(as positive – pos., negative – neg., or no substantial change)

Alt.	Alt. Description	Entrance Ebb	Current at West Cut	Maint. of West Cut	Comments
0	No action	–	–	–	–
1	Mine flood shoal to -10.5 ft mtl	No change	No change	Pos.	Mining in area of compatible material will reduce deposition in the West Cut as the mined area reforms
2	Mine flood shoal to –4.1 ft mtl	No change	Slight pos.	Pos.	
3	Mine flood shoal to -14.3 ft mtl	No change	Slight pos.	Pos.	
4	Mine flood shoal to -14.3 ft mtl; follow contours	No change	Slight pos.	Pos.	
5	Mine western portion of shoal	No change to slight neg.	Slight neg.	Slight pos.	Exploratory, similar to Alts. 1-4
6	Dredge a channel northeast from Ponquogue Bridge	No change	No change	No change	Exploratory, ineffective alternative
7	Mine Ponquogue attachment bar	Neg.	Neg.	Neg.	Stronger flood sweeps material into West Cut
8	8a. Lengthen west jetty 8b. Lengthen west jetty, mine as Alt. 3	Needs further analysis	8a. Neg on flood; no change on ebb 8b. Neg on flood and ebb	8a. Slight pos. 8b. Pos.	Thalweg and channel would be centered where none exist now
9	9a. Shorten east jetty 9b. Shorten east jetty, mine as Alt. 3	Same as Alt. 8	9a. Neg on flood and ebb 9b. Neg on flood and ebb	9a. Slight pos. 9b. Pos.	Same as Alt. 8
10	Mine wedge-shaped channel in flood shoal	Slight neg.	Slight neg. on flood; no change on ebb	Pos.	Not favorable, flood shoal would grow into bay
11	Combine Alts 6 and 10	"	Slight neg. on flood; no change on ebb	Neg.	Not favorable, flood shoal would grow into bay
12	Mine extended wedge-shaped channel in flood shoal	"	Slight neg. on flood; no change on ebb	Neg.	Not favorable, flood shoal would grow into bay
13	Mine a rotated wedge-shaped channel flood shoal	"	Slight neg. on flood; no change on ebb	Neg.	Not favorable, flood shoal would grow into bay
14	Reposition deposition basin on channel thalweg	Needs further analysis	No change	No change	Area of maximum ebb changes location
15	Reposition deposition basin to trend southeast	Needs further analysis	No change	No change	Area of maximum ebb changes location

speed of the current west of the west jetty on both ebb and flood tide. Alternatives 9a,b have similar patterns of change in speed of the current as compared to Alternatives 8a,b, but the jet is not displaced as far to the east. Correspondingly, the reduction in speed of the current west of the west jetty is smaller.

The changes in strength and patterns of the current for Alternatives 8 and 9 would act to reduce scour at the seaward end of the west jetty but promote scour at the east jetty. The area with the strongest current is shifted toward the center

of the inlet. During ebb, the speed of the current along the east jetty is increased by about 0.2 m/s, an increase great enough to promote scour. At the inlet entrance, the equal-length jetties (same distance offshore) act to align the current along the inlet center line. On flood tide, this alignment is different from the existing condition in which strong flow enters from the tip of the west jetty and moves diagonally across the inlet. Scour at the tip of the west jetty may be reduced if the jetties were at the same distance offshore because the strongest current would be centered at the inlet entrance.

On ebb tide, the equal lengths of the jetties of Alternatives 8 and 9 will tend to promote a straight navigation channel. The current within the inlet would be centered and parallel to the jetties. Migration of the ebb jet westward would be reduced, tending to create a nearly straight navigation channel. The speed of the ebb jet is sufficient to transport sand and maintain a navigation channel. Locating the jet east of its present position will tend to keep the navigation channel aligned with the inlet. The ebb shoal would migrate eastward in response to a shift in the location of the ebb jet.

Current at the Ponquogue Bridge

The preferred alternatives (Alternatives 1, 2, 3, and 4) are not expected to substantially modify the speed of the current at the Ponquogue Bridge. Alternatives 1-4 will slightly decrease the current in a small area at the bridge during flood, with no change at ebb. The current is strong at and under the bridge because of the natural constriction created by Ponquogue Point. Flow area has been further reduced, hence the velocity of the flow increased, by construction of landfill and fishing piers near the bridge.

References

Bruun, P., and Gerritsen, F. (1960). *Stability of coastal inlets.* North Holland, Amsterdam.

Bruun, P., Mehta, A. J., and Jonsson, I. G. (1978). *Stability of tidal inlets.* Elsevier, New York.

Carr De Betts, E. E. (1999). "An examination of flood tidal deltas at Florida's tidal inlets," M.S. thesis, Coastal and Oceanographic Engineering Department, University of Florida, Gainesville, FL.

Czerniak, M. T. (1977). "Inlet interaction and stability theory verification," *Proceedings Coastal Sediments '77*, American Society of Civil Engineers, Reston, VA, 754-773.

Dean, R. G., and Walton, T. L. (1973). "Sediment transport processes in the vicinity of inlets with special reference to sand trapping," *Estuarine Research.* L. E. Cronin, ed., Academic Press, Inc., New York, 129-149.

Environmental Modeling Research Laboratory. (1999). "SMS v6.0 reference manual," Environmental Modeling Research Laboratory, Brigham Young University, Provo, UT.

Escoffier, F. F. (1940). "The stability of tidal inlets," *Shore & Beach*, 8(4), 114-115.

FitzGerald, D. M. (1996). "Geomorphic variability and morphologic and sedimentologic controls on tidal inlets," *Journal of Coastal Research,* SI 23, 47-71.

Gofseyeff, S. (1952). "Case history of Fire Island Inlet, N.Y.," *Proceedings of Third Conference on Coastal Engineering*, Council on Wave Research, 272-305.

Harris, D. L. (1981). "Tides and tidal datums in the United States," Special Report No. 7, U.S. Army Corps of Engineers, Coastal Engineering Research Center, Fort Belvoir, VA.

Hayes, M. O. (1980). "General morphology and sediment patterns in tidal inlets," *Sedimentary Geology*, 26, 139-156.

Jarrett, J. T. (1976). "Tidal prism – inlet area relationships," General Investigation of Tidal Inlets GITI Report 3, U.S. Army Engineer Waterways Experiment Station, Vicksburg, MS.

Kana, T. W. (1995). "A mesoscale sediment budget for Long Island, New York," *Marine Geology*, 126, 87-110.

Keulegan, G. H. and Hall, J. V. (1950). "A formula for the calculation of tidal discharge through an inlet," U.S. Army Corps of Engineers, Beach Erosion Board Bulletin, 4, 15-29.

Komar, P. D. (1996). "Tidal-inlet processes and morphology related to the transport of sediments," *Journal of Coastal Research*, SI 23, 23-45.

Kraus, N. C. (1998). "Inlet cross-sectional area calculated by process-based model," *Proceedings 26th Coastal Engineering Conference*, American Society of Civil Engineers, Reston, VA, 3, 265- 3,278.

Kraus, N. C. (2000a). "Reservoir model of ebb-tidal shoal evolution and sand bypassing," *Journal of Waterway, Port, Coastal, and Ocean Engineering*, 126(6), 305-313.

Kraus, N. C. (2000b). "Prediction of ebb-tidal shoal volume change and sand bypassing," *Proceedings 12th Conference on Beach Preservation Technology*, Florida Shore and Beach Preservation Association, Tallahassee, FL, 268-280.

Kraus, N. C., Hanson, H., and Blomgren, S. (1994). "Modern functional design of groins," *Proceedings 24th Coastal Engineering Conference*, American Society of Civil Engineers, New York, 1327-1342.

Leatherman, S. P. and Allen, Jr., ed. (1985). "Geomorphologic analysis of south shore of Long Island barriers, New York," Report to U.S. Army Engineer District, New York.

LeConte, L. J. (1905). "Discussion on river and harbor outlets," Discussion of "Notes on the Improvement of river and harbor outlets in the United States," Paper No. 1009, D. A. Watts, *Transactions*, *American Society of Civil Engineers*, 55, 306-308.

Le Provost, C., Genco, M. L., Lyard, F., Vincent, P., and Canceill, P. (1994). "Spectroscopy of the world ocean tides from a hydrodynamic finite element model," *Journal of Geophysical Research*, 99(C12), 24,777-24,797.

Lillycrop, W. J., Parson, L. E., and Irish, J. L. (1996). "Development and operation of the SHOALS Airborne Lidar Hydrographic Survey System." Laser remote sensing of natural waters: from theory to practice. V. I. Feigels and Y. I. Kopilevich, ed., *SPIE—The International Society for Optical Engineering*, 2964, 26-37

Luettich, R. A., Westerink, J. J., and Scheffner, N. W. (1992). "ADCIRC: An advanced three-dimensional circulation model for shelves, coasts, and estuaries; Report 1, theory and methodology of ADCIRC-2DDI and ADCIRC-3DL," Technical Report DRP-92-6, U.S. Army Engineer Waterways Experiment Station, Vicksburg, MS.

Marino, J. N., and Mehta, A. J. (1987). "Inlet ebb shoals related to coastal parameters," *Proceedings Coastal Sediments '87*, American Society of Civil Engineers, New York, 1608-1623.

Militello, A., and Zarillo, G. A. (2000). "Tidal motion in a complex inlet and bay system, Ponce de Leon Inlet, Florida," *Journal of Coastal Research*, 16(3), 848-860.

Morang, A. (1999) "Shinnecock Inlet, New York, Site Investigation, Report 1 morphology and historical behavior," Technical Report CHL-98-32, U.S. Army Engineer Waterways Experiment Station, Vicksburg, MS.

O'Brien, M. P. (1931). "Estuary and tidal prisms related to entrance areas," *Civil Engineering.* 1(8), 738-739.

O'Brien, M. P. (1969). "Equilibrium flow areas of inlets on sandy coasts," *Journal of Waterways and Harbors Division* 95(WW1), 43-52.

Offshore & Coastal Technologies, Inc. (1999). "Evaluation of flood and ebb shoal sediment source alternatives, West of Shinnecock Interim Project, New York," Final Report prepared for U.S. Army Engineer District, New York.

Pratt, T. C., and Stauble, D. K. (2000). "Selected field collection efforts at Shinnecock Inlet, New York, Report 3, selected field data report for 1997, 1998, 1999, velocity and sediment surveys," Technical Report CHL-98-32, U.S. Army Engineer Research and Development Center, Vicksburg, MS.

Panuzio, F. L. (1968). "The Atlantic coast of Long Island," *Proceedings of Eleventh Conference on Coastal Engineering*, American Society of Civil Engineers, New York, 1222-1241.

Resio, D. T. (1987). "Shallow-water waves. I: Theory," *Journal of Waterway, Port, Coastal, and Ocean Engineering*, ASCE, 113(3), 264-281.

Resio, D. T. (1988). "Shallow-water waves. II: Data comparisons," *Journal of Waterway, Port, Coastal, and Ocean Engineering*, 114(1), 50-65.

Rosati, J. D., Gravens, M. B., and Smith, W. G. (1999). "Regional sediment budget for Fire Island to Montauk Point, New York, USA," *Proceedings Coastal Sediments '99*, American Society of Civil Engineers, Reston, VA, 802-817.

Seabergh, W. L., and Kraus, N. C. (1997). "PC program for coastal inlet stability using Escoffier method," CETN-IV-11, U.S. Army Engineer Research and Development Center, Coastal and Hydraulics Laboratory, Vicksburg, MS.

Smith, F. B., and FitzGerald, D. M. (1994). "Sediment transport patterns at the Essex River Inlet ebb-tidal delta, Massachusetts, U.S.A.," *Journal of Coastal Research*, 10, 752-744.

Smith, J. M., Resio, D. T., and Zundel, A. K. (1999). "STWAVE: steady-state spectral wave model, Report 1: User's manual for STWAVE version 2.0," Instructional Report CHL-99-1, U.S. Army Engineer Waterways Experiment Station, Vicksburg, MS.

U.S. Army Engineer District, New York. (1986). "General design memorandum Shinnecock Inlet project, Long Island, New York," Reformulation study and environmental impact statement, September 1986, draft report, New York.

U.S. Army Engineer District, New York. (1999). "The Fire Island to Montauk Point, Long Island, NY, Reach 2, west of Shinnecock Inlet draft decision document; An evaluation of an interim plan for storm damage protection," New York.

Van Rijn, L. C. (1993). "*Principles of sediment transport in rivers, estuaries, and coastal seas.*" Aqua Publications, Amsterdam.

Walton, T. L., Jr., and Adams, W. D. (1976). "Capacity of inlet outer bars to store sand," *Proceedings 15th Coastal Engineering Conference*, American Society of Civil Engineers, New York, 1919-1937.

Williams, G. L., Morang, A., and Lillycrop, L. (1998). "Shinnecock Inlet, New York, site investigation, Report 2, evaluation of sand bypass options," Technical Report CHL-98-32, U.S. Army Engineer Waterways Experiment Station, Vicksburg, MS.

Appendix A
Plots of Calculated Velocity

Plan-view plots of current velocity are provided for each alternative during spring peak flood and ebb tide. The images contain velocity vectors over contoured bottom topography, contoured current speed, and velocity vectors plotted over contoured speed. For each alternative, the following plots are given:

a. Flood shoal, flood tide.

   1. Velocity vectors over bottom topography.
   2. Contoured current speed.

b. Flood shoal, ebb tide.

   1. Velocity vectors over bottom topography.
   2. Contoured current speed.

c. Velocity vectors over contoured current speed, inlet and ebb shoal, ebb tide.

Plots listed as A and B are presented as upper and lower panels, respectively, in the figures. Velocity patterns over bottom topography are given for the flood shoal because this is the area in which most alternatives were dredged. Color scales refer to contours of either elevation or current speed.

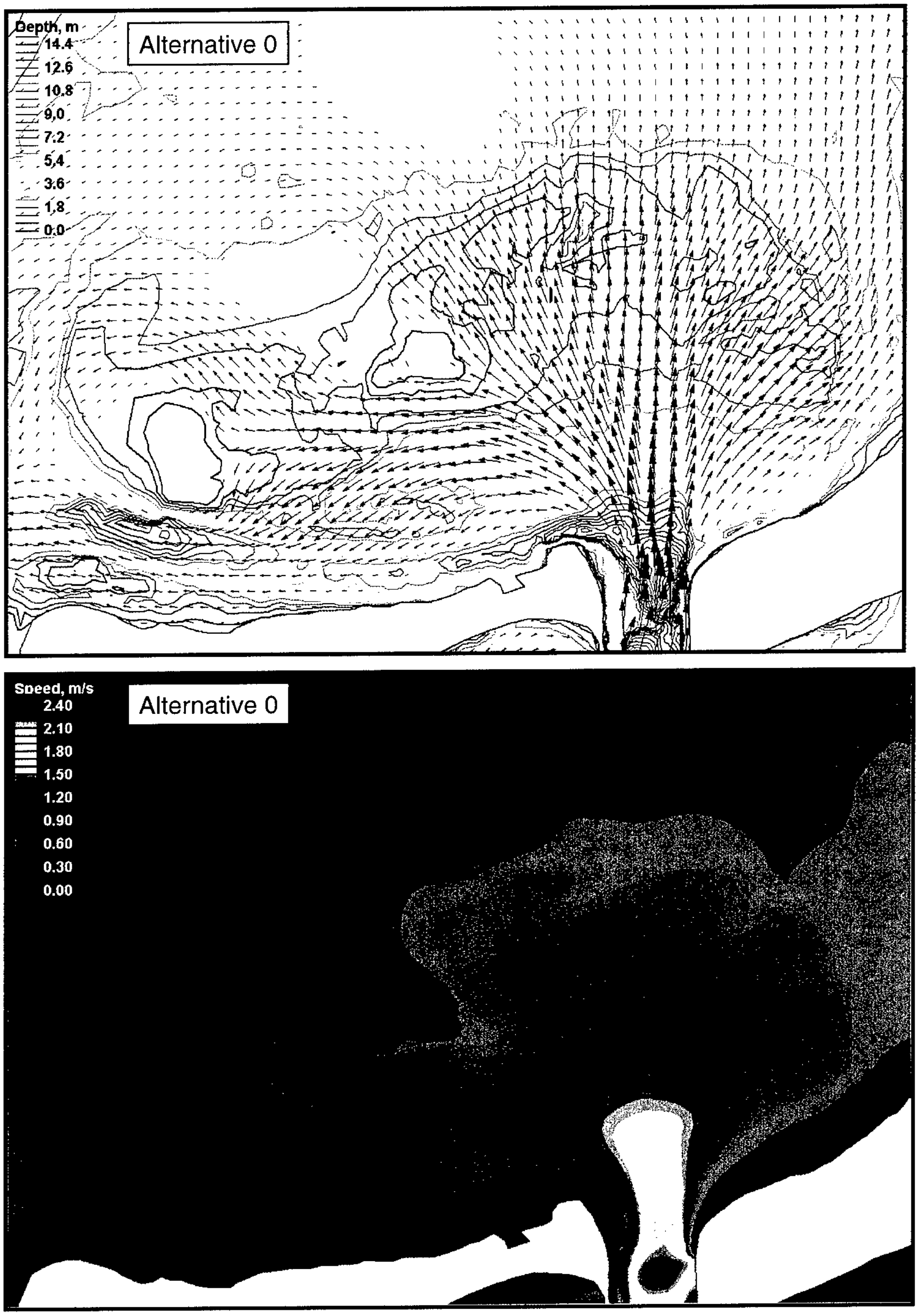

Figure A1. Alternative 0 velocity vectors and speed at flood shoal, peak flood tide

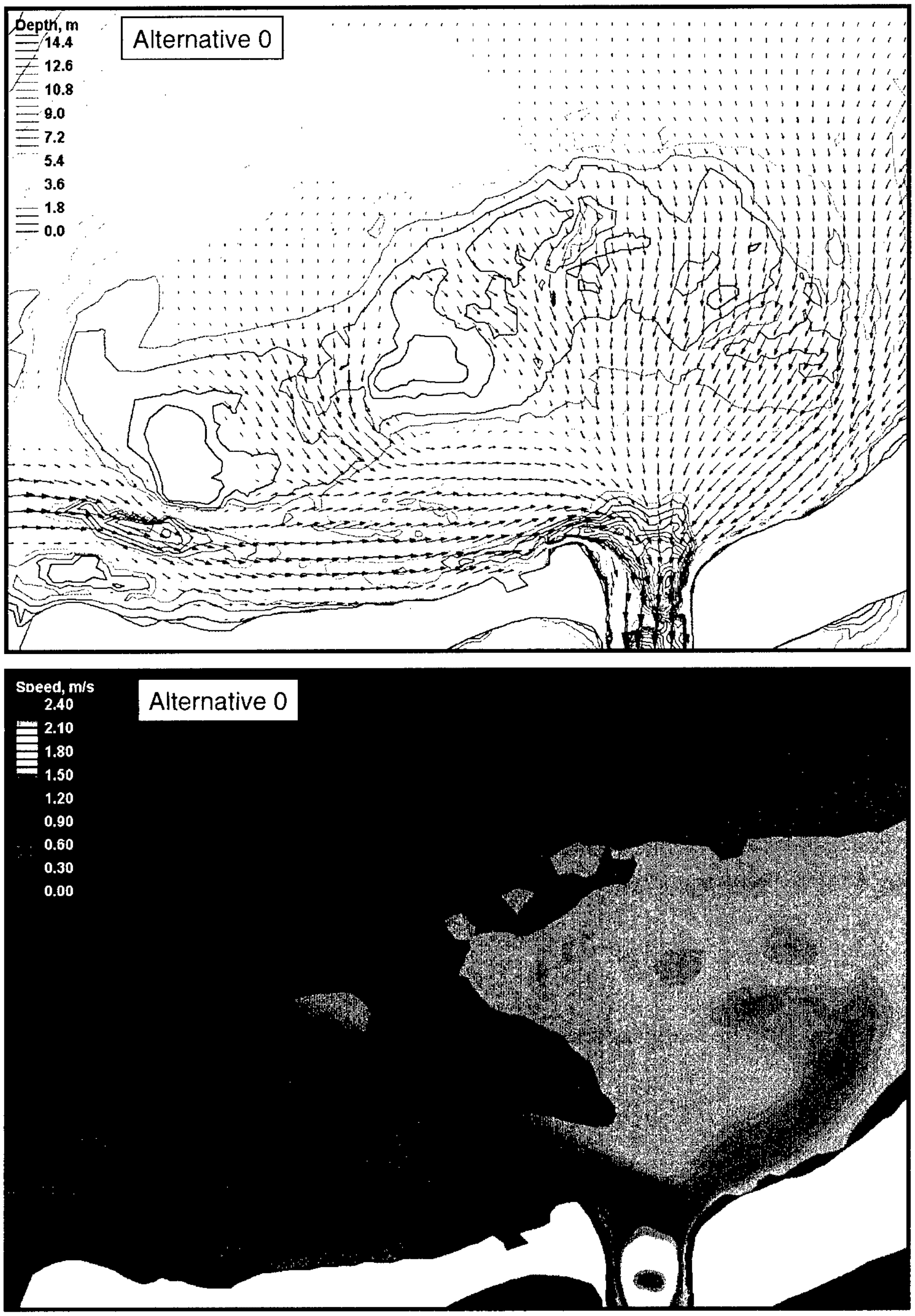

Figure A2. Alternative 0 velocity vectors and speed at flood shoal, peak ebb tide

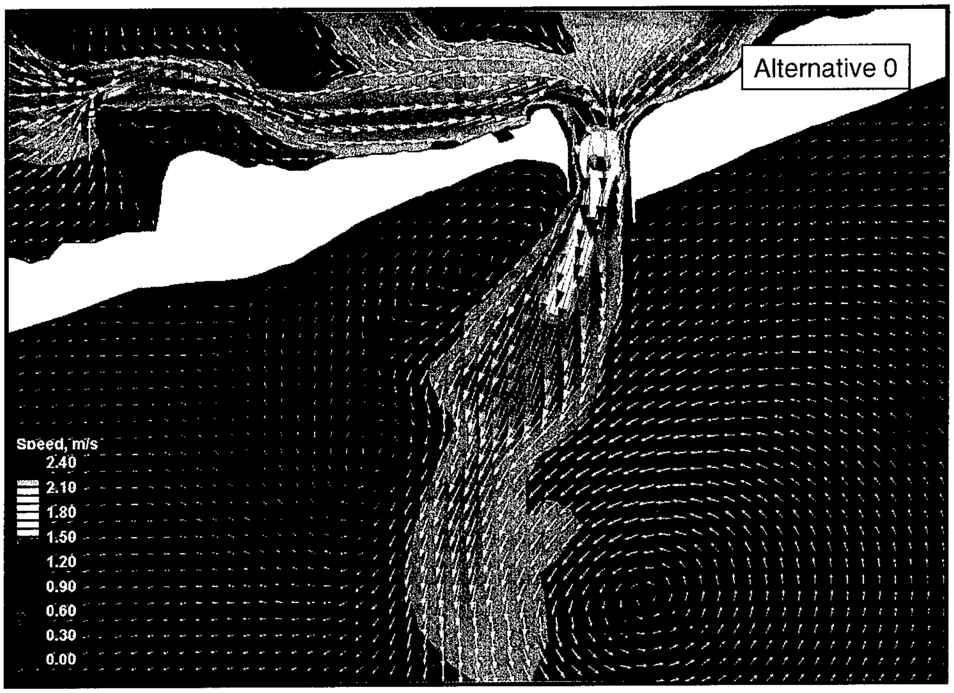

Figure A3. Alternative 0 velocity vectors and speed at inlet and ebb shoal, peak ebb tide

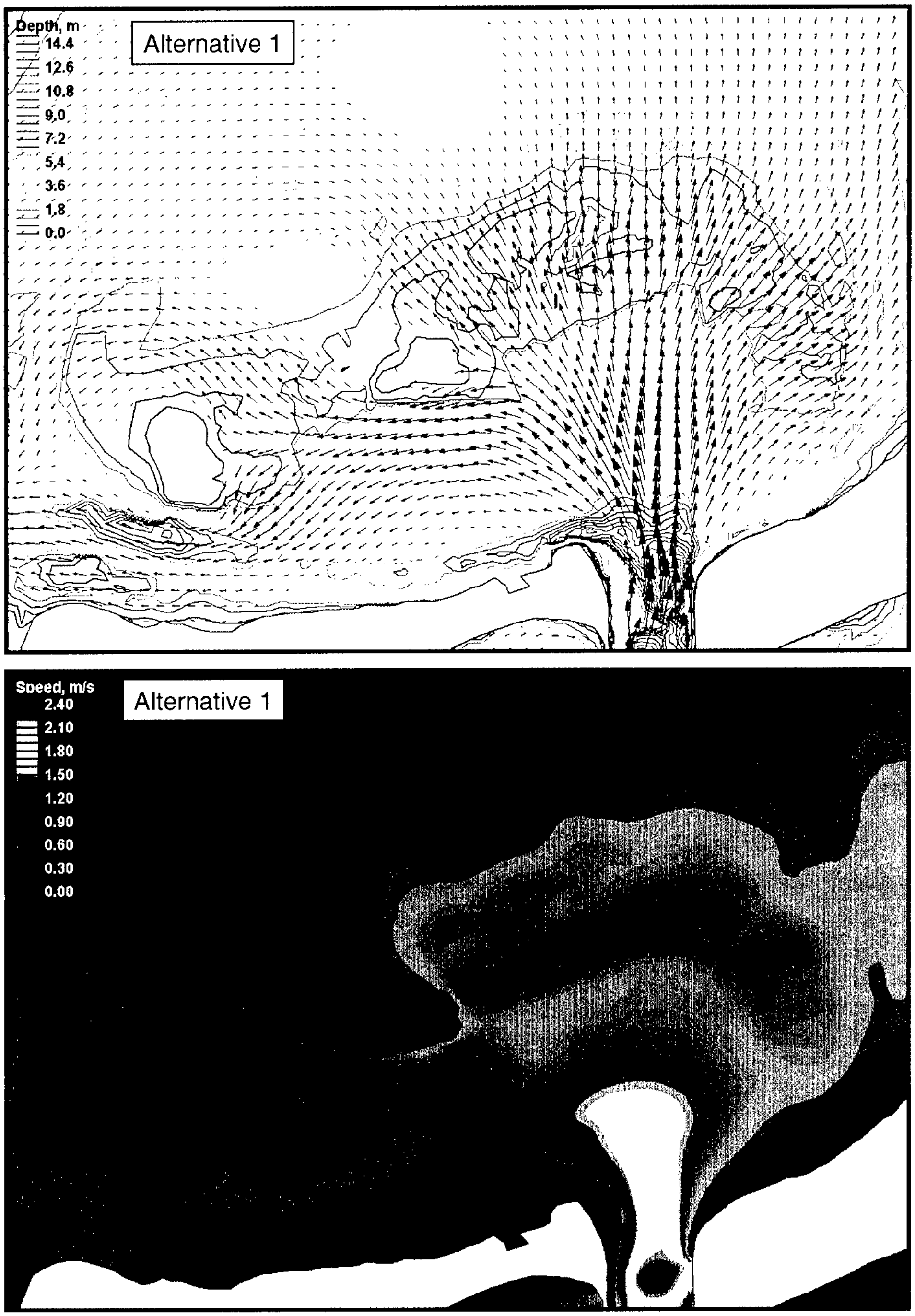

Figure A4. Alternative 1 velocity vectors and speed at flood shoal, peak flood tide

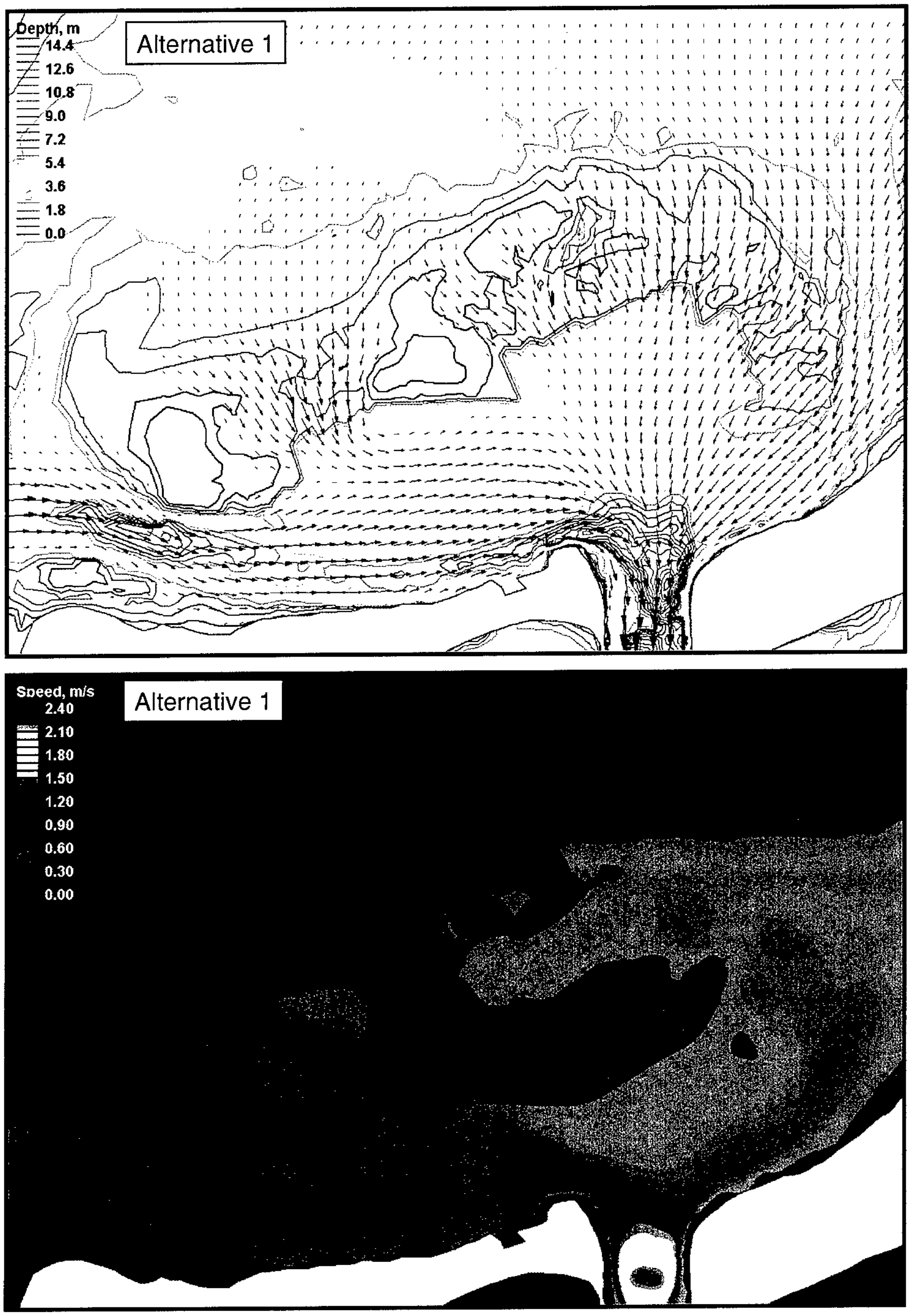

Figure A5. Alternative 1 velocity vectors and speed at flood shoal, peak ebb tide

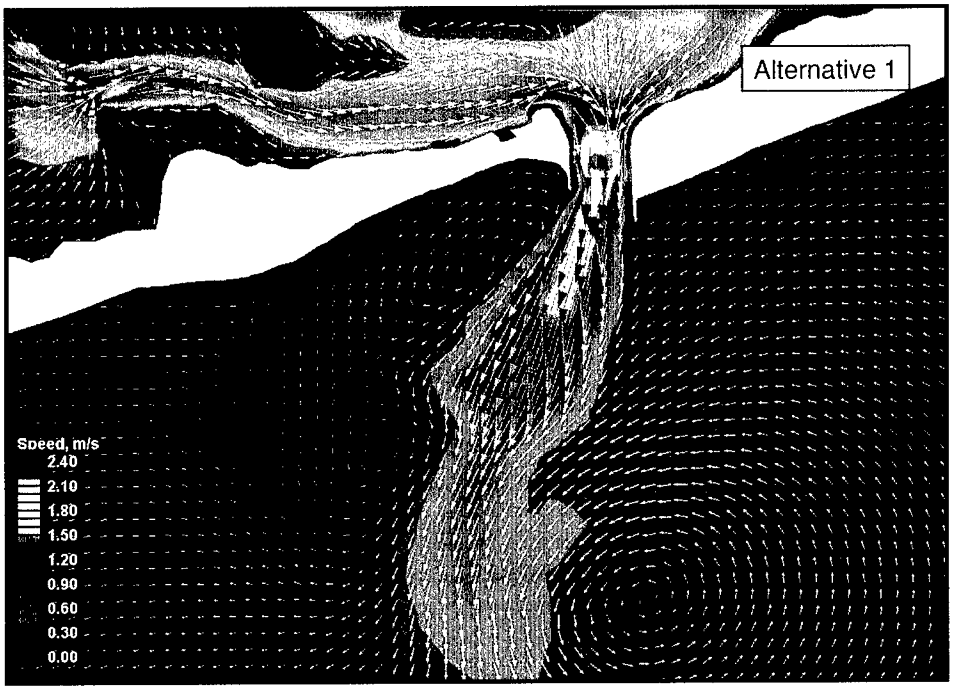

Figure A6. Alternative 1 velocity vectors and speed at inlet and ebb shoal, peak ebb tide

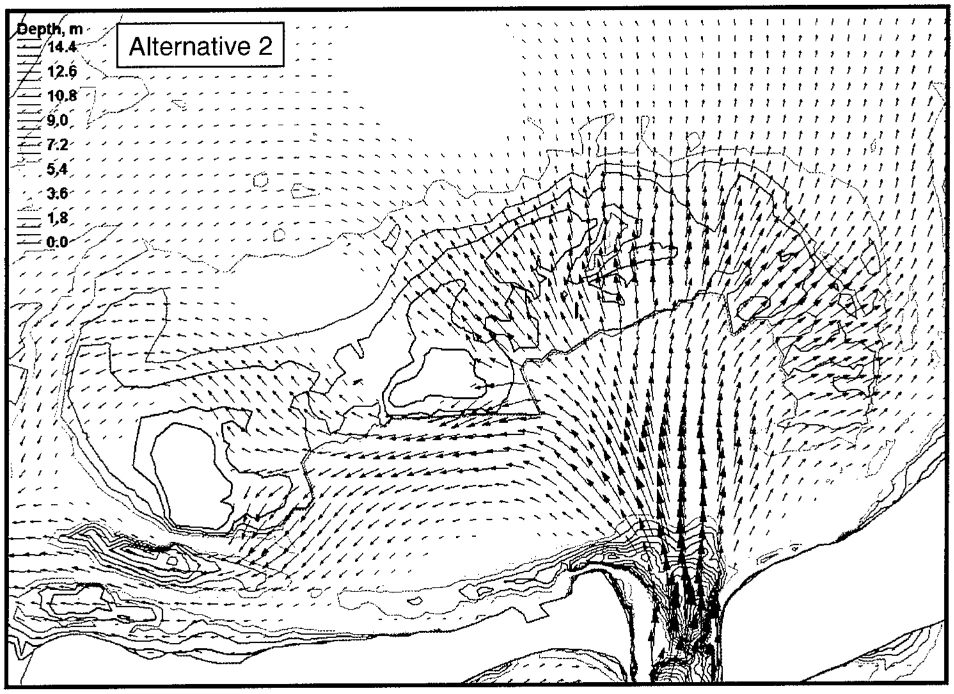

Figure A7. Alternative 2 velocity vectors and speed at flood shoal, peak flood tide

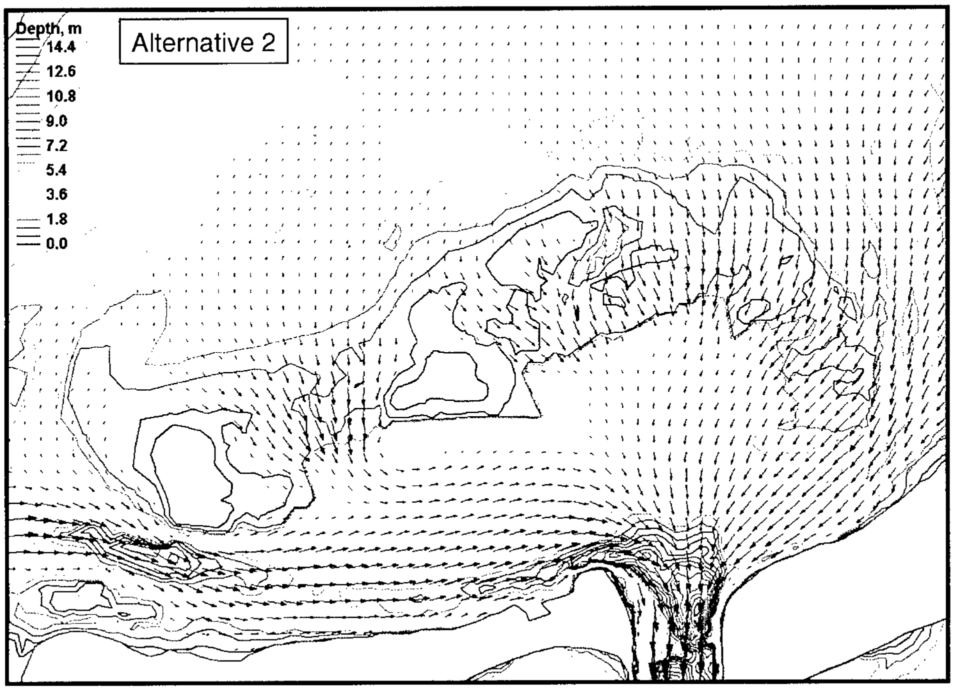

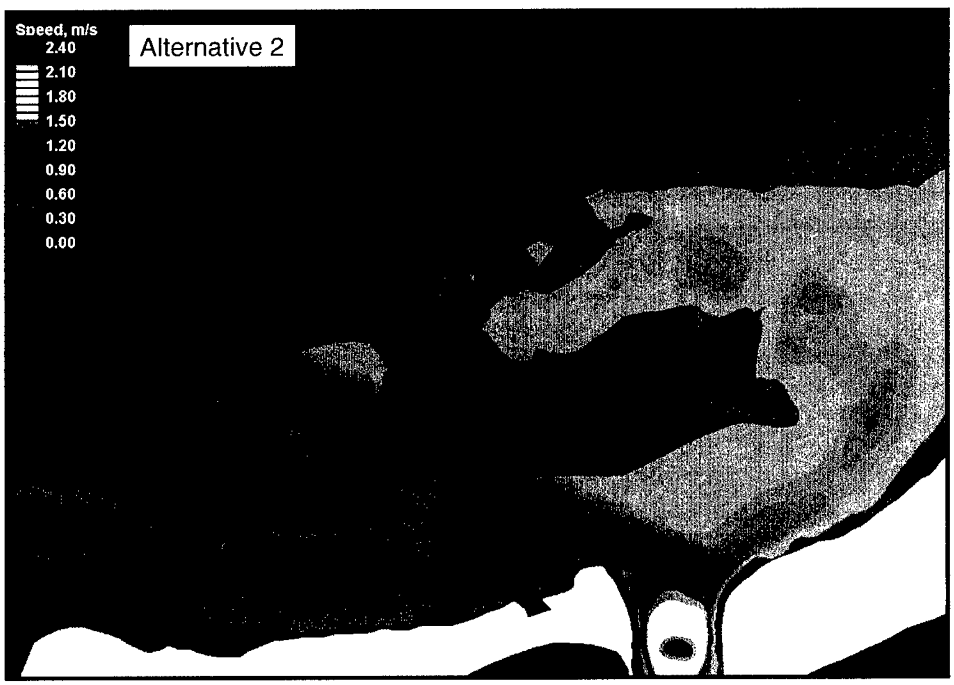

Figure A8. Alternative 2 velocity vectors and speed at flood shoal, peak ebb tide

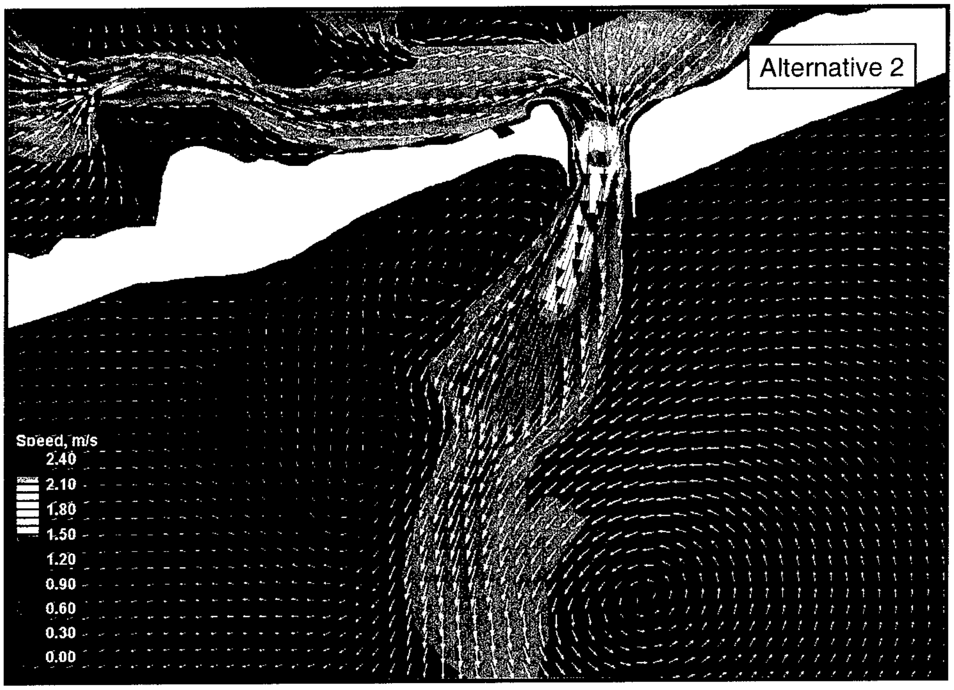

Figure A9. Alternative 2 velocity vectors and speed at inlet and ebb shoal, peak ebb tide

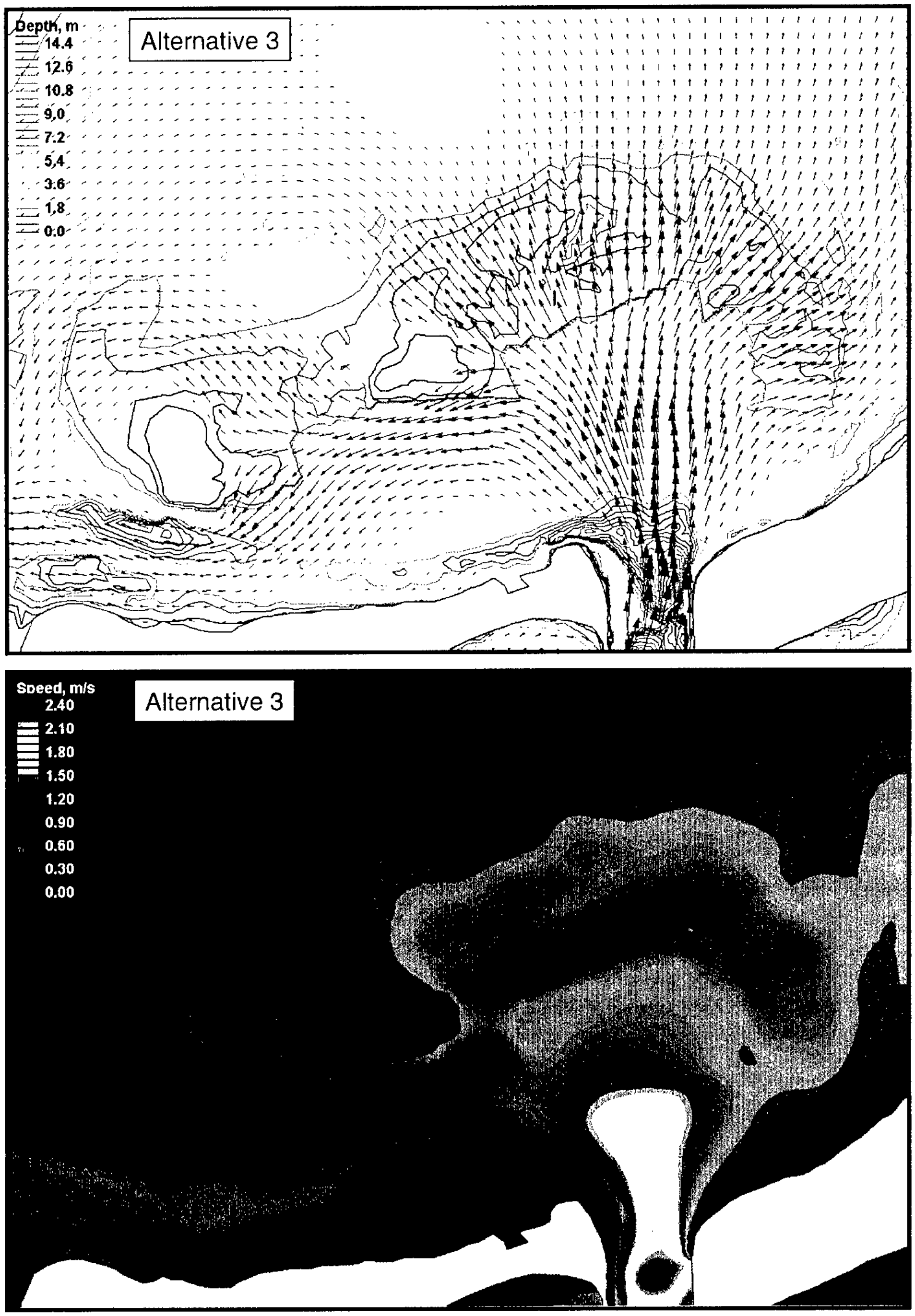

Figure A10. Alternative 3 velocity vectors and speed at flood shoal, peak flood tide

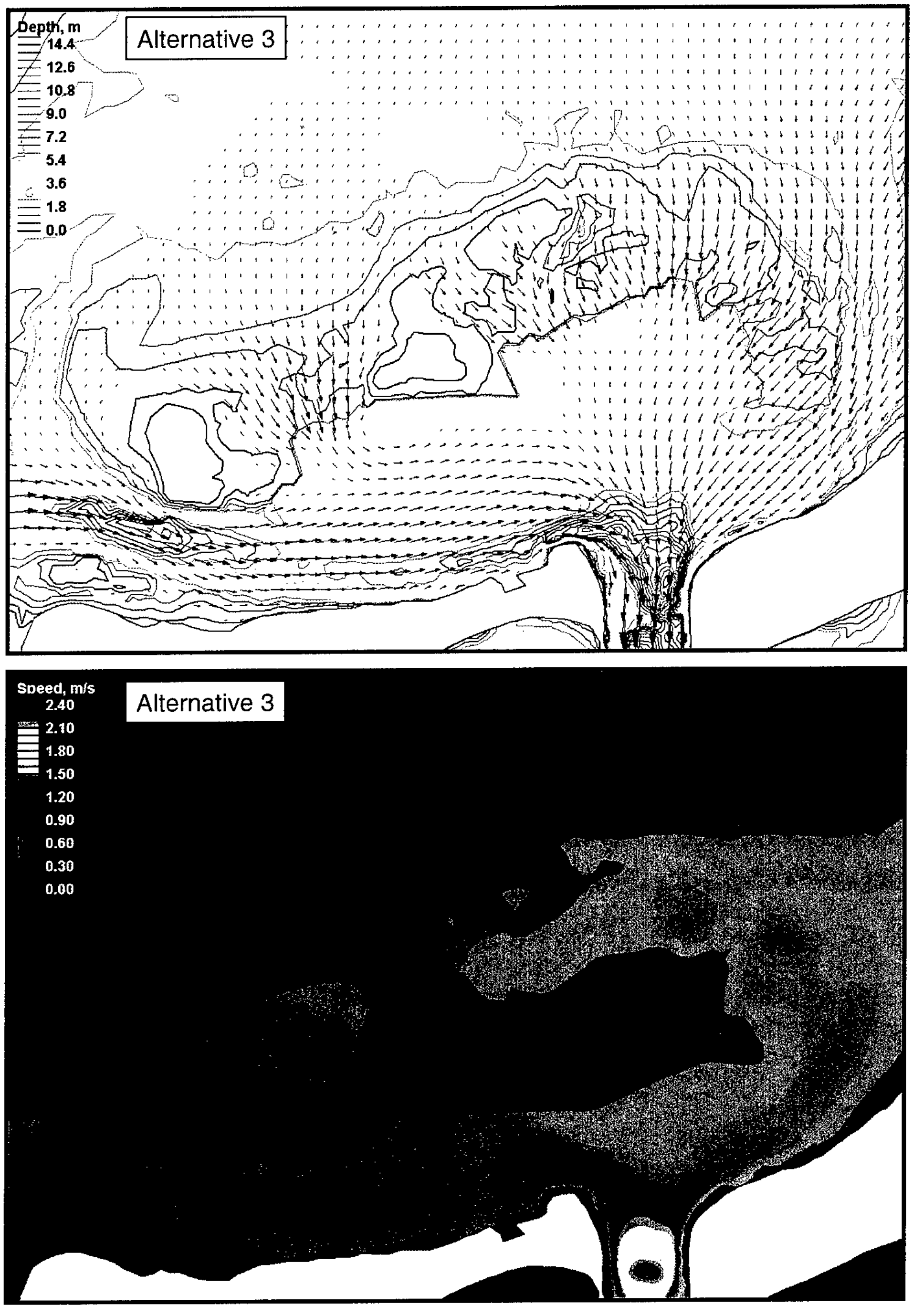

Figure A11. Alternative 3 velocity vectors and speed at flood shoal, peak ebb tide

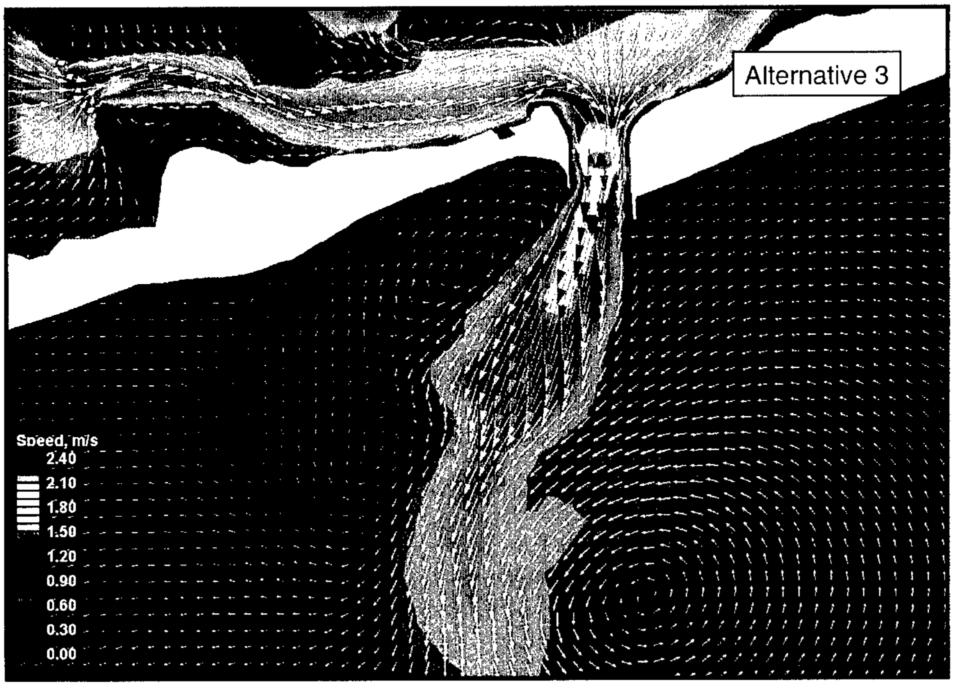

Figure A12. Alternative 3 velocity vectors and speed at inlet and ebb shoal, peak ebb tide

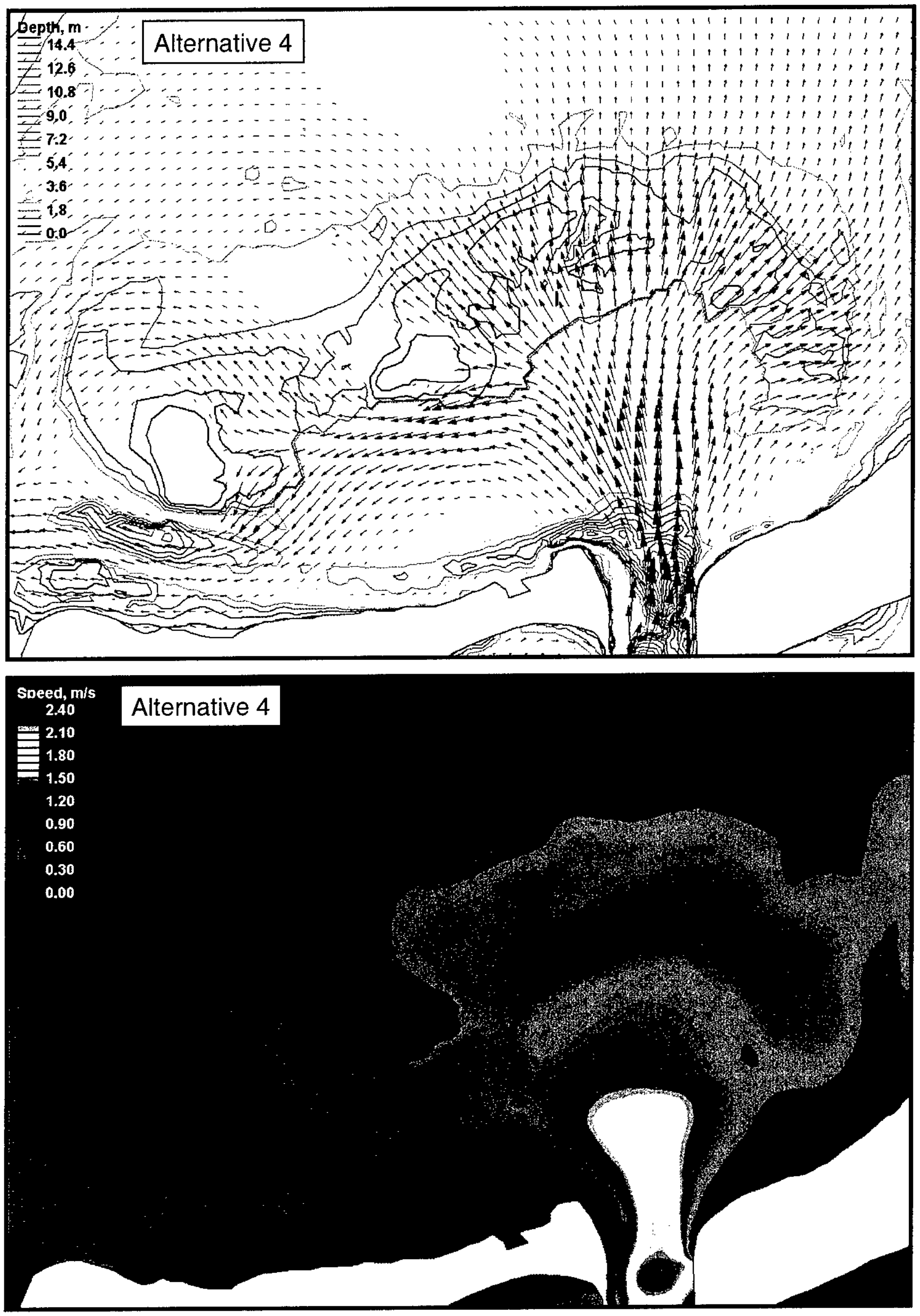

Figure A13. Alternative 4 velocity vectors and speed at flood shoal, peak flood tide

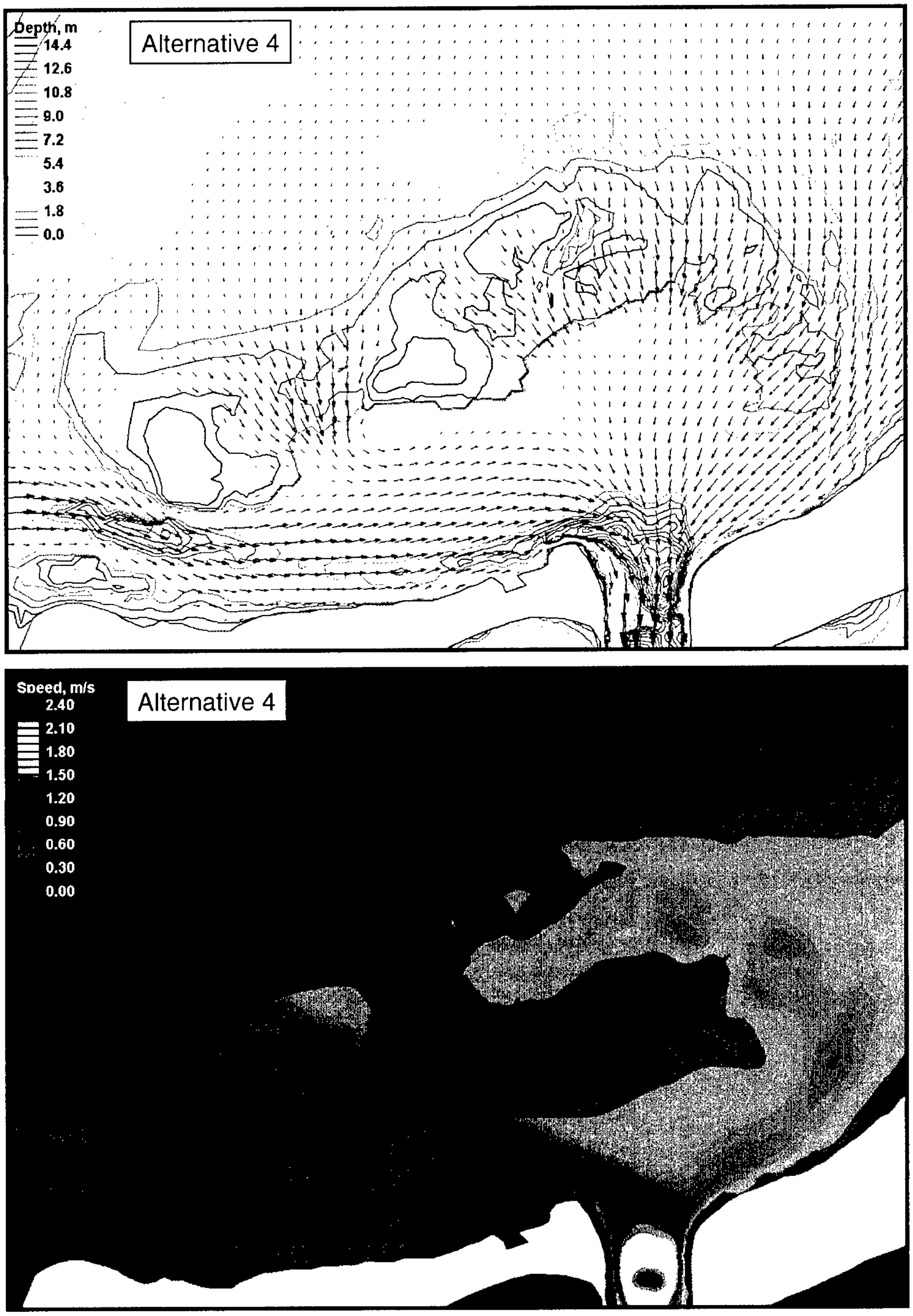

Figure A14. Alternative 4 velocity vectors and speed at flood shoal, peak ebb tide

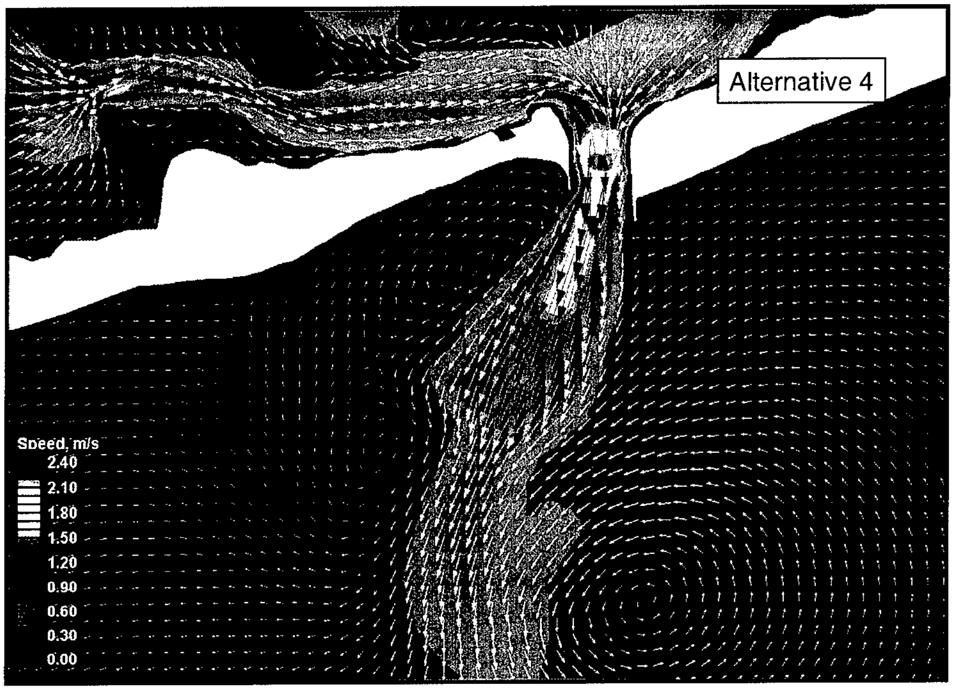

Figure A15. Alternative 4 velocity vectors and speed at inlet and ebb shoal, peak ebb tide

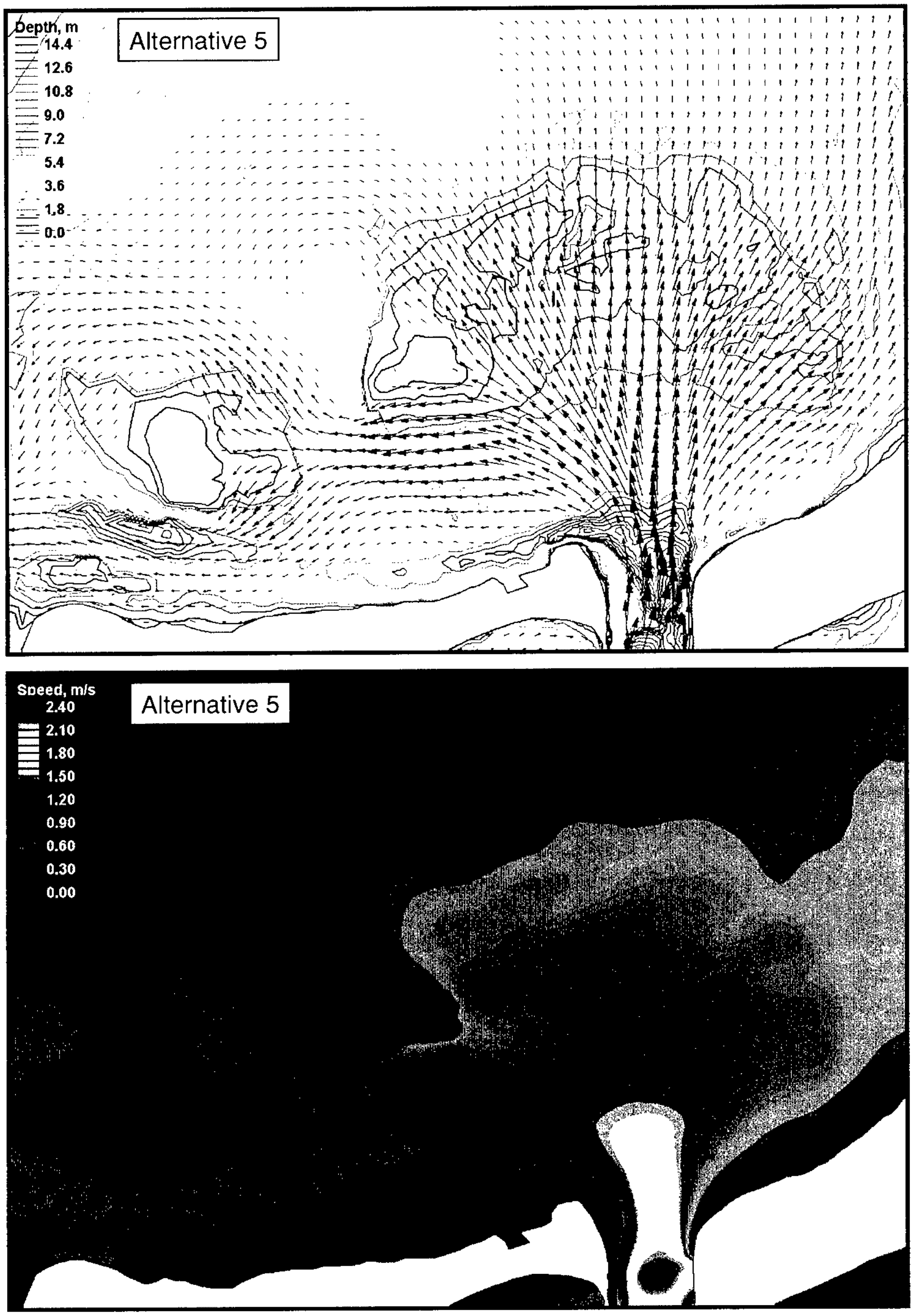

Figure A16. Alternative 5 velocity vectors and speed at flood shoal, peak flood tide

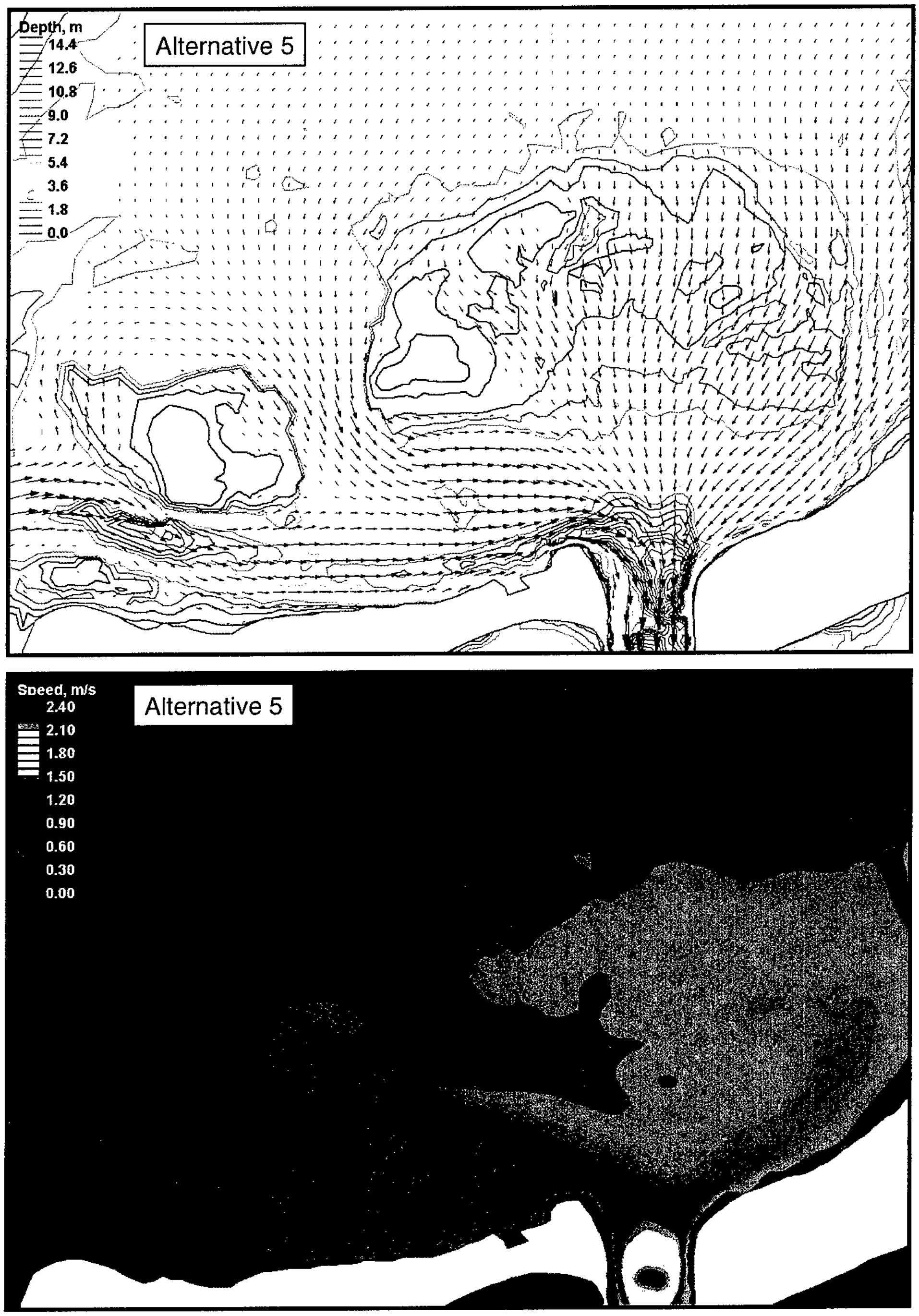

Figure A17. Alternative 5 velocity vectors and speed at flood shoal, peak ebb tide

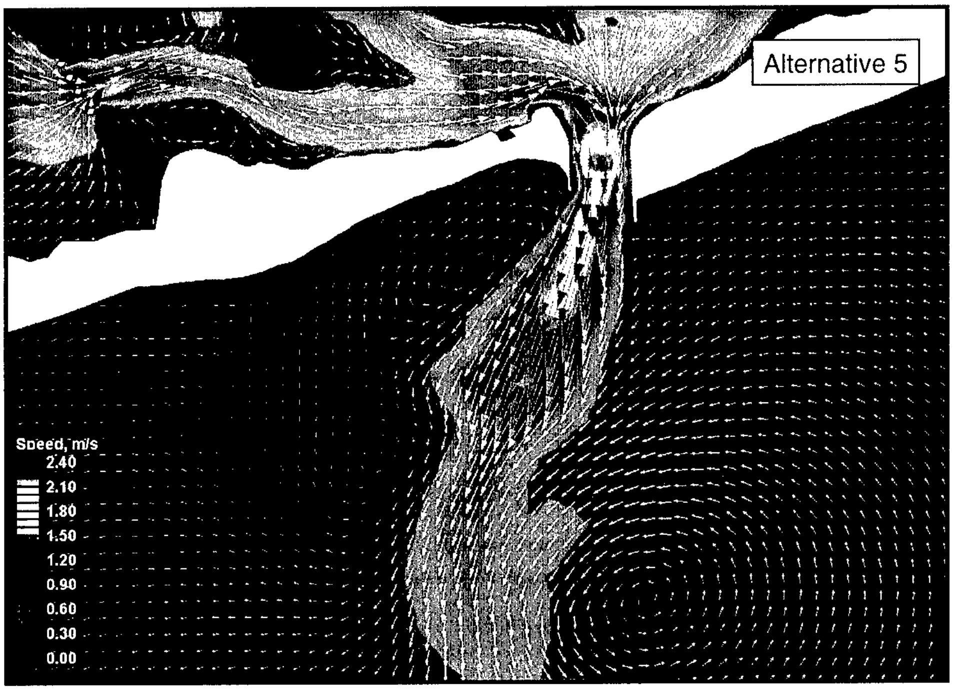

Figure A18. Alternative 5 velocity vectors and speed at inlet and ebb shoal, peak ebb tide

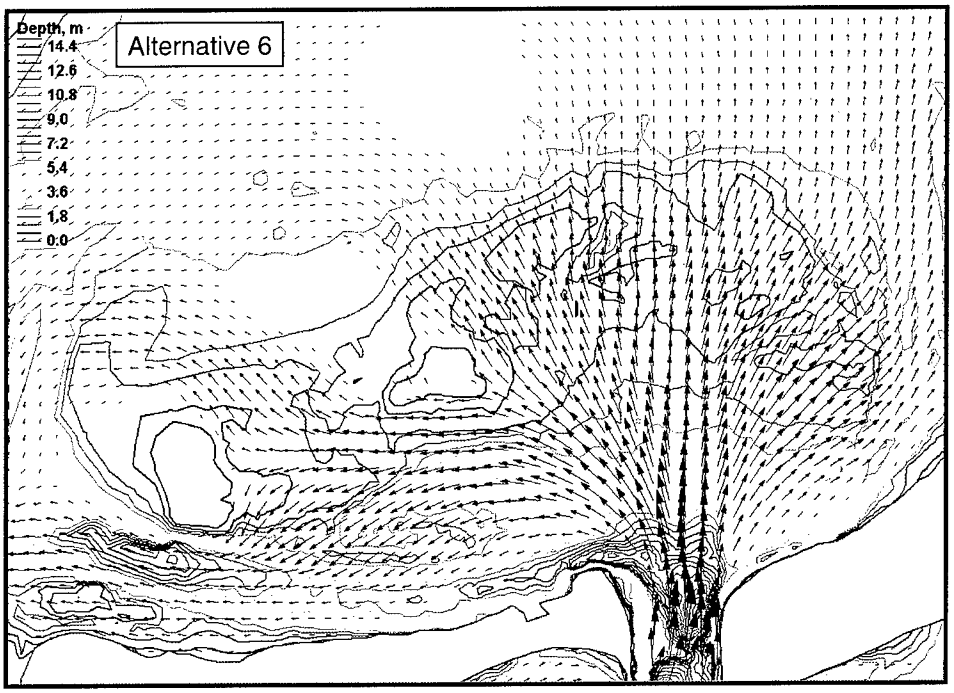

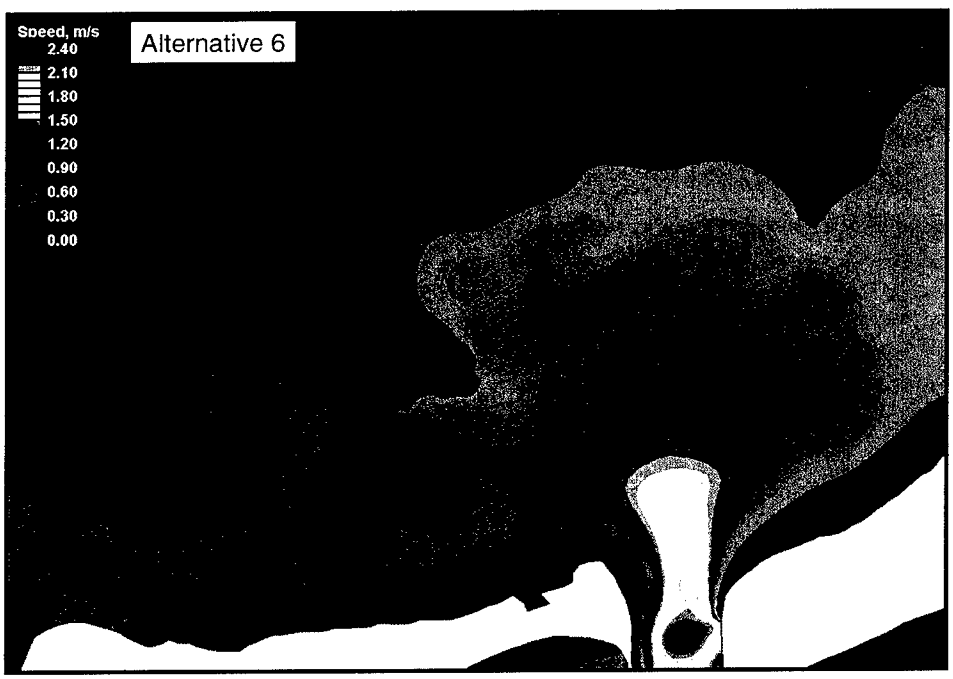

Figure A19. Alternative 6 velocity vectors and speed at flood shoal, peak flood tide

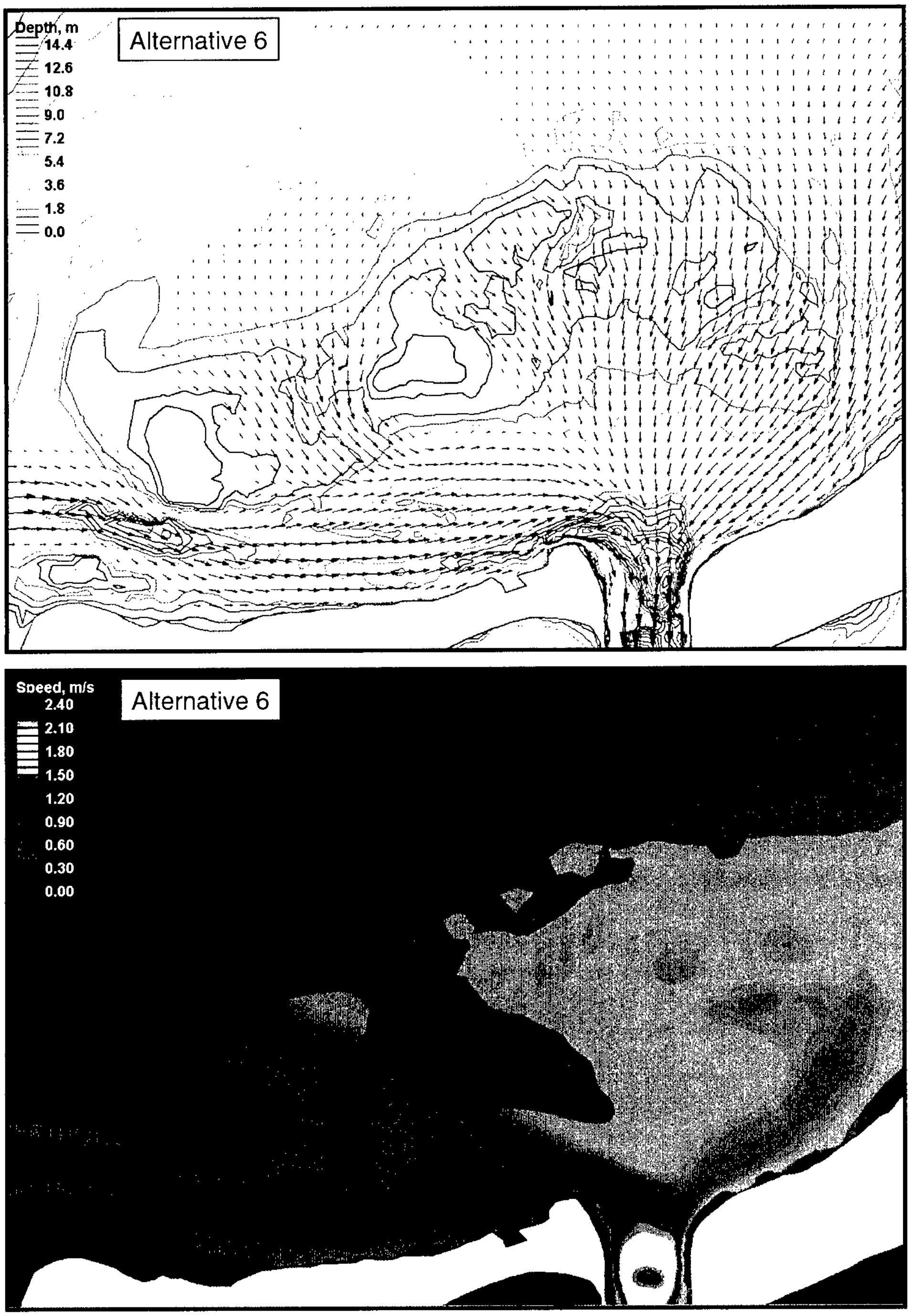

Figure A20. Alternative 6 velocity vectors and speed at flood shoal, peak ebb tide

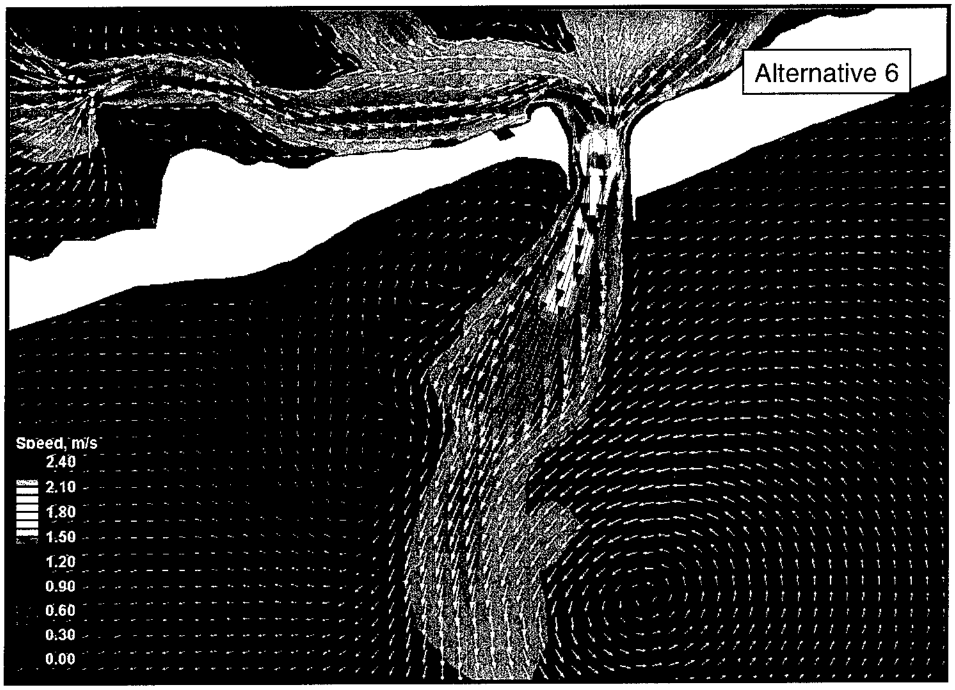

Figure A21. Alternative 6 velocity vectors and speed at inlet and ebb shoal, peak ebb tide

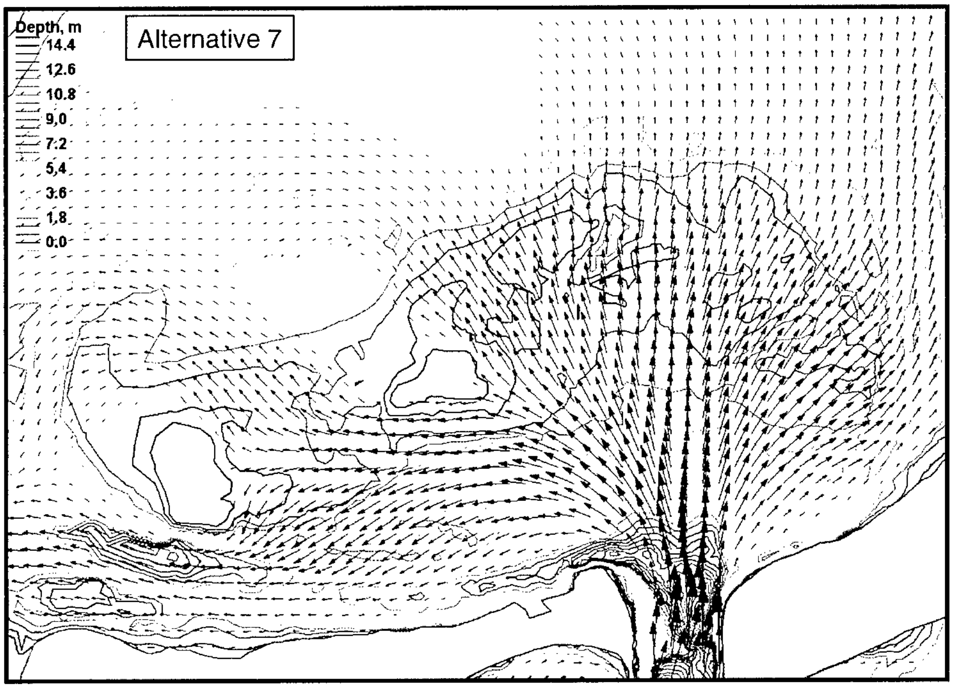

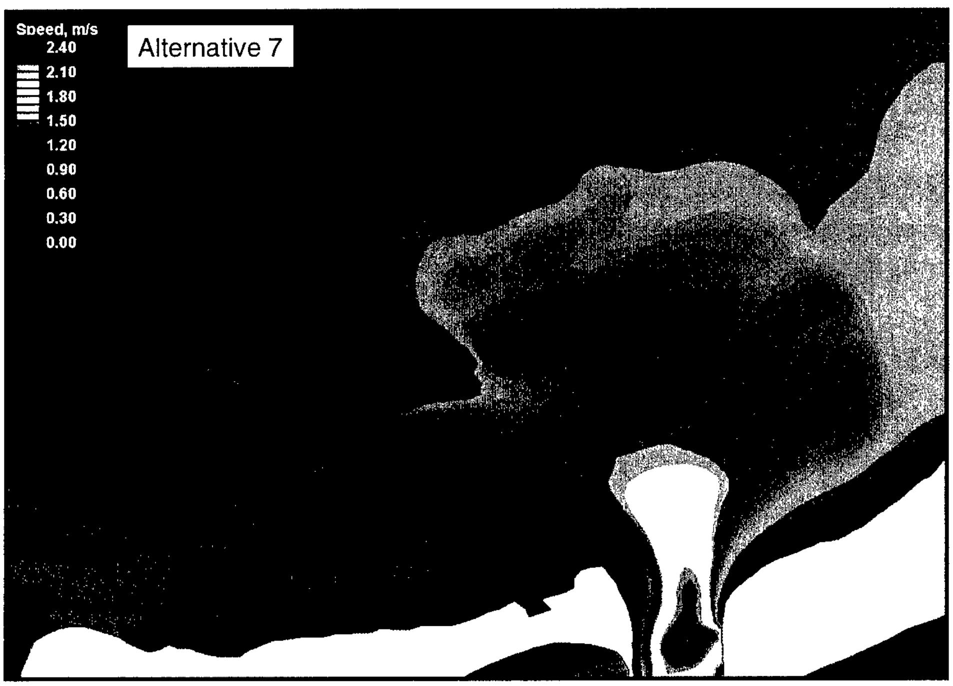

Figure A22. Alternative 7 velocity vectors and speed at flood shoal, peak flood tide

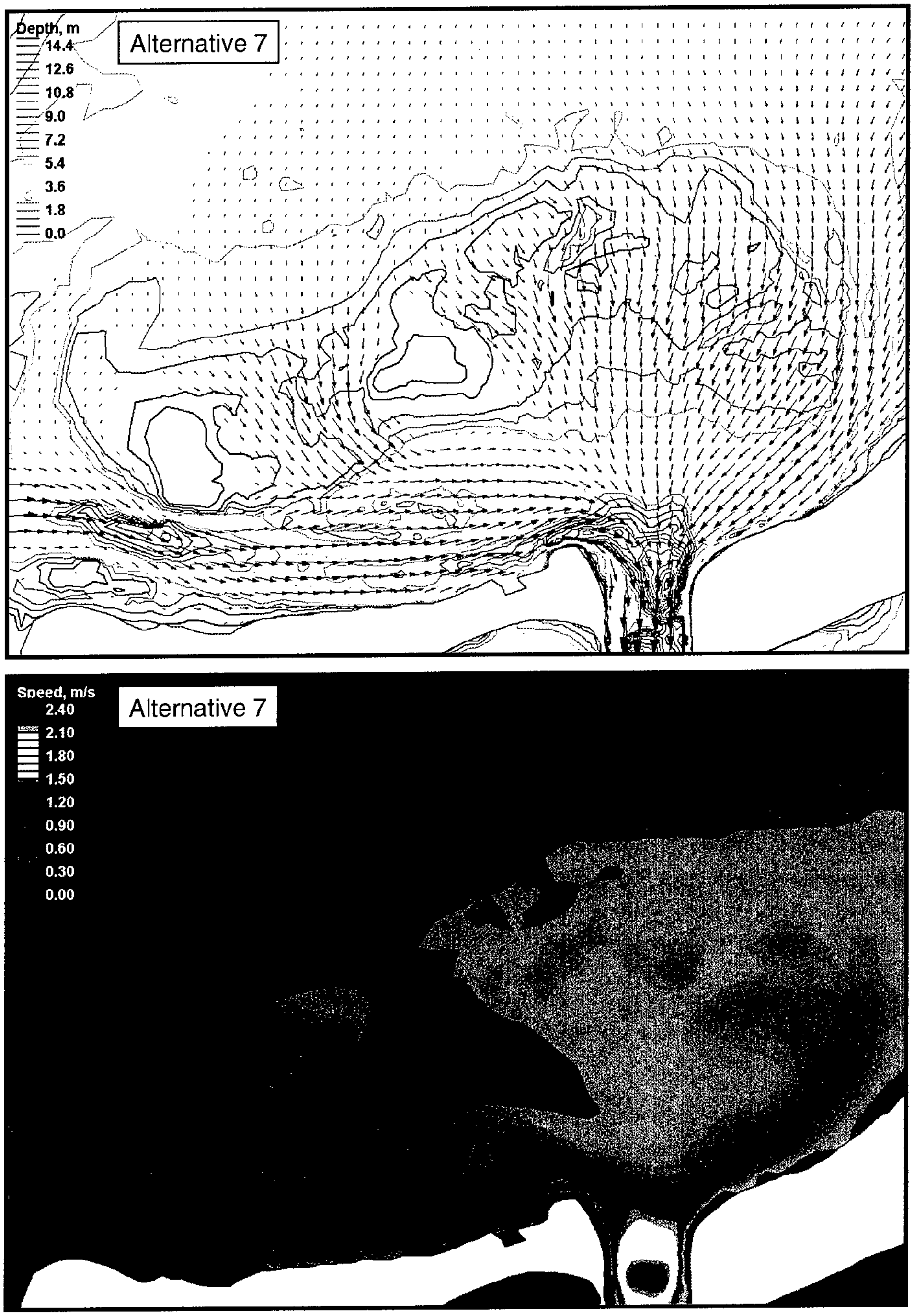

Figure A23. Alternative 7 velocity vectors and speed at flood shoal, peak ebb tide

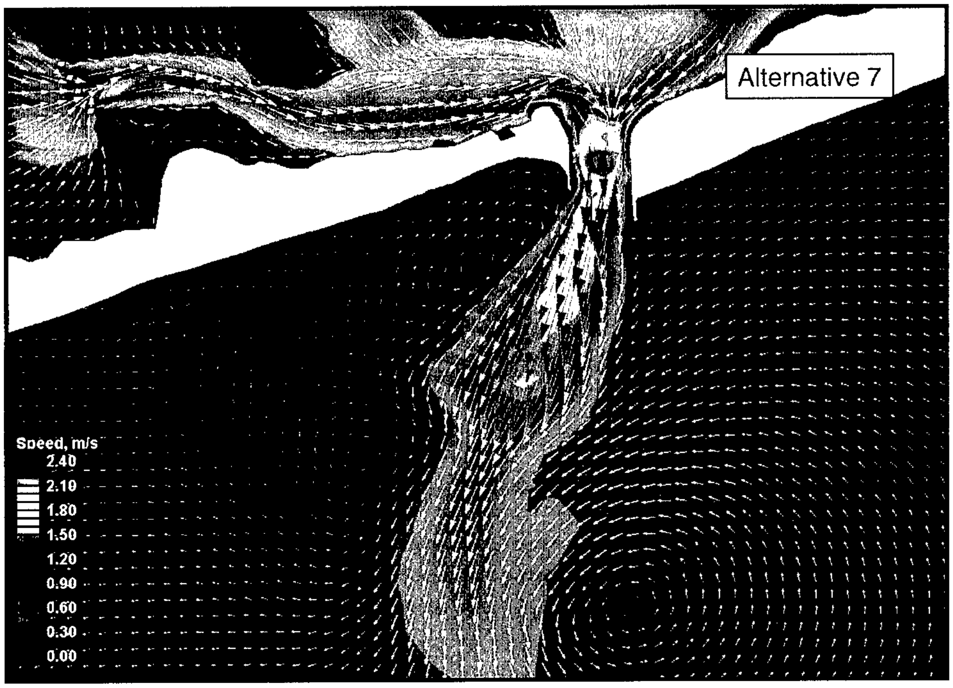

Figure A24. Alternative 7 velocity vectors and speed at inlet and ebb shoal, peak ebb tide

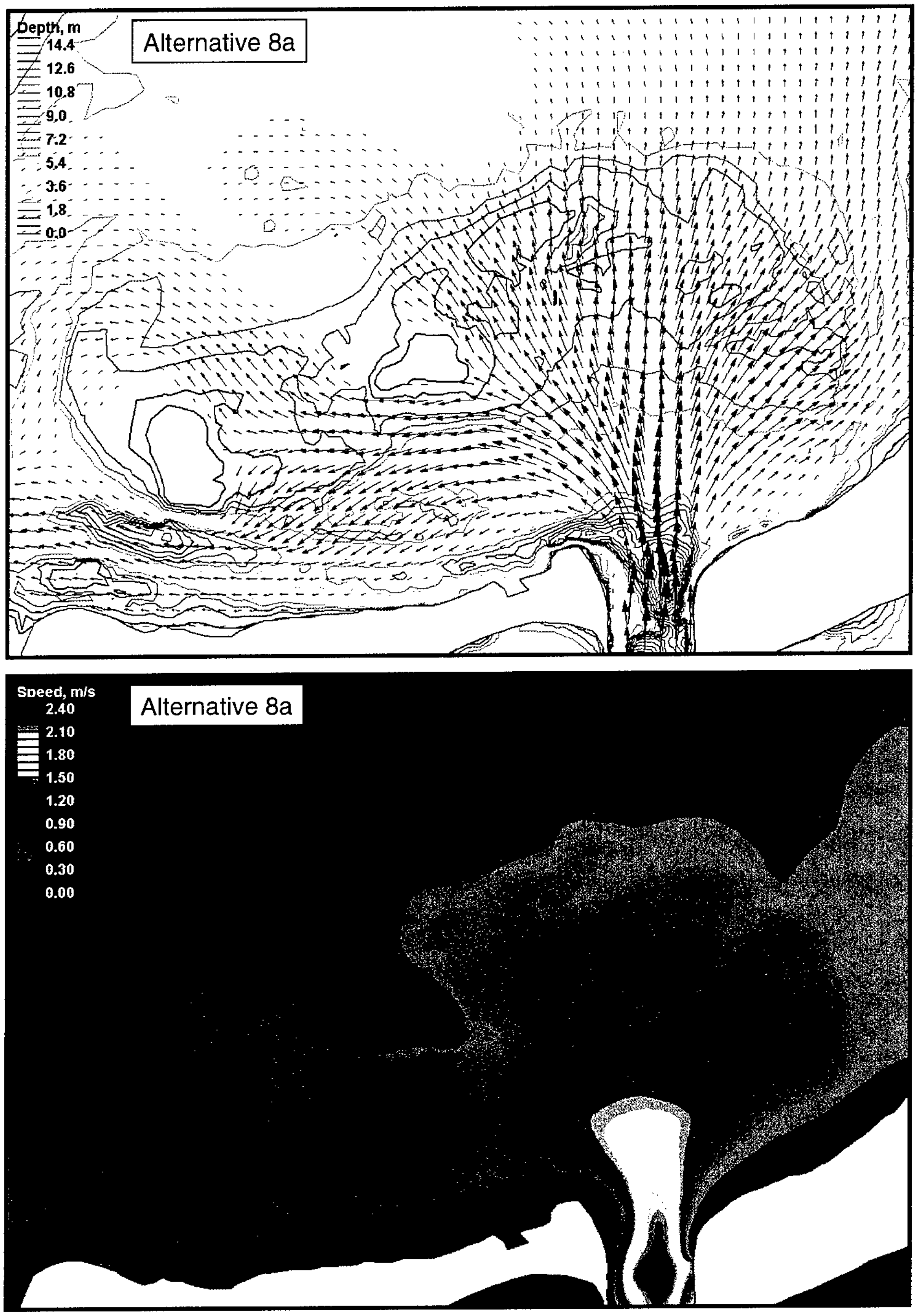

Figure A25. Alternative 8a velocity vectors and speed at flood shoal, peak flood tide

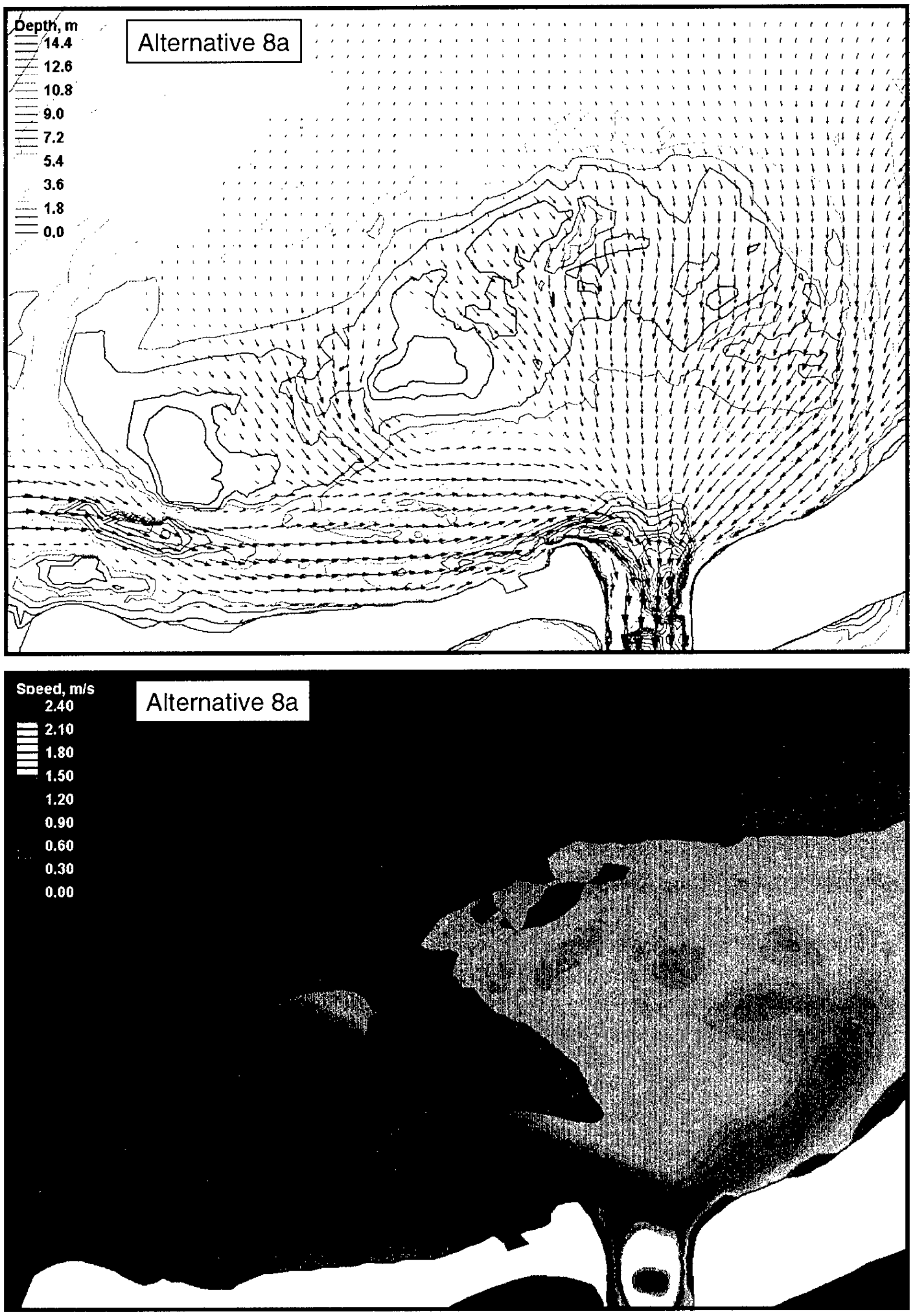

Figure A26. Alternative 8a velocity vectors and speed at flood shoal, peak ebb tide

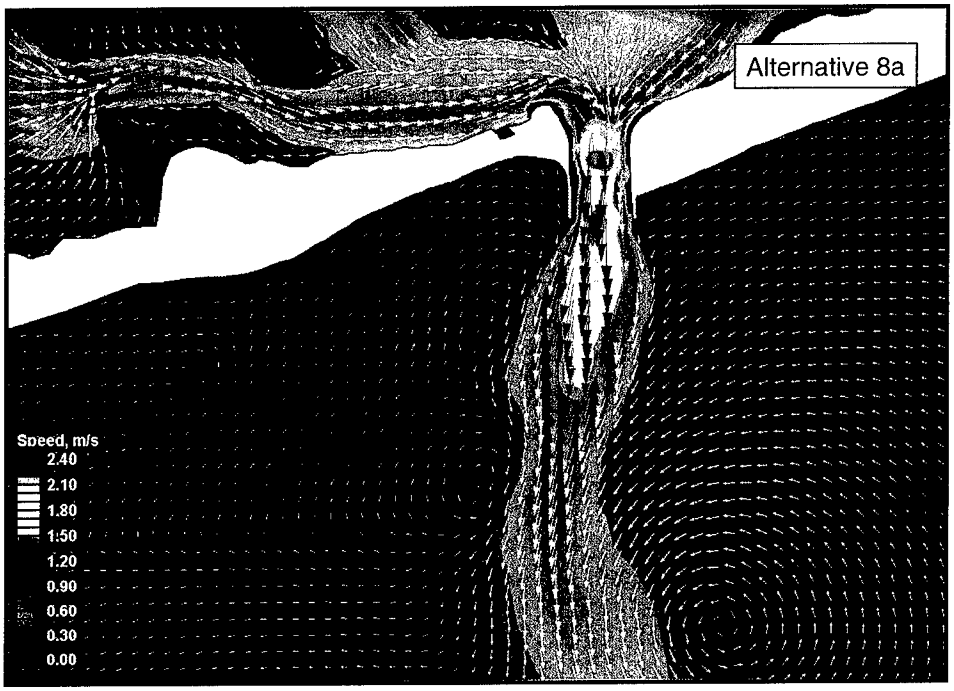

Figure A27. Alternative 8a velocity vectors and speed at inlet and ebb shoal, peak ebb tide

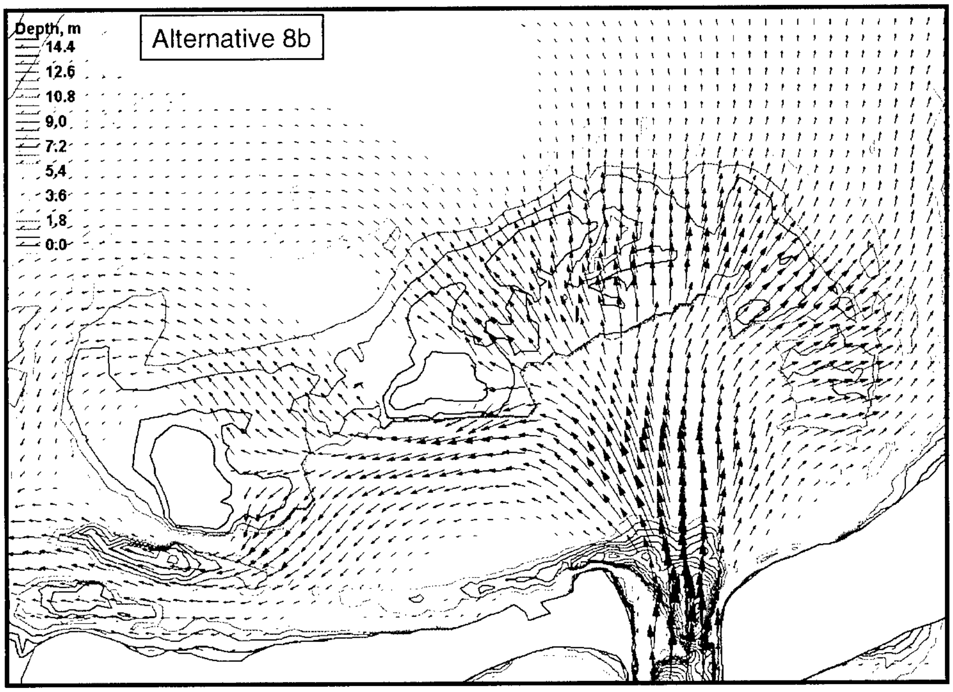

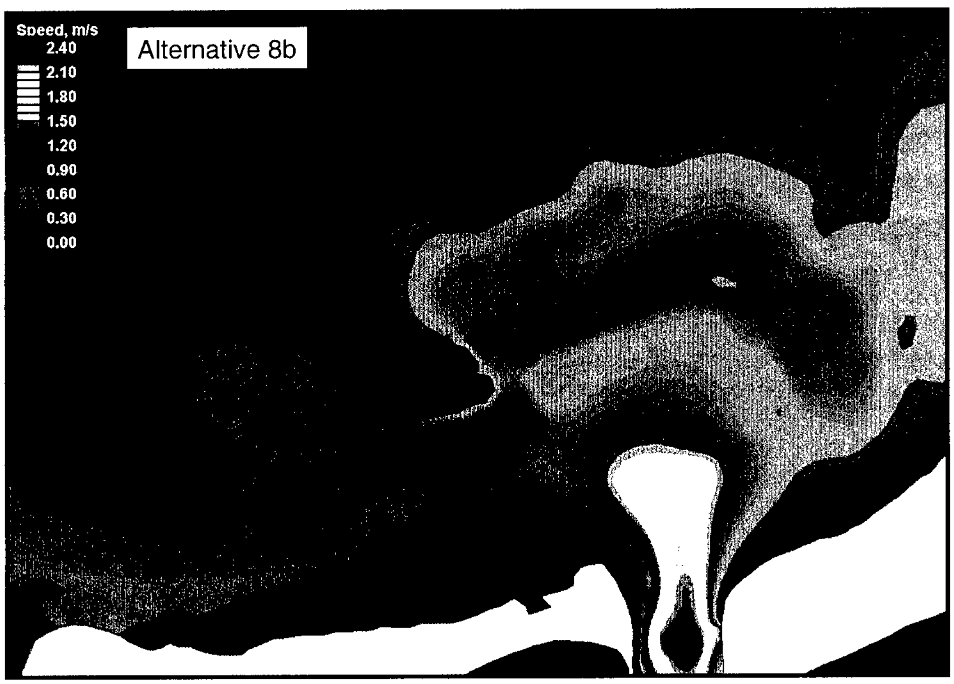

Figure A28. Alternative 8b velocity vectors and speed at flood shoal, peak flood tide

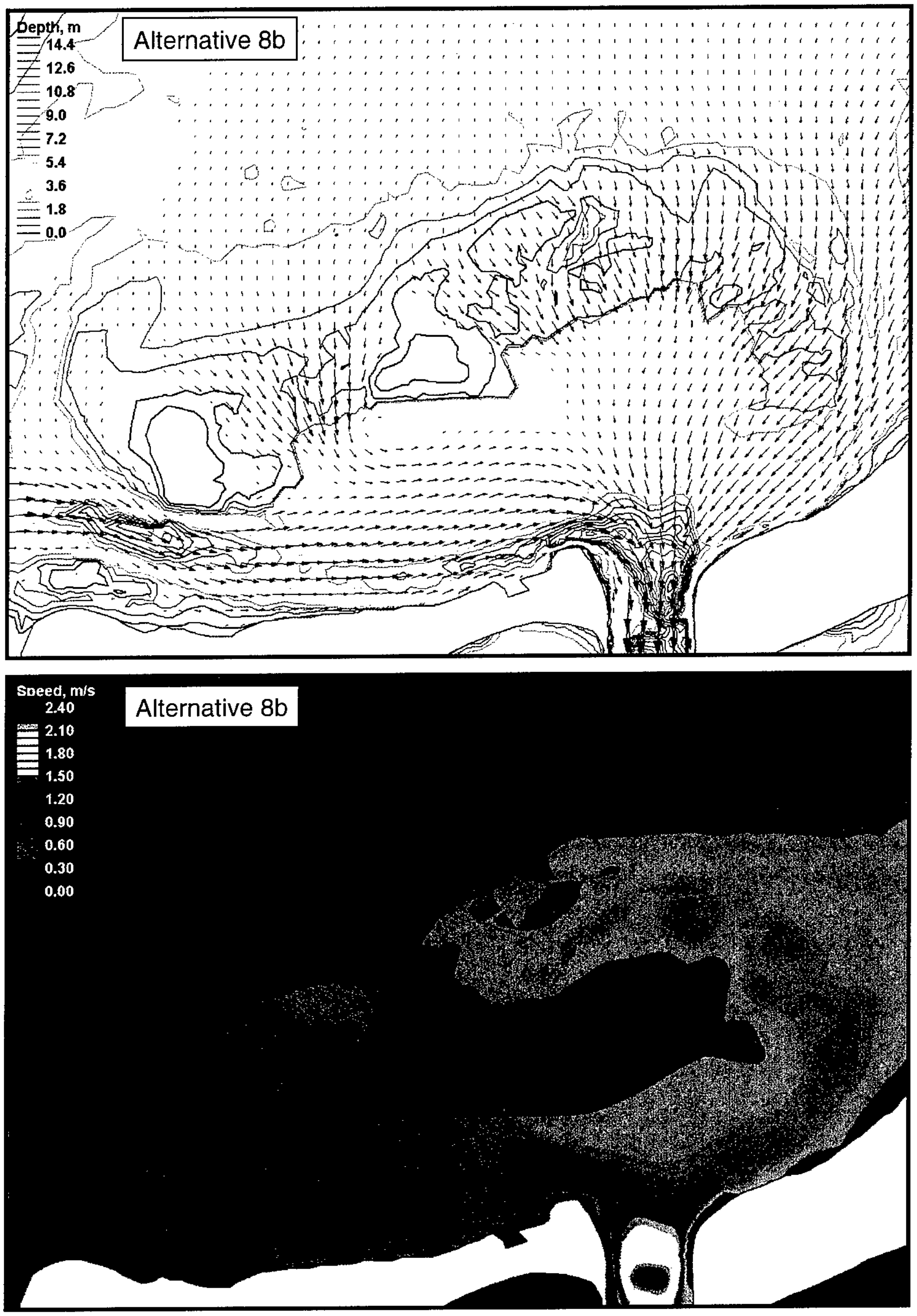

Figure A29. Alternative 8b velocity vectors and speed at flood shoal, peak ebb tide

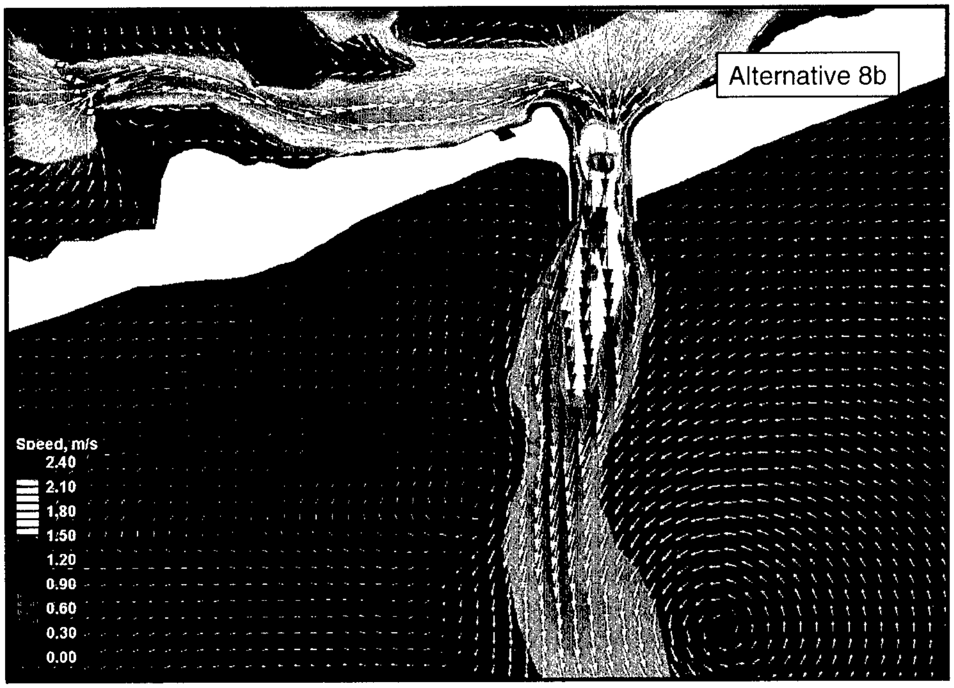

Figure A30. Alternative 8b velocity vectors and speed at inlet and ebb shoal, peak ebb tide

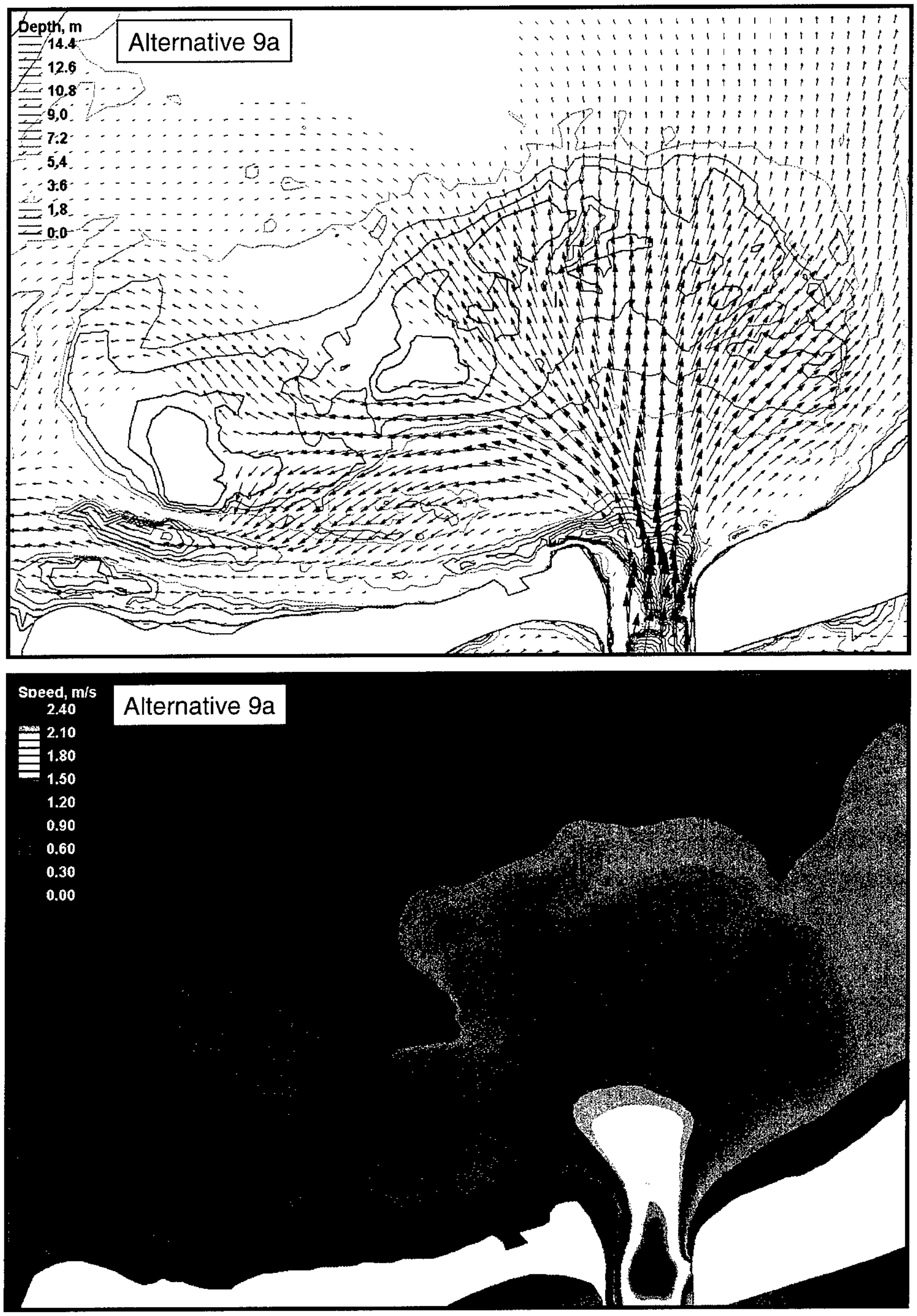

Figure A31. Alternative 9a velocity vectors and speed at flood shoal, peak flood tide

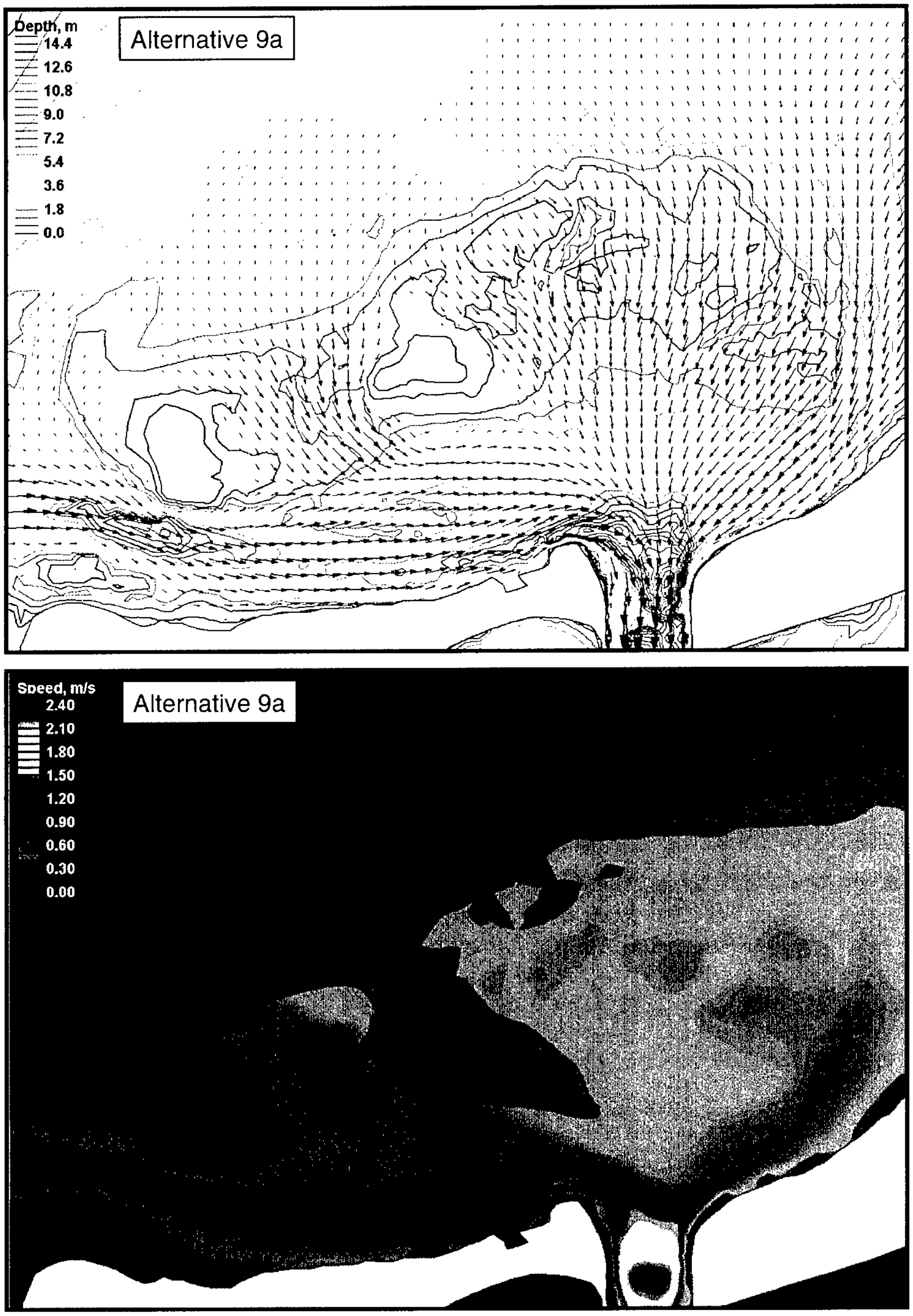

Figure A32. Alternative 9a velocity vectors and speed at flood shoal, peak ebb tide

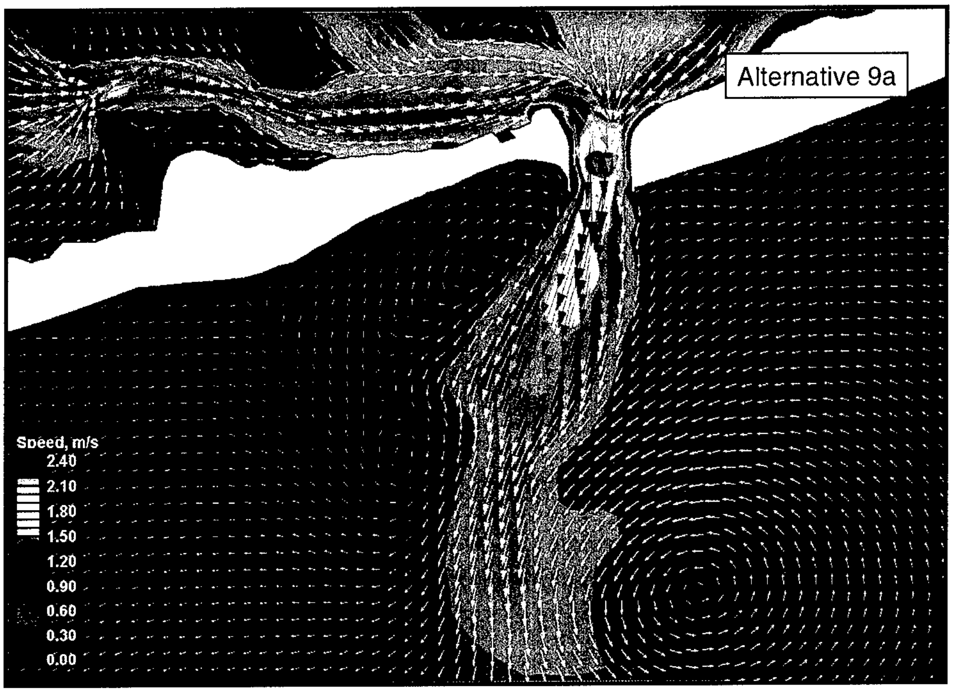

Figure A33. Alternative 9a velocity vectors and speed at inlet and ebb shoal, peak ebb tide

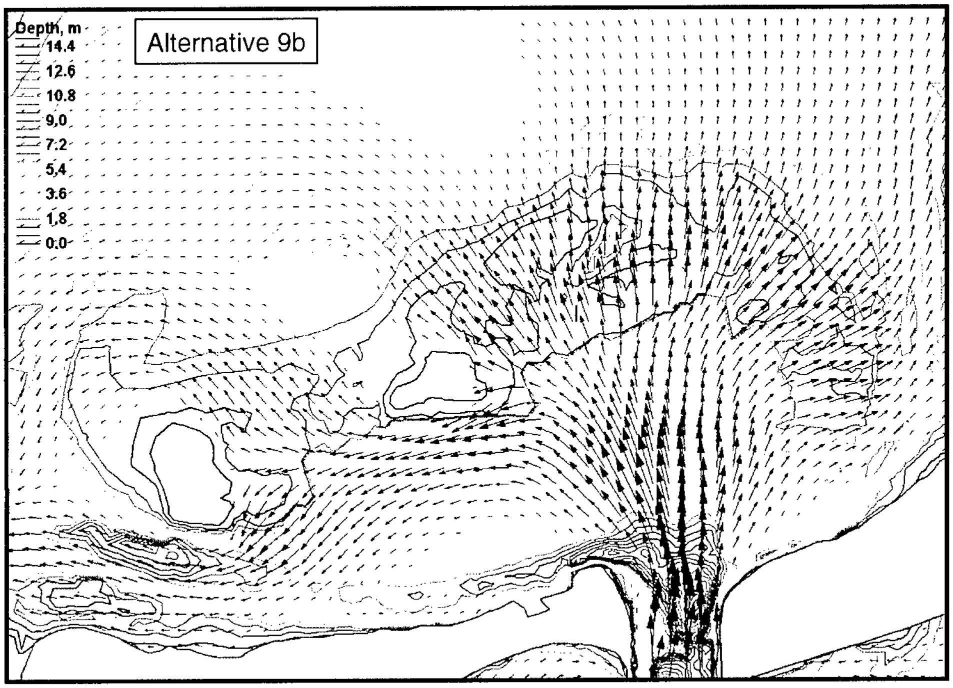

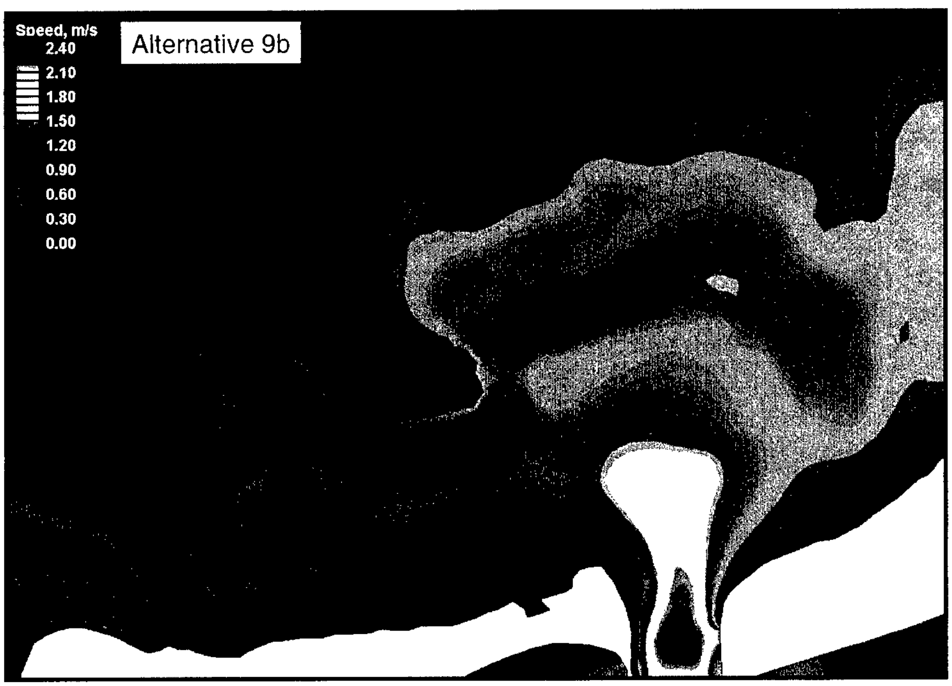

Figure A34. Alternative 9b velocity vectors and speed at flood shoal, peak flood tide

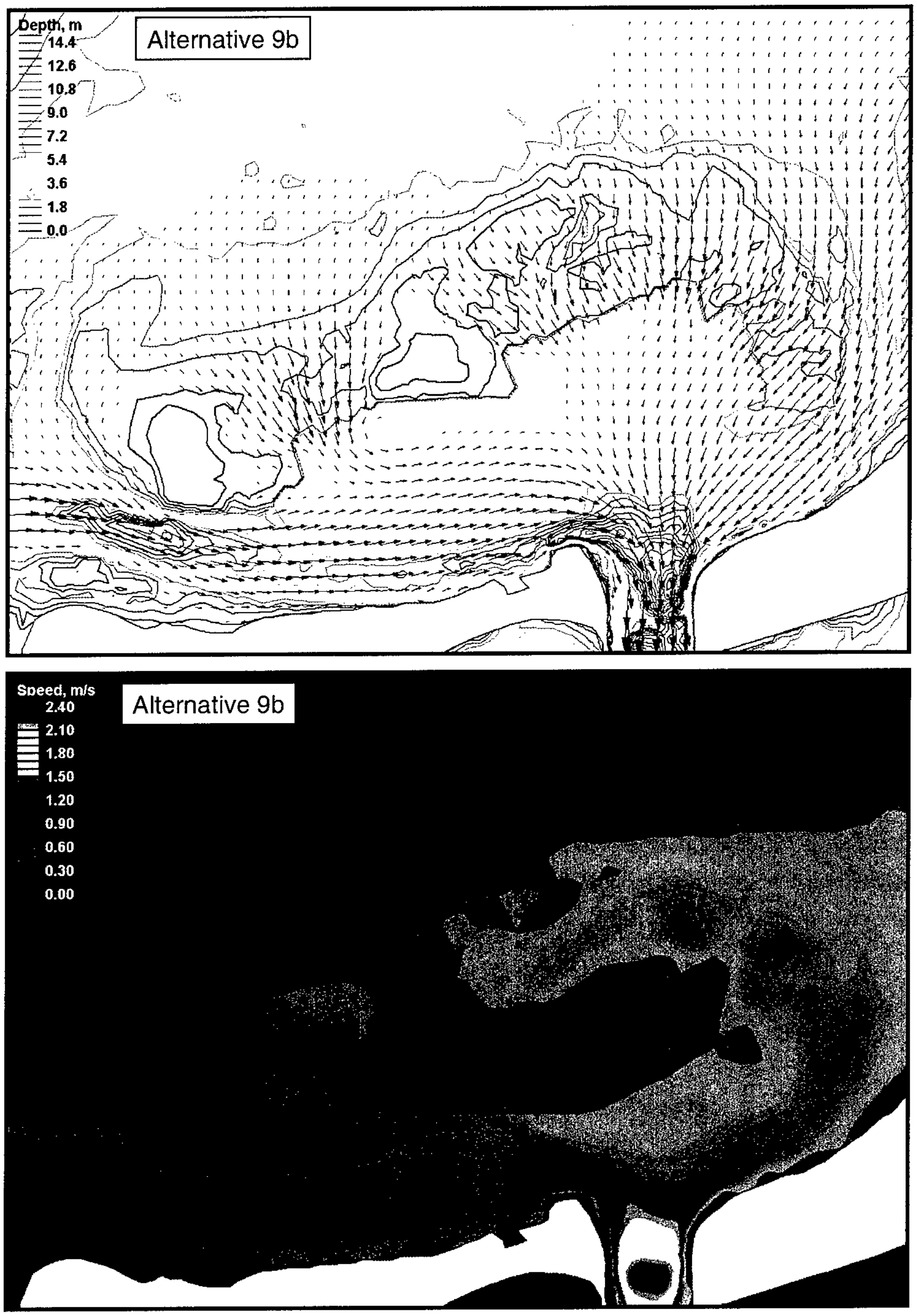

Figure A35. Alternative 9b velocity vectors and speed at flood shoal, peak ebb tide

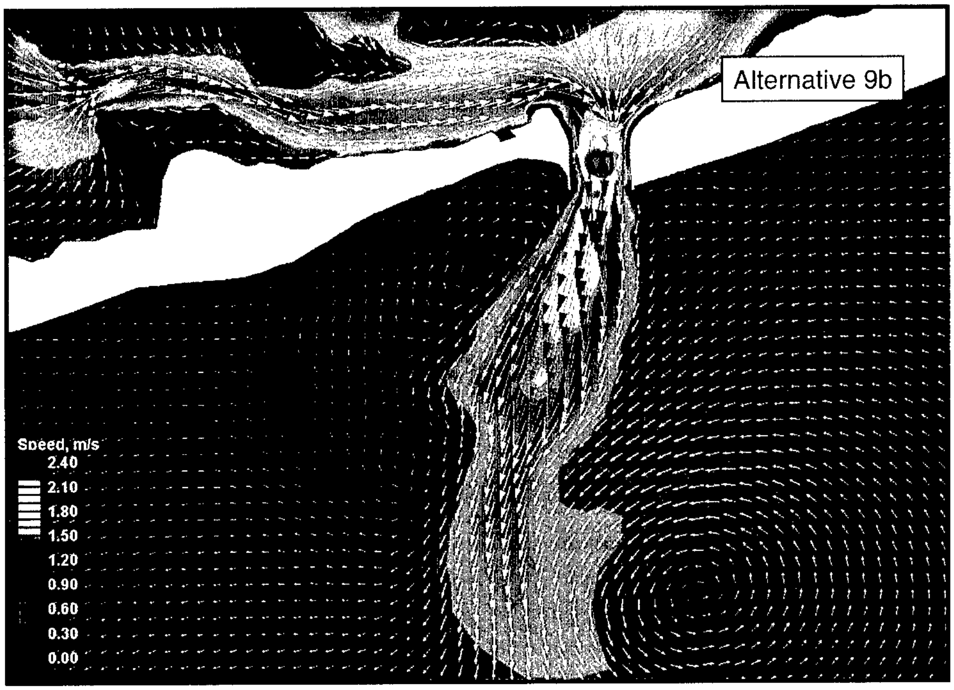

Figure A36. Alternative 9b velocity vectors and speed at inlet and ebb shoal, peak ebb tide

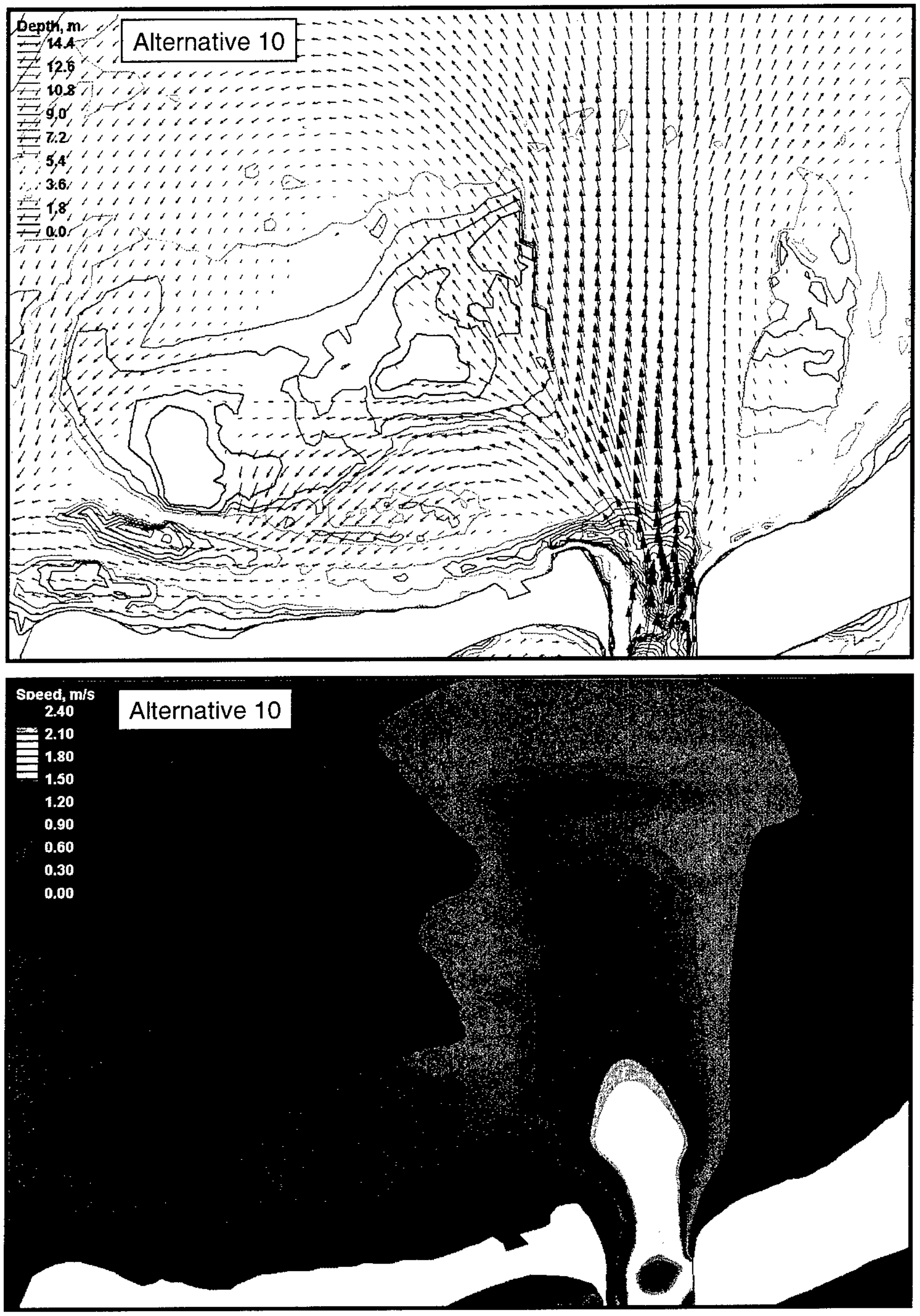

Figure A37. Alternative 10 velocity vectors and speed at flood shoal, peak flood tide

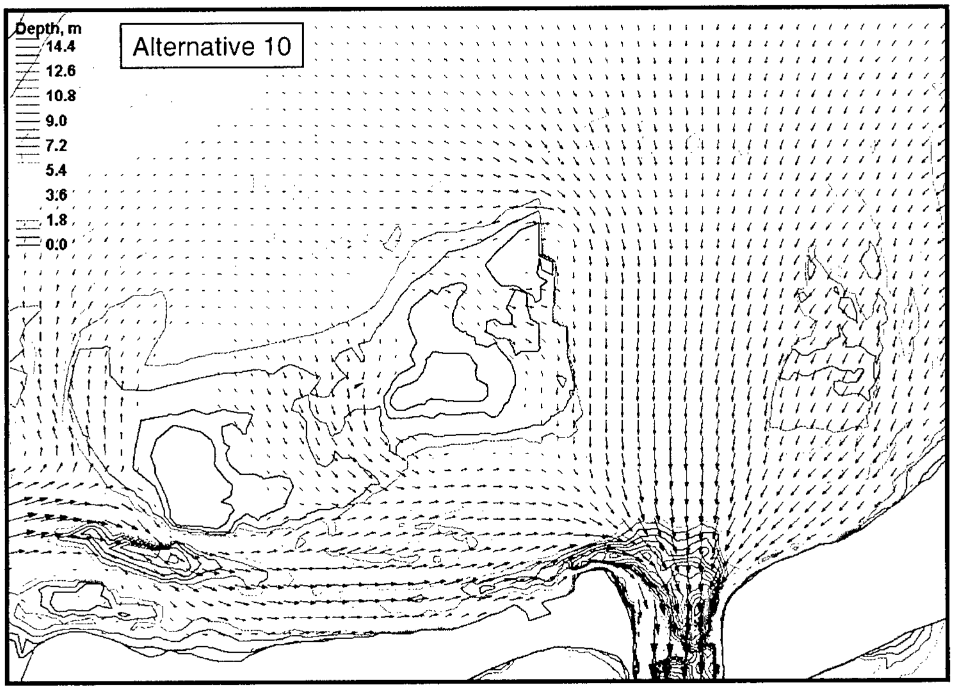

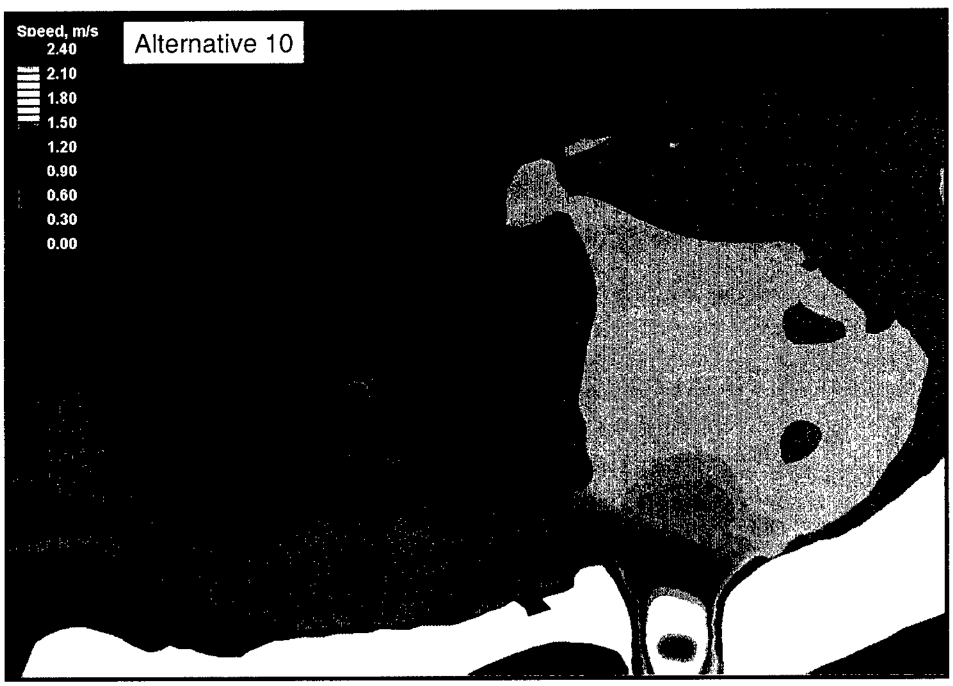

Figure A38. Alternative 10 velocity vectors and speed at flood shoal, peak ebb tide

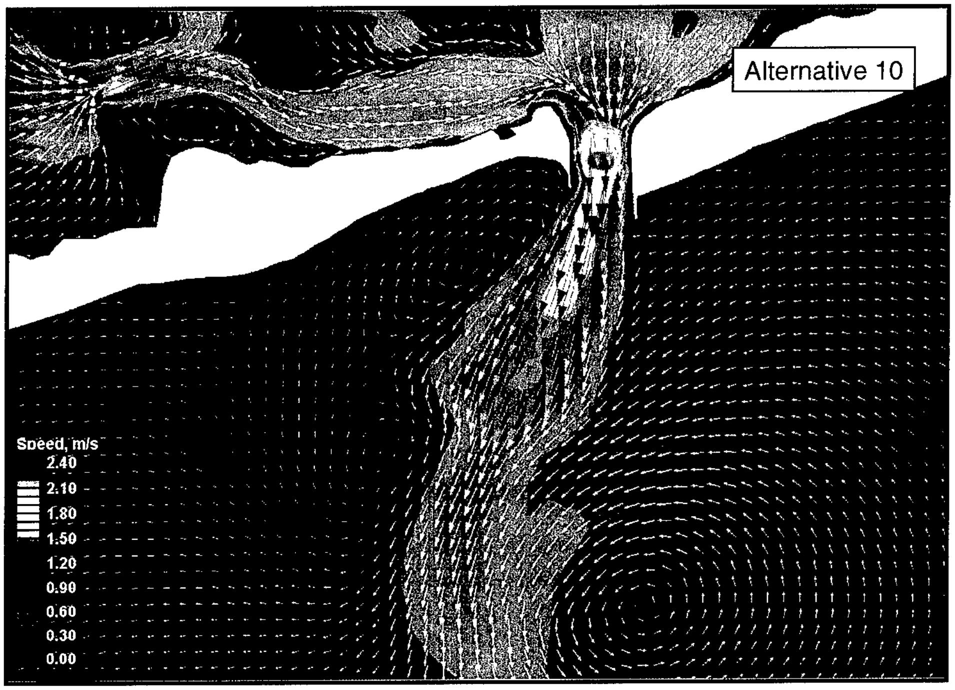

Figure A39. Alternative 10 velocity vectors and speed at inlet and ebb shoal, peak ebb tide

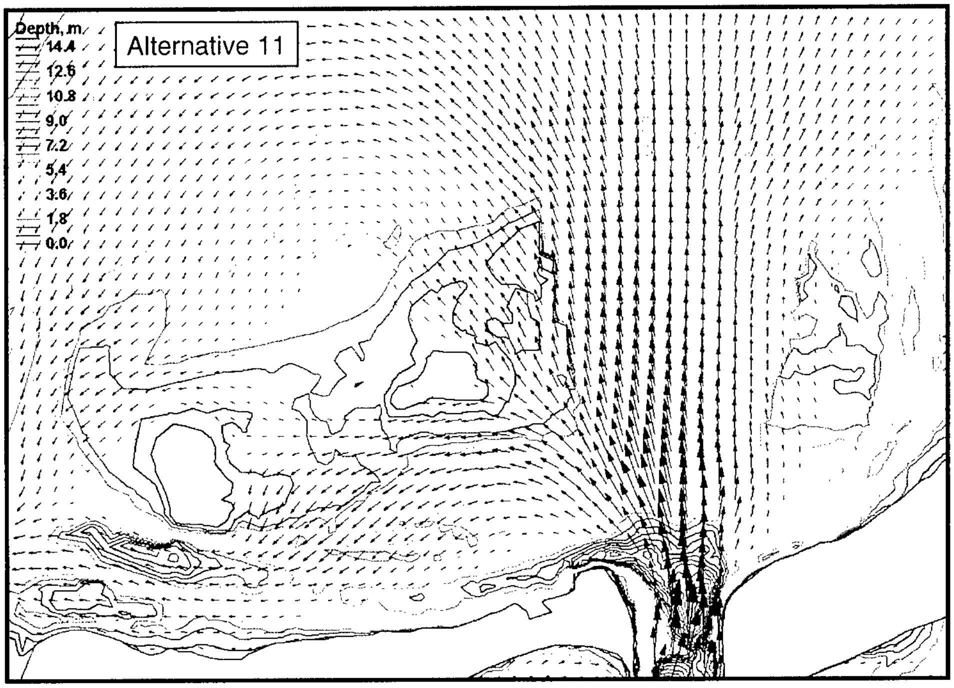

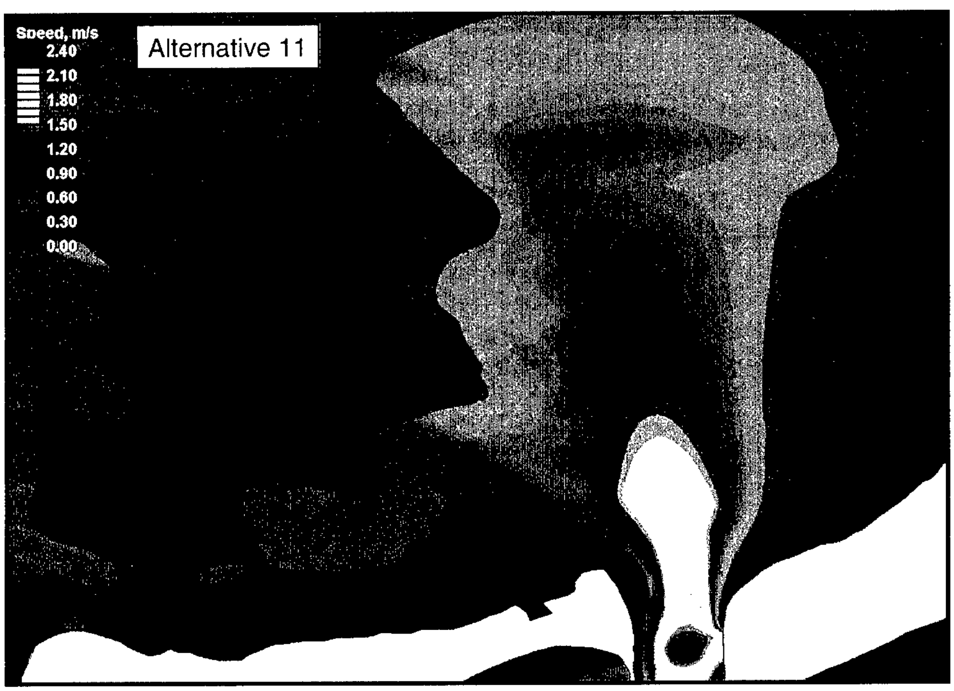

Figure A40. Alternative 11 velocity vectors and speed at flood shoal, peak flood tide

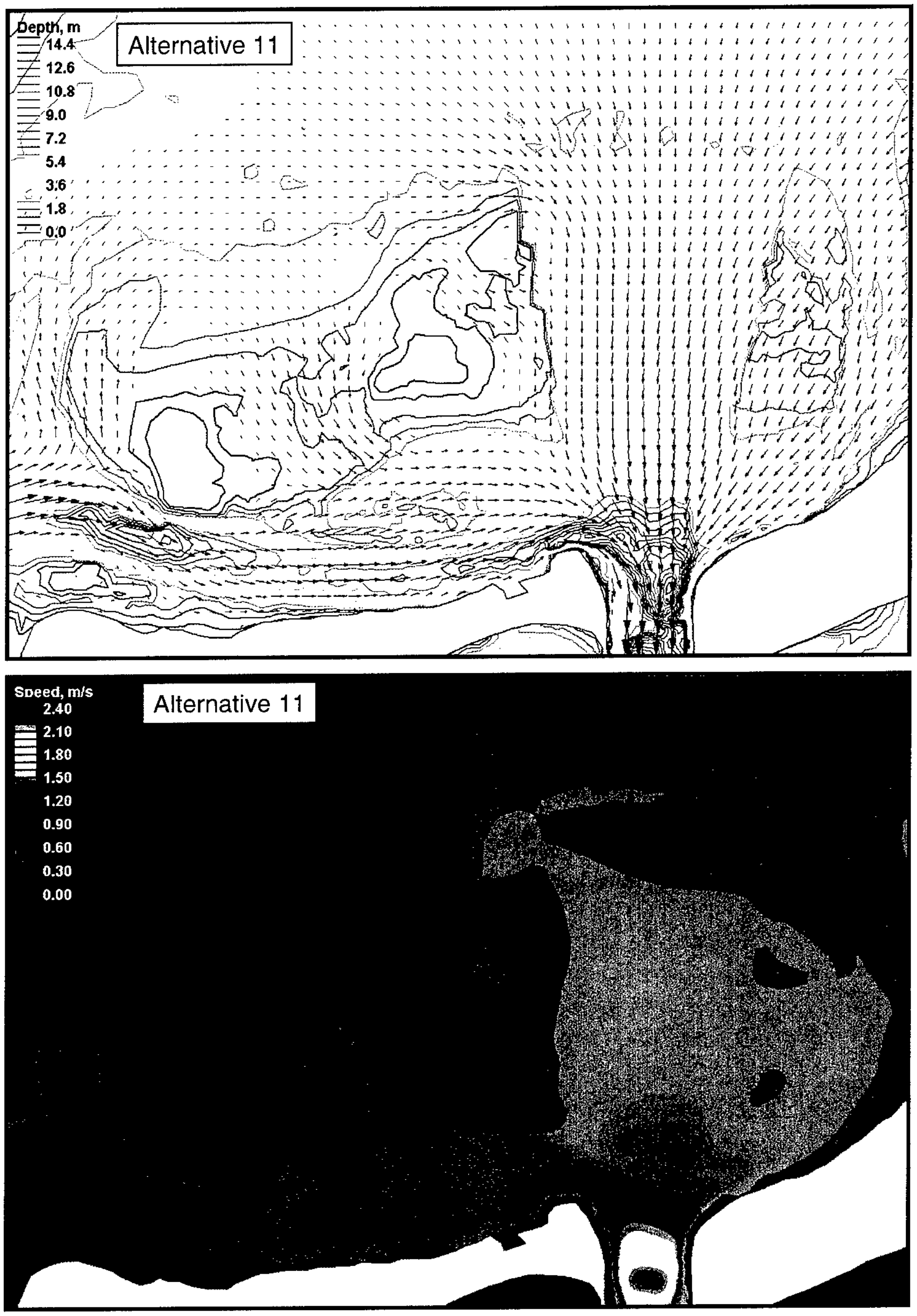

Figure A41. Alternative 11 velocity vectors and speed at flood shoal, peak ebb tide

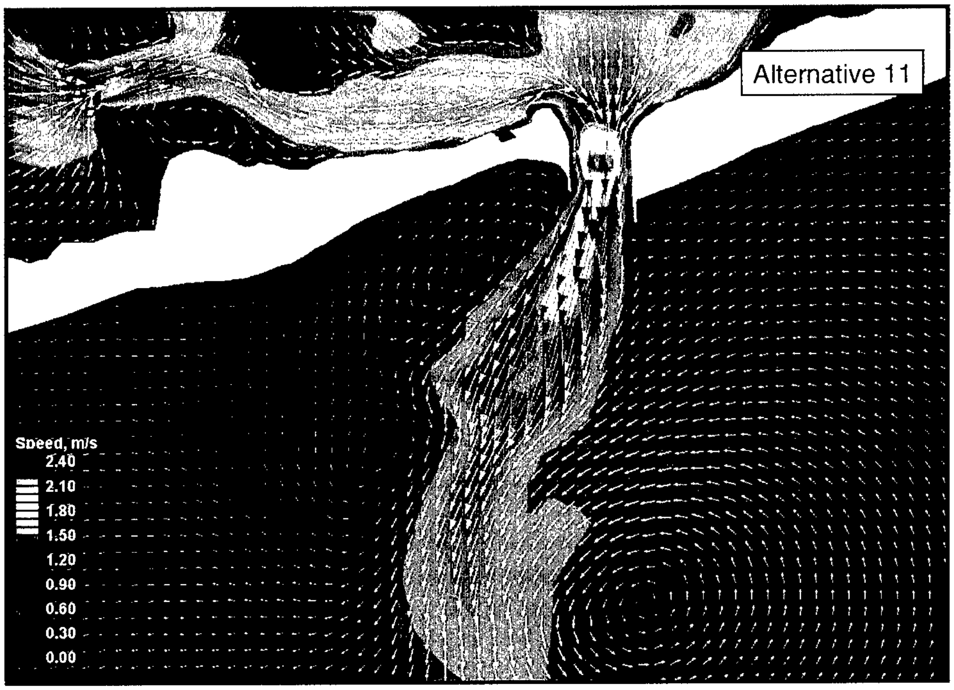

Figure A42. Alternative 11 velocity vectors and speed at inlet and ebb shoal, peak ebb tide

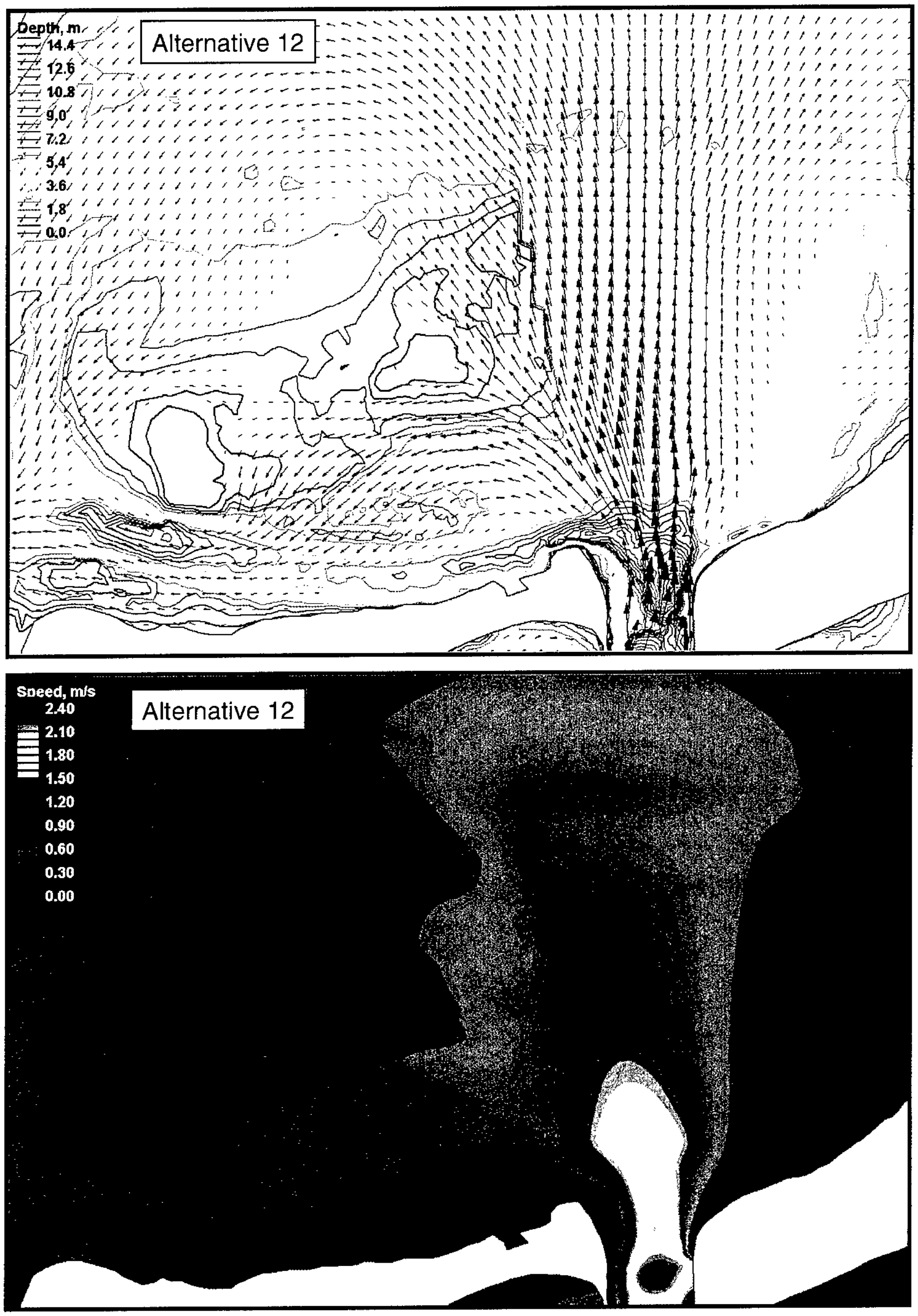

Figure A43. Alternative 12 velocity vectors and speed at flood shoal, peak flood tide

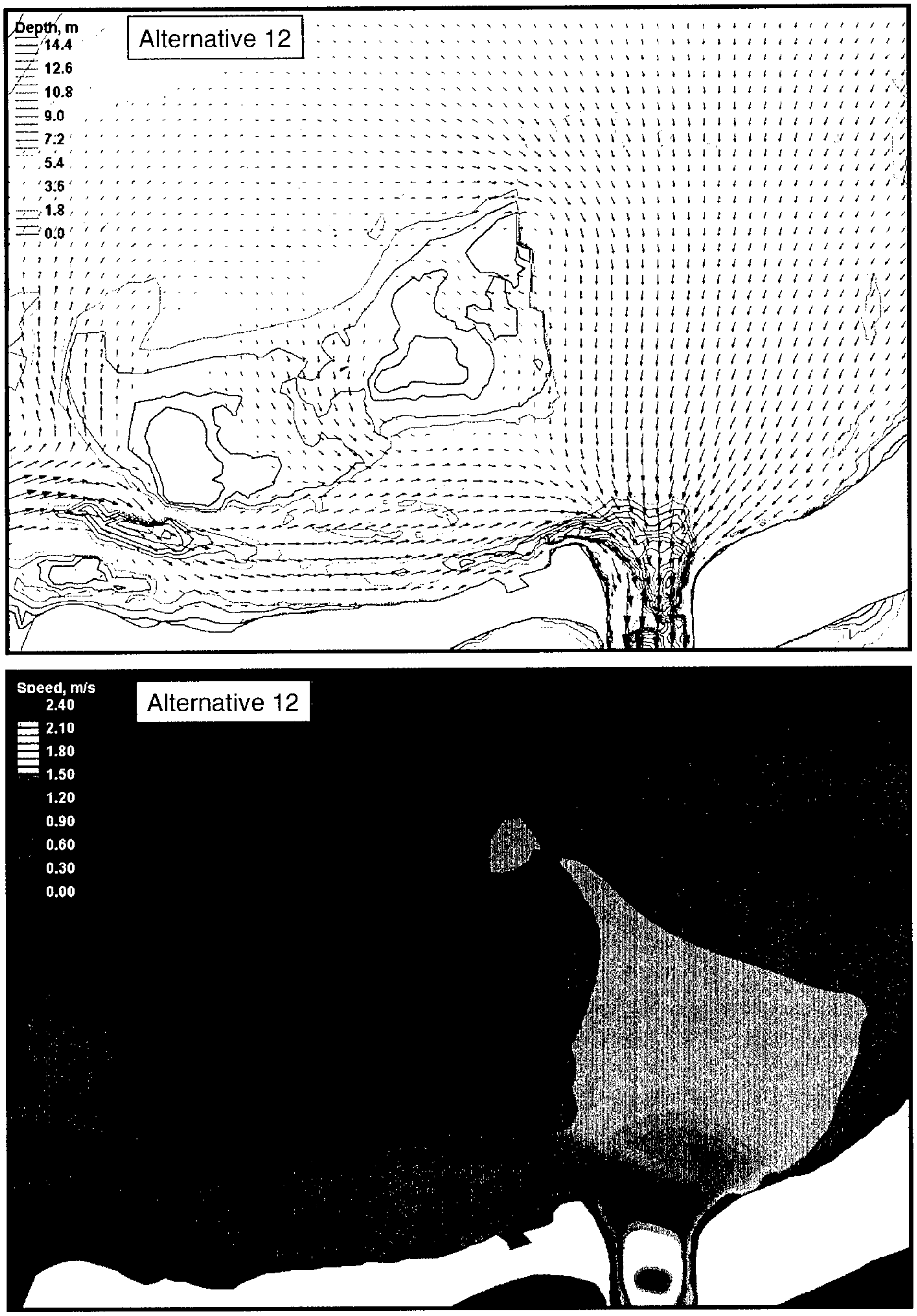

Figure A44. Alternative 12 velocity vectors and speed at flood shoal, peak ebb tide

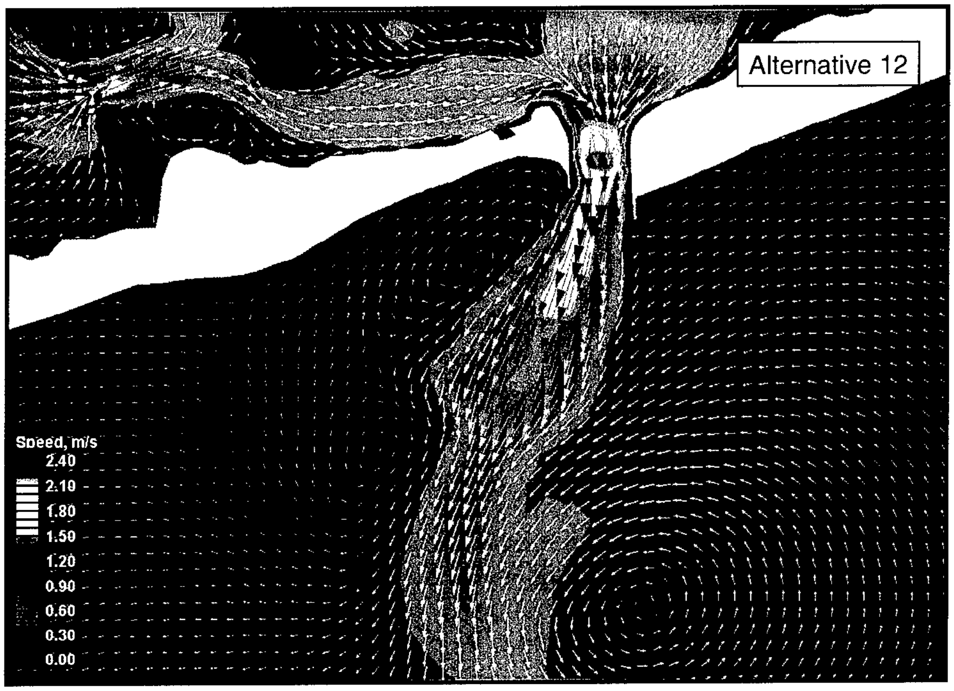

Figure A45. Alternative 12 velocity vectors and speed at inlet and ebb shoal, peak ebb tide

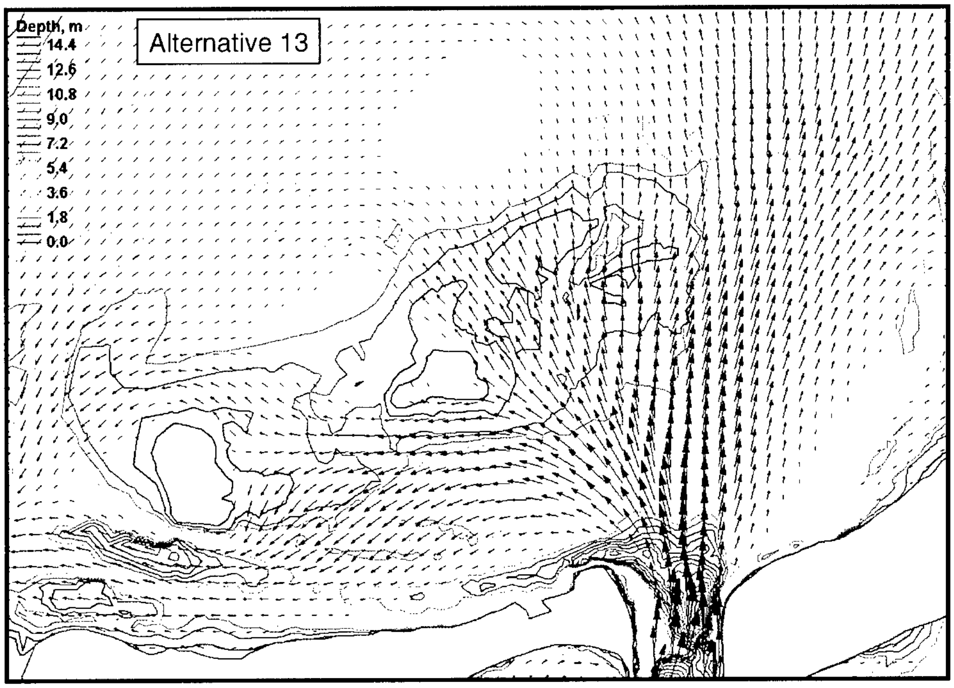

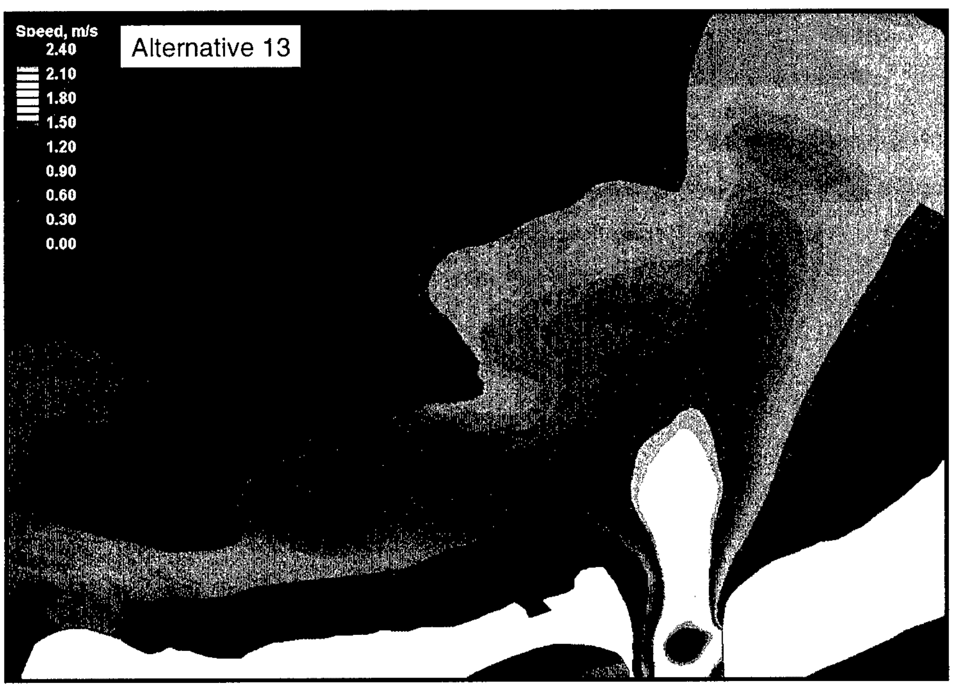

Figure A46. Alternative 13 velocity vectors and speed at flood shoal, peak flood tide

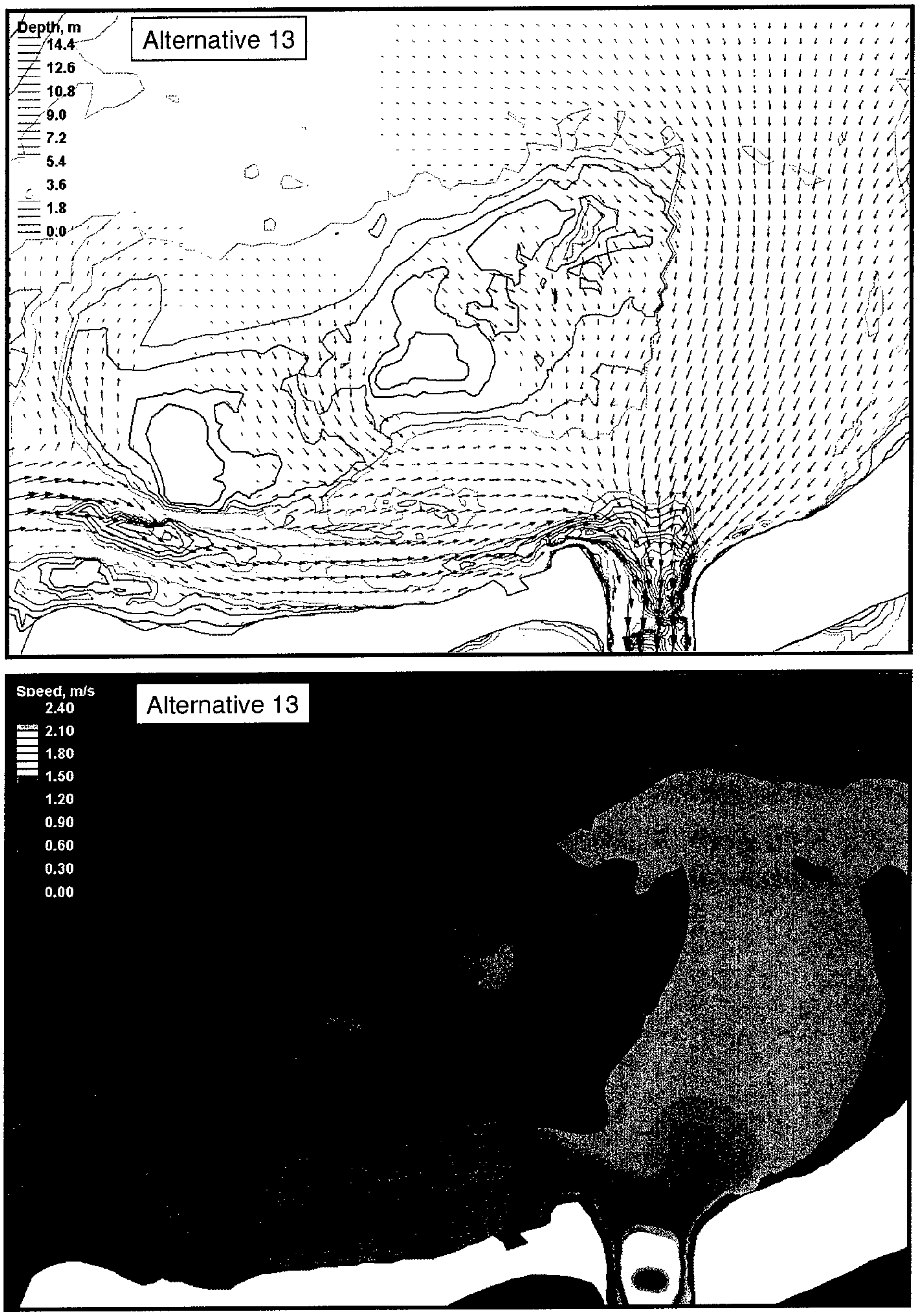

Figure A47. Alternative 13 velocity vectors and speed at flood shoal, peak ebb tide

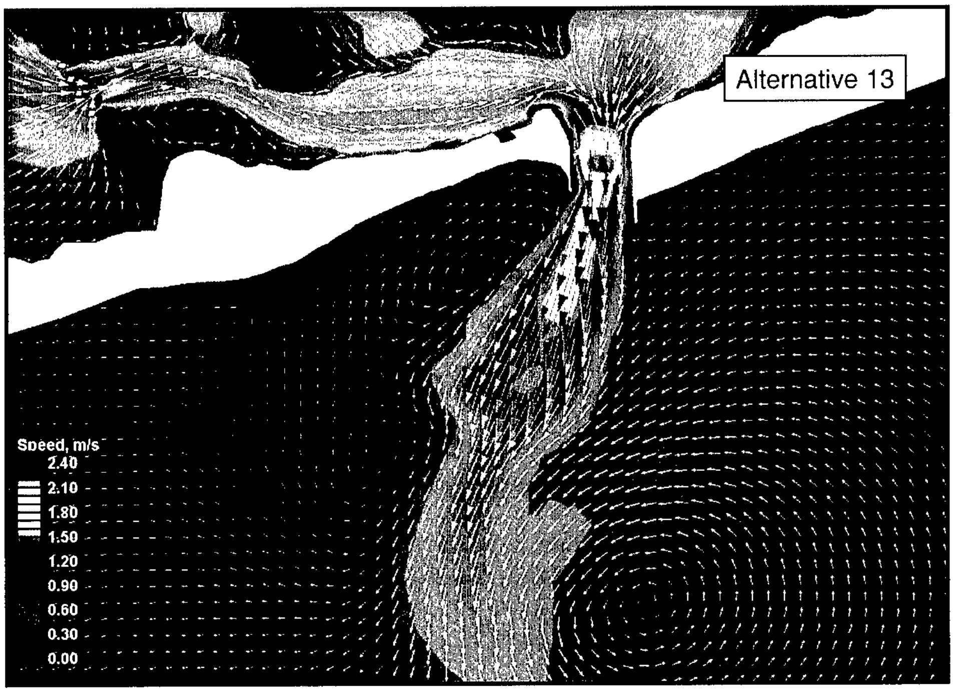

Figure A48. Alternative 13 velocity vectors and speed at inlet and ebb shoal, peak ebb tide

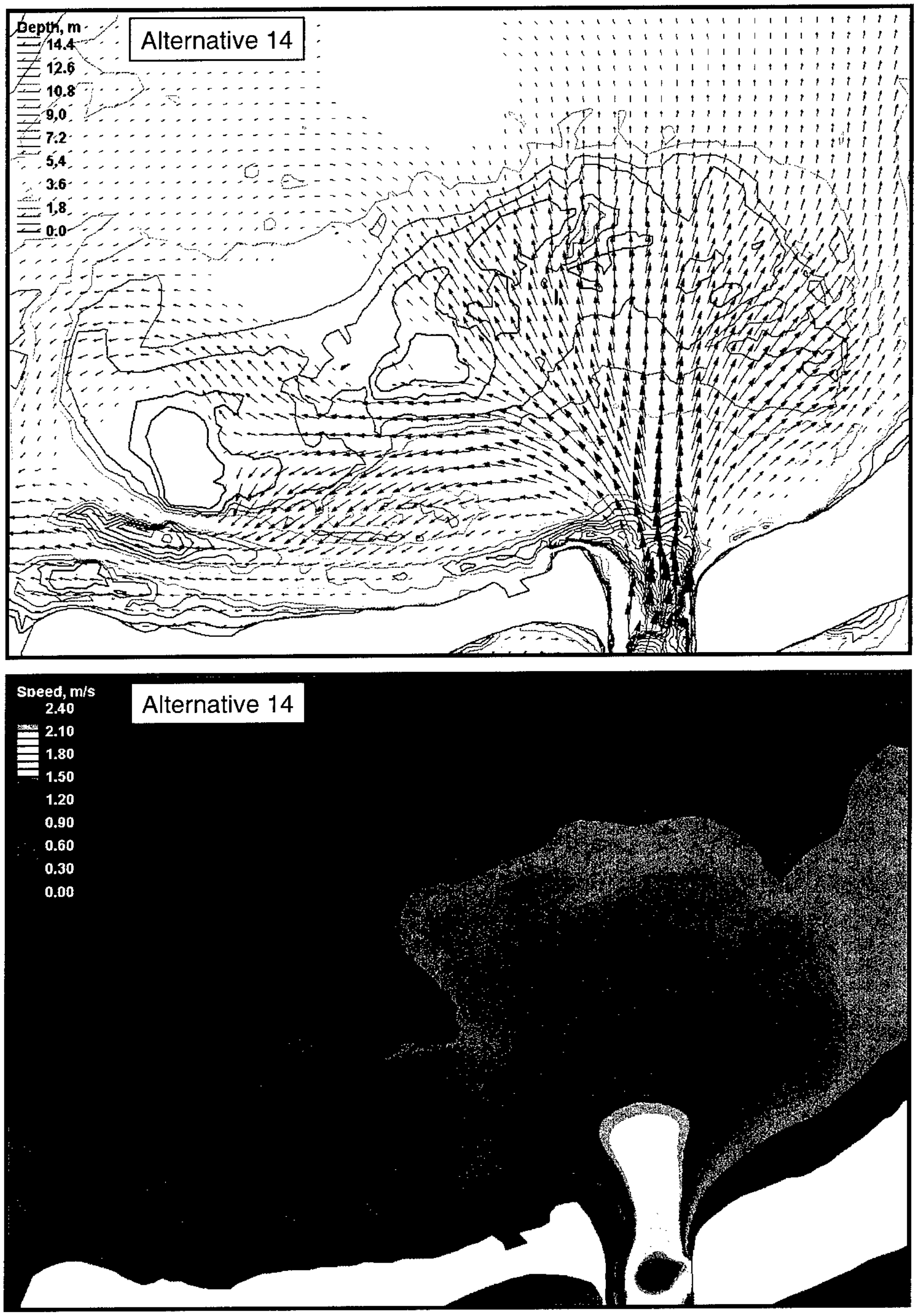

Figure A49. Alternative 14 velocity vectors and speed at flood shoal, peak flood tide

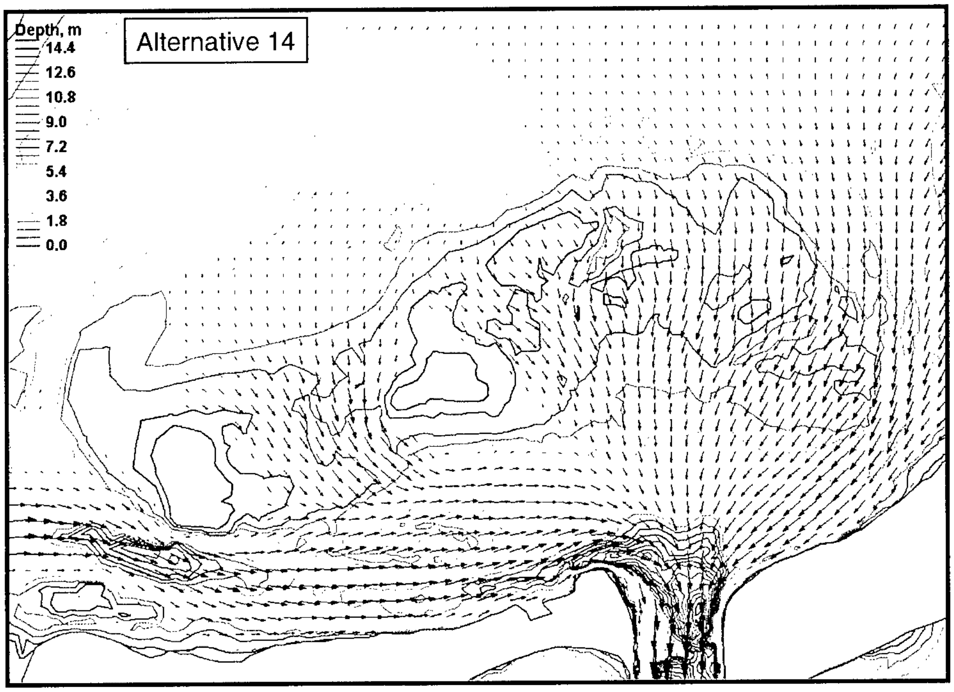

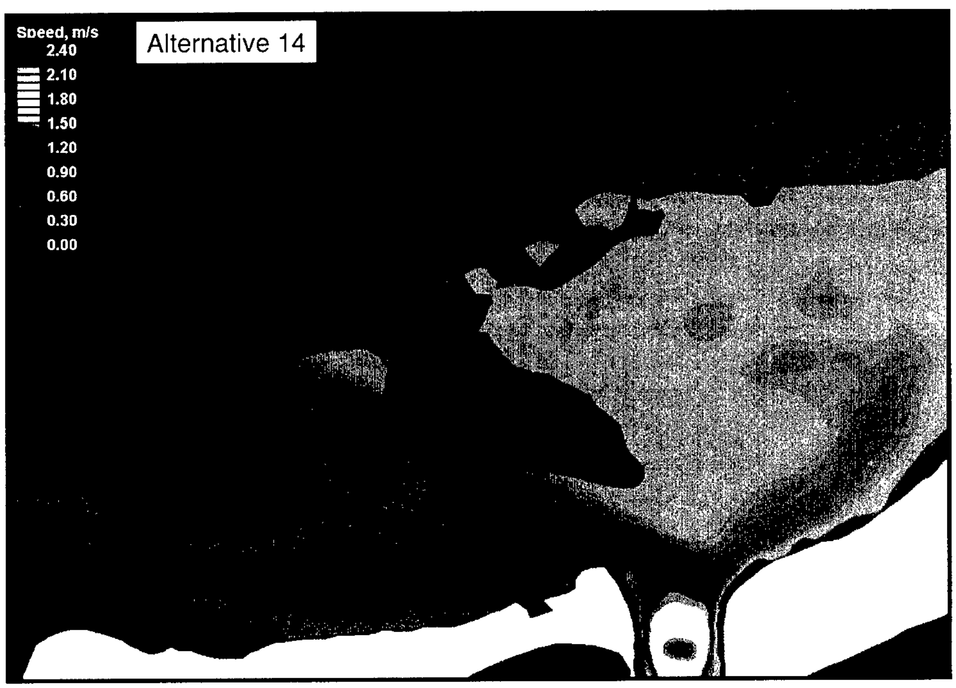

Figure A50. Alternative 14 velocity vectors and speed at flood shoal, peak ebb tide

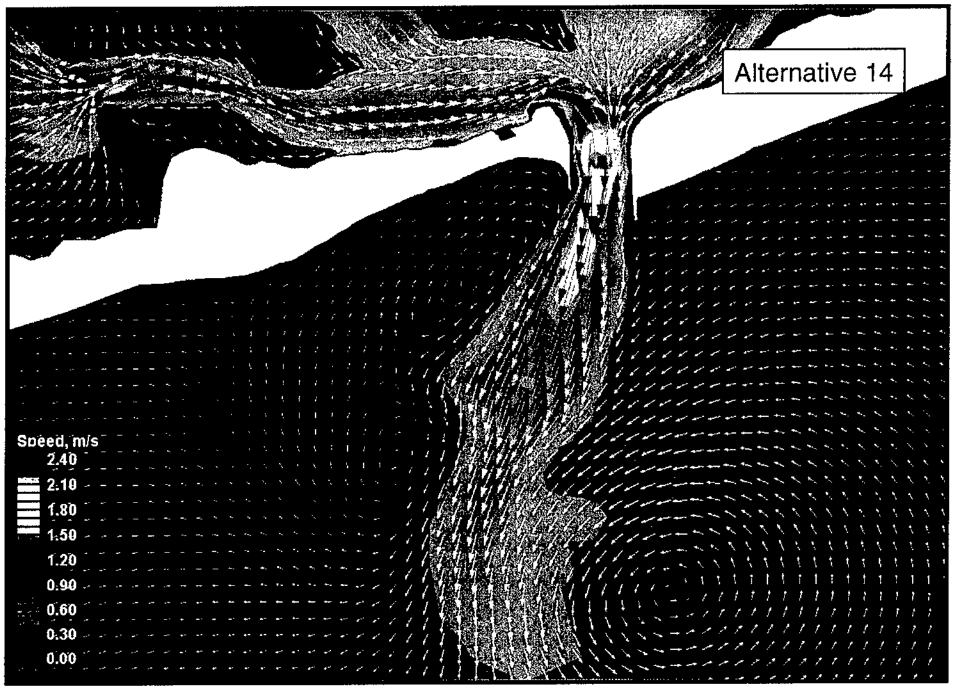

Figure A51. Alternative 14 velocity vectors and speed at inlet and ebb shoal, peak ebb tide

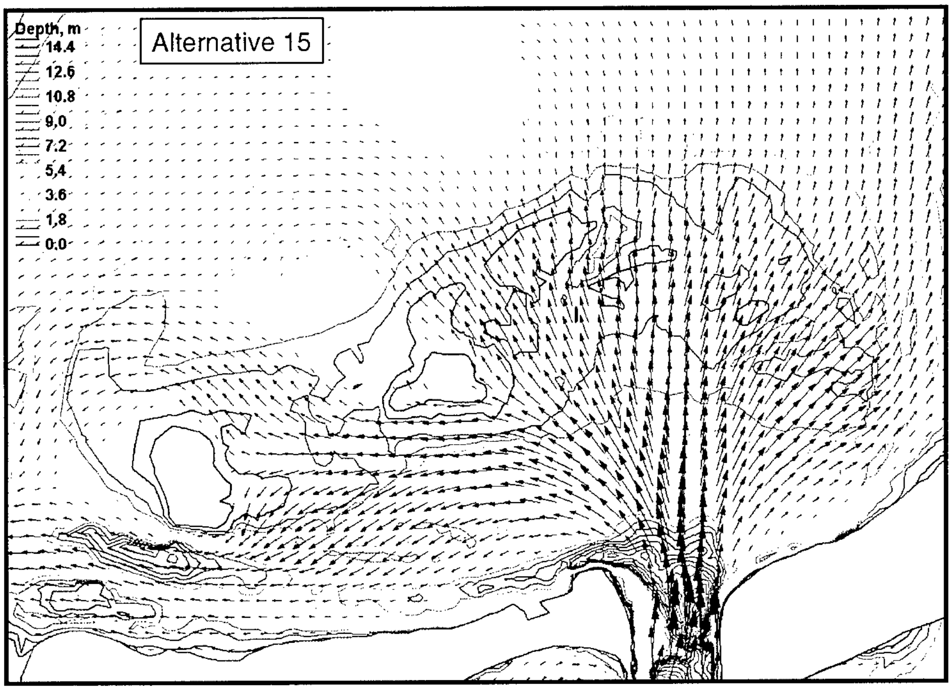

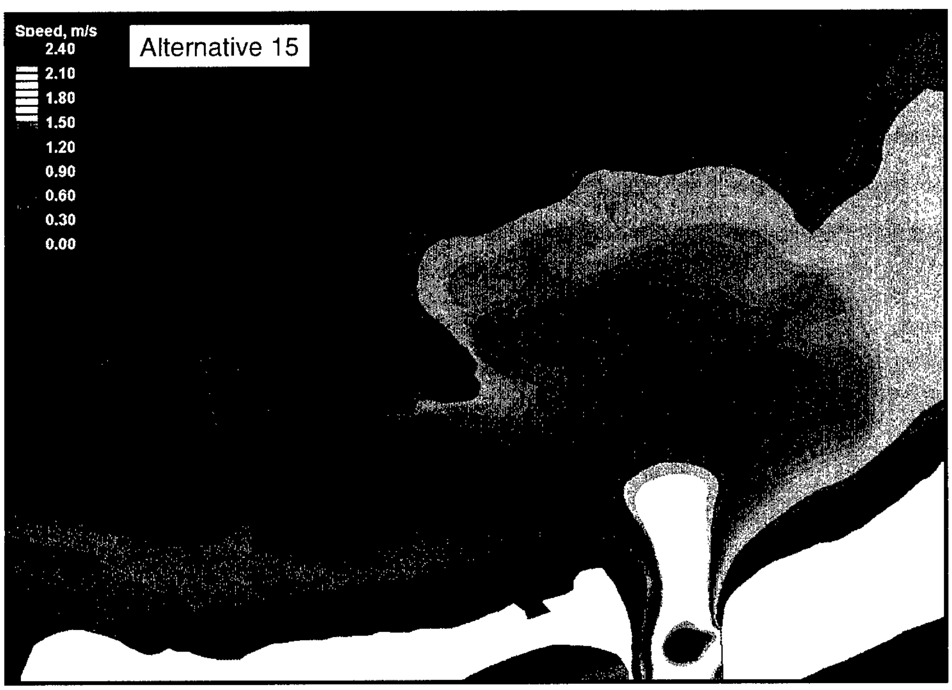

Figure A52. Alternative 15 velocity vectors and speed at flood shoal, peak flood tide

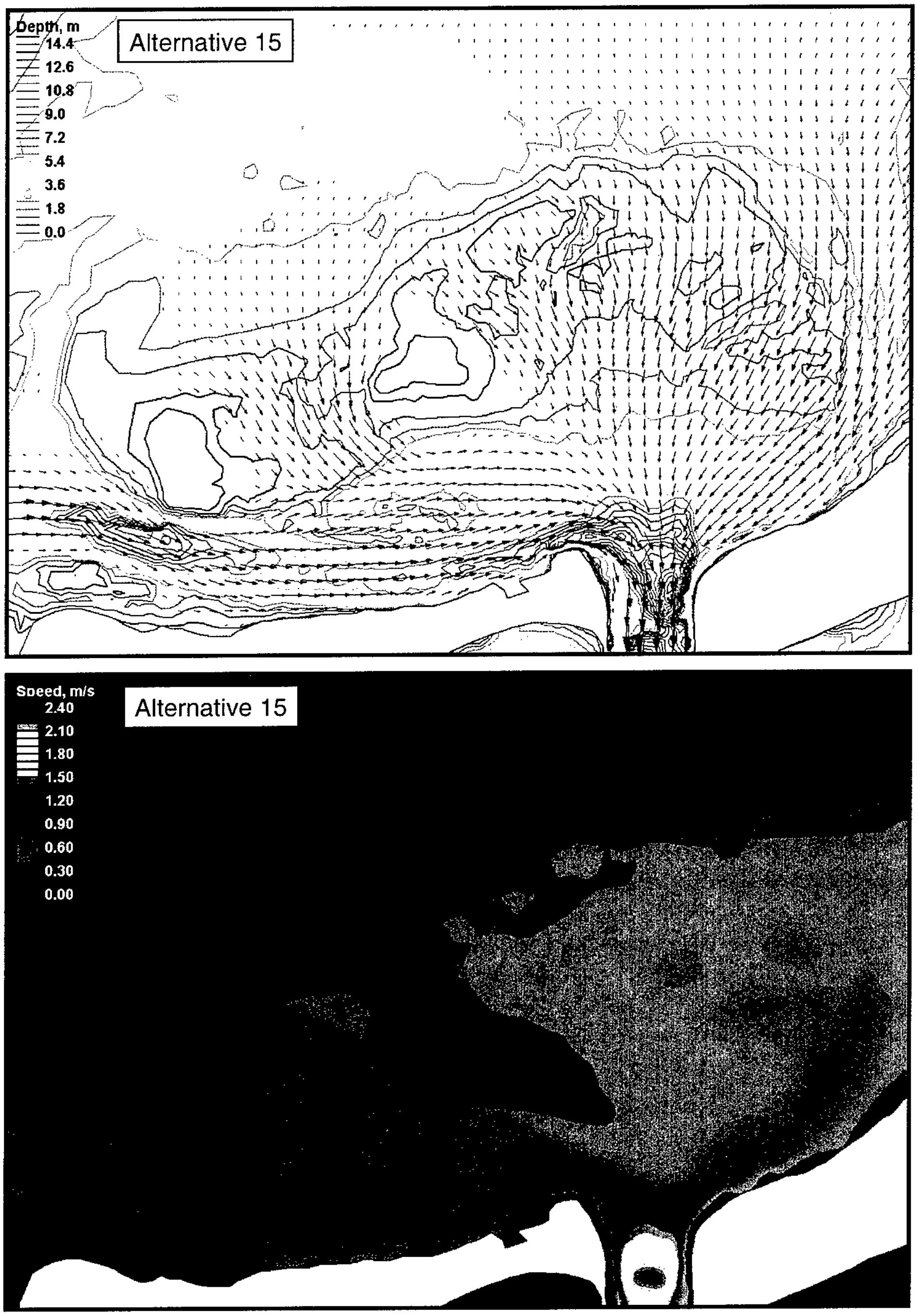

Figure A53. Alternative 15 velocity vectors and speed at flood shoal, peak ebb tide

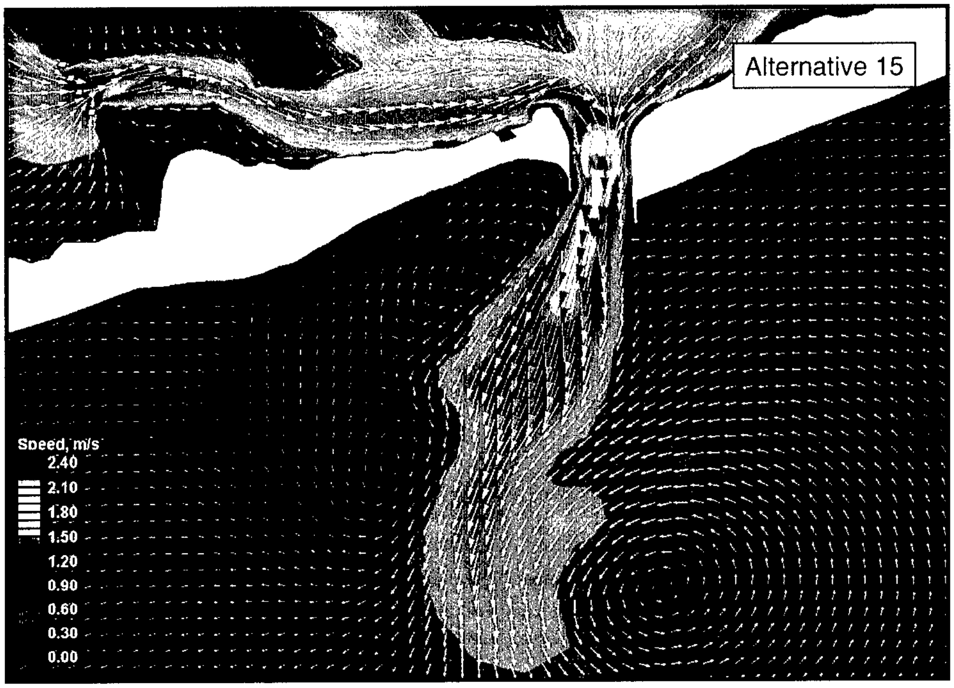

Figure A54. Alternative 15 velocity vectors and speed at inlet and ebb shoal, peak ebb tide

Appendix B
Plots of Calculated Change in Current Speed

Plan-view plots of change in current speed relative to the existing condition are presented for peak spring flood and ebb tide. Change in current speed was calculated by subtracting the speed corresponding to the existing condition from the speed for each alternative. Thus, positive change indicates increased speed for alternatives and negative change indicates decreased speed.

Contour plots over the inlet, flood shoal, and ebb shoal area are given for each action (dredging and/or structural modification) alternative. Two panels are given for each alternative. The upper panel shows change in current speed during flood tide and the lower panel shows the change for ebb tide.

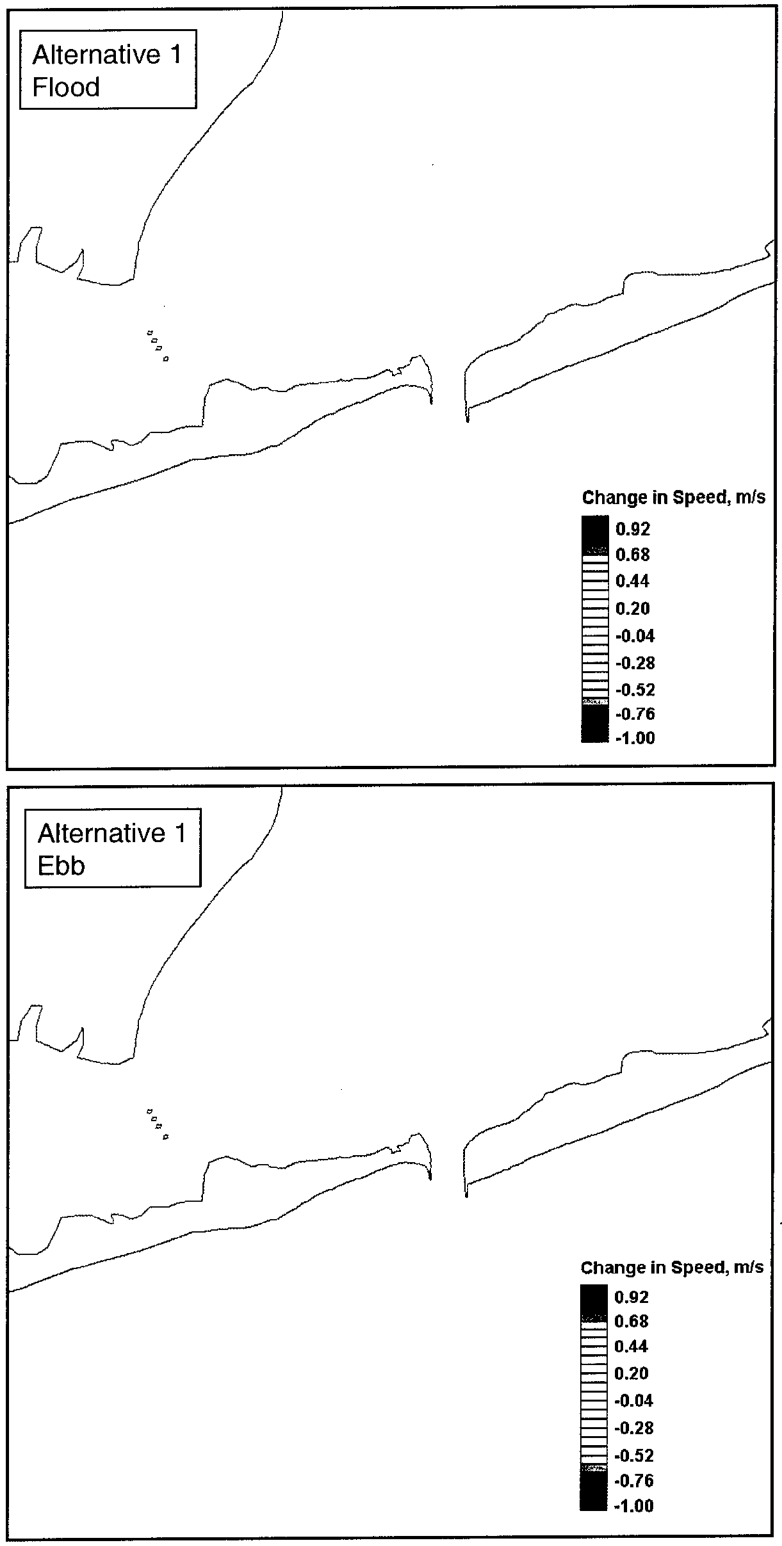

Figure B1. Change in current speed for Alternative 1

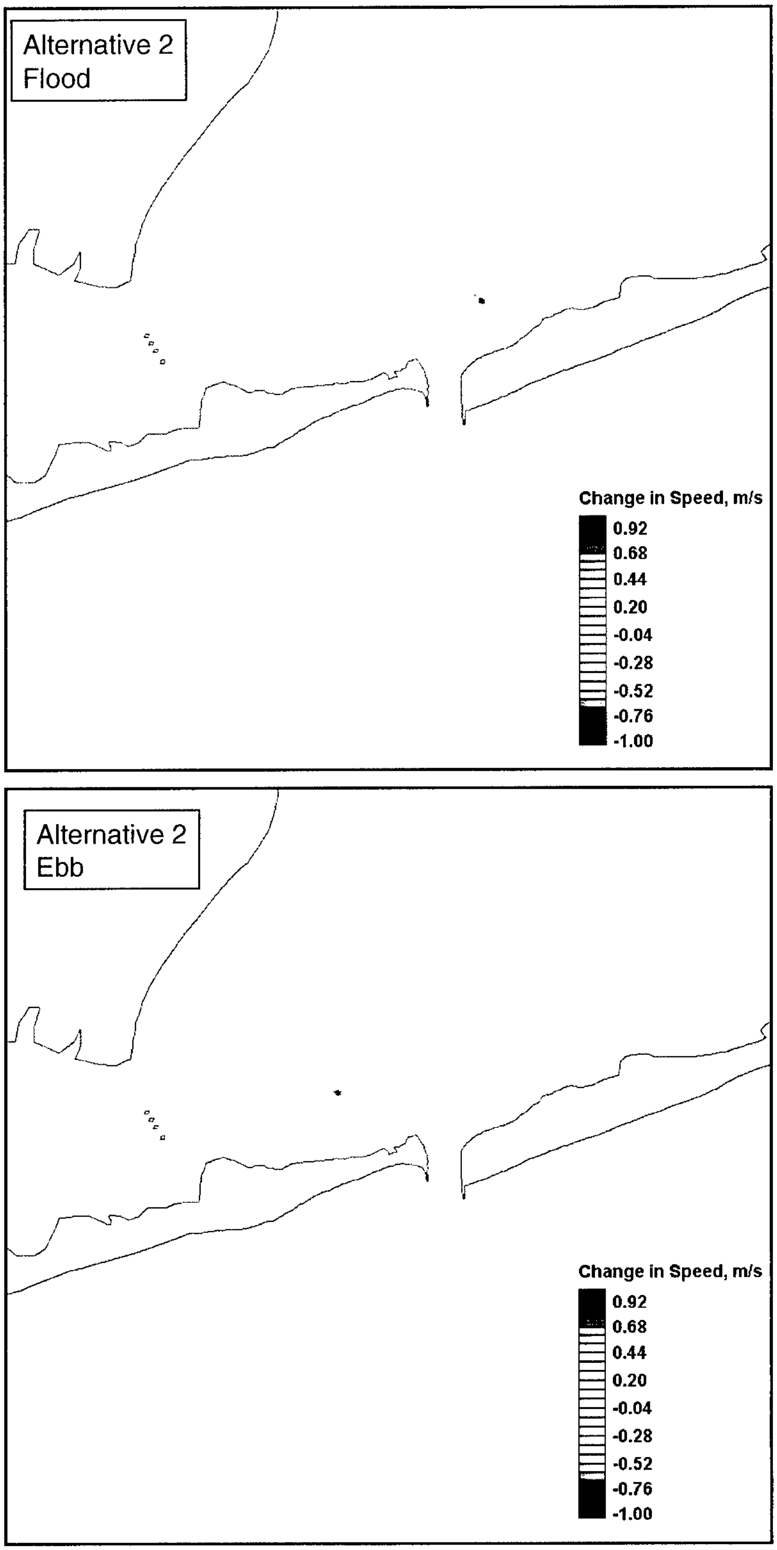

Figure B2. Change in current speed for Alternative 2

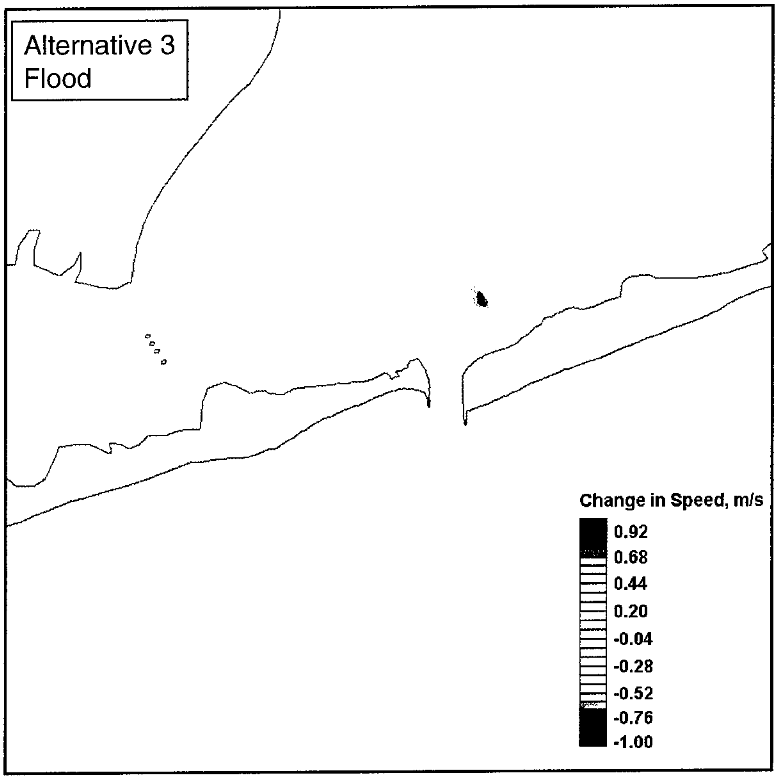

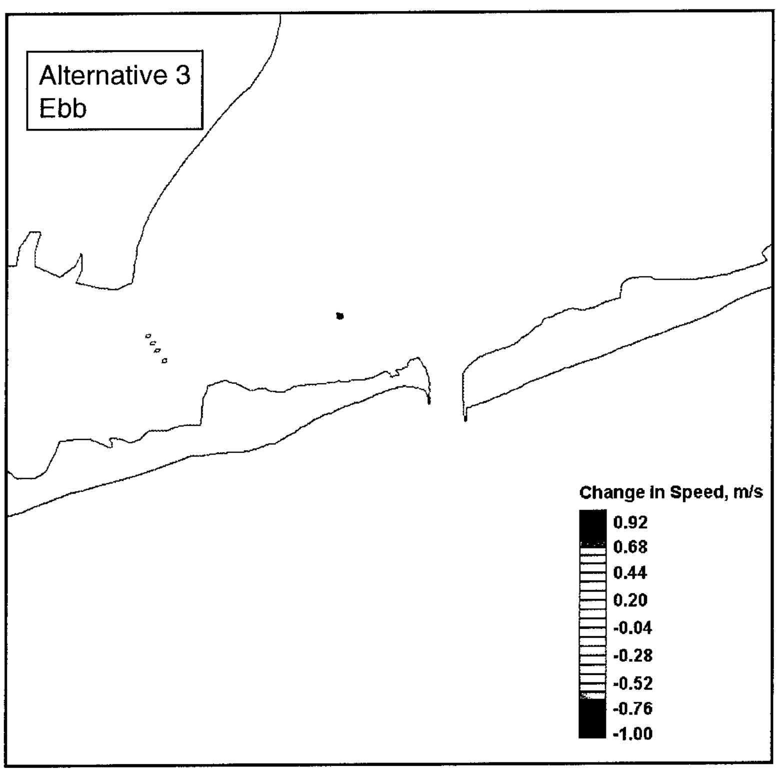

Figure B3. Change in current speed for Alternative 3

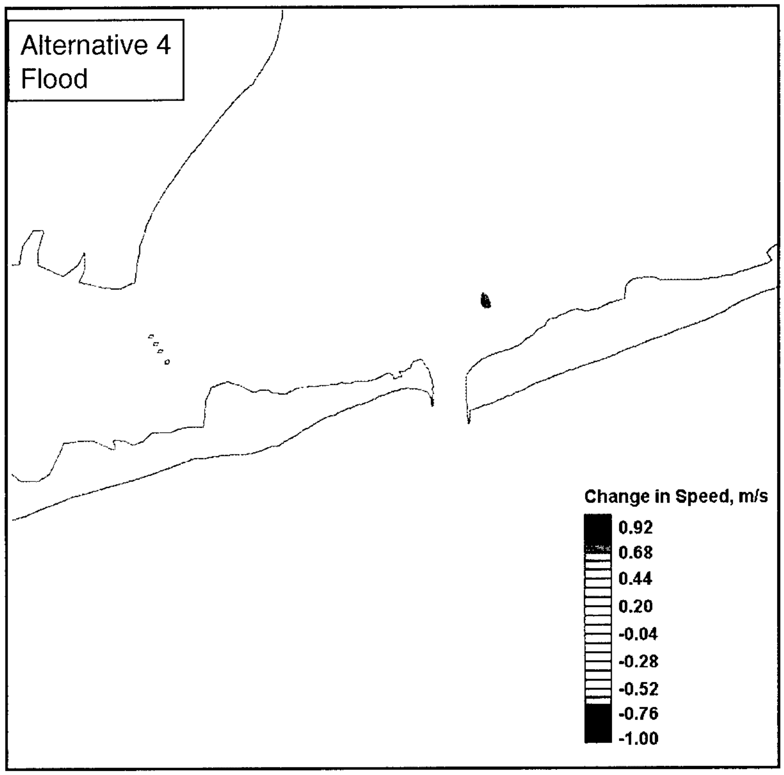

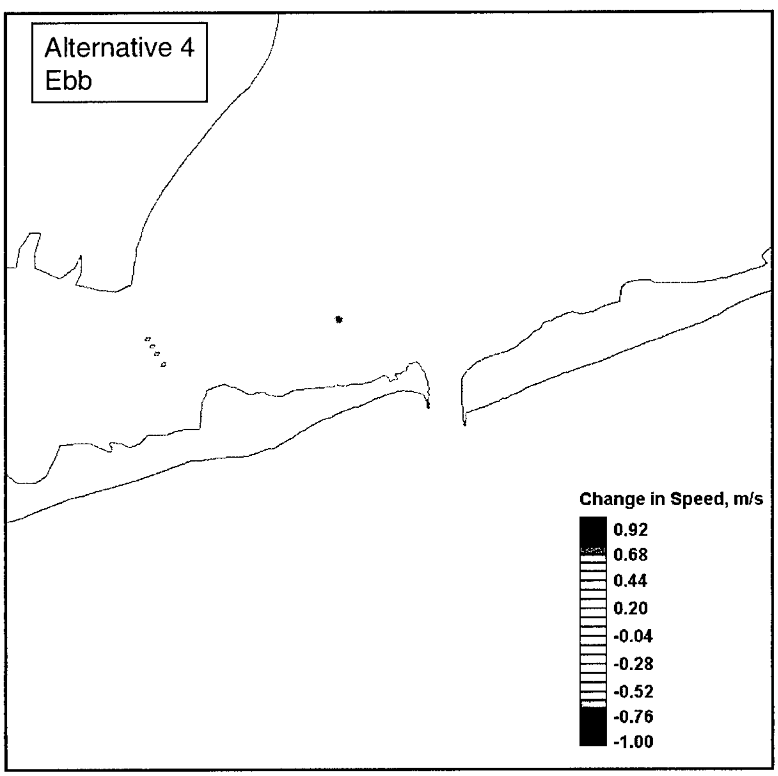

Figure B4. Change in current speed for Alternative 4

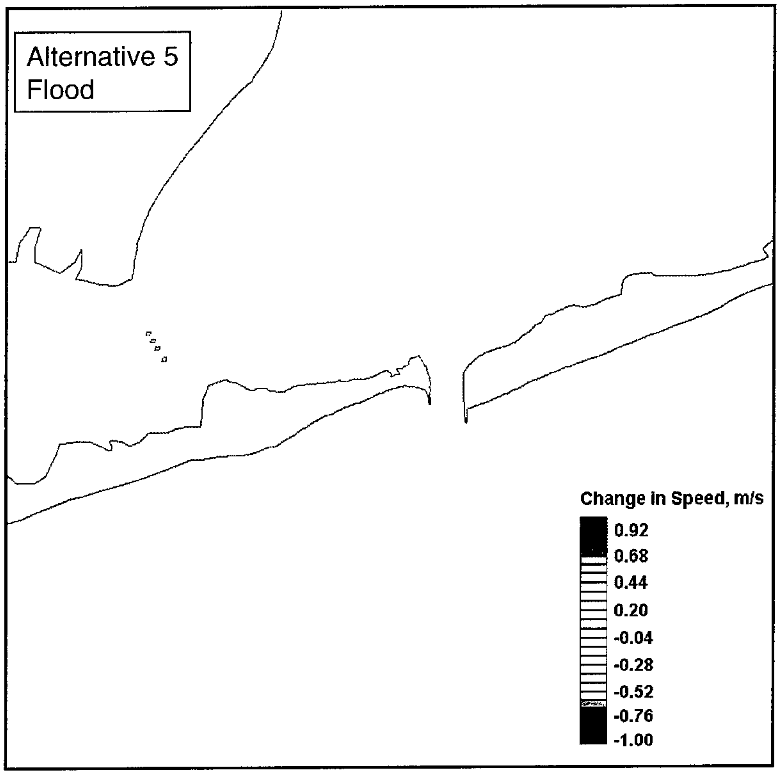

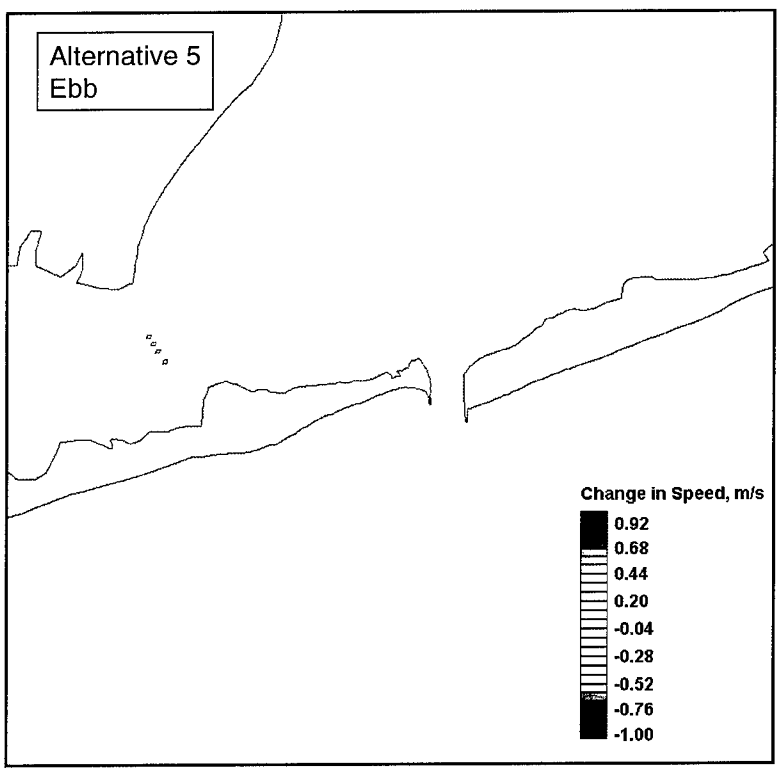

Figure B5. Change in current speed for Alternative 5

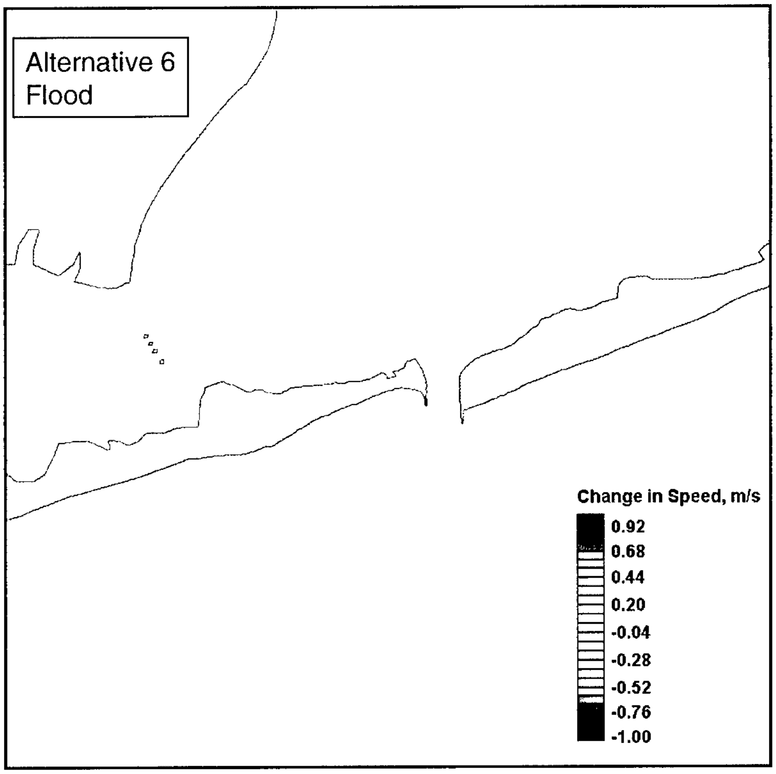

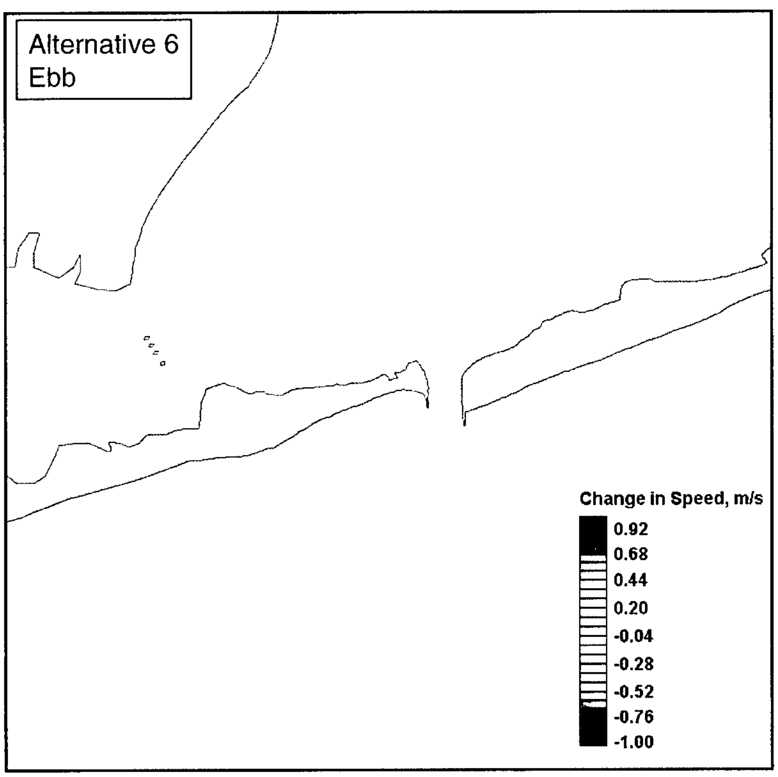

Figure B6. Change in current speed for Alternative 6

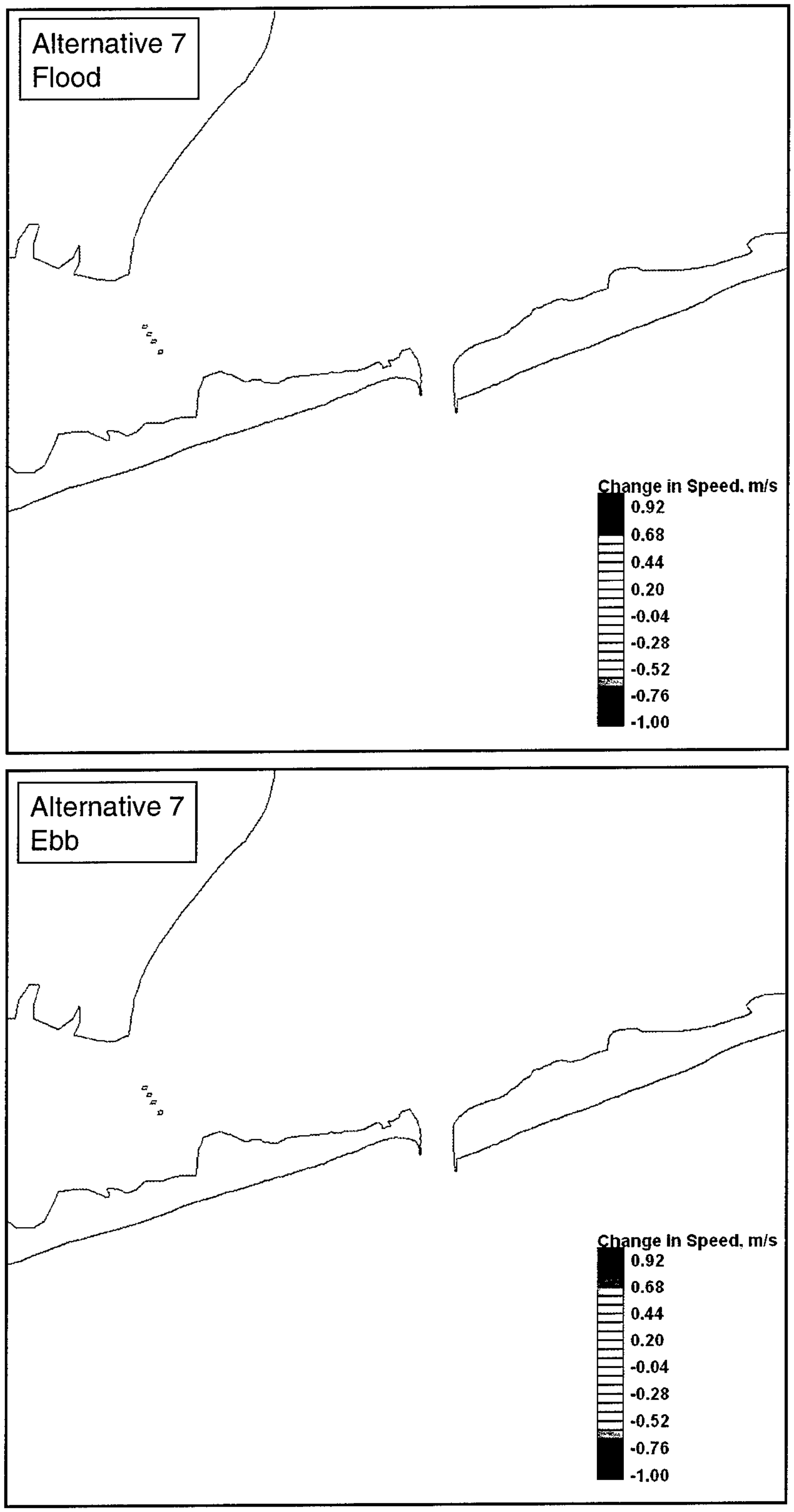

Figure B7. Change in current speed for Alternative 7

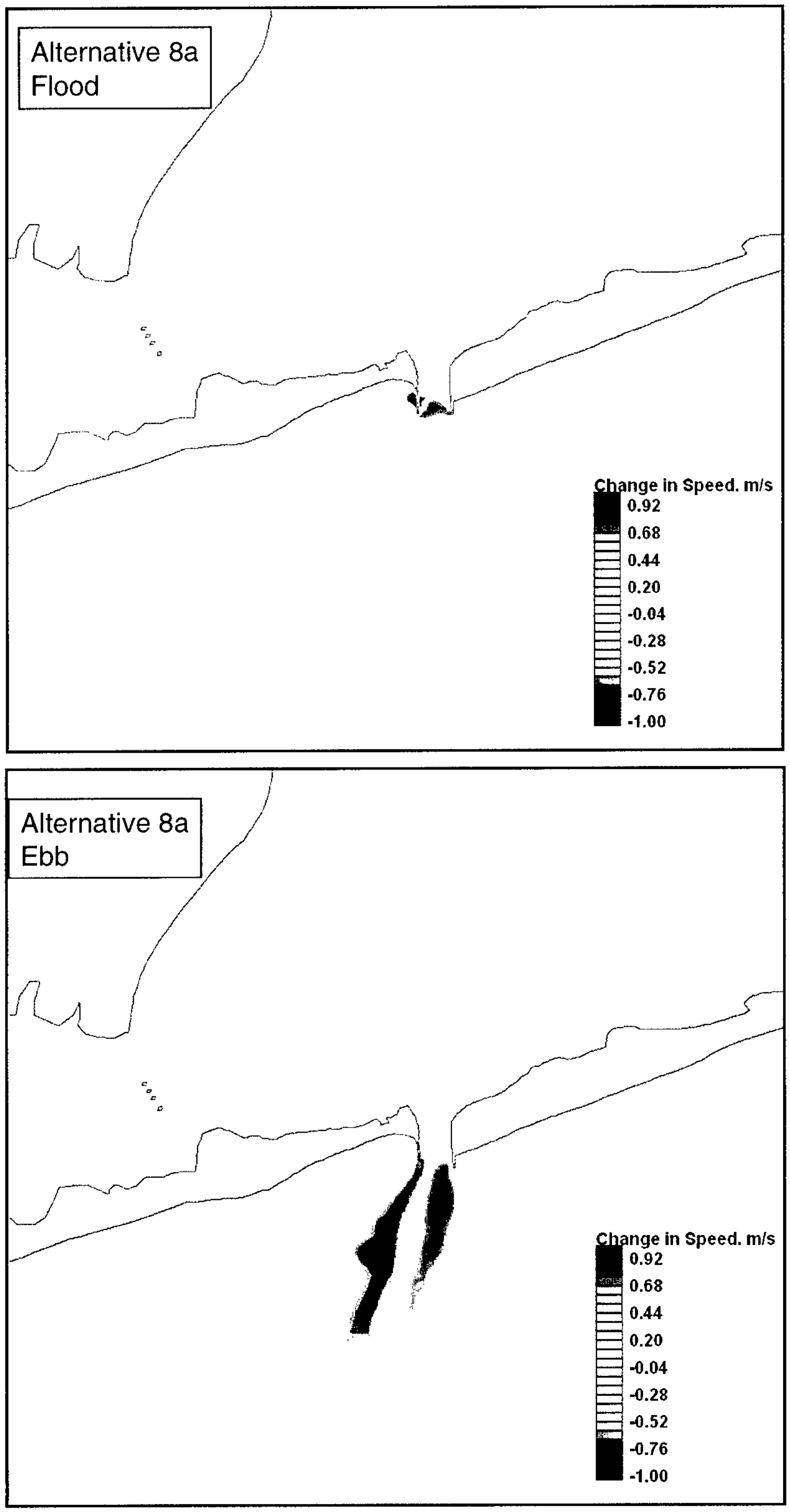

Figure B8. Change in current speed for Alternative 8a

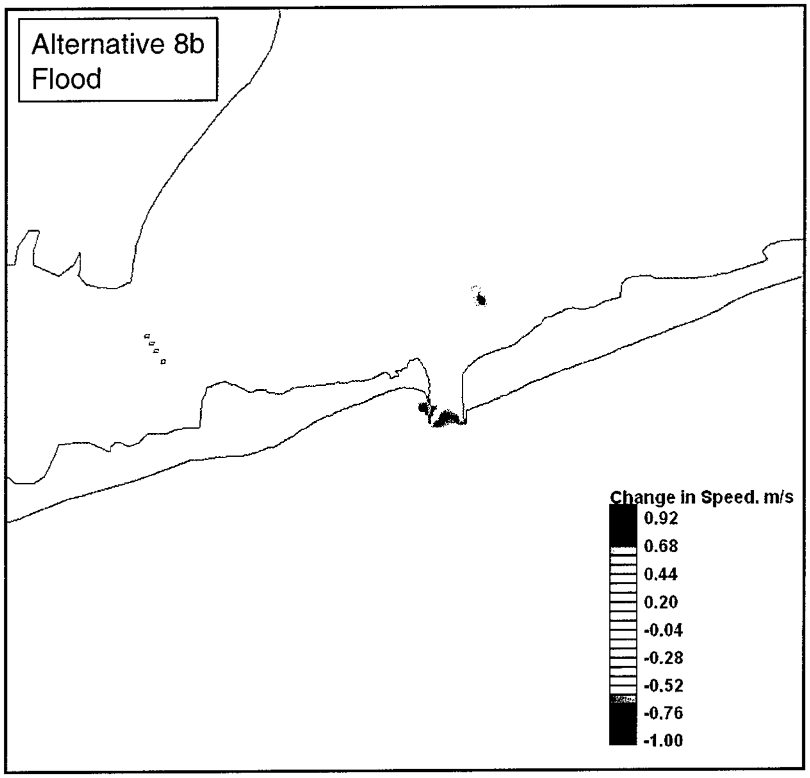

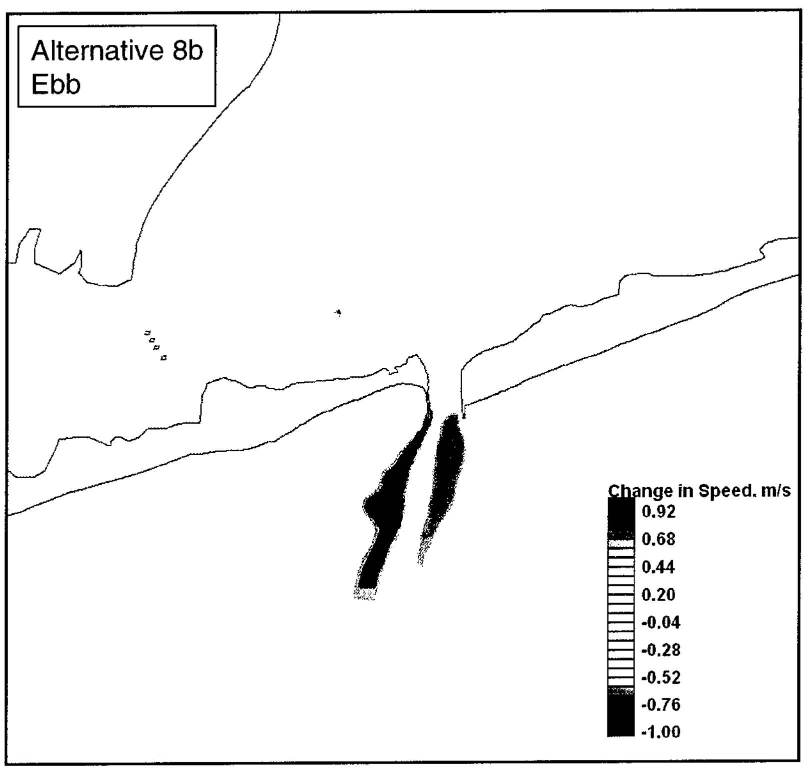

Figure B9. Change in current speed for Alternative 8b

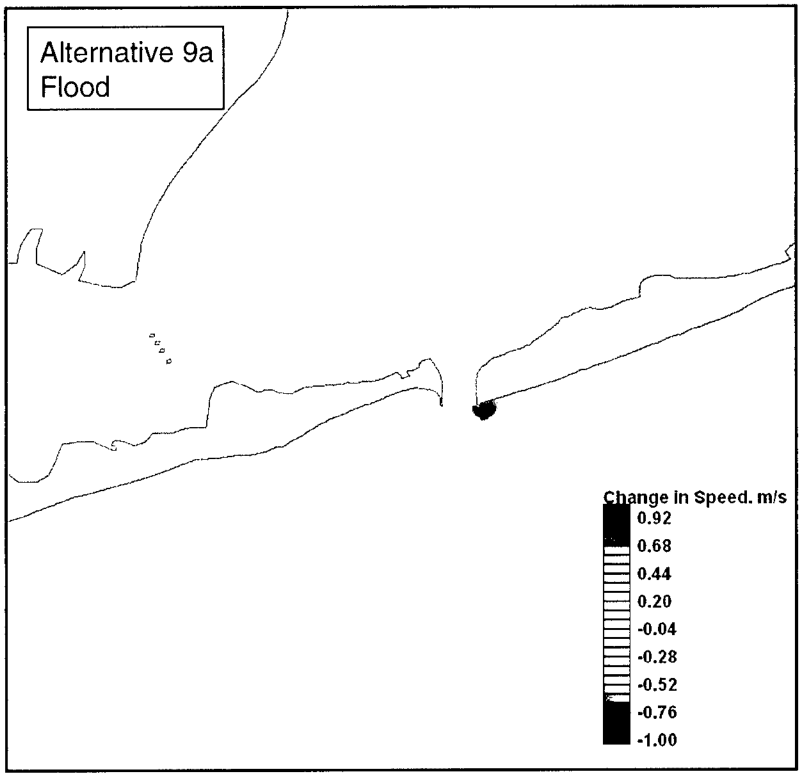

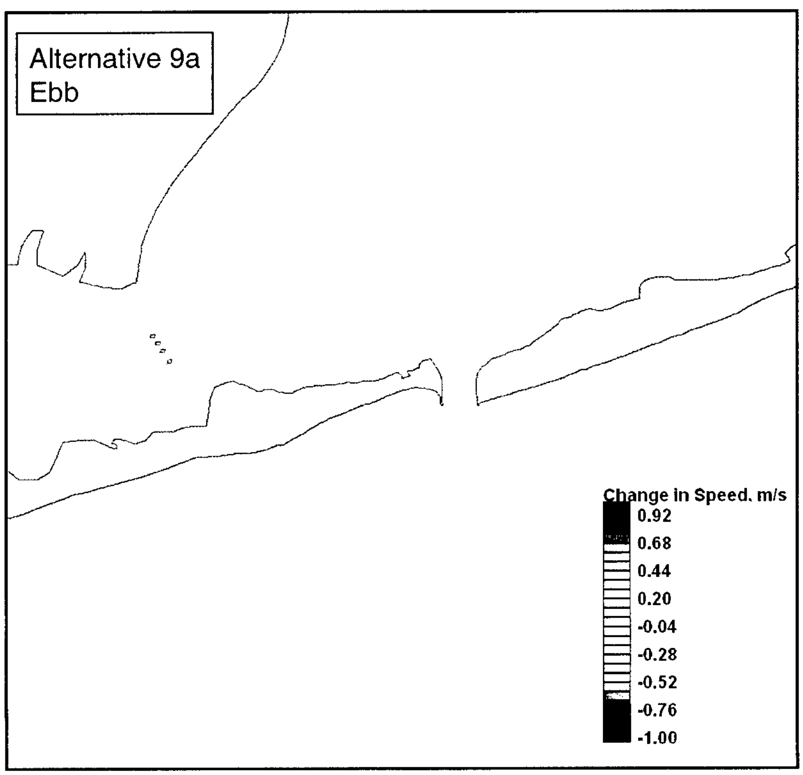

Figure B10. Change in current speed for Alternative 9a

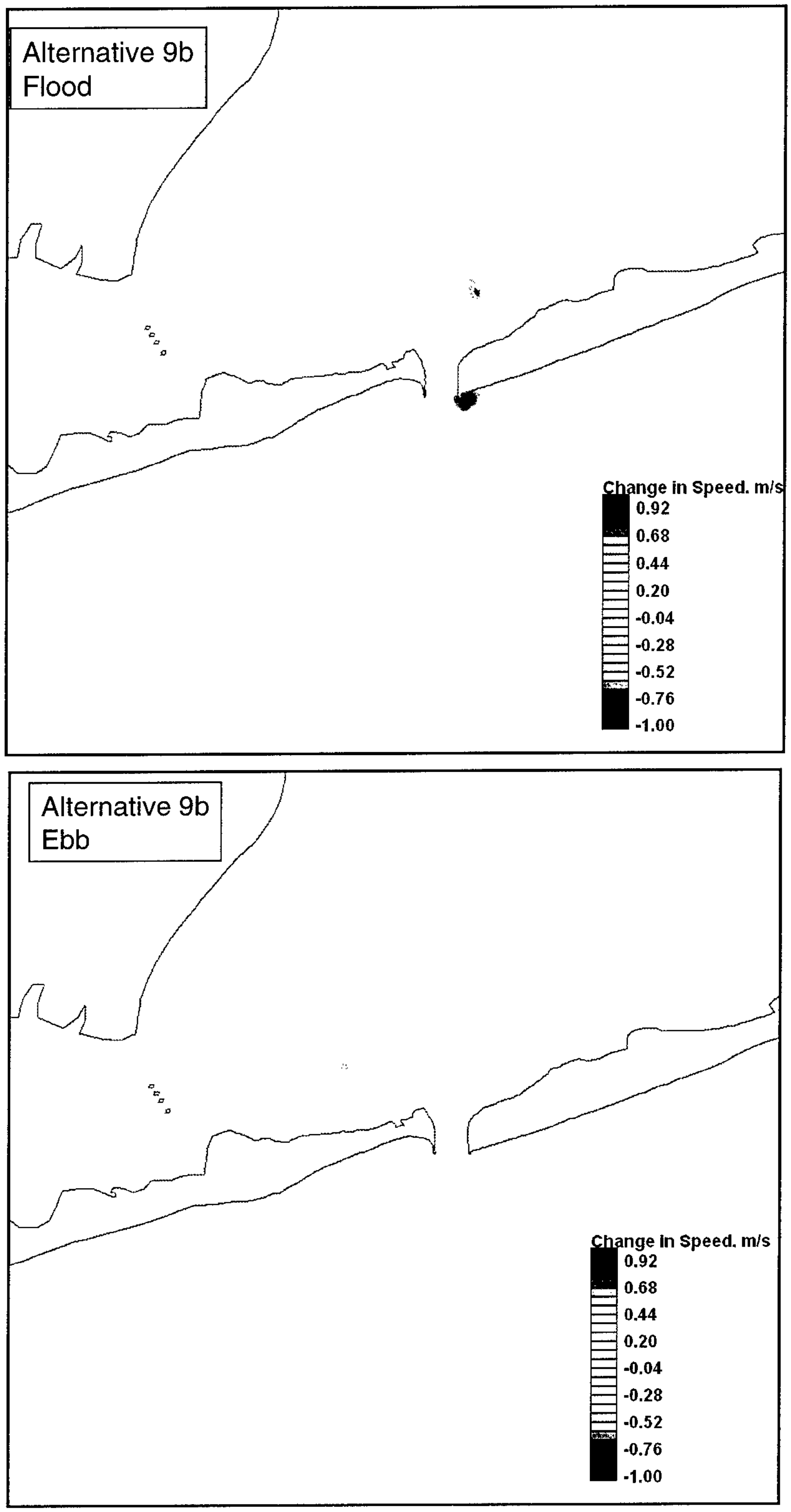

Figure B11. Change in current speed for Alternative 9b

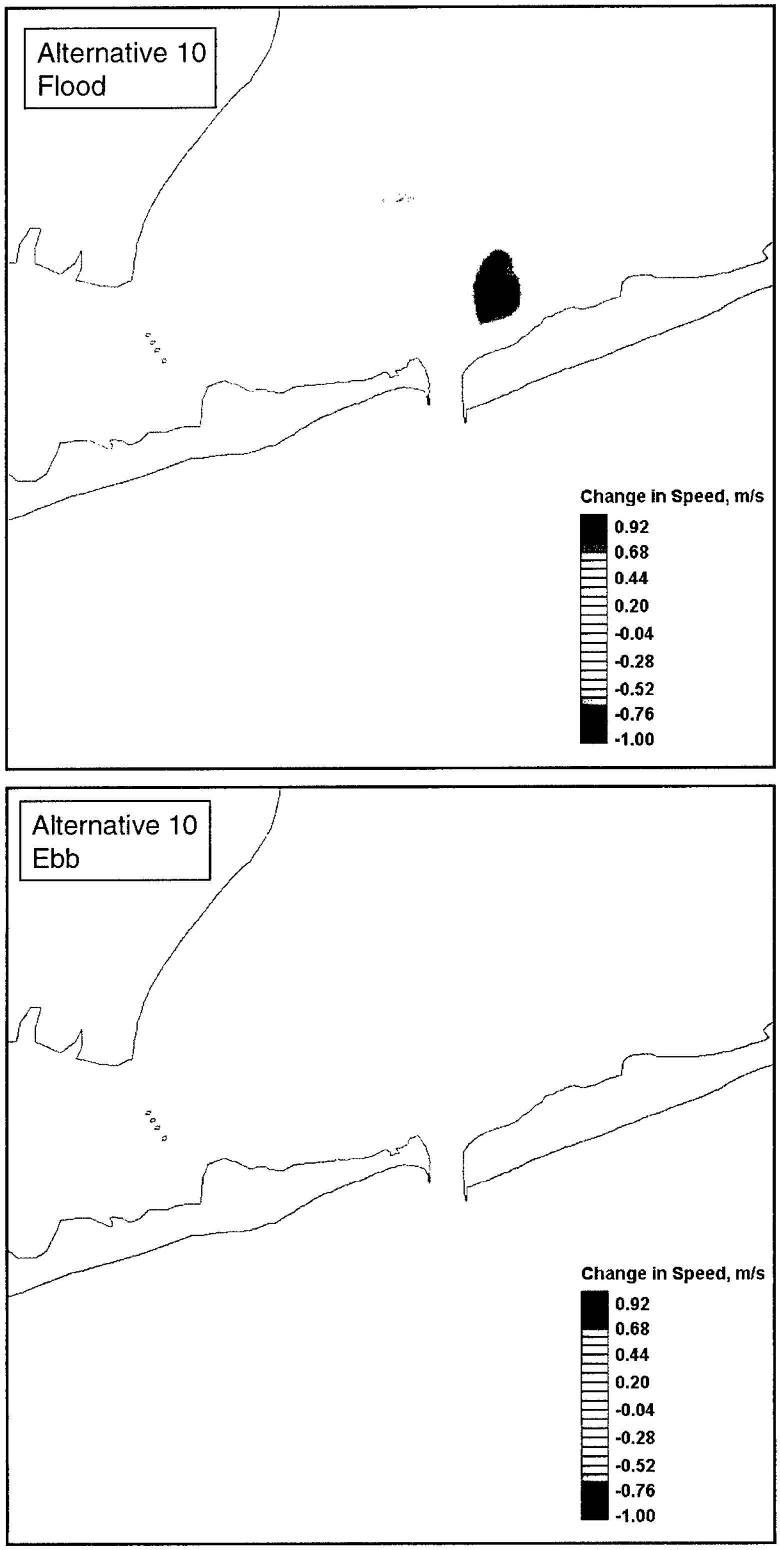

Figure B12. Change in current speed for Alternative 10

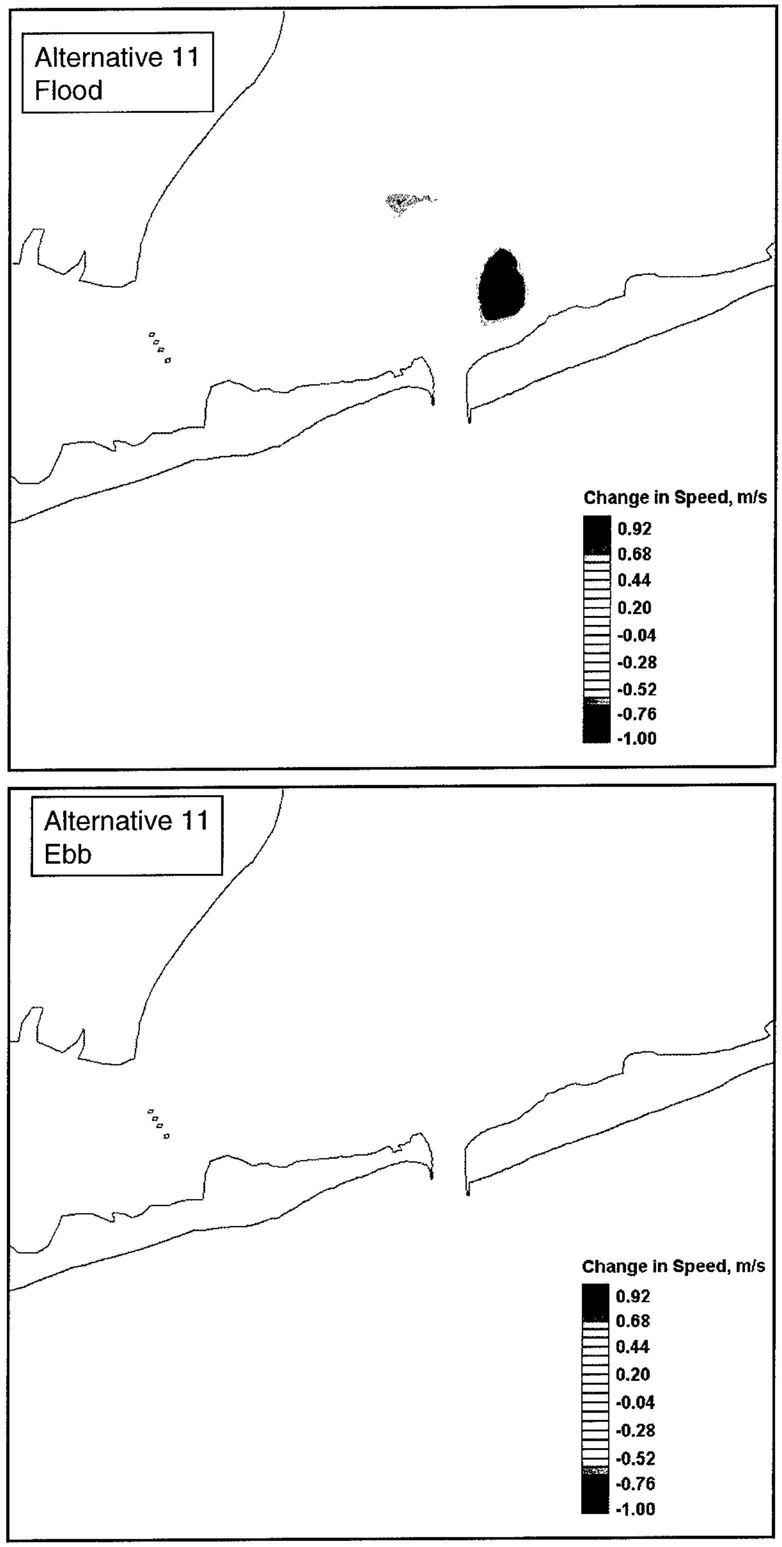

Figure B13. Change in current speed for Alternative 11

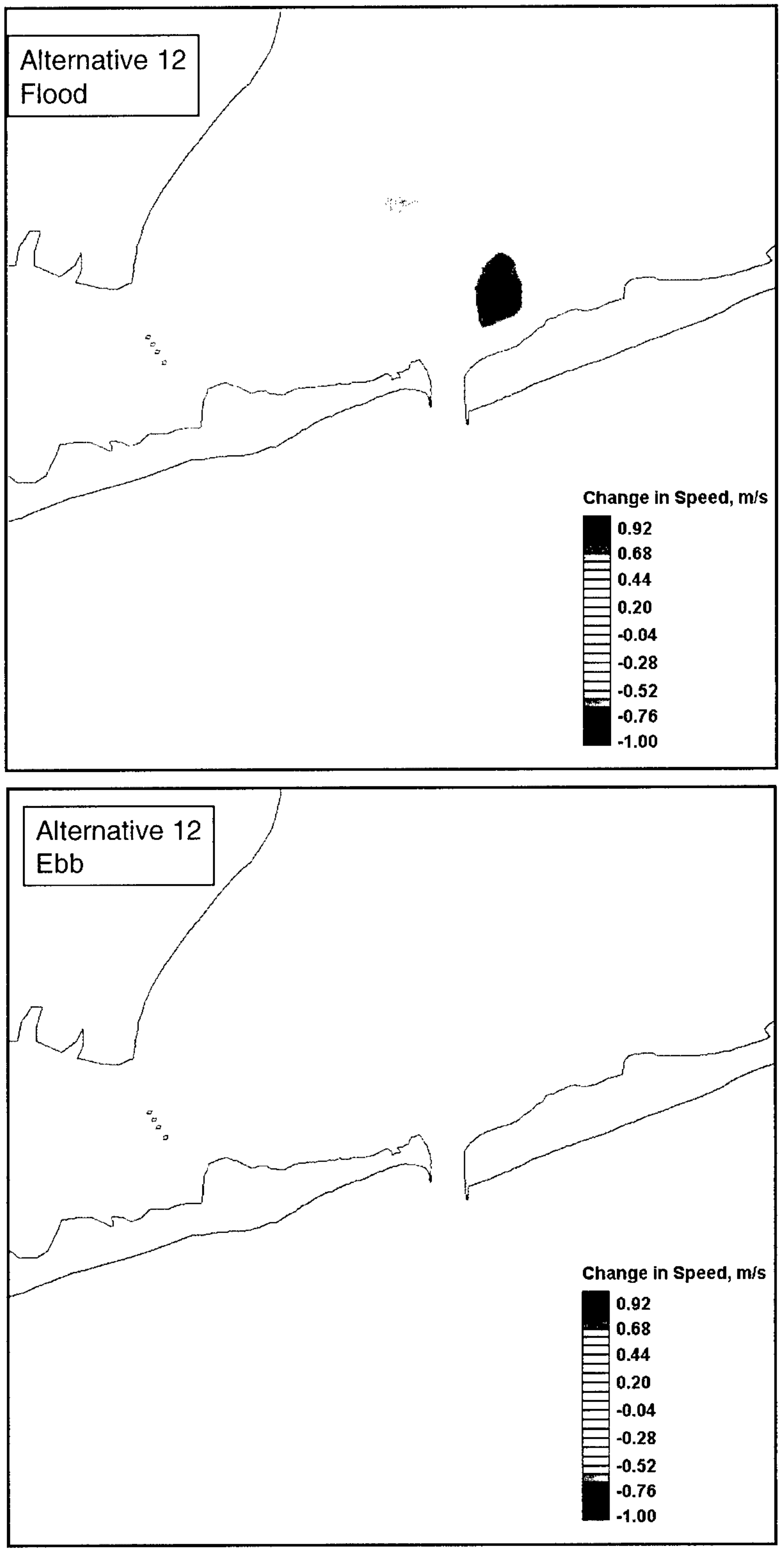

Figure B14. Change in current speed for Alternative 12

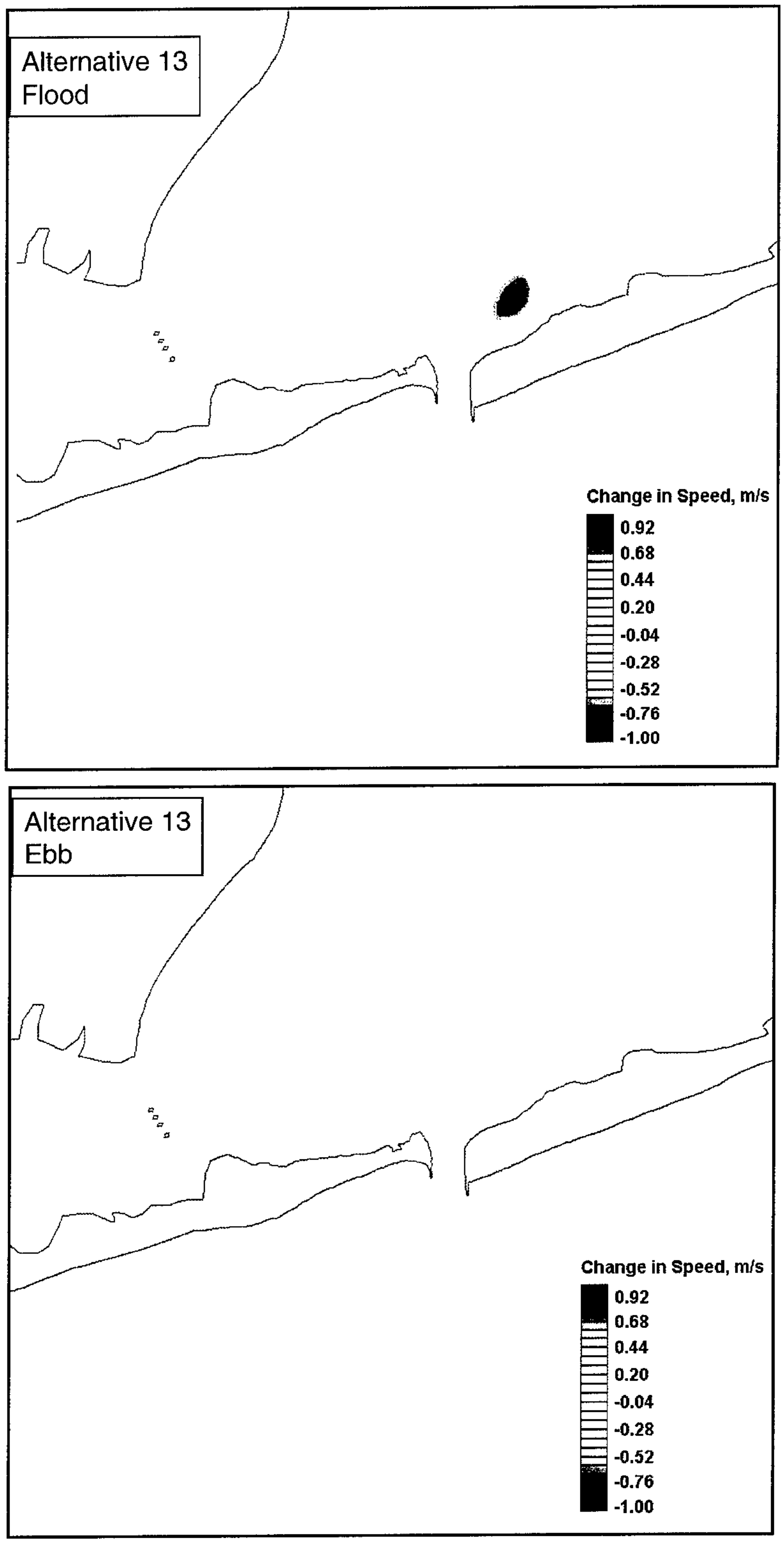

Figure B15. Change in current speed for Alternative 13

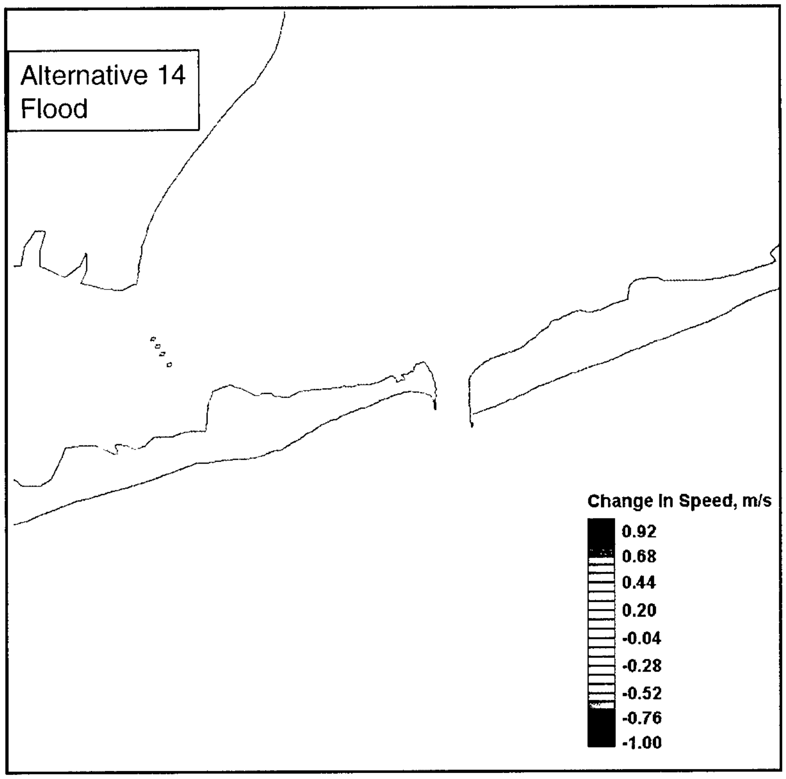

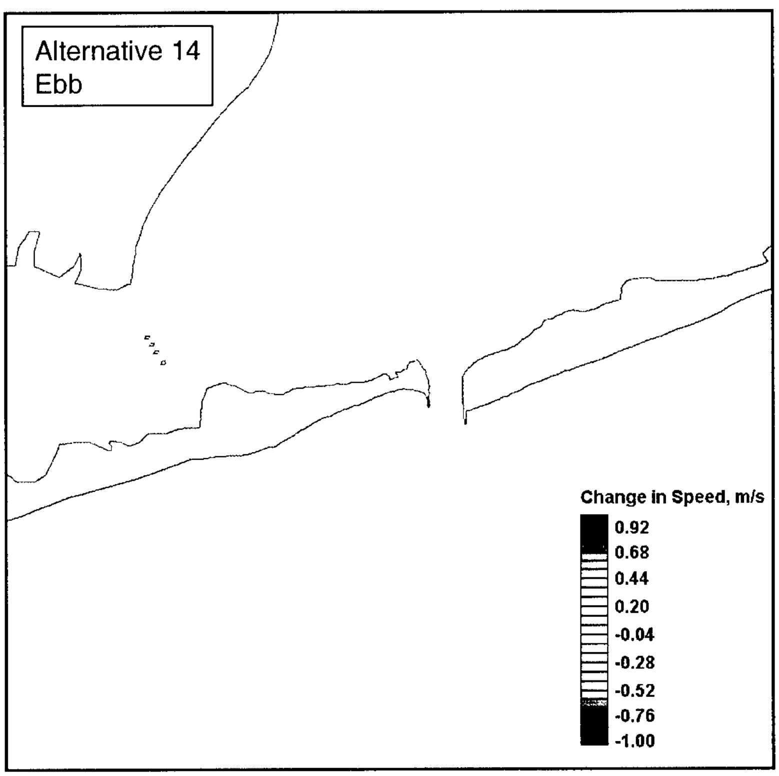

Figure B16. Change in current speed for Alternative 14

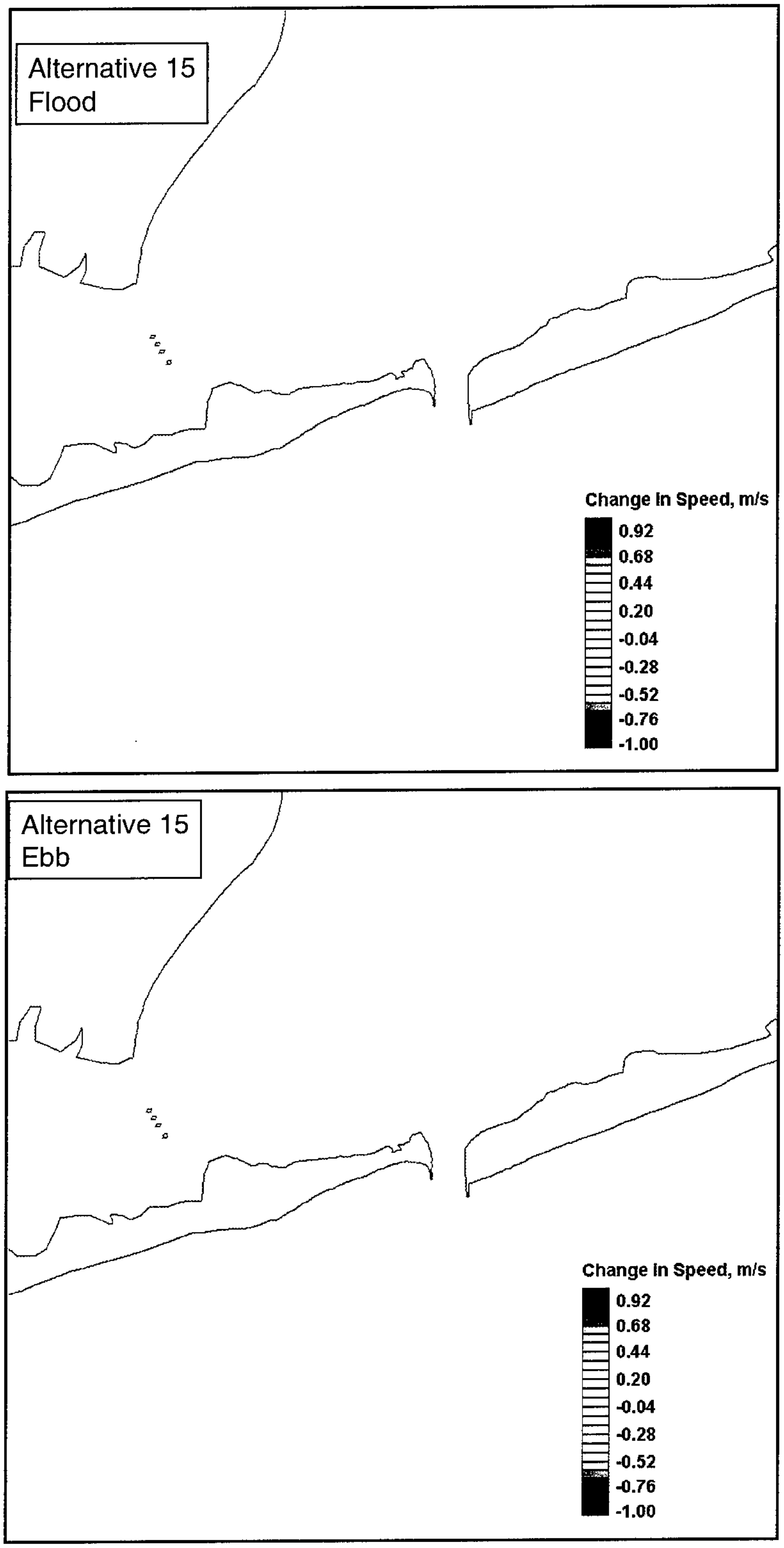

Figure B17. Change in current speed for Alternative 15

Appendix C
Analysis of Alternative 16

This appendix to the main report was prepared at the request of the U.S. Army Engineer District, New York, to supplement evaluation of the proposed alternatives for a flood-shoal sand source to nourish the beach west of Shinnecock Inlet, New York. The main report documents analysis of 15 action alternatives. This appendix extends the analysis to an additional alternative (Alternative 16). Notation and other conventions as appear in the main report are followed here.

Alternative 16 specifies dredging the seaward half of the area of compatible material to a depth of –16 ft mlw (CENAN-EM-HC Memorandum of 22 October 1999, Comment 3), as shown in Figure C1. The dredged depth corresponds to –17.7 ft (-5.4 m) mean tide level (mtl). Dredging of the southern half of the area of compatible material is in accordance with the request of the Southampton Town Trustees. The template for Alternative 16 lies outside of the area of compatible material along a portion of its southern edge. This extension beyond the area of compatible material removes sand that would otherwise be left as a ridge. The volume of sand removed for Alternative 16 is 1,560,000 m^3 (2,040,000 yd^3).

Analysis of Alternative 16 follows that of the alternatives described in the main report. Changes in current speed relative to the existing (1998) condition are first described for flood and ebb tide. Then, calculation of the excess suspension speed is discussed with relation to changes in sediment transport. Plots of flood and ebb current fields are also provided.

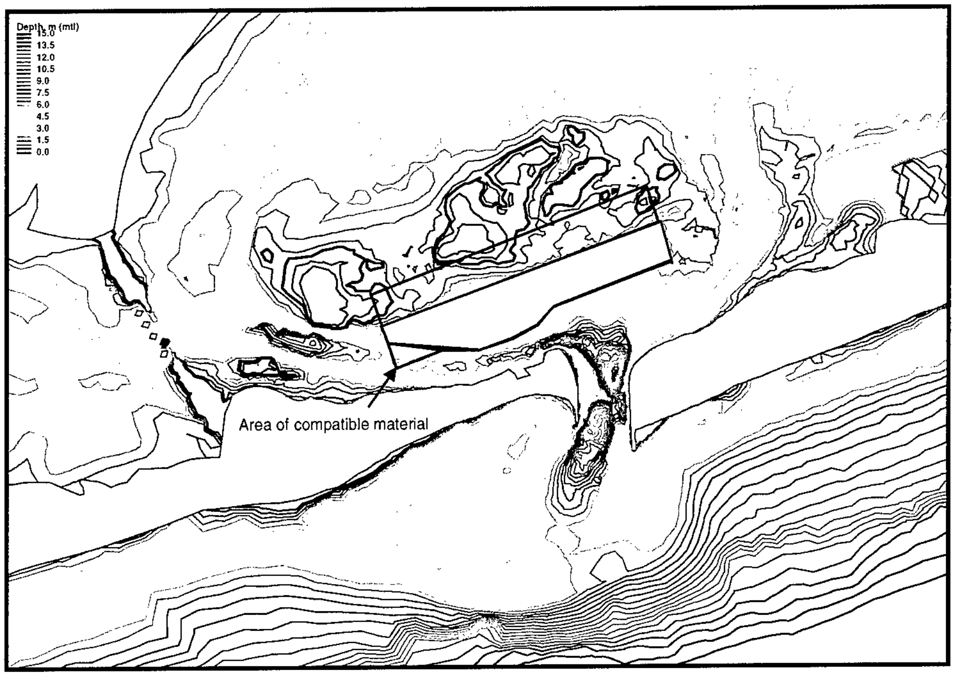

Figure C1. Alternative 16: Dredge seaward portion of flood shoal

Change in current speed

a. Flood tide (Figure C2). Current speed is increased where the inlet meets the flood shoal and adjacent to the shoreline along the West and East Cuts over limited reaches. The flood shoal experiences a decrease in current speed, whereas the back flood shoal has increased speed. The northwest portion of the flood shoal also experiences decreased speed. Speed in the East Cut is reduced, except for a reach that is adjacent to the shore. Maximum speed increase occurs where the inlet meets the flood shoal and in the eastern back flood shoal. Maximum speed decrease occurs on the eastern flood shoal.

b. Ebb tide (Figure C3). Increased current speed occurs where the inlet meets the flood shoal, and on the western and eastern portions of the flood shoal. The area of increased speed on the eastern flood shoal is small. Decreased current speed occurs on the flood shoal and in the West and East Cuts. A small increase in speed occurs east of the Ponquogue Bridge.

Changes in current speed for Alternative 16 are similar to those calculated for Alternatives 1, 2, 3, and 4 (discussed in the main report).

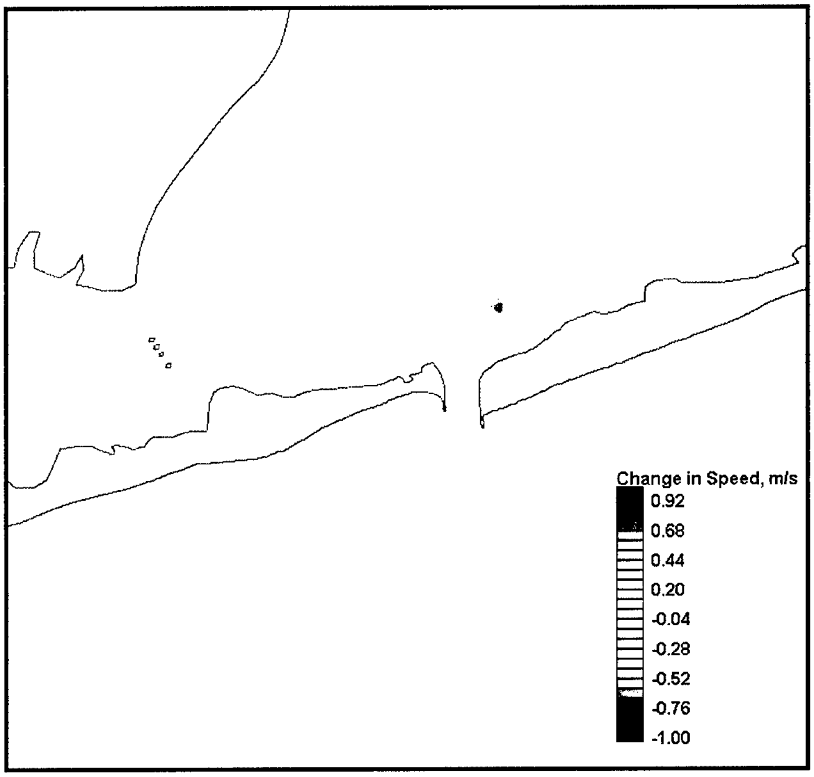

Figure C2. Change in current speed for Alternative 16, flood tide

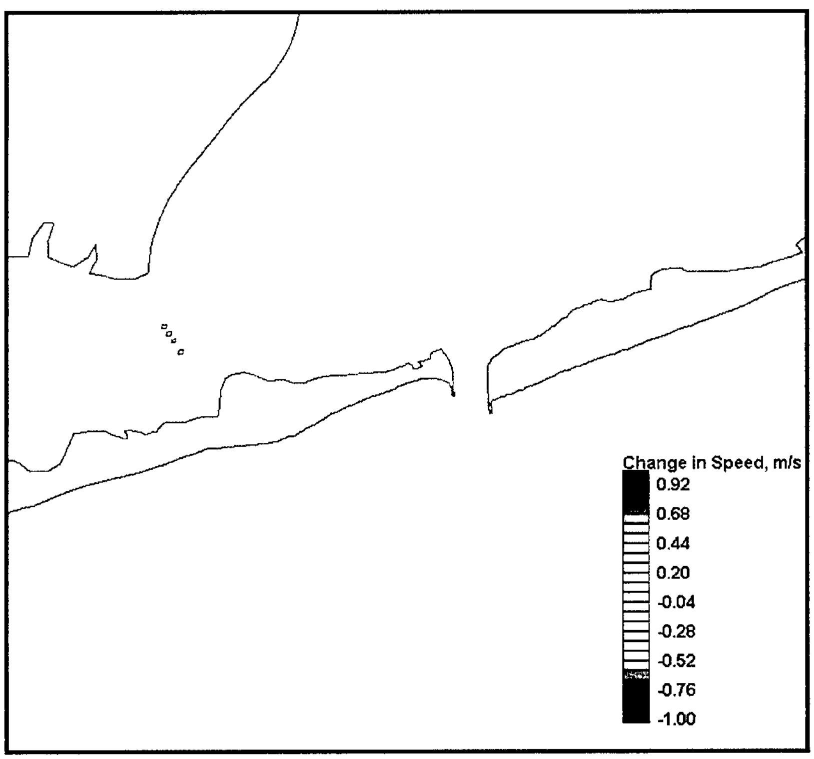

Figure C3. Change in current speed for Alternative 16, ebb tide

Change in patterns of erosion and deposition

Areas of erosion and deposition were estimated by subtracting the critical depth-averaged speed of initiation of suspension from the peak flood and ebb current speeds to obtain the excess suspension speed. The resultant patterns were compared to those for the existing condition (Alternative 0). The procedure for the excess suspension speed calculation and plots of the excess suspension speed for the existing condition are contained in the main report.

Figure C4 plots the excess suspension speed for Alternative 16 at peak flood tide. The pattern is similar to that for Alternative 0. Areas with excess suspension speed are the inlet, much of the flood shoal, and the vicinity of the Ponquogue Bridge. Weak excess suspension speed in the area where the inlet flood flow meets the flood shoal indicates that deposition may occur there over most of the tidal cycle. Thus, the mined area would have a tendency to fill. Based on this analysis, no areas of Alternative 16 would experience increased erosion as compared to the existing condition during flood tide.

Figure C5 plots the excess suspension speed for Alternative 16 for peak ebb tide. The pattern is almost identical to that for Alternative 0. The eastern portion of the flood shoal shows some small variations from Alternative 0, but significant changes to deposition or erosion are not indicated. Based on this analysis, no areas of Alternative 16 would experience substantial erosion as compared to the existing condition during ebb tide.

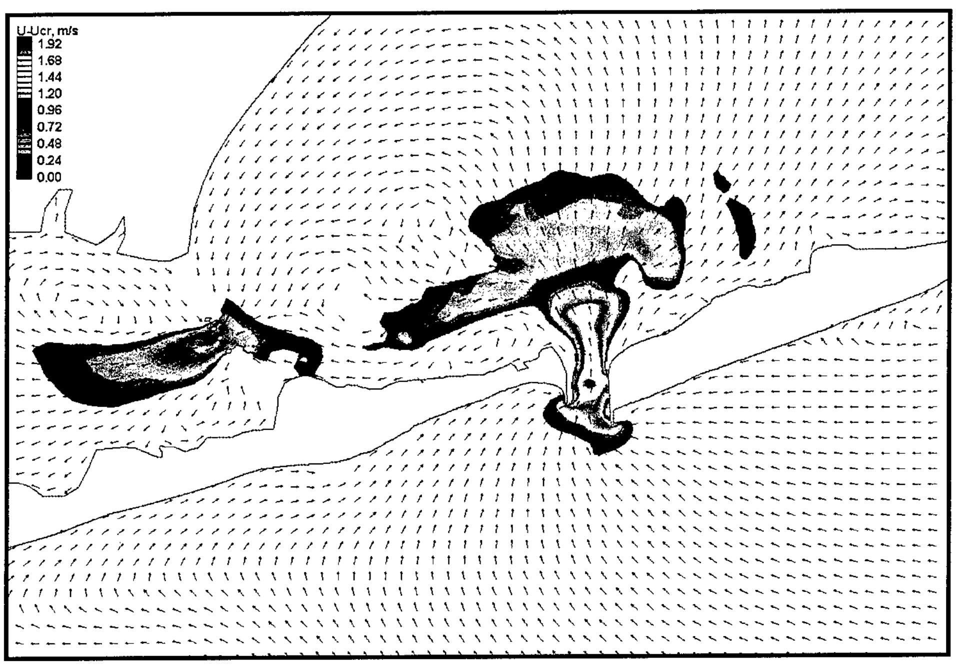

Figure C4. Excess suspension speed at peak flood tide, Alternative 16

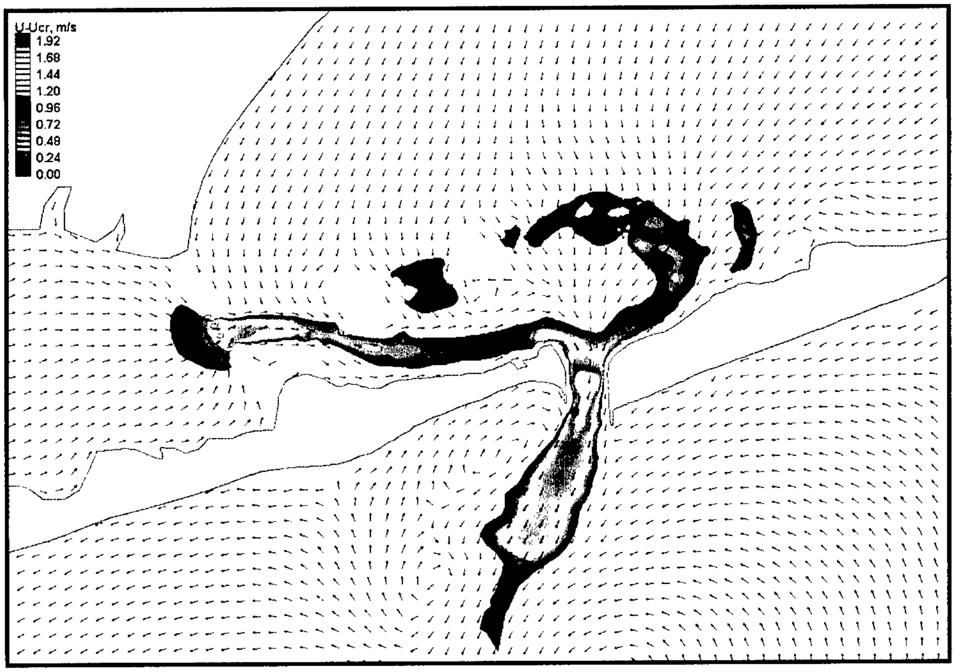

Figure C5. Excess suspension speed at peak ebb tide, Alternative 16

Plan-view plots of current velocity are shown in Figures C6, C7, and C8 for Alternative 16 during spring peak flood and ebb tide. The figures contain velocity vectors over contoured bottom topography, contoured current speed, and velocity vectors plotted over contoured speed. Color scales refer to contours of elevation in the upper panels of Figures C6 and C7, and to contours of current speed in the lower panels of Figures C6 and C7 and also in Figure C8. This set of plots shows circulation patterns similar to the existing condition and to Alternatives 1, 2, 3, and 4.

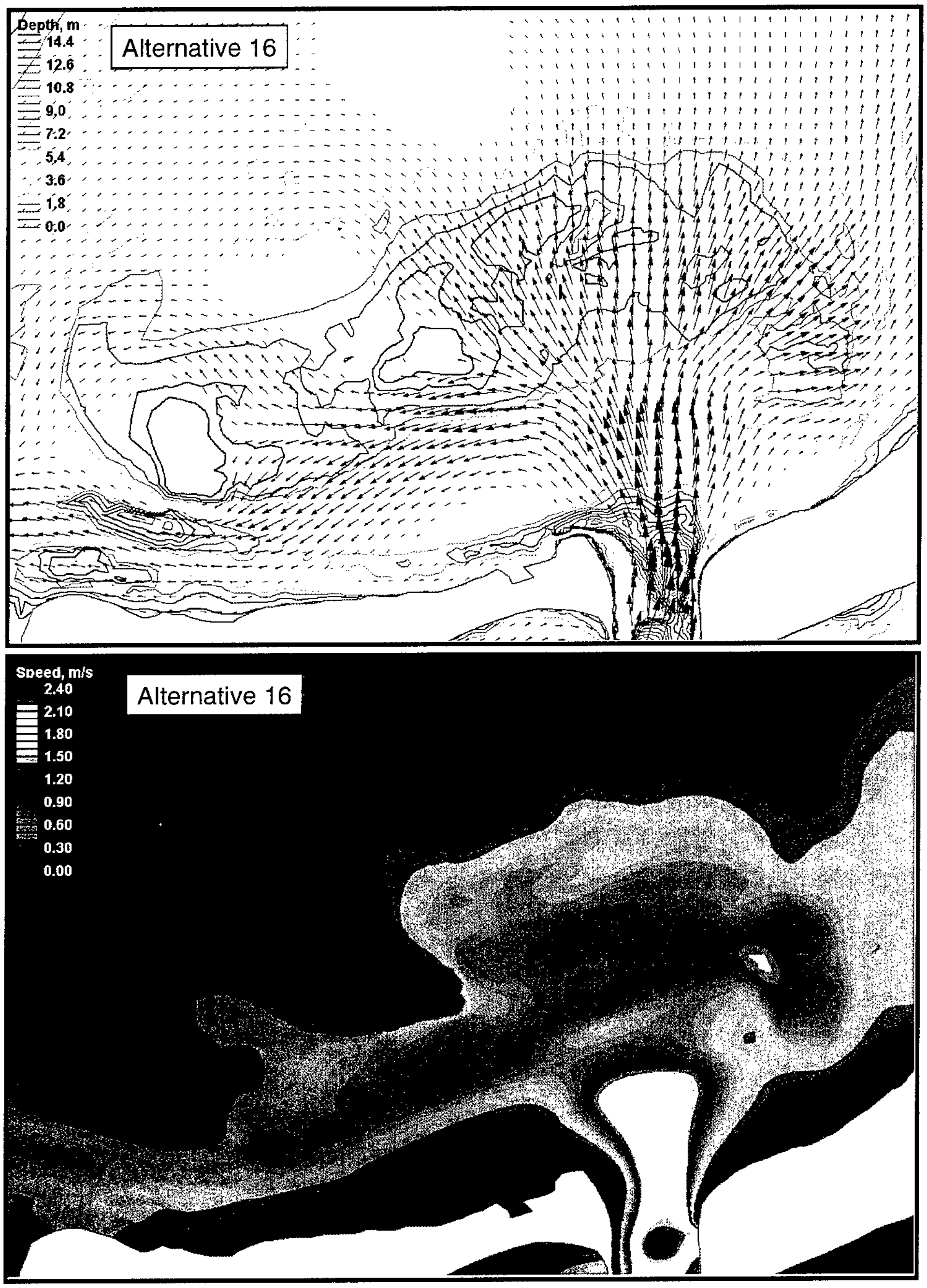

Figure C6. Alternative 16 velocity vectors and speed at flood shoal, peak flood tide

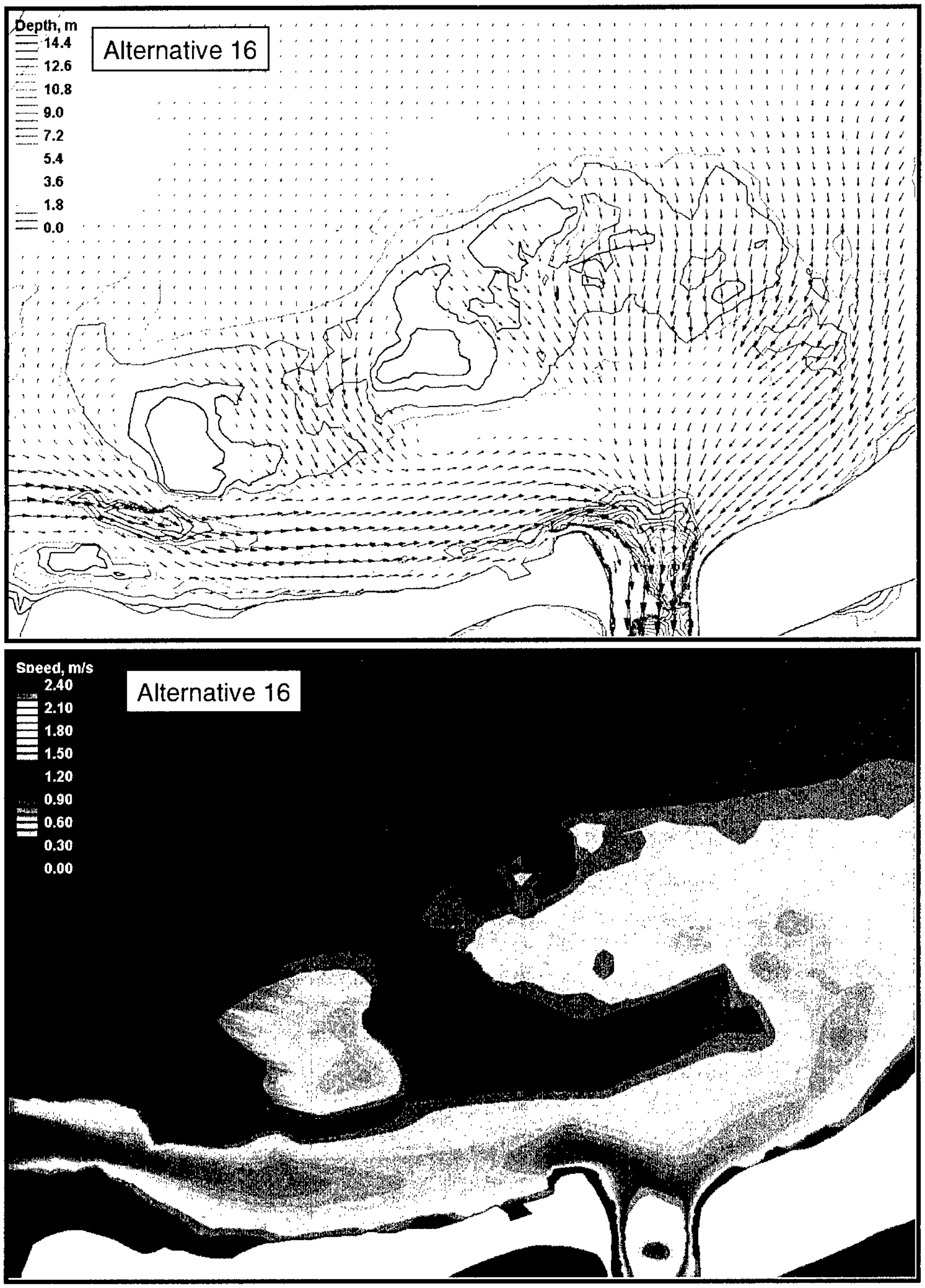

Figure C7. Alternative 16 velocity vectors and speed at flood shoal, peak ebb tide

Figure C8. Alternative 16 velocity vectors and speed at inlet and ebb shoal, peak ebb tide

Conclusions for Alternative 16

Analysis of Alternative 16 indicates that dredging the seaward half of the flood shoal in the area of compatible material is feasible. Calculated current patterns and strength show that the flood shoal and East and West Cuts are the only areas of change. Current speed in the inlet is not expected to change if Alternative 16 is implemented.

Calculated erosion and deposition patterns show little change from the existing condition. The mined area will act as a sediment trap, providing a renewable source of sand. Alternative 16 did not modify the current along the beach adjacent to the west jetty. Erosion of the west beach will not be increased by implementation of this alternative.

Navigation benefits for Alternative 16 are similar to those for Alternatives 1, 2, 3, and 4. This alternative is also not expected to cause shoaling or scour in the inlet or modify the navigation channel. In addition, the current near the Ponquogue Bridge is not expected to change significantly.

REPORT DOCUMENTATION PAGE

Form Approved
OMB No. 0704-0188

1. REPORT DATE *(DD-MM-YYYY)*
March 2001

2. REPORT TYPE
Final Report

3. DATES COVERED *(From - To)*

4. TITLE AND SUBTITLE
Shinnecock Inlet, New York, Site Investigation
Report 4, Evaluation of Flood and Ebb Shoal Sediment Source Alternatives for the West of Shinnecock Interim Project, New York

5a. CONTRACT NUMBER

5b. GRANT NUMBER

5c. PROGRAM ELEMENT NUMBER

6. AUTHOR(S)
Adele Militello, Nicholas C. Kraus

5d. PROJECT NUMBER

5e. TASK NUMBER

5f. WORK UNIT NUMBER

7. PERFORMING ORGANIZATION NAME(S) AND ADDRESS(ES)

U.S. Army Engineer Research and Development Center
Coastal and Hydraulics Laboratory
3909 Halls Ferry Road
Vicksburg, MS 39180-6199

8. PERFORMING ORGANIZATION REPORT NUMBER

Technical Report CHL-98-32

9. SPONSORING / MONITORING AGENCY NAME(S) AND ADDRESS(ES)
U.S. Army Engineer District, New York
26 Federal Building
New York, NY 10278-0090;

U.S. Army Corps of Engineers
Washington, DC 20314-1000

10. SPONSOR/MONITOR'S ACRONYM(S)

11. SPONSOR/MONITOR'S REPORT NUMBER(S)

12. DISTRIBUTION / AVAILABILITY STATEMENT
Approved for public release; distribution is unlimited.

13. SUPPLEMENTARY NOTES

14. ABSTRACT

Shinnecock Inlet, New York, is a dual-jettied inlet located on the south shore of Long Island connecting Shinnecock Bay to the Atlantic Ocean. The down-drift beach, west of the inlet, experiences chronic erosion, and cost-effective and innovative measures for beach nourishment are being examined by the U.S. Army Engineer District, New York. The feasibility of mining of the flood and ebb shoals to serve as sources of material was examined in this report. Emphasis is on the concept of "flood-shoal engineering" within an integrated inlet and beach system. Fifteen action alternatives were developed that involved dredging, modification of the jetties, and combined dredging and structural changes. The alternatives were evaluated by their potential changes to navigation conditions, availability of material for placement on the beach, changes to inlet and channel currents that would modify scour and deposition patterns, and changes in current strength near the beach that would modify erosion. The area of compatible material, established for the flood shoal from analysis of core samples, was the targeted mining area for the study and contains approximately 1.8×10^6 yd^3 of beach-compatible sand. Exploratory alternatives were also evaluated that involved dredging in other locations. Evaluation of alternatives was conducted through circulation, wave, and morphology modeling. A calibrated circulation model was applied to simulate each alternative and compare current strength and patterns to those for the existing condition. Wave modeling was conducted for one alternative that consisted of mining the attachment bar

(Continued)

15. SUBJECT TERMS

Ebb shoal	Flood shoal	New York	Sand mining	Tidal inlet
Erosion	Navigation channel	Numerical modeling	Shinnecock Inlet, New York	

16. SECURITY CLASSIFICATION OF:			17. LIMITATION OF ABSTRACT	18. NUMBER OF PAGES	19a. NAME OF RESPONSIBLE PERSON
a. REPORT	**b. ABSTRACT**	**c. THIS PAGE**			**19b. TELEPHONE NUMBER** *(include area code)*
UNCLASSIFIED		UNCLASSIFIED		211	

14. (Concluded).

to determine changes in the wave patterns near the shore. Morphology modeling was conducted to calculate the long-term recovery rates of the system to mining of the flood shoal. The study found that mining of the flood shoal in the area of compatible material (the front portion of the shoal containing relatively coarse material) is a feasible method of obtaining sand for placement on the beach. Mining in this area resulted in little change to the current strength and patterns in the bay, and no change in the inlet. The mined area would have reduced current speed over its present condition and would act as a sediment trap, providing a regenerating source of material for the beach. Calculated recovery times for mining of the flood shoal are 15 yr for removal of 400,000 yd^3 (planned placement volume) and 35 yr for removal of 1×10^6 yd^3.